Wave Propagation Sensors for Structural Control

By

Darryll J. Pines

B.S., Mechanical Engineering
University of California at Berkeley, 1986

S.M., Mechanical Engineering
Massachusetts Institute of Technology, 1988

SUBMITTED TO THE DEPARTMENT OF MECHANICAL ENGINEERING
IN PARTIAL FULLFILLMENT OF THE
REQUIREMENTS FOR THE DEGREE OF

DOCTOR OF PHILOSOPHY

at the

MASSACHUSETTS INSTITUTE OF TECHNOLOGY

February 1992

Signature redacted

Signature of Author_____
Department of Mechanical Engineering
October 21, 1991

Signature redacted

Certified by_____
Prof. Andreas H. von Flotow
Thesis Supervisor

Signature redacted

Certified by_____
Prof. Jean-Jacques E. Slotine
Chairman

Signature redacted

Accepted by_____
Prof. Ain A. Sonin
Chairman, Department Committee on Graduate Students

Wave Propagation Sensors for Structural Control

By

Darryll J. Pines

October 21, 1991

Submitted to the Department of Mechanical Engineering
in February of 1992, in Partial Fulfillment of
the Degree of Doctor of Philosophy
at the Massachusetts Institute of Technology

Abstract

This research develops novel methods for sensing actual disturbance information which can propagate along one-dimensional structural waveguides. The motivation for this work arises from the inability to realize most active wave control designs using output information from physical measurements such as deflection, slope, curvature and internal shear force. Often the use of actual physical measurements leads to instability and sub-optimal performance of certain active wave control loops. Thus, there is a desire to develop wave-component filters which can extract magnitude and direction of structural disturbances along dispersive and non-dispersive members. In this work two sensing schemes are reported. In each case, the solution of the partial differential equation which characterizes the dynamics of a one-dimensional structural member is written in terms of travelling waves. This form of the solution is then exploited in the first method to combine a sequence of spatially discrete measurements through a frequency dependent decoupling matrix to yield magnitude and direction of travelling wave components. This approach works well for non-dispersive members, however, for dispersive members a low order approximation to the frequency dependent decoupling matrix is not guaranteed to be causal. A further limitation is the introduction of spatial aliasing. In the second approach, a spatially distributed sensor which convolves past and future measurements along a member into a single temporal signal overcomes these problems of causality and aliasing for a dispersive member. Here mapping between the temporal and spatial domains permits acausal temporal filters to be realized by spatial filters. Thus, by imposing specific shapes to spatially distributed sensors, it is possible to combine the output of these sensors with point measurements to observe various propagating wave components. Because both methods require some approximation of the spatial domain, there will be errors due to spatial discretization and truncation. This work addresses these issues and presents some preliminary experimental results to confirm analytical examples.

Thesis Supervisor, Andreas H. von Flotow
Title-Associate Professor of Aeronautics and Astronautics

Chairman, Jean-Jacques E. Slotine
Title-Associate Professor of Mechanical Engineering

Committee Member, Steven H. Crandall
Title-Professor of Mechanical Engineering

Committee Member, Dr. David W. Miller
Title-Research Associate

Acknowledgements

There are many individuals who have played an integral role in helping me achieve my degree objective . First of all there is my distinguished dissertation committee which included Professors Andreas H. von Flotow, Stephen H. Crandall, Jean-Jacques E. Slotine and Dr. David W. Miller. Of this group I am particularly grateful to Professor Andreas H. von Flotow who has not only served as my thesis supervisor but also as my landlord for 5 years. I thank him for opening both his home and his mind to me. It has truly been an honor to work with an individual with such a creative technical mind. I thank Professor Crandall for helping me convey my thoughts so that others could understand what I was talking about. I thank Professor Slotine for his thoughtful discussions and encouragement. Finally, I am grateful to Dr. Miller for forcing me to pay closer attention to details. Indeed my haste caused me many unnecessary hardships.

I thank many members of Space Engineering Research Center for their direct or indirect help with this work. Specifically, I am grateful to Simon Collins, Gary Blackwood, Eric Anderson, Ken Lazarus, Erik Saarma, David Vos, Norman Wereley, Mathieu Mercadal and Paul Bauer.

I also thank members of the BGSA for providing a forum for thought and discussion. This truly helped me to relieve some of my technical frustrations while opening my mind to other global and national issues.

Last, but certainly not least, I am forever grateful to my parents, Claude and Maureen, and my siblings Derek and Denise. Their constant support and love throughout the course of my degree programs gave me the strength to endure many difficult moments.

This work was partially supported by a grant from the Office of Naval Research under Contract No. N00014-88-K-0720 and by the Patricia Harris Roberts Fellowship Foundation.

TABLE OF CONTENTS

List of Figures

List of Tables

Nomenclature

Roman Notation	**Units**
A = cross-sectional area	(m^2)
A= matrix operator, spatial or temporal	
a = pole locations in complex plane	
B = matrix operating on point inputs	
b = width of beam	(m)
C = ouput vector matrix operator	
D = observer matrix operator	
d = downstream	
E = Young's modulus of elasticity	(N/m^2)
F = external point excitation	(N)
f = circular frequency	(Hz.)
H = approximate transfer function	(ND)
I = identity matrix	
I = moment of inertia	($kg\text{-}m^2$)
i = complex variable	
j = index	
K = observer gain operator	
k = non-dispersive/dispersive wavenumber	(m^{-1})
l = length	(m)
M = external point moment applied to beam	(N-m)
m = integer	
n = noise vector	
P = power Flow matrix	
p = spatial Laplace variable	
Q = Lyapunov Functional	
Q = excitation vector	
q = interpolation function	(ND)
S = scattering matrix	
s = temporal Laplace variable	
t = time	(sec)
u = physcial deflection(displacement)	(m)
u = upstream	
v = distributed sensor output	
w = wave-mode vector	
x = position along 1-D member	
y = physical state vector	
Y = state transformation matrix	

Greek Notation	
α = bending constant	(ND)
β = closed loop characteristic equation, constant	
Δ = distance between discrete sensors	

ε = strain
ϕ = weighting function
η = loss factor (ND)
Λ = uncertainty matrix (ND)
ψ = face rotation (ND)
Ψ = generation matrix
ρ = density (kg/m^3)
ξ = transition matrix
ω = radian frequency (rad/sec)
ζ = damping ratio (ND)

Subscripts

A = actuator
b = beam
c = control
cl = closed loop
d = 1/2 length of distributed sensor
e = evanescent-(near field)
ol = open loop
p = passive
p = propagating
t = truncated spatial domain
T = travelling
1, 2, 3, 4= junction interface locations
+ = positive going disturbance
- = negative going disturbance

CHAPTER 1

Introduction

1.1 Controlled-Structures Problem

Active control of one and two dimensional structures whose dynamics are typically described using partial differential equations has received a considerable amount of attention in the past two decades. Two current examples receiving increasing attention include large scale dynamic systems known as Large Space Structures-LSS-[1,2] and more recently the area of Structural Acoustics-[3]. LSS typically consist of complex structural networks which are derived from simple one and two-dimensional structures. The size of these systems has been proposed to have dimensions of tens of kilometers. More realistically, however, visions of structures which support interferometers, reflectors and antennas are planned to have dimensions on the order of hundreds of meters. Because of mission objectives and launch requirements many of these structures will be composed of long lightweight slender members which are essentially one-dimensional. These particular members will be quite flexible often including several of the structure's natural frequencies when excited. This is also true in the area of structural acoustics where coupling between structures such as aircraft skins and submarine hulls with fluid media may often involve

hundreds of natural modes of the structure. Consequently, the central concern has been how to accurately predict and control the behavior of such structures over a broad frequency spectrum where several local and global elastic modes may contribute to the overall response of the structure.

1.2 Modelling/Control Options

1.2.1 Global Models

Several modelling options exist for describing the dynamics of complex structural networks; each with its advantages and limitations. Historically, modal analysis has been used to describe most complex structural systems. This method suppresses the distributed nature of one and two-dimensional structures in favor of an equivalent lumped-parameter representation. This representation characterizes the system dynamics in terms of the interaction of several structural modes. Such a characterization can be approximated by Linear Time Invariant-(LTI) dynamics where the infinite-dimensionality of the distributed parameter system is suppressed for practical control purposes. This approximation gives the following truncated form of the system dynamics:

$$\begin{aligned} \dot{\vec{x}} &= A\,\vec{x} + B\,\vec{u} + \vec{w} \\ \vec{y} &= C\,\vec{x} + D\,\vec{u} + \vec{v} \end{aligned} \qquad (1.1)$$

where A is a nxn matrix containing the homogeneous dynamic properties of the structure, B has dimensions nxp and defines how the control forces affect the system dynamics, C-(mxn) connects the vector of actual measurements to their modal states-$\vec{x}$ *and* D-(mxp) *affects the DC response and zero locations.* $\vec{w}(t)$ and $\vec{v}(t)$ represent vectors of process and measurement noise respectively. Equation (1.1) is the ideal LTI description of a controlled structures problem.

LTI descriptions are useful because a host of multivariable control design methods have been developed to handle such systems. These methods-[4] include *LQR-Linear Quadratic Regulator, LQG-Linear Quadratic Gaussian, LQG/LTR-Linear Quadratic Gaussian/Loop Transfer Recovery*, and norm based methods such as H_2 and H_∞. Most of these design methods, however, assume that the plant model and disturbances are well known. This is rarely the case in most feedback systems and is definitely not the case in modally rich systems found in the fields of LSS and structural acoustics where global modal models are rarely valid to the required precision.

1.2.2 Statistical Models

To handle modally rich-(>100 modes) structures two modelling approaches have evolved from classical modal analysis; Statistical Energy Analysis-SEA-[5] and Asymptotic Modal Analysis-AMA-[6,7]. Both of these approaches attempt to minimize the effects of modelling uncertainty by approximating the reverberant response of a structure over a broad frequency range in terms of an average root mean square-(rms) value. Unfortunately, both of these methods suffer from the loss of phase information which is critical to most control applications. Hence SEA and AMA methods cannot be used for active control purposes.

1.2.3 Local (Wave) Models

An alternative to representing the dynamics of complex structures in terms of the global interaction of several elastic modes, is to describe structural motion in terms of the propagation of elastic waves-[8-10]. These elastic waves, natural responses of an individual waveguides, can circumnavigate a network of waveguides exchanging energy with one-another at structural discontinuities and junctions. These travelling wave components can be assembled to obtain the reverberant response of the system. Such global predictions are equivalent to that obtained via modal methods, exhibiting the same level of uncertainty.

An advantage of this approach, however, is that active control designs can be implemented on a local scale where the model is thought to be much more accurate. Thus, instead of relying on a global feedback model a local feedforward scheme is developed based on point actuation and sensing of propagating wave dynamics-(See Figure 1.1a). A typical open loop frequency representation of a wave component input/output relation has the following form:

$$\vec{w}_o(\omega)=S(\omega)\vec{w}_i(\omega)+\Psi(\omega)\vec{Q}(\omega) \qquad (1.2)$$

where $\vec{w}_i(\omega)$ and $\vec{w}_o(\omega)$ represent vectors of incoming and outgoing wave components respectively, $S(\omega)$ is the scattering matrix of reflection and transmission coefficients, $\Psi(\omega)$ is the generation matrix and $\vec{Q}(\omega)$ is the vector of control forces and moments. In this form several wave control objectives such as vibration isolation-(zero transmission of energy to other parts of a structure) or damping augmentation-(energy removal) have been studied with feedforward compensation in which the control signal $\vec{Q}(\omega)$ is derived from measurement of the incoming waves-(See Figure 1.1a);

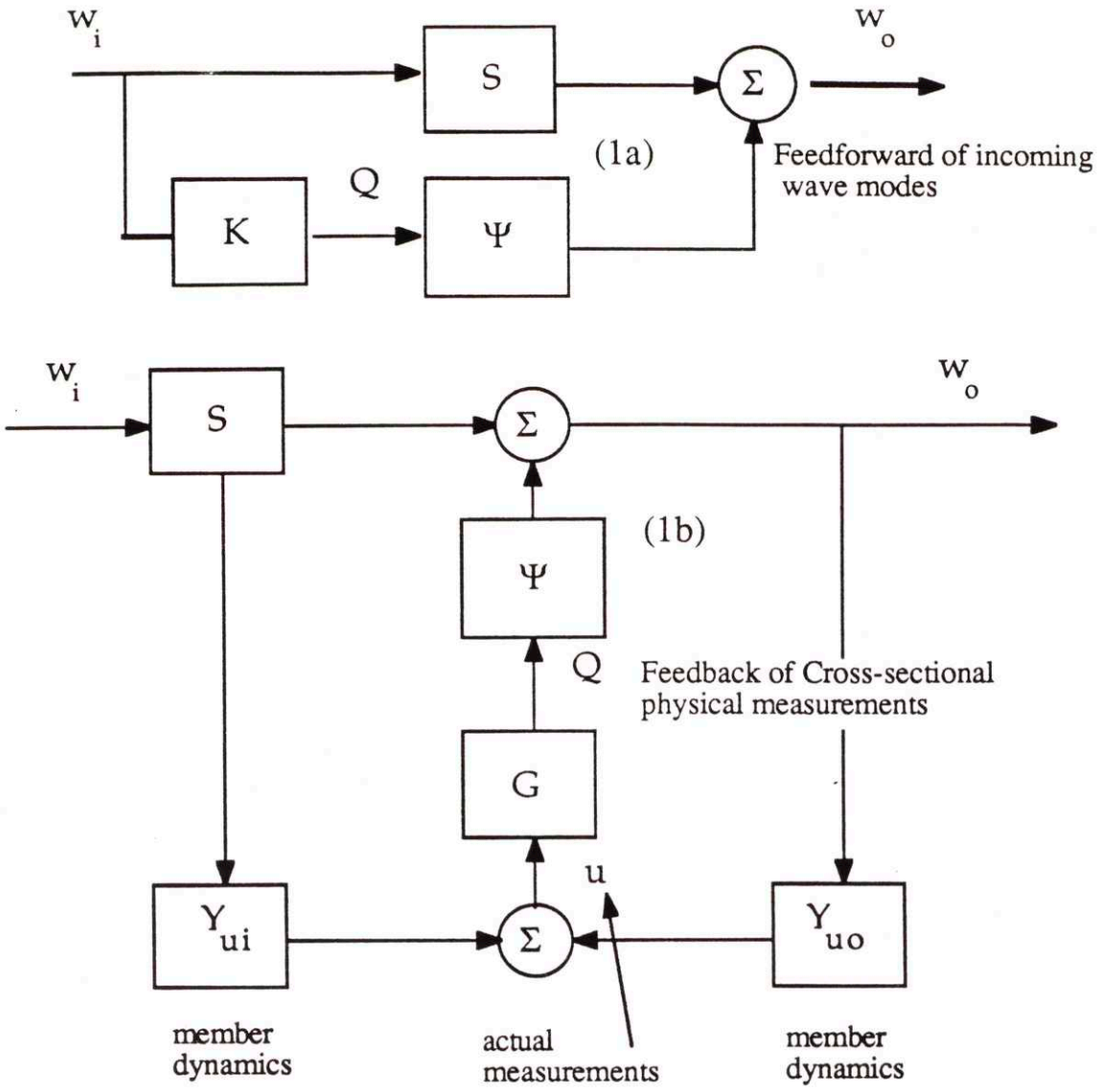

Figure 1.1: Structure of an Feedforward-(a) and Actual Feedback-(b) implementation of a typical Wave Control

$$\vec{Q}(\omega)=K(\omega)\vec{w}_i(\omega) \qquad (1.3)$$

where $K(\omega)$ is the dynamic compensation matrix. Since individual wave-states have not been measurable, all feedforward compensation schemes must be transformed to their equivalent feedback representation-(See Figure 1.1b) where physical state measurements are used in conjunction with causal compensation in the form of $G(\omega)$.

$$\vec{Q}(\omega)=G(\omega)\vec{u}(\omega) \qquad (1.4)$$

Notice that in this loop structure outgoing waves are fed back into the control actuator, giving rise to a local closed-loop with possible instabilities. An approach which attempts to overcome this difficulty along with causality limitations centers around realization of the feedforward form given in equation-*(1.3)*. Such an approach requires the sensing of wave propagation dynamics and implementing appropriate filters, $K(\omega)$, which achieve feedforward control.

The research discussed here focuses on developing wave sensors to solve this specific problem. However, the need for wave sensors extends far beyond the structural control problem. Some of these other applications are also alluded to in the text of this thesis.

1.3 The Need for Wave Sensors for Control

The cancellation of incident disturbances by active means is not a new concept. In fact its first application might be traced to the field of sound propagation where in 1973 Swinbanks-[11] attempted to control the transmission of sound in a slender duct using an array of point sources. Later his work was experimentally verified by Poole and Leventhall-[12-14]. In their work cancellation was achieved by using secondary sources to superpose an equal but opposite sound field upon an incident noise field so that summation of the two fields resulted in destructive interference. Ffowcs Williams-[15] later refered to this opposing sound field as "anti-sound." Hence, it was found that if interest was restricted to signals with wave-lengths much greater than the duct cross-sectional dimensions (frequencies below 100 Hz. for most air conditioning ducts), the duct would act essentially as a single-mode, non-dispersive waveguide.

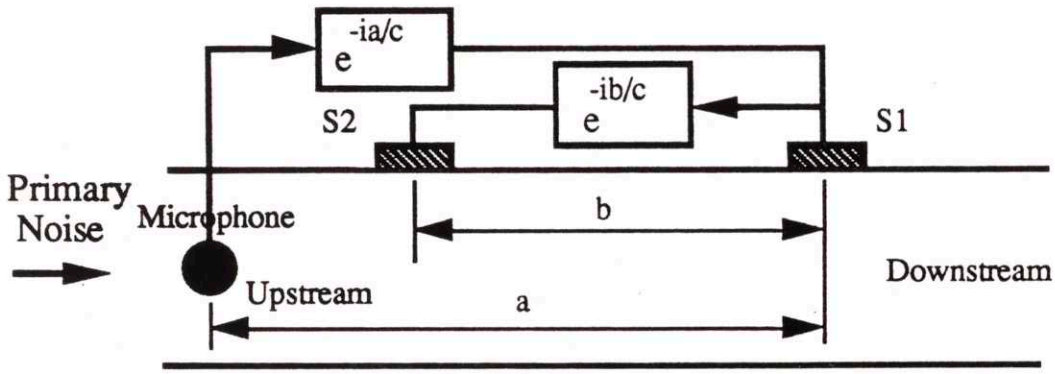

Figure 1.2: Geometric arrangement of Swinbank's noise attentuator system using two secondary sources.

Many structural idealizations such as plates, shells, cables and beams can also be viewed as waveguides-(See Appendix A1). Directly analogous to the air duct at low frequencies is the class of slender structural members described by the one-dimensional wave equation $u_{xx}=u_{tt}$; elastic rods in compression and torsion, and taut cables undergoing lateral deflections. Many of the techniques developed for active control of sound in ducts ought to be applicable to these structural components, albeit with different sensors and actuators. Most structural idealizations are however dispersive; different frequency components of a given excitation travel at different speeds, and the signal distorts as it propagates. Nevertheless, for a class of 1-D structures including both dispersive and non-dispersive members several active control schemes-[16-52] have evolved based on altering the local scattering properties of incoming and outgoing waves at particular actuator/sensor locations. Some methods have been ad-hoc while others have provided a rigorous approach to deriving local control laws based on wave propagation dynamics.

The first notable publication in this area was the PhD thesis of von Flotow-[10] in 1984. In his work he views one-dimensional structures as elastic waveguides to develop a uniform approach to controlling a network of 1-D structural members. His goal is to change the global dynamics of LSS by affecting the local scattering properties of wave components which circumnavigate the network. He points out that a wave description leads to two potential control objectives

Active Damping-(Energy Absorption)
Active Isolation-(Energy Shunting)

Active Damping has been investigated by a host of researchers-[], both analytically and experimentally. Some of the more notable contributions include the power flow ideas of Miller-[32,36,39], the impedance matching theory of MacMartin and Hall-[47,48l, and the non-collocated sensing/control scheme of Scheuren-[16,45,46]. In Miller's approach, the choice of power flow as a performance objective, leads to optimal causal, non-causal and fixed-form compensators derived for the pinned-end of a pinned-free Bernoulli-Euler beam. As expected a non-causal compensator achieves the best absorption of incident energy using a dual sensor/actuator pair. Miller found that such a control attempts to match the impedance at the controlled-end. Experimentally, he verified his causal solutions on an brass beam and found good agreement between theory and experiment. Following the lead of Miller, MacMartin develops a scheme for matching the impedance at any location in a

structure in the presence of unmodelled dynamics. Again this leads to causal compensators and suboptimal performance.

To overcome the problem of causality Scheuren-[16,45,46] motivated a non-collocated control approach to absorping energy on a flexural beam. The key to his scheme was the manipulation of an array of point measurments which facilitated digital realization of feedforward wave filters/compensators for controlling the propagating wave componenet of the structural dynamics. Resonant response was suppressed by covering the free end of the beam with sand boxes.

Active Isolation was studied in the work of Mace-[25] and Mckinnell-[31]. Both motivated the use of point control forces to cancel the evanescent and propagating waves on a beam using only point sensors. While Mace pointed out that the approach lead to irrational compensators, Mckinnell found a transformation which suppressed the underlying wave dynamics to obtain realizable compensators based on physical measurements only. Again a digital approximation was required for implementation. Experimental verification of Mckinnell's approach resulted in marginal isolation-(6 db in reduction of the transmission coefficient) being achieved on an experimental fixed-free beam.

More recently, Elliott Stothers, and Billet-[49] have applied Adaptive Filtering concepts to the control of flexural waves in a beam. Their work complements the non-collocated control schemes proposed by Scheuren and Mckinnell. Again as in many other experimental tests they confirm their predictions on a non-resonant experimental beam. Remarkable cancellation is achieved for a 128 order FIR compensator.

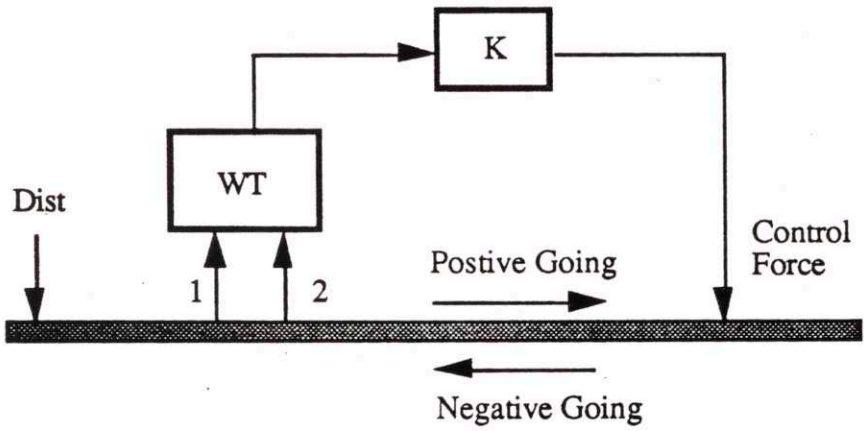

Figure 1.3: Feedforward non-collocated directional control scheme of Scheuren using point sensors-(1,2).

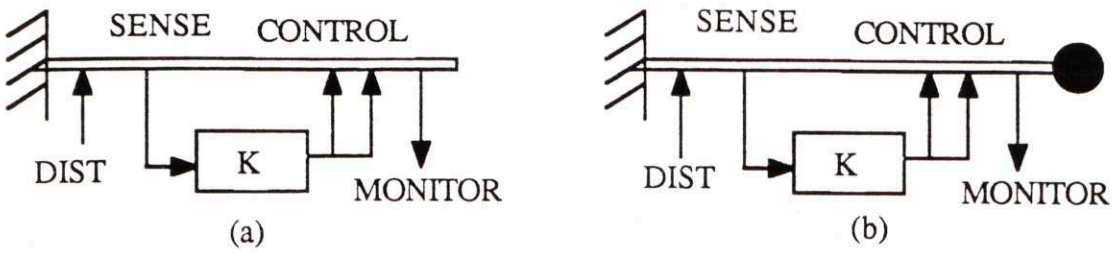

Figure 1.4: Mckinnell's feedfoward cancellation scheme on a B-E beam.(a) free end. (b) mass-loaded end.

In all of the above approaches one of the following issues either limits or complicates active control schemes based on a wave-description of the system dynamics

- causality-(irrationality of compensators)
- stability of control loops
- the use of physical point measurements
- boundaries/structural discontinuities
- collocation/non-collocation of sensors/actuators
- presence of evanescent-(nearfield) dynamics

If wave-states which characterize the physical responses in a member were available, pure feedforward control could be achieved and many of the above issues would be resolved with the exception of the presence of evanescent dynamics. However, the finite dimensionality of an actual structure insures that beyond some finite scale length-(kl) on a beam, these terms will contribute negligibly to its response. Thus, beyond this point a purely propagating view of the beam structural dynamics should suffice.

With this assumption in mind this thesis develops techniques for sensing wave motion of simple one-dimensional structures using the output from collocated distributed/point sensor pairs. Specifically, the approach uses purely analog components to realize directional wave dynamics. Causality is not an issue since the compensation is embedded in the sensing of directional information. Also boundaries do not present a problem since the approach uses collocated sensing. Both active damping and isolation are possible and a digital computer is only required for implementation of non-linear spatial phase lags.

Polyvinylidene Flouride-PVDF-[53] film is used in this work as a transducer to help aid in the realization of directional wave filters. This material has been previously used in numerous other structural control applications because of it's high piezoelectric stress

coefficients, resulting in a large field being developed under a given stress. This material is also lightweight, very compliant-(E=2 GPa) and is easy to use.

1.4 Research Objectives

The objective of this research is to develop both analytically and experimentally wave-type estimators/sensors for determining rightward and leftward wave components which can propagate along along 1-dimensional structures. Concomitant with this objective is the identification of the local wave-model. This model is defined by the specific wavenumber-frequency relation which characterizes dispersive and non-despersive evolution of waves along a member. Using this information along with the estimated wave states, feedforward wave control designs can be implemented on simple 1-dimensional members and compared to their modal counterparts. The goal of this research is to verify the use of local wave control models for broadband control of global structural dynamics.

Methods for estimating of local wave components are derived from both a discrete and distributed approximation of the spatial domain. The discrete approach exploits phase lags to infer past and future information which affect the dynamics at a point location in the structure. Analysis of the discrete approach yields criteria on the minimal sensors required to estimate local wave dynamics. The distributed approach is a bit more elegant, exploiting properties of Hilbert spaces, Fourier Analysis and Complex Variable theory to derive spatial weighting functions which can directly yield propagating wave components which are free of the effects of aliasing or artificial dispersion. In addition, spatially distributed sensors are better equiped to handle known point disturbances.

Examples are presented for various 1-D structures to illustrate the advantages and disadvantages of each approach. Some of the potential contributions of this research are given below:

- Analog measurement of wave coordinates/amplitudes-(magnitude and direction).
- Experimental determination of scattering properties of boundaries.
- Realization of 90 degree spatial phase shifters and differentiators.
- Realization of collocated and non-collocated control designs on a resonant beam.
- The use of distributed sensors for broadband control.

CHAPTER 2

Models of Wave Propagation in 1-Dimensional Structural Elements

2.1 Introduction

Modelling of one-dimensional structures begins with the introduction of kinematic approximations which attempt to adequately predict member deflection to a certain order of accuracy for a given perturbed state away from its equilibrium configuration. The 1-D classification makes the assumption that these physical variables are a function of only 1 spatial variable-x along with a dependance on the temporal variable-t. The internal deformation characteristics of the structural element are accounted for using the laws of elasticity where constitutive relations relating material properties to force variables are approximated to first order. Combining these constitutive relations with the kinematic assumptions for perturbations away from the equilibrium state leads to idealized partial differential equations for structural elements such as rods and beams.

2.2 Travelling Wave Models

Travelling wave descriptions begin with the modelling of continuum 1-D structural elements in terms of partial differential equations. These equations can then be transformed into ordinary differential equations by transforming the temporal variable into the frequency domain-ω. Such an approach leads to a generic ordinary differential equation-(ode) representation with constant coefficients given by

$$\frac{\partial^m u}{\partial x^m} + a_1 \frac{\partial^{m-1} u}{\partial x^{m-1}} + a_2\, i\omega \frac{\partial^{m-1} u}{\partial x^{m-1}} + \ldots + u + b_1\, i\omega u - b_2\, \omega^2 u + \ldots + (i\omega)^m u = 0 \qquad (3.1)$$

where a suitable state-space description in terms of a system of 1st order ordinary differential equations is given by

$$\frac{d\,\vec{y}}{dx} = A(\omega)\,\vec{y} \qquad (2.2)$$

where $\vec{y}(x,\omega)$ represents a vector of member deflections and/or internal force variables. $A(\omega)$ is a frequency dependent matrix which charcterizes homogeneous member dynamics.

2.2.1 Wave-Mode Coordinates

Following the frequency domain formalism developed in references-[8,9,10] and [32], the dynamic behaviour of each structural element can be obtained by superposing independently propagating travelling wave-modes at every frequency. To expose this wave nature equation-(2.2) can be diagonalized to give the following decoupled description of the spatial evolution of normalized wave-mode variables, $\vec{w}(x,\omega)$

$$\frac{d\,\vec{w}}{dx} = \Gamma(\omega)\,\vec{w} \qquad (2.3)$$

where the entries of

$$\Gamma(\omega) = Y^{-1}(\omega) A(\omega) Y(\omega) = \begin{bmatrix} -k_1(\omega) & & & & & \\ & \ddots & & 0 & & \\ & & -k_p(\omega) & & & \\ & & & k_1(\omega) & & \\ & 0 & & & \ddots & \\ & & & & & k_p(\omega) \end{bmatrix}$$

are termed the propagation coefficients-(with $k_j(\omega)=k_{rj}(\omega)+ik_{ij}(\omega)$) of travelling wave-modes. The collection of these coefficients define the dispersion relations for a member which intimately connects the spatial and temporal domains. Depending on the 1-D structural element these coefficients can be very complex functions of the temporal

frequency variable ω. Structrual elements which have linear dispersion relations, i.e. k *vs.* ω, are termed non-dispersive while members with non-linear relations are termed dispersive. The difference between the two types of classifications lies in how fast information and energy flows at each frequency. The wave components $\vec{w}$ thus appear in rightward and leftward pairs with the eigenvalues of $A(\omega)$ being restricted to the first and third quadrant of the complex spatial transform plane which adheres to the conservation of energy principle for a conservative system.

The invertible matrix $Y(\omega)$ represents a frequency dependent set of complex eigenvectors which transform member deflections and internal forces into leftward and rightward travelling wave-modes which propagate along the structure

$$\vec{y}\,(x,\omega) = Y\,(\omega)\,\vec{w}\,(x,\omega) \qquad (2.4)$$

Each column of this matrix yields the relative magnitude and phase of the physical variables $\vec{y}(x,\omega)$ which are present in the correponding wave type.

2.2.2 Junction Dynamics

Travelling waves which propagate independently along each member can be scattered or generated at structural discontinuities or at locations where external excitations alter the homogeneous evolution of member dynamics. Locations at which the scattering or generation of travelling waves occur are referred to as junctions. A generic junction in Figure 2.1-(Adapted from Reference-[10]) shows how incoming waves along with external forces generate outgoing waves along attached members 1thru m. Associated with each member is a physical state vector $\vec{y}_m(x,\omega)$ defined at the interface of the member and the structural discontinuity. The junction boundary condition can then be described in terms of a composite state vector $\vec{y}_c=(\vec{y}_1{}^T, \ldots, \vec{y}_m{}^T)^T$, as ($B$ is a rectangular matrix with half as many rows as columns).

$$\begin{aligned} B\,(\omega)\,\vec{y}_c\,(x,\omega) &= \vec{Q}\,(\omega) \\ B\,(\omega)Y\,(\omega)\,\vec{w}_c\,(x,\omega) &= \vec{Q}\,(\omega) \end{aligned} \qquad (2.5)$$

where the member transformation matrices have been used to substitute $\vec{w}_c$ for $\vec{y}_c$. Partitioning this equation into incoming and outgoing dynamics leads to

$$\begin{bmatrix} B_o(\omega) & B_i(\omega) \end{bmatrix} \begin{bmatrix} \vec{w}_o \\ \vec{w}_i \end{bmatrix} = \vec{Q}\,(\omega) \qquad (2.6)$$

where the open loop description relating the generation of outgoing waves $\vec{w}_o(x,\omega)$ to the scattering of incoming waves $\vec{w}_i(x,\omega)$ and external excitation-$\vec{Q}(\omega)$, is given by

$$\vec{w}_o(x,\omega) = S(\omega)\,\vec{w}_i(x,\omega) + \Psi(\omega)\,\vec{Q}(\omega) \qquad (2.7)$$

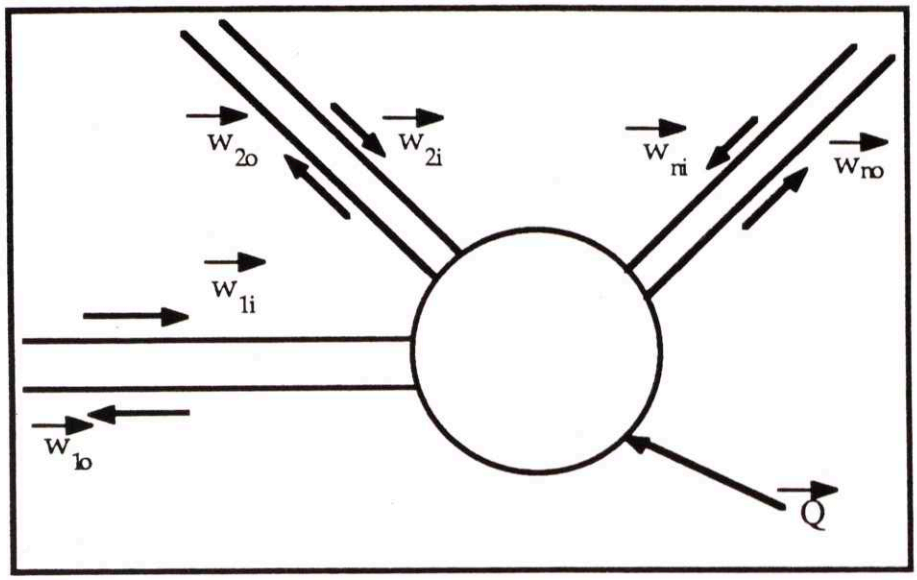

Figure 2.1: Wave Scattering at a Joint of a Truss Structure. Outgoing waves are generated by incoming waves and external excitations. (Adapted from Reference-[10])

2.2.3 Transmission Dynamics

Wave-modes at different locations in a structural member are related to wave-modes at any other location of the same member through a frequency dependent transition matrix. This matrix is diagonal and consists of transcendental functions whose arguments depend on the path length between the two points in which the wave-mode amplitudes are desired. A typical representation can be written as

$$\begin{aligned}\vec{w}(x_2,\omega) &= \xi(x_2,x_1,\omega)\,\vec{w}(x_1,\omega) \\ &= e^{\Gamma(\omega)(x_2-x_1)}\,\vec{w}(x_1,\omega)\end{aligned} \qquad (2.8)$$

where $\vec{w}(x_1,\omega)$ and $\vec{w}(x_2,\omega)$ correspond to wave mode vectors at locations x_1 and x_2 respectively.

2.2.4 Phase Closure

On finite structures waves generated by external point forces can circumnavigate the structure, interacting with structural discontinuities to close upon themselves in a constructive or destructive manner-[32]. This constructive behaviour characterizes the resonant dynamics of the member. Thus, the response at any location of a finite structure can be obtained by tracking the motion of individual leftward and rightward travelling wave components as they circulate a member and close upon themselves.

2.3 Examples of 1-D Structural Elements

2.3.1 Compression Rod

The simple one-dimensional wave equation which characterizes longitudinal vibrations along a rod is given by

$$EA\frac{\partial^2 u(x,t)}{\partial x^2} = \rho A\frac{\partial^2 u(x,t)}{\partial t^2} \qquad (2.9)$$

where $u(x,t)$ represents longitudinal deflection and EA and ρA are constants which determine the wave speed of structural disturbances. Transforming the temporal variable gives an o.d.e. which can be put into the following state-space form:

$$\frac{d\vec{y}}{dx} = \begin{bmatrix} 0 & 1 \\ \frac{\rho A}{EA}\omega^2 & 0 \end{bmatrix}\vec{y} \qquad (2.10)$$

where $\vec{y}=(u,u')^T$. The dispersion relation is given by

$$k = \pm\,\omega\sqrt{\frac{\rho A}{EA}} \qquad (2.11)$$

and is displayed in Figure 2.2 for an aluminum rod with $EA=1.06\ kN\text{-}m^2$ and $\rho A=0.27\ kg\text{-}m^{-1}$.

The diagonalization of equation (2.10) suggests that the reponse of a rod can be written in terms of two propagating wave-modes; one travelling to the left and one travelling to the right.

$$u(c,\omega) = w_{rp}(0,\omega)e^{-ikx} + w_{lp}(0,\omega)e^{ikx} \qquad (2.12)$$

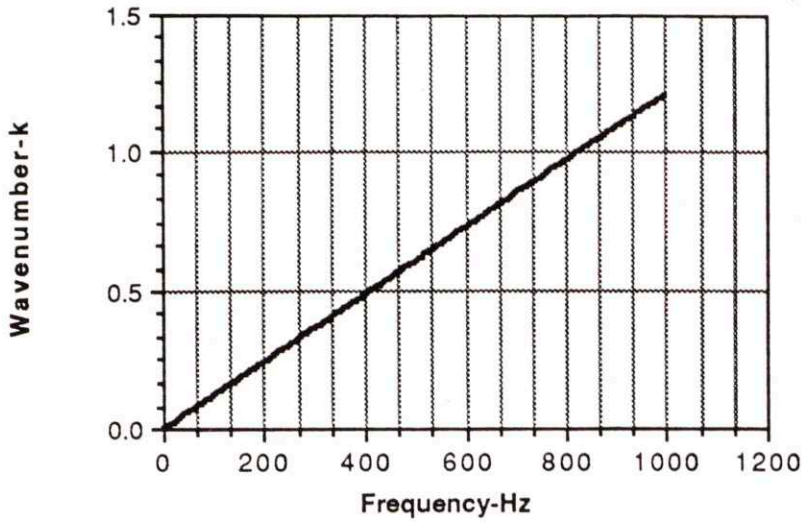

Figure 2.2: Dispersion Relation for an Aluminum Rod

2.3.2 Bernoulli-Euler Beam

In the 18th century the work of Daniel Bernoulli and Leonard Euler inspired the following partial differential equation which governs the transverse vibration of a beam.

$$EI\frac{\partial^4 u(x,t)}{\partial x^4} + \rho A\frac{\partial^2 u(x,t)}{\partial t^2} = 0 \qquad (2.13)$$

where u corresponds to transverse deflection and E, I, ρ and A characterize material and geometric propeties of the member. Transforming this equation into state space form leads to the equivalent first order system description given by

$$\frac{d\vec{y}}{dx} = \begin{bmatrix} 0 & 1 & 0 & 0 \\ 0 & 0 & \frac{1}{EI} & 0 \\ 0 & 0 & 0 & 1 \\ -\rho A\omega^2 & 0 & 0 & 0 \end{bmatrix} \vec{y} \qquad (2.14)$$

where the physical state vector $\vec{y} = (u, u', EIu'', -EIu''')^T$ has been chosen to include deflection, slope, curvature and internal shear force. Diagonalizing this equation and solving for the eigenvalues leads to the following disperion relation:

$$k = \pm\sqrt{\omega\sqrt{\frac{\rho A}{EI}}}, \quad \pm i\sqrt{\omega\sqrt{\frac{\rho A}{EI}}} \qquad (2.15)$$

The resulting dispersion curves are plotted in Figure 2.3 for specific values of beam bending stiffness $EI=1.0\ N\text{-}m^2$, mass density-$\rho A=1.0\ kg\text{-}m^{-1}$. Notice that in equation-*(2.15)* k is proportional to $\omega^{(1/2)}$ making the beam a dispersive system. In this case broadband information travels at different wave speeds causing a pulse of energy to spread as it propagates along the member.

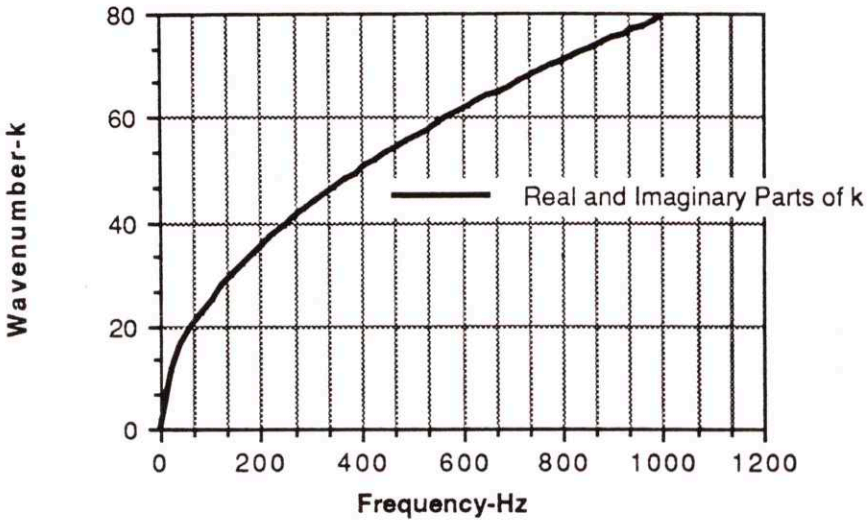

Figure 2.3: Dispersion Relation for a generic B-E Beam

The dispersion relation implies that four wave-modes are necessary to characterize the dynamics of a B-E beam; two far-field modes and two near-field modes. Thus, the response of the structure can be written as

$$u(x,\omega) = w_{rp}(0,\omega)e^{-ikx} + w_{re}(0,\omega)e^{-kx} + w_{lp}(0,\omega)e^{ikx} + w_{le}(0,\omega)e^{kx} \qquad (2.16)$$

where the vector of wave-mode amplitudes-$\vec{w}$ has units of position with subscripts defined as

rp: rightward propagating
lp: leftward propagating
re: rightward evanescent
le: leftward evancescent

2.3.3 Timoshenko Beam

A more accurate beam model which accounts for shear deformation and rotary inertia of a cross-section was developed by Timoshenko. This model consists of two coupled pde's given by

$$GA_s\left(\frac{\partial \psi}{\partial x}+\frac{\partial^2 u}{\partial x^2}\right)=\rho A\frac{\partial^2 u}{\partial t^2}$$
$$EI\frac{\partial^2 \psi}{\partial x^2}-GA_s\left(\psi+\frac{\partial u}{\partial x}\right)=\rho I\frac{\partial^2 \psi}{\partial t^2} \qquad (2.17)$$

where the kinematic variables ψ and u describe face deflection and rotation respectively. Transforming the temporal variable of equation-(2.17) and defining the physical state vector to be $\vec{y}=(-u,\psi,EI\psi',GA_s(u'+\psi))^T$ leads to the following system of first-order differential equations:

$$\frac{d\vec{y}}{dx}=\begin{bmatrix} 0 & 1 & 0 & \frac{-1}{GA_s} \\ 0 & 0 & \frac{1}{EI} & 0 \\ 0 & -\rho I\omega^2 & 0 & 0 \\ \rho A\omega^2 & 0 & 0 & 0 \end{bmatrix}\vec{y} \qquad (2.18)$$

where the constants GA_S and ρI correspond to the shear stiffness and rotary inertia of the member. Diagonalizing this expression leads to the following dispersion relation

$$k=\pm\left(\frac{1}{2}\left(\left(\sqrt{\frac{\rho A}{GA_s}}\right)^2+\left(\sqrt{\frac{\rho I}{\rho A}}\sqrt{\frac{\rho A}{EI}}\right)^2\right)\omega^2 \pm\sqrt{\left(\omega\sqrt{\frac{\rho A}{EI}}\right)^2+\frac{1}{4}\left(\left(\sqrt{\frac{\rho A}{GA_s}}\right)^2-\left(\sqrt{\frac{\rho I}{\rho A}}\sqrt{\frac{\rho A}{EI}}\right)^2\right)^2\omega^4}\right) \qquad (2.19)$$

Notice that in the high frequency limit-($\omega\Rightarrow\infty$) two propagating modes travel along the beam with the wavenumber k becoming proportional to

$$k_{1,2}\Rightarrow\omega\sqrt{\frac{\rho I}{\rho A}}\sqrt{\frac{\rho A}{EI}},\quad \omega\sqrt{\frac{\rho A}{GA_s}} \qquad (2.20)$$

Therefore, unlike the B-E beam model the Timoshenko model does not predict infinite wave speed at high frequency. In fact at high frequency the structure becomes non-dispersive with homogeneous solution given by two equations

$$u(x,\omega) = w_{rpb}(0,\omega)e^{-ik_1 x} + w_{rps}(0,\omega)e^{-ik_2 x} + w_{lpb}(0,\omega)e^{ik_1 x} + w_{lps}(0,\omega)e^{ik_2 x} \tag{2.21}$$

and

$$\psi(x,\omega) = \frac{ikGA_s}{GA_s k^2 - \rho A\omega^2} u(x,\omega) \tag{2.22}$$

2.4 Summary

The models presented in this chapter represent descriptions of wave dynamics along 1-D structural members commonly found in the areas of structural acoustics and LSS. These models, however, only account for the homogeneous dynamics of these members. Non-homogeneous behaviour can be included using the junction relations of equation (2.7). Thus, the purpose of this chapter was to introduce the notation used in this thesis and to point out the underlying differences between transverse and longitudinal disturbance propagation. Additional examples including both homogeneous and non-homegenous dynamics can be found in references-[10] and-[32].

CHAPTER 3

Wave Filtering Using Discrete Sensors

3.1.0 Introduction

This chapter presents model based approaches for local observation of wave components which propagate along one-dimensional structures. Two approaches are developed, which under appropriate approximations yield identical procedures. In each case, the solution of the partial differential equation which characterizes the dynamics of a one-dimensional structural component is written in terms of travelling waves. This form of the solution is then exploited in the first method to combine a sequence of spatially discrete measurements through a frequency dependent decoupling matrix to yield magnitude and direction of travelling wave components. In the second method a finite difference scheme is employed to estimate local deflections and internal forces at a cross-section in a member. A frequency domain transformation is then applied to this local state information to obtain the decoupled wave components. Several useful algebraic expressions are derived for waves on rods and beams. However, because both of these methods require local discretization of the spatial domain, perfect resolution of decoupled wave components will suffer from the effects of spatial aliasing. Measurements corrupted by noise are also

considered from the point of view of optimal resolution of travelling wave components using Wiener-Hopf filtering concepts. Here we derive an expression for the spacing which maximizes the signal-to-noise ratio. We also discuss issues associated with causal realization, transient performance, implementation and accuracy of the estimated wave-states.

3.2.0 Discretization Methods

Many techniques are available for discretizing the spatial domain of one-dimensional structures. Some of these include *Finite Element Methods-FEM, Galerkin Methods-GM, Raleigh Ritz Methods-RRM, Modal Analysis-MA* and *Finite Difference Methods-FDM.* Finite Difference formulations employ several nearby point measurements-[55-62] to estimate local spatial derivatives. This approach is thus well suited for observation of wave propagation dynamics at a point along a member. This chapter discusses the use of FDM to solve the full-state wave estimation problem at a point location in a member using a sequence of discrete measurements which can be either collocated or non-collocated.

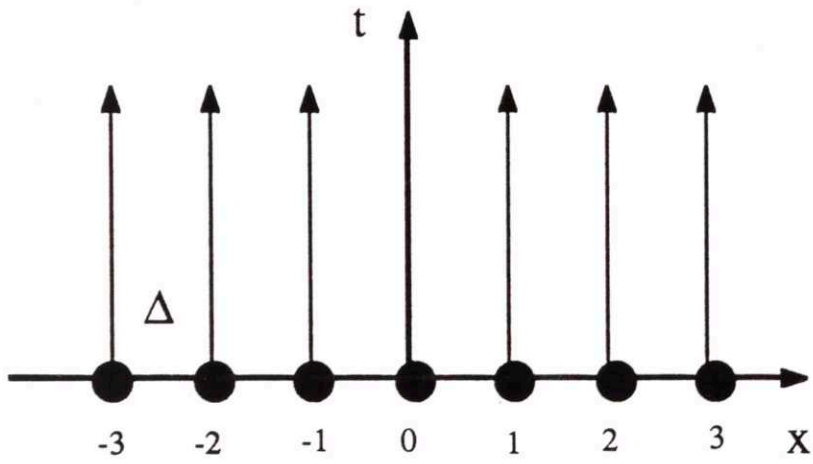

Figure 3.1 Spatial Grid

3.2.1 Discretizing the Spatial Domain-(See Figure 3.1)

Let $\Delta>0$ be a fixed space step with $x_j=j\Delta$ for integer j. The points (x_j,t) define a linear grid in the spatial domain such that $R\supset\Delta Z$ Therefore, the response at any x_j along a 1-dimensional structure can be approximated by the values at the grid points,

$$v_j \approx u(x_j, t) \tag{3.1}$$

where $u(x_j,t)$ corresponds to longitudinal or transverse displacement. Now lets define the spatial shift operator K as

$$Kv_j = v_{j+1} \tag{3.2}$$

and let I or 1 represent the identity operator s.t.

$$Iv_j = 1v_j = v_j \tag{3.3}$$

Utilizing this notation we can derive a host of common spatial difference operators which are frequently used in many numerical techniques. Table 3.1 lists some typical spatial difference operators.

Table 3.1: Typical 1st and 2nd order Spatial Difference Operators

$\mu_+ = \frac{1}{2}(I + K)$	$\mu_- = \frac{1}{2}(K^{-1} + I)$	$\mu_o = \frac{1}{2}(K^{-1} + K)$
$\delta_+ = \frac{1}{\Delta}(K - I)$	$\delta_- = \frac{1}{\Delta}(I - K^{-1})$	$\delta_o = \frac{1}{\Delta}(K - K^{-1})$
	$\delta_x = \frac{1}{\Delta^2}(K - 2I + K^{-1})$	

In this table the operators μ_+,μ_- and μ_o are termed the forward, backward and centered spatial averaging operators. Similarly, δ_+,δ_- and δ_o are the corresponding spatial difference operators of first order and δ_x is a centered spatial difference operator of 2nd order. The forward and backward operators find numerous applications in the field of numerical analysis of ordinary and partial differential equations with both time and space discretized. However, in this work the most useful operators for local wave sensing will involve the centered spatial averaging and difference operators.

The explicit dependency of these operators on separation distance suggest a more useful notation such as $\delta_+(\Delta)$, $\delta_-(\Delta)$, etc. For example

$$\delta_o(2\Delta)v_j = \frac{1}{4\Delta}(K^2 - K^{-2})v_j = \frac{1}{4\Delta}(v_{j+2} - v_{j-2}) \qquad (3.4)$$

where interpolated point responses are twice as far apart.

The uniqueness between many finite difference formulas is determined by four factors:

- the nature of the spaital grid-(uniform or nonuniform)
- the choice of interpolating function-(polynomial, trigonometric)
- the order of differentiation that is desired
- and the order of accuracy desired

Accuracy is a relative term defined with respect to the highest order Taylor series expansion in which the finite difference formula agrees with the actual spatial derivative $u'(x,t)$. Items 3 and 4 of this list determine the number of sensors required by the Finite Difference Formula. With these four factors in mind, we can compute the exact weights for any finite difference formula given a finite number of point sensors An efficient algorithm that performs this task was developed by Fornberg-[63] and is given in Table 3.2 for completeness. This algorithm computes the coefficients of both one-sided and centered difference formulas. For a regular grid simple formulas can be derived for a number of spatial derivatives-(See Table 3.3). From this table it is obvious that the minimum number of sensors required to approximate any spatial derivative must at least be equal to the order of the derivative+1. Thus, the first row of each spatial derivative approximation represents the fundamental stencil which achieves the minimum order of accuracy. Subsequent rows for the same derivative order can be derived from the fundamental spatial difference operator for each derivative order. Subsequent rows for the same derivative order can be derived from the fundamental spatial difference operator for each derivative order. To show this lets define the spatial derivative operator $D_{2p}{}^m$ to represent the spatial derivative of order m for $2p$ sensors such that $m<2p$. Now lets assume $p=1$ or 2 and suppose we are interested in an approximation to the first-$(m=1)$ derivative of the response at a discrete location in a member then according to the Fornberg algorithm

$$D_2^1 = \delta_O(\Delta) \qquad (3.5)$$

which corresponds to the fundamental-$(p=1)$ approximation to the first derivative. Similarly, a more accurate operator for 4-$(p=2)$ sensors is

$$D_4^1 = \frac{4}{3}\delta_O(\Delta) - \frac{1}{3}\delta_O(2\Delta) \qquad (3.6)$$

In the limit as the number of sensors $p \Rightarrow \infty$ the first order spatial derivative operator becomes

$$D_{\infty}^{1} = 2\,\delta_0(\Delta) - 2\,\delta_0(2\Delta) + 2\,\delta_0(3\Delta) - \ldots\ldots \qquad (3.7)$$

Table 3.2: Algorithm for Determining the Spatial Difference Coefficients

FDM on an Arbitrary Grid

Given $m_{max} > 0$ *and* $n_{max} \geq m_{max}$, $\frac{\partial^m u}{\partial x^m}$ *at* $x = 0$ *can be computed from*

$C_{00}^{0} = 1$: $\alpha = 1$

for $n = 1$ *to* n_{max}

$\beta = 1$

for $j = 0$ *to* $n - 1$

$\beta = \beta(x_n - x_j)$

if $n \leq m_{max}$ *then* $C_{n-1}^{n}, j = 0$

for $m = 0$ *to* $min(n, m_{max})$

$$C_{n,j}^{m} = \frac{\left(x_n C_{n-1,j}^{m} - m C_{n-1,j}^{m-1}\right)}{x_n - x_j}$$

for $m = 0$ *to* $min(n, m_{max})$

$$C_{n,m}^{m} = \frac{\left(\alpha C_{n-1,n-1}^{m-1} - m C_{n-1,n-1}^{m}\right)}{\beta}$$

$\alpha = \beta$

Table 3.3 Finite Difference Approximations-(Adapted From Ref [63])

	-4	-3	-2	-1	0	1	2	3	4
0					1				
1				$\frac{-1}{2}$	0	$\frac{1}{2}$			
			$\frac{1}{12}$	$\frac{-2}{3}$	0	$\frac{2}{3}$	$\frac{-1}{12}$		
		$\frac{-1}{60}$	$\frac{3}{20}$	$\frac{-3}{4}$	0	$\frac{3}{4}$	$\frac{-3}{20}$	$\frac{1}{60}$	
	$\frac{1}{280}$	$\frac{-4}{105}$	$\frac{1}{5}$	$\frac{-4}{5}$	0	$\frac{4}{5}$	$\frac{-1}{5}$	$\frac{4}{105}$	$\frac{-1}{280}$
2				1	-2	1			
			$\frac{-1}{12}$	$\frac{4}{3}$	$\frac{-5}{2}$	$\frac{4}{3}$	$\frac{-1}{12}$		
		$\frac{1}{90}$	$\frac{-3}{20}$	$\frac{3}{2}$	$\frac{-49}{2}$	$\frac{3}{2}$	$\frac{-3}{20}$	$\frac{1}{90}$	
	$\frac{-1}{560}$	$\frac{8}{315}$	$\frac{-1}{5}$	$\frac{8}{5}$	$\frac{-205}{72}$	$\frac{8}{5}$	$\frac{-1}{5}$	$\frac{8}{315}$	$\frac{-1}{560}$
3			$\frac{-1}{2}$	1	0	-1	$\frac{1}{2}$		
		$\frac{1}{8}$	-1	$\frac{13}{8}$	0	$\frac{-13}{8}$	1	$\frac{-1}{8}$	
	$\frac{-7}{240}$	$\frac{3}{10}$	$\frac{-169}{120}$	$\frac{61}{30}$	0	$\frac{-61}{30}$	$\frac{169}{120}$	$\frac{-3}{10}$	$\frac{7}{240}$

3.2.2 Difference Operators Imply Convolution

One useful way to interpret these infinite and finite spatial operators is to think of them as discrete interpolation kernels which convolve spatially discrete measurements to obtain properties locally at points along a structural member. Thus, the operator in equation-(3.5) acting on a finite set of discrete measurements-u can be represented as

$$v(x_k) = D_2^1 u = \frac{1}{\Delta^2}(\ldots\ldots 0\ 0\ 0\ \frac{1}{2}\ 0\ \frac{-1}{2}\ 0\ 0\ 0\ldots\ldots) * u$$

$$= \Delta \sum_{-\infty}^{\infty} \phi(x_k - x_j) u(x_j, t) \qquad (3.8)$$

where

$$\phi(x_j) = \begin{cases} \dfrac{-1}{2\Delta^2}, & x_1 = \Delta \\ \dfrac{1}{2\Delta^2}, & x_1 = -\Delta \\ 0, & otherwise \end{cases} \qquad (3.9)$$

Similarly, for the infinite domain operator D_∞, the convolution becomes

$$v(x_k, \omega) = \Delta \sum_{j=-\infty}^{\infty} \phi(x_k - x_j) u(x_j, \omega)$$

$$= \Delta \sum_{j=-\infty}^{\infty} \left(\frac{\sin\left(\frac{\pi}{\Delta}(x_k - x_j)\right)}{(x_k - x_j)} \right)' u(x_j, \omega) \qquad (3.10)$$

where the interpolation function $\phi(x)$ corresponds to the derivative of the sinc function with frequency properties given by

$$\Phi(k) = ik; \qquad k \in [-\frac{\pi}{\Delta}, \frac{\pi}{\Delta}] \qquad (3.11)$$

where k is the spatial frequency variable or wavenumber.

3.3.0 Wave-Mode Observation

Many sophisticated analytical procedures for control design are based on the assumption that the full-state vector is available for measurement. Wave control is no exception; it would exploit full knowledge of a "local state." In addition wave-control methods add more complexity since most wave control designs yield compensators which are dynamic functions of the local state and are often difficult to realize-[32]. As in most control design methods performance is limited when the full state of the dynamic system is not available. We are thus faced with the common dilemma of approximating state information from a few measurements. In the work to follow we present two passive procedures for estimating wave-modes along one-dimensional structures from a limited number of measurements. We label these wave-mode estimates $\hat{w}$ to explicitly differentiate them from the unknown, actual wave-modes, w.

3.3.1 Spatially Collocated Measurements

The most direct approach to sensing waves propagating along one-dimensional members is to infer this information from full-knowledge of the dynamic state of the system at a cross-section. This is done by inverting the wave-mode transformation matrix-(equation *3.4*) relating physical cross-sectional measurements to wave-mode coordinates.

$$\begin{bmatrix} \hat{w}_r(x, \omega) \\ \hat{w}_l(x, \omega) \end{bmatrix} = Y^{-1}(\omega) \vec{y}(x, \omega) \qquad (3.12)$$

where subscripts r and l denote the rightward and leftward wave components respectively. Difficulties with such an approach are specific to the case at hand. It may be physically

impractical to measure all of $\vec{y}(x,\omega)$ at a single point, (e.g. measurement of the internal shear force in a beam is difficult). Further, the frequency dependence of this matrix is such that temporal filters cannot always be built to implement equation (*3.12*); as the theoretical matrix $Y^{-1}(\omega)$ may be non-causal.

Example L1-(Longitudinal Waves in a Rod)

In the case of a longitudinal rod the dynamics are described according to the partial differential equation

$$EA\frac{\partial^2 u(x,t)}{\partial x^2} = \rho A\frac{\partial^2 u(x,t)}{\partial t^2} \qquad (3.13)$$

which has steady-state harmonic solutions of the form

$$u(x,t) = (w_r(0)e^{-ikx} + w_l(0)e^{ikx})e^{i\omega t} \qquad (3.14a)$$

and the corresponding broadband solution of the form

$$u(x,\omega) = (w_r(0,\omega)e^{-ikx} + w_l(0,\omega)e^{ikx}) \qquad (3.14b)$$

where the subscripts r and l refer to rightward and leftward travelling components respectively. The wavenumber k is given by

$$k = \omega\sqrt{\frac{\rho A}{EA}}$$

Transforming equation (*3.13*) into the frequency domain and obtaining a state-space representation of the dynamics in the form of equation (*2.3*) leads to the following relation between wave-mode coordinates and physical states at a cross-section

$$\begin{bmatrix}\hat{w}_r(x,\omega)\\ \hat{w}_l(x,\omega)\end{bmatrix} = \begin{bmatrix}\frac{1}{2} & \frac{1}{2i\omega}\sqrt{\frac{EA}{\rho A}}\\ \frac{1}{2} & -\frac{1}{2i\omega}\sqrt{\frac{EA}{\rho A}}\end{bmatrix}\begin{bmatrix}u(x,\omega)\\ u'(x,\omega)\end{bmatrix} \qquad (3.15)$$

where steady-state behavior is not implied.

Estimates for the local right and left-going wave modes are thus available from a linear combination of local deflection, u, and strain, u'. Temporally, only an integration of strain is required. This appears to be a viable technique for observing wave components along a rod.

Example B1-(Bending waves in a B-E Beam)

The governing partial differential equation describing the dynamics of a Bernoulli-Euler beam is given by

$$EI\frac{\partial^4 u(x,t)}{\partial x^4} + \rho A\frac{\partial^2 u(x,t)}{\partial t^2} = 0 \qquad (3.16)$$

where the Fourier transformed solution in terms of waves can be represented as

$$u(x,\omega) = w_{rp}(0,\omega)e^{-ikx} + w_{re}(0,\omega)e^{-kx} + w_{lp}(0,\omega)e^{ikx} + w_{le}(0,\omega)e^{kx} \qquad (3.17)$$

where the subscripts p,e refer to whether a wave component is a propagating or an evanescent term, and r and l refer to whether it is rightward or leftward going. Inverting the transformation relation between wave-modes and physical member measurements at x we find that

$$\begin{bmatrix} \hat{w}_{rp}(x,\omega) \\ \hat{w}_{re}(x,\omega) \\ \hat{w}_{lp}(x,\omega) \\ \hat{w}_{le}(x,\omega) \end{bmatrix} = \begin{bmatrix} \frac{1}{4} & \frac{i}{4k} & \frac{i}{4EIk^3} & -\frac{1}{4EIk^2} \\ \frac{1}{4} & \frac{1}{4k} & -\frac{1}{4EIk^3} & \frac{1}{4EIk^2} \\ \frac{1}{4} & -\frac{i}{4k} & -\frac{i}{4EIk^3} & -\frac{1}{4EIk^2} \\ \frac{1}{4} & -\frac{1}{4k} & \frac{1}{4EIk^3} & \frac{1}{4EIk^2} \end{bmatrix} \begin{bmatrix} u(x,\omega) \\ u'(x,\omega) \\ -EIu'''(x,\omega) \\ EIu''(x,\omega) \end{bmatrix} \qquad (3.18)$$

In this expression the wavenumber k for transverse bending motion is given by

$$k = \omega^{\frac{1}{2}}\sqrt[4]{\frac{\rho A}{EI}}$$

Thus equation (*3.18*), if implemented as written, would require measurement of lateral deflection, u, slope, u', bending moment $M = EIu''$ and shear force, $V = -EIu'''$. Measurements of internal shear force V, with a point sensor, may not be practical. These would be combined using temporal filters with gain characteristics of 1, $\omega^{(-1/2)}$, ω^{1}, $\omega^{(-3/2)}$, and with various constant phases. Not all are implementable in real time since they are acausal.

However, if we are only interested in observing the propagating components travelling along the beam from 4 collocated state sensors then rows one and three of the matrix in equation (*3.18*) give

$$\begin{bmatrix} \hat{w}_{rp} \\ \hat{w}_{lp} \end{bmatrix} = \begin{bmatrix} \frac{1}{4} & \frac{e^{-i\frac{\pi}{4}}}{4\sqrt{i\omega}\sqrt[4]{\frac{EI}{\rho A}}} & \frac{e^{i\frac{\pi}{4}}}{4\,(i\omega)^{\frac{3}{2}}\sqrt[4]{EI\,(\rho A)^3}} & \frac{e^{-i\frac{\pi}{2}}}{4\,i\omega\sqrt{EI\rho A}} \\ \frac{1}{4} & \frac{-e^{-i\frac{\pi}{4}}}{4\sqrt{i\omega}\sqrt[4]{\frac{EI}{\rho A}}} & \frac{-e^{i\frac{\pi}{4}}}{4\,(i\omega)^{\frac{3}{2}}\sqrt[4]{EI\,(\rho A)^3}} & \frac{e^{-i\frac{\pi}{2}}}{4\,i\omega\sqrt{EI\rho A}} \end{bmatrix} \begin{bmatrix} u \\ u' \\ -EIu''' \\ EIu'' \end{bmatrix} \tag{3.19}$$

where we have substituted for k and rearranged to illustrate elements having positive and negative phase delays. Notice that elements of the second and third column are non-causal; requiring prior knowledge of the internal shear at a point in the beam. This complicates direct observation of w_{rp} and w_{lp} from 4 collocated state sensors. Several wavelengths removed from structural discontinuities near field terms contribute negligibly to the response $u(x,\omega)$ given in equation (*3.17*). Thus, at high frequencies we can interpret the response of the beam in terms of propagating components only. Such an assumption reduces the number of sensors required for observation to two. Nevertheless, there is not one combination of physical cross-sectional-$\vec{y}(x,\omega)$ measurements which leads to causal filtering of propagating compononents.

These two examples have highlighted two difficulties with the simple concept of employing the transformation of $\vec{y}(x,\omega)$ between physical measurements at a point and the wave components at that point. The first is simply the difficulty of measuring all the necessary variables at the cross-section in question. The second difficulty is the impossibility of achieving the needed (acausal) temporal filtering in real time. This requirement for acausal filtering appears to be related to dispersive wave propagation.

3.3.2 Spatially Sequential Non-collocated Measurements

In this section we relax a requirement implicitly imposed in the previous section; that all measurements be spatially collocated. Rather we suggest a spatial stencil of point sensors, (implicitly assumed to be strain gages) and discuss possible signal processing approaches to extract wave components from this sensor array. Such techniques are widespread in ocean acoustics and geophysics, where the domain is three-dimensional and the wave propagating is essentially non-dispersive. Real-time implementation is not an issue in these fields, since active control is not contemplated. Acausal signal processing is thus not ruled out in these fields.

3.3.2.1 Exploiting Phase Delays

One approach might involve a sequence of similar measurements at multiple locations along a member(See Figure 3.2). This implies that waves propagating without attenuation along the member will only have relative phase leads or lag between spatially discrete points and that a signal processing scheme might exploit this known phase relation to identify the wave component of interest. This problem has been extensively studied in the case of sound propagation in ducts-[11-14]. However, only recently has this approach been considered for elastic waveguides-[16,45,46].

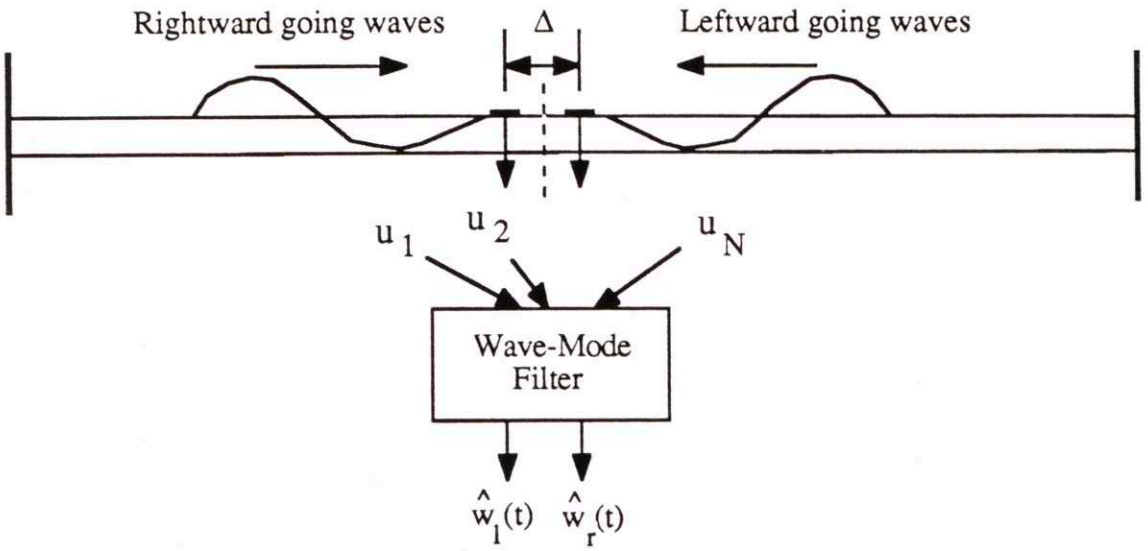

Figure 3.2: Spatially Sequential Measurement Method for Observation of Travelling Wave Components along a 1-dimensional member.

Example L2-(Longitudinal Waves in a Rod)

Consider again the longitudinal rod with successive axial strain measurements given by

$$u'\left(-\frac{\Delta}{2},\omega\right) = ik\left(-w_r(0,\omega)e^{ik\frac{\Delta}{2}} + w_l(0,\omega)e^{-ik\frac{\Delta}{2}}\right) \qquad (3.21)$$

and

$$u'\left(\frac{\Delta}{2},\omega\right) = ik\left(-w_r(0,\omega)e^{-ik\frac{\Delta}{2}} + w_l(0,\omega)e^{ik\frac{\Delta}{2}}\right) \qquad (3.22)$$

where Δ is the separation between the two strain gages and $x=0$ is taken to identify a point midway between them. Solving for the rightward and leftward wave-modes leads to an expression (for this non-dispersive example involving both positive and negative delays)

$$\begin{bmatrix} w_{ndr}(0,\omega) \\ w_{ndl}(0,\omega) \end{bmatrix} = F(\Delta,\omega) \begin{bmatrix} u'(-\frac{\Delta}{2},\omega) \\ u'(\frac{\Delta}{2},\omega) \end{bmatrix}$$

$$= \frac{1}{ik_{nd}(e^{-ik\Delta} - e^{ik\Delta})} \begin{bmatrix} e^{ik\frac{\Delta}{2}} & -e^{-ik\frac{\Delta}{2}} \\ e^{-ik\frac{\Delta}{2}} & -e^{ik\frac{\Delta}{2}} \end{bmatrix} \begin{bmatrix} u'(-\frac{\Delta}{2},\omega) \\ u'(\frac{\Delta}{2},\omega) \end{bmatrix} \qquad (3.23)$$

where $F(\Delta,\omega)$ is referred to as the observation matrix. This is similar to the approach outlined by Swinbanks-[11].

To avoid spatial aliasing, $k\Delta<p$, the sensor spacing is less than a half wavelength. Thus, if one can assume $k\Delta<<1$(the sensor spacing is much less than a wavelength) some straightforward algebraic manipulation leads to the following form of equation-(*3.23*)-(low order in $k\Delta$)

$$\begin{bmatrix} \hat{w}_{ndr}(0,\omega) \\ \hat{w}_{ndl}(0,\omega) \end{bmatrix} \cong \begin{bmatrix} \frac{1}{2k^2\Delta^2} - \frac{1}{4ik\Delta} & -\frac{1}{2k^2\Delta} - \frac{1}{4ik\Delta} \\ \frac{1}{2k^2\Delta^2} + \frac{1}{4ik\Delta} & -\frac{1}{2k^2\Delta} + \frac{1}{4ik\Delta} \end{bmatrix} \begin{bmatrix} u'(-\frac{\Delta}{2},\omega) \\ u'(\frac{\Delta}{2},\omega) \end{bmatrix} \qquad (3.24)$$

Evaluation of this expression requires up to two causal temporal integrations of each local strain measurement. Figure 3.3 compares the non-dimensional matrix elements corresponding to the exact solution-(*3.23*) with those of the linearized approximation-(*3.24*). Here we define the non-dimensional amplitude and frequency to be

$$\hat{w}_{nd} = \frac{\hat{w}}{\Delta} \quad \text{and} \quad k_{nd} = k\Delta = \frac{\omega\Delta}{\sqrt{\frac{EA}{\rho A}}} \qquad (3.25)$$

Notice that in this figure there is close agreement between the linear and non-linear elements up to $k\Delta=1$. However, as $k\Delta>>1$, the error between the linear and nonlinear elements becomes significant. In this region the phenomenon of spatial aliasing appears in the form of resonance behavior in the magnitude and phase of the nonlinear elements. These resonances arise because spatially discrete measurements are incapable of resolving all possible wavelengths propagating along the member. Therefore, whenever

$$k\Delta > \pi \text{ or } \omega > (\pi/\Delta)(EA/\rho A)^{(1/2)}$$

there will be ambiguity in determining the true wavelength of a disturbance propagating along a rod.

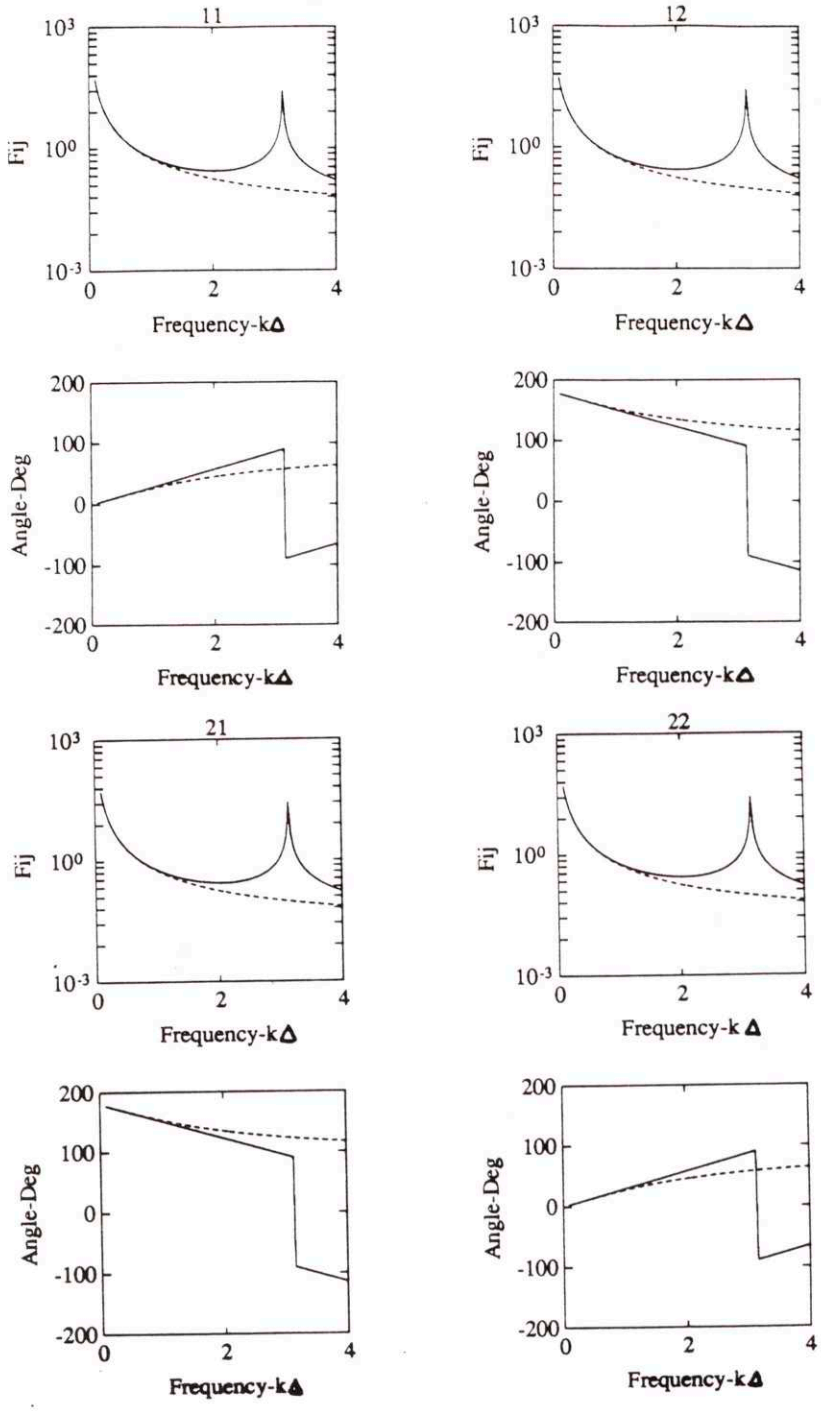

Figure 3.3: Elements-(solid) of the observation matrix $F(\Delta,\omega)$-(equation 3.23) which yields propagating wave components traversing a longitudinal rod from local strain measurements. The low-order approximation-(equation 3.24) of these elements-(dashed) are also shown.

Example B2-(Bending Waves in a B-E beam)

As in the case of the longitudinal rod, we can infer information about wave-modes from sequential strain measurements at spatially discrete locations along a simple Bernoulli-Euler beam member. Applying the same approach we can write local expressions for bending strains in terms of wave-mode amplitudes as

$$\varepsilon_b(x,\omega) = -\frac{t_b}{2}k^2\,(-w_{rp}(0,\omega)e^{-ikx} + w_{re}(0,\omega)e^{-kx} - w_{lp}(0,\omega)e^{ikx} + w_{le}(0,\omega)e^{kx}) \tag{3.26}$$

where ε_b refers to bending strain on the surface of a member of rectangular cross-section, t_b denotes the thickness of the beam, and x takes on four values. If the strain gage stencil is equally spaced about $x=0$, these values are $(\pm\Delta/2)$, $(\pm 3\Delta/2)$, where Δ is the gage spacing.

Solving for the frequency dependent wave-mode amplitudes at $x=0$ we arrive at the following matrix expression

$$\hat{w}(0,\omega)_{4x1} = F(\Delta,\omega)_{4x4}\,\varepsilon_b(\Delta,\omega)_{4x1} \tag{3.27}$$

where each element in $F(\Delta,\omega)$ represents the contribution to the evolution of a particular wave-mode from a discrete non-collocated measurement. The elements of this matrix contain frequency dependent exponential and transcendental terms.

$$F_{11}(\Delta,\omega) = (-e^{0.5ik\Delta-2k\Delta} + e^{-0.5ik\Delta-k\Delta} + e^{1.5ik\Delta-k\Delta} - e^{-0.5ik\Delta+k\Delta} - e^{1.5ik\Delta+k\Delta} + e^{0.5ik\Delta+2k\Delta})/D_1(\Delta,\omega) \tag{a}$$

$$F_{12}(\Delta,\omega) = (e^{0.5ik\Delta-3k\Delta} - e^{1.5ik\Delta-2k\Delta} - e^{-1.5ik\Delta-k\Delta} + e^{-1.5ik\Delta+k\Delta} + e^{1.5ik\Delta+2k\Delta} - e^{0.5ik\Delta+3k\Delta})/D_1(\Delta,\omega) \tag{b}$$

$$F_{13}(\Delta,\omega) = (-e^{-0.5ik\Delta-3k\Delta} + e^{-1.5ik\Delta-2k\Delta} + e^{1.5ik\Delta-k\Delta} - e^{1.5ik\Delta+k\Delta} - e^{-1.5ik\Delta+2k\Delta} + e^{-0.5ik\Delta+3k\Delta})/D_1(\Delta,\omega) \tag{c}$$

$$F_{14}(\Delta,\omega) = (e^{-0.5ik\Delta-2k\Delta} - e^{-1.5ik\Delta-k\Delta} - e^{0.5ik\Delta-k\Delta} + e^{-1.5ik\Delta+k\Delta} + e^{0.5ik\Delta+k\Delta} - e^{-0.5ik\Delta+2k\Delta})/D_1(\Delta,\omega) \tag{d}$$

$$F_{21}(\Delta,\omega) = (e^{-ik\Delta-0.5k\Delta} - e^{-ik\Delta-0.5k\Delta} - e^{-2ik\Delta+0.5k\Delta} + e^{2ik\Delta+0.5k\Delta} + e^{-ik\Delta+k\Delta} - e^{ik\Delta+1.5k\Delta})/D_1(\Delta,\omega) \tag{e}$$

$$F_{22}(\Delta,\omega) = (-e^{-ik\Delta-1.5k\Delta} + e^{ik\Delta-1.5k\Delta} + e^{-3ik\Delta+0.5k\Delta} - e^{3ik\Delta+0.5k\Delta} - e^{-2ik\Delta+1.5k\Delta} + e^{2ik\Delta+1.5k\Delta})/D_1(\Delta,\omega) \quad (f)$$

$$F_{23}(\Delta,\omega) = (e^{-2ik\Delta-1.5k\Delta} - e^{2ik\Delta-1.5k\Delta} - e^{-3ik\Delta-0.5k\Delta} + e^{3ik\Delta-0.5k\Delta} + e^{-ik\Delta+1.5k\Delta} - e^{ik\Delta+1.5k\Delta})/D_1(\Delta,\omega) \quad (g)$$

$$F_{24}(\Delta,\omega) = (-e^{-ik\Delta-1.5k\Delta} + e^{ik\Delta-1.5k\Delta} + e^{-2ik\Delta-0.5k\Delta} - e^{2ik\Delta-0.5k\Delta} - e^{-ik\Delta+0.5k\Delta} + e^{ik\Delta+0.5k\Delta})/D_1(\Delta,\omega) \quad (h)$$

$$F_{31}(\Delta,\omega) = (e^{-0.5ik\Delta-2k\Delta} - e^{-1.5ik\Delta-k\Delta} - e^{0.5ik\Delta-k\Delta} + e^{-1.5ik\Delta+k\Delta} + e^{0.5ik\Delta+k\Delta} - e^{-0.5ik\Delta+2k\Delta})/D_1(\Delta,\omega) \quad (i)$$

$$F_{32}(\Delta,\omega) = (-e^{-0.5ik\Delta-3k\Delta} + e^{-1.5ik\Delta-2k\Delta} + e^{1.5ik\Delta-k\Delta} - e^{1.5ik\Delta+k\Delta} - e^{-1.5ik\Delta+2k\Delta} + e^{-0.5ik\Delta+3k\Delta})/D_1(\Delta,\omega) \quad (j)$$

$$F_{33}(\Delta,\omega) = (e^{0.5ik\Delta-3k\Delta} - e^{1.5ik\Delta-2k\Delta} - e^{-1.5ik\Delta-k\Delta} + e^{-1.5ik\Delta+k\Delta} + e^{1.5ik\Delta+2k\Delta} - e^{0.5ik\Delta+3k\Delta})/D_1(\Delta,\omega) \quad (k)$$

$$F_{34}(\Delta,\omega) = (-e^{0.5ik\Delta-2k\Delta} + e^{-0.5ik\Delta-k\Delta} + e^{1.5ik\Delta-k\Delta} - e^{-0.5ik\Delta+k\Delta} - e^{1.5ik\Delta+k\Delta} + e^{0.5ik\Delta+2k\Delta})/D_1(\Delta,\omega) \quad (l)$$

$$F_{41}(\Delta,\omega) = (-e^{-ik\Delta-1.5k\Delta} + e^{ik\Delta-1.5k\Delta} + e^{-2ik\Delta-0.5k\Delta} - e^{2ik\Delta-0.5k\Delta} - e^{-ik\Delta+0.5k\Delta} + e^{ik\Delta+0.5k\Delta})/D_1(\Delta,\omega) \quad (m)$$

$$F_{42}(\Delta,\omega) = (e^{-2ik\Delta-1.5k\Delta} - e^{2ik\Delta-1.5k\Delta} - e^{-3ik\Delta-0.5k\Delta} + e^{3ik\Delta-0.5k\Delta} + e^{-ik\Delta+1.5k\Delta} - e^{ik\Delta+1.5k\Delta})/D_1(\Delta,\omega) \quad (n)$$

$$F_{43}(\Delta,\omega) = (-e^{-ik\Delta-1.5k\Delta} + e^{ik\Delta-1.5k\Delta} + e^{-3ik\Delta+0.5k\Delta} - e^{3ik\Delta+0.5k\Delta} - e^{-2ik\Delta+1.5k\Delta} + e^{2ik\Delta+1.5k\Delta})/D_1(\Delta,\omega) \quad (o)$$

$$F_{44}(\Delta,\omega) = (e^{-ik\Delta-0.5k\Delta} - e^{ik\Delta-0.5k\Delta} - e^{-2ik\Delta+0.5k\Delta} + e^{2ik\Delta+0.5k\Delta} + e^{-ik\Delta+1.5k\Delta} - e^{ik\Delta+1.5k\Delta})/D_1(\Delta,\omega) \quad (p)$$

where the denominator $D_1(\Delta,\omega)$ is given by

$$D_1(\Delta,\omega) = \frac{-t_b}{2}k^2\,(-e^{-ik\Delta-3\,k\Delta} + e^{ik\Delta-3\,k\Delta} + 2e^{-2\,ik\Delta-2\,k\Delta} - 2e^{2\,ik\Delta-2\,k\Delta}$$
$$- e^{-3\,ik\Delta-k\Delta} - 2e^{-ik\Delta-k\Delta} + 2e^{ik\Delta-k\Delta} + e^{3\,ik\Delta-k\Delta} + e^{-3\,ik\Delta+k\Delta}$$
$$+ 2e^{-ik\Delta+k\Delta} - 2e^{ik\Delta+k\Delta} - e^{3\,ik\Delta+k\Delta} - 2e^{-2\,ik\Delta+2\,k\Delta}$$
$$+ 2e^{2\,ik\Delta+2\,k\Delta} + e^{-ik\Delta+3\,k\Delta} - e^{ik\Delta+3\,k\Delta}) \qquad (q)$$

The magnitude and phase of the elements of this matrix are plotted versus non-dimensional frequency-(k_{nd}) in Figure 3.4 where

$$\hat{w}_{nd} = \frac{\hat{w}\,t_b}{\Delta^2} \qquad \text{and} \qquad \omega_{nd} = \frac{\omega}{\Delta}^{\frac{1}{2}}\sqrt[4]{\frac{EI}{\rho A}} \qquad (3.28)$$

Unfortunately, attempts at linearizing the elements of $F(\Delta,\omega)$(for $k\Delta<<1$) causes the matrix to become singular. This singularity occurs because we cannot infer four wave-modes from a strain field which is approximated as locally linear in space. Only two sensors are actually needed to determine this strain field approximation. Hence, the linearized version of matrix $F(\Delta,\omega)$ is no longer of full rank, and we would be forced to higher order-(in $k\Delta$) approximations.

Several wavelengths removed from structural discontinuities and boundary effects, near field components contribute negligibly to the response of the beam. As a result we can interpret the response of the beam at high frequencies in terms of travelling components only. With this assumption the rightward and leftward travelling wave-mode can be found from an expression which only accounts for the contributions of travelling components-(and is analogous to equation *3.23*);

$$\begin{bmatrix}\hat{w}_{ndrp}(0,\omega)\\ \hat{w}_{ndlp}(0,\omega)\end{bmatrix} \approx \frac{2}{(k\Delta)^2\,(e^{ik\Delta}-e^{-ik\Delta})}\begin{bmatrix} e^{ik\frac{\Delta}{2}} & -e^{-ik\frac{\Delta}{2}} \\ -e^{-ik\frac{\Delta}{2}} & e^{ik\frac{\Delta}{2}}\end{bmatrix}\begin{bmatrix}\varepsilon_b(-\frac{\Delta}{2},\omega)\\ \varepsilon_b(\frac{\Delta}{2},\omega)\end{bmatrix} \qquad (3.29)$$

If we neglect the non-causal $(k\Delta)^2$ term in the denominator of equation (*3.29*) the elements of the observation matrix become functions of transcendental expressions. Because these terms violate Bode's Gain/Phase Theorem-[64] analog realizations are not possible. Digital realizations, however, are possible using *Finite Impulse Reponse Filters*.. Scheuren-[45,46] has demonstrated that good agreement exists between the FIR approximation and the ideal observation matrix elements for $k\Delta$ near *1*. However, for $k\Delta<<1$ the approximation suffers. This is largely due to the fact that unlike the rod, the beam has a non-linear dispersion relation $k\propto\omega^{1/2}$. Thus, an infinitely long filter is required to resolve all frequency components in the spectrum.

These limits are further exposed by approximating the elements of this matrix for small separation distance-($k\Delta<<1$). Such a linearized approximation transforms the transcendental terms in equation-(*3.29*) into the non-causal matrix expression given by

$$\begin{bmatrix} \hat{w}_{ndrp}(0,\omega) \\ \hat{w}_{ndlp}(0,\omega) \end{bmatrix} \approx \begin{bmatrix} -\frac{1}{i(k\Delta)^3} - \frac{1}{2(k\Delta)^2} & \frac{1}{i(k\Delta)^3} - \frac{1}{2(k\Delta)^2} \\ \frac{1}{i(k\Delta)^3} - \frac{1}{2(k\Delta)^2} & -\frac{1}{i(k\Delta)^3} - \frac{1}{2(k\Delta)^2} \end{bmatrix} \begin{bmatrix} \varepsilon_b(-\frac{\Delta}{2},\omega) \\ \varepsilon_b(\frac{\Delta}{2},\omega) \end{bmatrix}$$

(3.30)

The matrix elements of equations (*3.29*) and (*3.30*) are plotted in Figure 3.5. As in the case of the rod this figure shows that there is close agreement between the transcendental matrix elements and their linearized approximations in both phase and magnitude over a broad frequency range. Spatial aliasing is again apparent in the form of resonance behavior in the observation matrix elements whenever

$$k_{nd} = k\Delta > \pi, (n=1,2,3,...) \quad or \quad \omega > (\pi)^2\Delta^2(\rho A/EI)^{(1/2)}$$

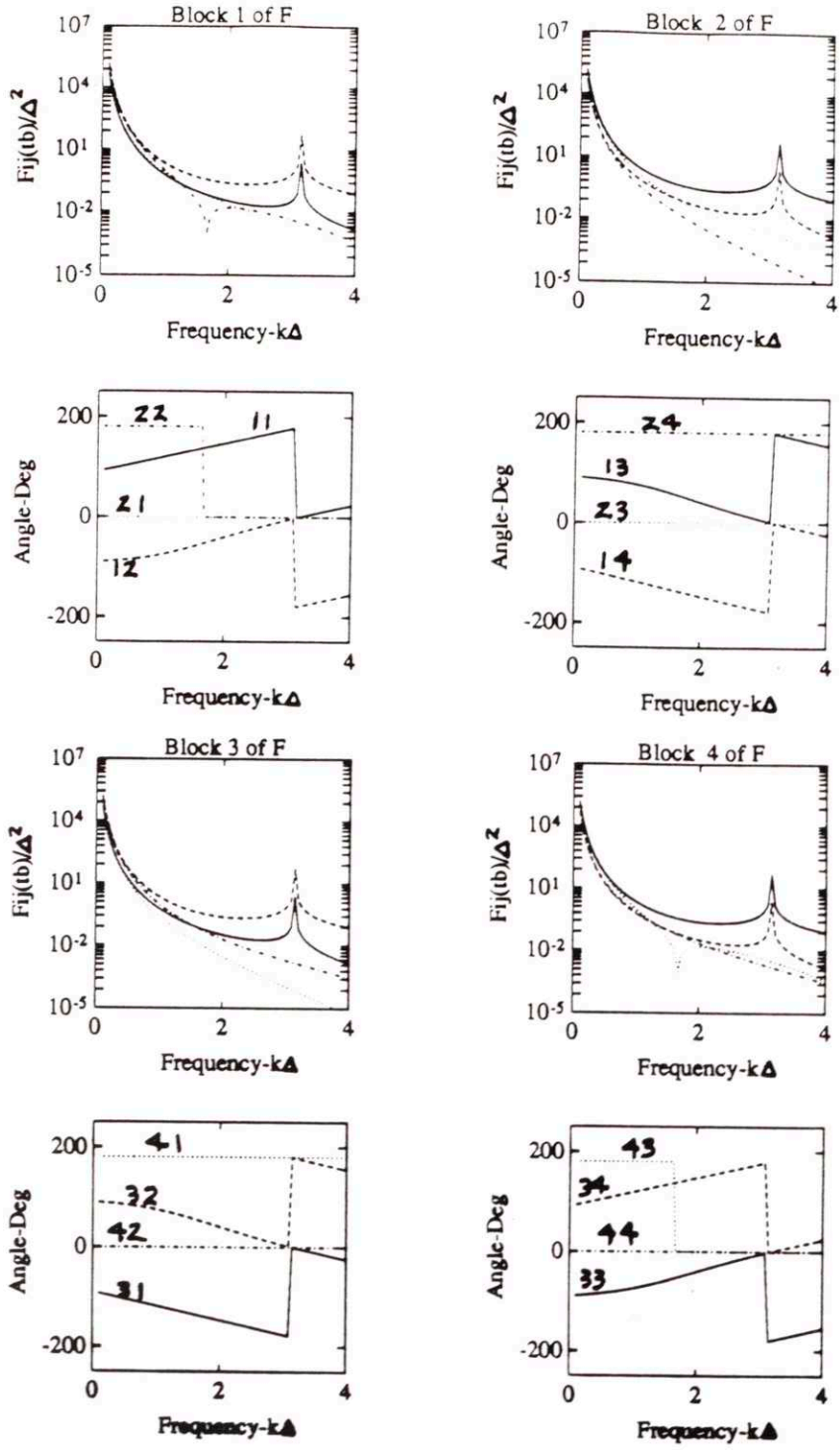

Figure 3.4 **Elements of the observation matrix $F_{4x4}(\Delta,\omega)$-(equation 3.27) which yields travelling wave components traversing a B-E beam from local strain measurements.**

$$\vec{W} = \begin{bmatrix} F_1 & F_2 \\ F_3 & F_4 \end{bmatrix}_{4\times4} \vec{\varepsilon}$$

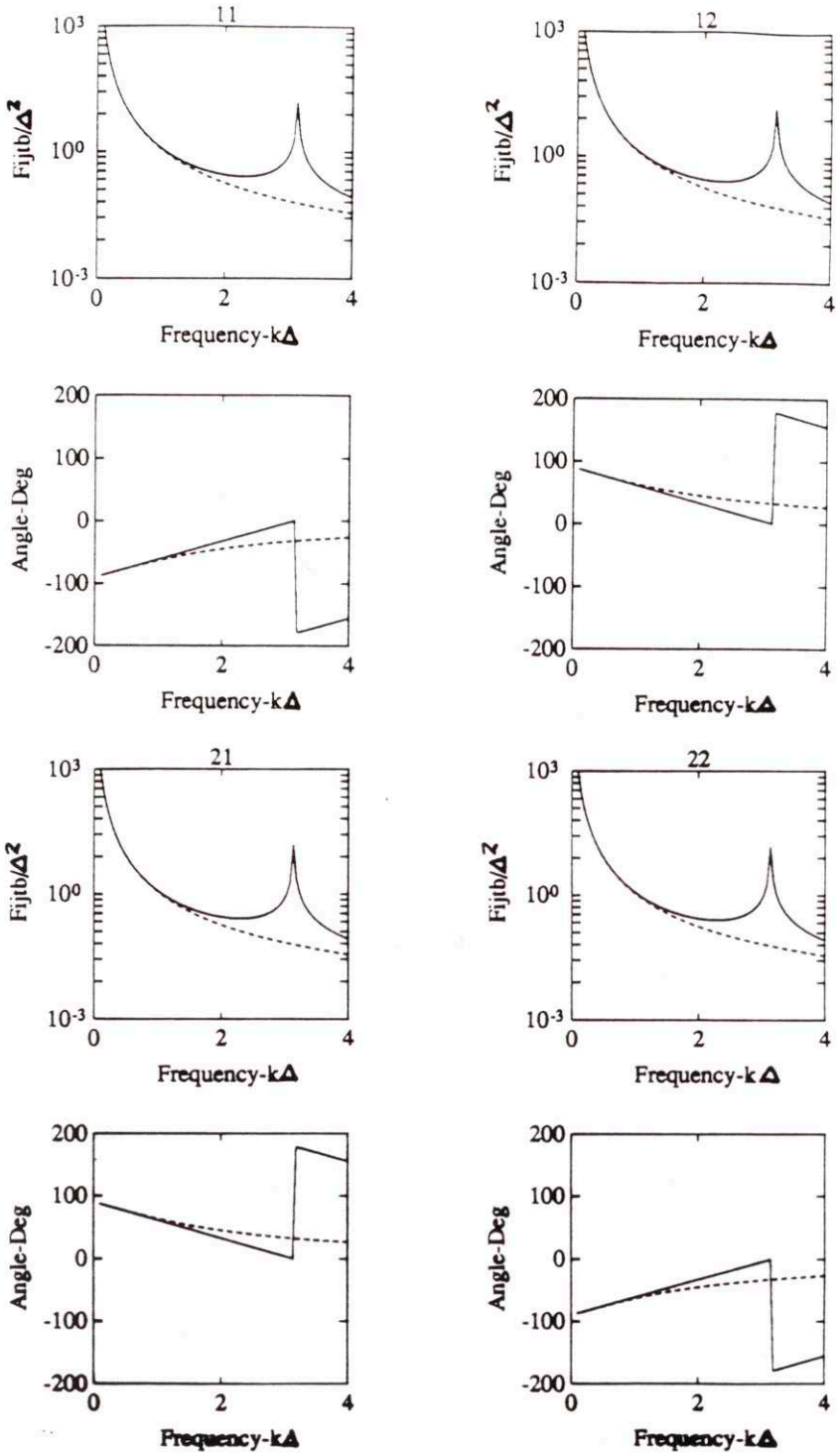

Figure 3.5: Elements-(solid) of the observation matrix $F(\Delta,\omega)$-(equation 3.29) which yields propagating wave components traversing a B-E beam from local strain measurements. The low-order approximation-(equation 3.30) of these elements-(dashed) are also shown.

3.3.2.2 Finite Difference Approximation of Spatial Derivatives

Strain gauges are the most convenient types of sensors used to infer an element of the physical state vector at spatially discrete points along one-dimensional members. The reason for this is that they are lightweight, thin and inexpensive. More importantly the impedance contribution to the overall impedance of the structure is negligible. This implies that this type of measuring instrument has very little effect on the propagation and scattering properties of waves as they traverse individual members in a network.

Swinbanks-[11] and Pavic'-[58,60] also demonstrate that strain sensors can be used to estimate spatial derivatives at locations along a member which are far removed from structural discontinuities. At such locations Pavic' employs a finite difference scheme which he uses to approximate the first and second derivatives of strain for both beams and plates. He uses this information to determine local inertial acceleration, effectively using the local (beam or plate) mass as the accelerometer proof mass. This same approach can be used as an effective way of determining the direction and amplitude of longitudinal and transverse travelling waves.

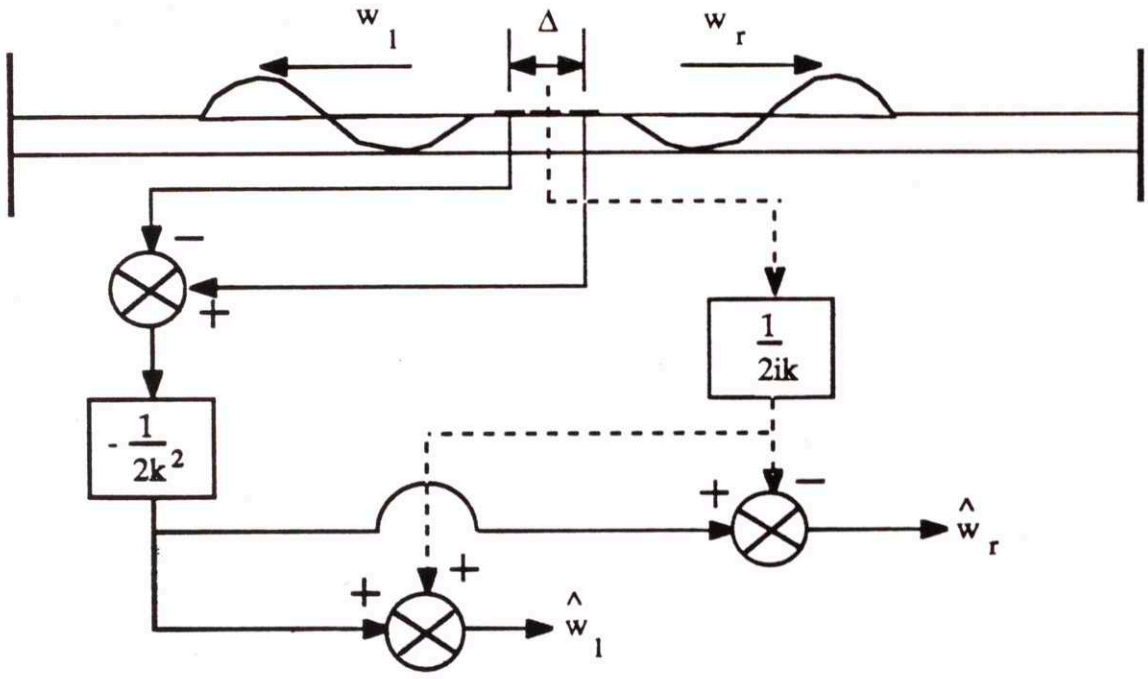

Figure 3.6: Illustration of the Spatial Derivative Approximaton for estimating deflections and internal forces to complete the physical state vector at a cross-section. Example of local estimation along a longitudinal rod.

Example L3-(Longitudinal Waves in a Rod)

Equation (*3.13*), presented earlier, describes the dynamics of a rod in compression or tension without distributed loading. The longitudinal strain at any location in the member is given by

$$\varepsilon_L(x_j,\omega) = \frac{\partial u(x_j,\omega)}{\partial x} \tag{3.31}$$

Using this relation in conjunction with the central difference method the second spatial derivative can be approximated as follows

$$\varepsilon'_L(x_j,\omega) \approx \frac{\varepsilon_L(x_j+\frac{\Delta}{2},\omega) - \varepsilon_L(x_j-\frac{\Delta}{2},\omega)}{\Delta} \tag{3.32}$$

where Δ is separation between the two strain sensors and the error is on the order of the square of the separation distance (See Figure 3.6). Following the sign convention shown in this figure the direction and amplitude of wave-modes given in equation (*3.15*) can be approximated by the following relation

$$\begin{bmatrix} \hat{w}_{rdr}(0,\omega) \\ \hat{w}_{rdl}(0,\omega) \end{bmatrix} \equiv \begin{bmatrix} \frac{1}{2ik\Delta} & -\frac{1}{2k^2\Delta} \\ -\frac{1}{2ik\Delta} & -\frac{1}{2k^2\Delta} \end{bmatrix} \begin{bmatrix} \varepsilon_L(0,\omega) \\ \varepsilon'_L(0,\omega) \end{bmatrix} \tag{3.33}$$

where $x_j = 0$. This expression is equivalent to the sequential measurement scheme in the approximation $k\Delta << 1$ (equation *3.24*). The two methods are related by the following finite difference transformation

$$\begin{bmatrix} \varepsilon_L(0,\omega) \\ \varepsilon'_L(0,\omega) \end{bmatrix} \equiv \begin{bmatrix} \frac{1}{2} & \frac{1}{2} \\ -\frac{1}{\Delta} & \frac{1}{\Delta} \end{bmatrix} \begin{bmatrix} \varepsilon_L(-\frac{\Delta}{2},\omega) \\ \varepsilon_L(\frac{\Delta}{2},\omega) \end{bmatrix} \tag{3.34}$$

The equivalence is not surprising since both methods are based upon the approximation that the strain field is locally linear in space.

Example B3-(Bending waves in a B-E beam)

Because the second spatial derivative of displacement is related to the curvature of the member, the bending strain corresponding to transverse propagating waves is given by

$$\varepsilon_b(x_j,\omega) = -\frac{t_b}{2}\frac{\partial^2 u(x_j,\omega)}{\partial x^2} \tag{3.35}$$

Again applying the central difference scheme the third spatial derivative can be approximated as

$$\varepsilon'_b(x_j,\omega) \equiv \left\{\frac{\varepsilon_b(x_j+\frac{\Delta}{2},\omega) - \varepsilon_b(x_j-\frac{\Delta}{2},\omega)}{\Delta}\right\} \equiv -\frac{2}{t_b}\frac{\partial^3 u(x_j,\omega)}{\partial x^3} \tag{3.36}$$

The second derivative of strain yields the fourth derivative of displacement which by equation (*3.16*) is related to the actual beam deflection. Applying the central difference method for the second derivative of bending strain, and exploiting equation (*3.16*) leads to the following expression for the transverse beam deflection

$$u(0,\omega) \equiv \frac{2}{t_b}\frac{EI}{\rho A}\frac{1}{s^2}\left\{\frac{\varepsilon_b(\frac{\Delta}{2},\omega) + \varepsilon_b(-\frac{\Delta}{2},\omega) - 2\,\varepsilon_b(0,\omega)}{\Delta^2}\right\} \tag{3.37}$$

where $x_j=0$ and s is the Laplace variable.

The only element of the physical cross-sectional state vector yet to be accounted for is the local slope. Since the slope represents the rate of change of deflection with respect to position along the member, the deflection at two neighboring points must be found using equation (*3.37*) before the slope can be estimated. Applying this method the local slope can be approximated as

$$u'(0,\omega) \equiv \frac{u(\frac{\Delta}{2},\omega) - u(-\frac{\Delta}{2},\omega)}{\Delta}$$

$$= \frac{2}{t_b}\frac{EI}{\rho A}\frac{1}{s^2}\left\{\frac{\varepsilon_b(\frac{3}{2}\Delta,\omega) - \varepsilon_b(-\frac{3}{2}\Delta,\omega) - 3\,\varepsilon_b(\frac{\Delta}{2},\omega) + 3\,\varepsilon_b(-\frac{\Delta}{2},\omega)}{\Delta^3}\right\} \tag{3.38}$$

The error in this expression is on the order of Δ, the separation between strain sensors.

Equation (*3.38*) completes the estimation of elements of the physical state vector at a particular location from only 4 local strain sensors. Combining equations (*3.35-38*) with equation (*3.12*) we can approximate the evolution of rightward and leftward going wave-modes along a beam member in terms of local strain measurement.

$$\begin{bmatrix} \hat{w}_{rp}(0,\omega) \\ \hat{w}_{re}(0,\omega) \\ \hat{w}_{lp}(0,\omega) \\ \hat{w}_{le}(0,\omega) \end{bmatrix} = \frac{2}{t_b} \begin{bmatrix} \frac{1}{4} & \frac{i}{4k} & \frac{i}{4EIk^3} & \frac{-1}{4EIk^2} \\ \frac{1}{4} & \frac{-1}{4k} & \frac{1}{4EIk^3} & \frac{1}{4EIk^2} \\ \frac{1}{4} & \frac{-i}{4k} & \frac{-i}{4EIk^3} & \frac{-1}{4EIk^2} \\ \frac{1}{4} & \frac{1}{4k} & \frac{-1}{4EIk^3} & \frac{1}{4EIk^2} \end{bmatrix} \begin{bmatrix} \frac{P}{\Delta^2} & \frac{-P}{\Delta^2} & \frac{-P}{\Delta^2} & \frac{P}{\Delta^2} \\ \frac{-P}{\Delta^3} & \frac{3P}{\Delta^3} & \frac{-3P}{\Delta^3} & \frac{P}{\Delta^3} \\ 0 & \frac{EI}{\Delta} & \frac{-EI}{\Delta} & 0 \\ 0 & \frac{-EI}{2} & \frac{-EI}{2} & 0 \end{bmatrix} \begin{bmatrix} \varepsilon_b(-\frac{3}{2}\Delta,\omega) \\ \varepsilon_b(-\frac{\Delta}{2},\omega) \\ \varepsilon_b(\frac{\Delta}{2},\omega) \\ \varepsilon_b(\frac{3}{2}\Delta,\omega) \end{bmatrix}$$

$$P = \frac{EI}{\rho A s^2}$$

(3.39)

As in the sequential sensor scheme, contributions due to the evanescent terms can be considered negligible when measurements are taken far away from structural discontinuities. This implies that the rightward and leftward propagating components can be found from extracting the 1st and 3rd rows of the matrix given in equation (*3.38*). It was pointed out earlier, however, that this expression is not realizable in real-time because the terms in the third column of the matrix in equation (*3.39*) are non-causal. However, since the evanescent terms have been considered negligible it is possible to exploit the remaining causal terms in equation (*3.39*) to derive an expression which uses only knowledge of local bending strain ε_b and slope-u' to estimate the propagating wave components w_{rp} and w_{lp}. Such an approximation would lead to the following equation for the propagating wave components for a beam

$$\begin{bmatrix} \hat{w}_{rp}(0,\omega) \\ \hat{w}_{lp}(0,\omega) \end{bmatrix} = \frac{2}{t_b} \begin{bmatrix} \frac{i}{2k} & \frac{-1}{2EIk^2} \\ \frac{-i}{2k} & \frac{-1}{2EIk^2} \end{bmatrix} \begin{bmatrix} \frac{-P}{\Delta^3} & \frac{3P}{\Delta^3} & \frac{-3P}{\Delta^3} & \frac{P}{\Delta^3} \\ 0 & \frac{-EI}{2} & \frac{-EI}{2} & 0 \end{bmatrix} \begin{bmatrix} \varepsilon_b(-\frac{3}{2}\Delta,\omega) \\ \varepsilon_b(-\frac{\Delta}{2},\omega) \\ \varepsilon_b(\frac{\Delta}{2},\omega) \\ \varepsilon_b(\frac{3}{2}\Delta,\omega) \end{bmatrix}$$

(3.40)

Again the acausality of the first matrix makes observation only possible for narrowband signals. Since the local deflection and slope represent a causal pair of physical measurements they can also be used to estimate propagating wave components far away from structural discontinuities. However, such a selection would introduce additional resolution errors associated with inaccuracies in estimating local deflection from four point strain measurements. Other non-realizable pairs include (deflection & strain) and those

physical measurements which are combined with an estimate of the internal shear force at a cross-section.

3.3.3 Optimal Sensor Spacing in the Presence of Noise

Up until this point we have omitted any restrictions imposed by the possibility of noisy strain measurements. Although the signal processing described in the preceeding sections invariably become simple for small gage spacing-($k\Delta<<1$), we will not be able to choose the separation distance Δ arbitrarily small since the difference between strain signals will become very small, potentially smaller than the noise level in the measurement. Further restrictions will be imposed by the occurrence of spatial aliasing, limiting the smallest resolvable wavelength that can be accurately detected by this measurement scheme. The optimal spacing between successive strain sensors will be based on our ability to achieve the maximum rms signal to noise level for each wave component for a given noise spectrum and stencil configuration.

Assuming that the sensors are corrupted with stationary, uncorrelated white noise, the wave sensor observation integral determines the estimated wave components from the following equation.

$$\hat{\vec{w}}(t) = \int_0^t \vec{f}(\Delta, t-\tau)\left(\vec{\varepsilon}(\tau) + \vec{n}(\tau)\right) \tag{3.41}$$

where $f(\Delta,t-\tau)$ is the convolution kernel associated with the observation matrix-$F(\Delta,\omega)$, $\vec{n}(\tau)$ is the noise vector and $\vec{\varepsilon}(\tau)$ is vector of discrete measurements. This convolution expression permits the covariance matrix-$\phi_{ww}(\tau)$ for the estimated wave components to be computed from

$$\begin{aligned}\phi_{ww}(\tau) &= E\left(\hat{\vec{w}}(t)\,\hat{\vec{w}}^T(t+\tau)\right) \\ &= \int_{-\infty}^{\infty} d\tau_1 \int_{-\infty}^{\infty} d\tau_2 f(\Delta,\tau_1) E\left(\left(\vec{\varepsilon}(t-\tau_1) + \vec{n}(t-\tau_1)\right)\right. \\ &\quad \left.\cdot\left(\vec{\varepsilon}(t+\tau-\tau_2) + \vec{n}(t+\tau-\tau_2)\right)^T\right) f(\Delta,\tau_2)^T\end{aligned} \tag{3.42}$$

where $\phi_{\varepsilon\varepsilon}(\tau)$ and $\phi_{nn}(\tau)$ are the covariance matrices for the deterministic and stochastic part of the measurement. The power spectral density matrix is found by taking the Fourier transform of the covariance matrix $\phi_{ww}(\tau)$. This leads to

$$\Phi_{ww}(\omega) = F(\Delta, s)\left(\begin{bmatrix} \Phi_{\varepsilon_1\varepsilon_1}(\omega) & \cdots & \Phi_{\varepsilon_1\varepsilon_n}(\omega) \\ \vdots & & \vdots \\ \Phi_{\varepsilon_n\varepsilon_1}(\omega) & \cdots & \Phi_{\varepsilon_n\varepsilon_n}(\omega) \end{bmatrix} + \begin{bmatrix} \Phi_{n_1n_1}(\omega) & & \\ & \ddots & 0 \\ & 0 & \Phi_{n_1n_1}(\omega) \end{bmatrix}\right) F(\Delta, -s)^T \tag{3.43}$$

Because wave propagation couples the spatially non-colocated strain measurements, there will be off-diagonal elements appearing in the $\Phi_{ww}(\omega)$ matrix. These cross-spectra terms are essential for determining the optimal sensor spacing along a member. However, if no correlation exists between the spatially non-collocated sensors then relative phase information between each sensor is lost and it is impossible to infer the magnitude and directionality of each wave component.

Example L4-(Longitudinal Waves in a Rod)

The power spectral density matrix for wave propagation along a longitudinal rod is given by

$$\Phi_{ww}(\omega) = \begin{bmatrix} F_{11}(\Delta, s) & F_{12}(\Delta, s) \\ F_{21}(\Delta, s) & F_{22}(\Delta, s) \end{bmatrix} \Phi_{\varepsilon\varepsilon}(\omega) + \Phi_{nn}(\omega) \begin{bmatrix} F_{11}(\Delta, -s) & F_{21}(\Delta, -s) \\ F_{12}(\Delta, -s) & F_{22}(\Delta, -s) \end{bmatrix} \tag{3.44}$$

where $\Phi_{\varepsilon 2\varepsilon 1}(\omega)=(\Phi_{\varepsilon 1\varepsilon 2}(\omega)^*)$-(*-denotes complex conjugate). The estimated rms response of the rightward and leftward wave components are available from the diagonal elements of this matrix.

$$\left(\Phi_{w_r w_r}(\omega)\right)_{rms} = \left(\Phi_{w_l w_l}(\omega)\right)_{rms}$$

$$= \sqrt{\frac{\Phi_{\varepsilon_1\varepsilon_1} + \Phi_{\varepsilon_2\varepsilon_2} + \Phi_{nn} - 2\cos(k\Delta)Re(\Phi_{\varepsilon_1\varepsilon_2}) - 2\sin(k\Delta)Im(\Phi_{\varepsilon_1\varepsilon_2})}{4k^2\sin^2(k\Delta)}} \tag{3.45}$$

where Re and Im denote the real and imaginary parts of the cross-spectra term $\Phi_{\varepsilon 1\varepsilon 2}(\omega)$ respectively.

The points where this expression has an extremum can be found by computing its derivative with respect to Δ and equating the result to zero. Hence, the necessary condition for the existence of a maximum is

$$\cos^2(k\Delta) - \frac{\Phi_{\varepsilon_1\varepsilon_1} + \Phi_{\varepsilon_2\varepsilon_2} + \Phi_{nn}}{Re(\Phi_{\varepsilon_1\varepsilon_2})}\cos(k\Delta) + \frac{Im(\Phi_{\varepsilon_1\varepsilon_2})}{Re(\Phi_{\varepsilon_1\varepsilon_2})}\sin(k\Delta)\cos(k\Delta) - 1 = 0 \tag{3.46}$$

This equation can be further manipulated to give the following 4th order equation

$$\left((Re(\Phi_{\varepsilon_1\varepsilon_2}))^2 + (Im(\Phi_{\varepsilon_1\varepsilon_2}))^2\right)\cos^4(k\Delta) - 2D\,Re((\Phi_{\varepsilon_1\varepsilon_2}))\cos^3(k\Delta)$$
$$+\left(D^2 - 2(Re(\Phi_{\varepsilon_1\varepsilon_2}))^2 - (Im(\Phi_{\varepsilon_1\varepsilon_2}))^2\right)\cos^2(k\Delta) +$$
$$2\,Re(\Phi_{\varepsilon_1\varepsilon_2})D\cos(k\Delta) + (Re(\Phi_{\varepsilon_1\varepsilon_2}))^2 = 0 \tag{3.47}$$

where

$$D = 2\,Re(\Phi_{\varepsilon_1\varepsilon_2}) - (\Phi_{\varepsilon_1\varepsilon_1} + \Phi_{\varepsilon_2\varepsilon_2} + \Phi_{nn})$$

Finding the exact solution of equation (*3.47*) is cumbersome. Therefore, to gain insight into the optimal sensor spacing we might make some limiting approximations. One such approximation is to assume that $k\Delta << 1$. This assumption leads to the following approximate optimal sensor spacing.

$$(k\Delta)_{opt} = \frac{\Phi_{\varepsilon_1\varepsilon_1} + \Phi_{\varepsilon_1\varepsilon_1} + \Phi_{nn} - 2\,Re(\Phi_{\varepsilon_1\varepsilon_2})}{Im(\Phi_{\varepsilon_1\varepsilon_2})} \tag{3.48}$$

This expression only applies to a narrowband signal. For broadband signals tradeoffs have to be made to select a stencil spacing that performs well in one frequency region as opposed to another. To increase performance in the frequency range of interest multiple sensor stencils can be used. .

3.3.4 The Wave Sensor Transfer Function

Because of the assumed form of the solution which is used to infer wave propagation along 1-dimensional structures, an inherent difficulty associated with the decoupling of rightward and leftward wave components is the realizability of elements of the observation matrix $F(\Delta,\omega)$. Since the elements of this matrix are typically infinite dimensional we must approximate them by first order elements-(linear in $k\Delta$) which are physically realizable. Unfortunately, this linearization limits our ability to achieve perfect decoupling of rightward and leftward wave components from discrete measurements. However, if the condition $k\Delta << 1$ is satisfied we expect that rightward and leftward components will be sufficiently decoupled from one another.

The required transfer function from actual wave-modes present to wave-mode estimates delivered by the sensor is given by

$$\hat{\vec{w}} = \Lambda(\Delta, \omega)\,\vec{w} + F(\Delta, \omega)\,\vec{n} \tag{3.49}$$

where $\Lambda(\Delta,\omega)$ is the wave sensor transfer function, $\vec{n}$ is the vector of uncorrelated noises, $\vec{w}$ is the vector of actual wave-modes and $\hat{\vec{w}}$ represents the vector of wave sensor estimates. In all of these approaches the wave-modes which are present in a member are inferred from physical variables $y(x,\omega)$ using a frequency dependent transformation of the form:

$$\vec{y} = \left[F^{-1}(\Delta, \omega) \text{ or } Y(\omega)\right]\vec{w} \tag{3.50}$$

Each approach works by attempting to invert $F^{-1}(\omega)$ or realize $Y^{-1}(\omega)$. This is done approximately for a variety of reasons:

1. Unable to measure all elements of the cross-sectional state vector $\vec{y}(x,\omega)$.
2. Not always possible to implement $F(\omega)$ with causal filters.
3. Prefer a low order approximation to $F(\omega)$ rather than an infinite-order solution.
4. The model is not accurate over all frequencies.

Further the physical measurements $\vec{y}(x,\omega)$ are corrupted with noise. This leads to two kinds of imperfections in the approaches outlined in this paper; $\hat{F}$ is not F and $\hat{\vec{y}}$ is not $\vec{y}$. The wave sensor output for $\vec{w}$ is thus $\hat{\vec{w}}$.

$$\begin{aligned}\hat{\vec{w}} &= \hat{F}(\Delta, \omega)\,\hat{\vec{y}} \\ &= \hat{F}(\Delta, \omega)(\vec{y} + noise)\end{aligned} \tag{3.51}$$

But $\vec{y} = F^{-1}(\Delta,\omega)\vec{w}$ This implies that

$$\hat{\vec{w}} = \hat{F}(\Delta, \omega)F^{-1}(\Delta, \omega)\,\vec{w} + \hat{F}(\Delta, \omega)(noise) \tag{3.52}$$

Example L6-(Longitudinal Waves in a Rod)

Considering examples L2 and L5 again we know from the exact model given in equations (*4.23*) and (*4.24*) that

$$\begin{bmatrix} u'\left(\frac{-\Delta}{2},\omega\right) \\ u'\left(\frac{\Delta}{2},\omega\right) \end{bmatrix} = F^{-1}w = ik\begin{bmatrix} -e^{ik\frac{\Delta}{2}} & e^{-ik\frac{\Delta}{2}} \\ -e^{-ik\frac{\Delta}{2}} & e^{ik\frac{\Delta}{2}} \end{bmatrix}\begin{bmatrix} w_r(0,\omega) \\ w_l(0,\omega) \end{bmatrix} \tag{3.53}$$

Substituting equations (*3.24*) and (*3.53*) into equation (*3.52*) gives the wave sensor transfer function to first order for a rod.

$$\begin{bmatrix} \hat{w}_r \\ \hat{w}_l \end{bmatrix} = \begin{bmatrix} 1 & \frac{k^2\Delta^2}{16} \\ \frac{k^2\Delta^2}{16} & 1 \end{bmatrix}\begin{bmatrix} w_r \\ w_l \end{bmatrix} + \begin{bmatrix} \frac{1}{2k^2\Delta} - \frac{1}{4ik} & -\frac{1}{2k^2\Delta} - \frac{1}{4ik} \\ \frac{1}{2k^2\Delta} + \frac{1}{4ik} & -\frac{1}{2k^2\Delta} + \frac{1}{4ik} \end{bmatrix}\begin{bmatrix} n_1 \\ n_2 \end{bmatrix} \tag{3.54}$$

The first order approximation to $F(\Delta,\omega)$ leads to off-diagonal terms of second order which couple actual rightward and leftward wave components to their estimates. However, for low frequencies-($k\Delta<<1$) these off-diagonal contributions can be considered to be negligible. The estimated wave components are thus decoupled except for the presence of measurement noise in the sensors.

3.3.5 Transient Behavior of the Spatially Sequential Approach

The preceding sections of this paper have developed all ideas in the frequency domain. Although general transients are not excluded from this frequency domain discussion, it is often difficult to make the transition to time response. This section presents a particular transient response of a particular wave sensing scheme. The example is motivated by a desire to enhance intuitive understanding of the wave decoupling procedure.

Example L5-(Longitudinal Waves in a Rod)

This section calculates the transient response of a first order-(linear in $k\Delta$) wave-mode filter using two strain sensors spaced a distance Δ apart. We excite the sensor with a sinusoidal wave train arriving from the left at $t=0$. If we assume that the rod is semi-infinite and that only a rightward travelling longitudinal wave is present in the member than we would hope that our approach would indicate the presence of only a rightward going wave. Before we attempt to examine how well the first order approximation achieves decoupling of wave components along a rod, it is convenient to express equation (*3.24*) in state-space form;

$$\dot{x} = A x + B\varepsilon$$
$$w = \begin{bmatrix} C_{11} \\ C_{21} \end{bmatrix} x + \begin{bmatrix} C_{12} \\ C_{22} \end{bmatrix} x + D\varepsilon \qquad (3.55)$$

where the linear time invariant matrices are

$$A = \begin{bmatrix} 0 & 1 \\ 0 & 0 \end{bmatrix}; \quad B = \begin{bmatrix} 0 \\ 1 \end{bmatrix}; \quad C_{11} = \begin{bmatrix} \frac{c^2}{2\Delta} & \frac{c}{4} \end{bmatrix}; \quad C_{12} = \begin{bmatrix} -\frac{c^2}{2\Delta} & \frac{c}{4} \end{bmatrix};$$
$$C_{21} = \begin{bmatrix} \frac{\beta^2}{2\Delta} & -\frac{\beta}{4} \end{bmatrix}; \quad C_{22} = \begin{bmatrix} -\frac{c^2}{2\Delta} & -\frac{c}{4} \end{bmatrix}; \quad D = [0]; \quad c = \sqrt{\frac{EA}{\rho A}}$$

Assuming that we have perfect strain sensors, we can describe the evolution of rightward and leftward components using the following convolution integrals

$$\begin{bmatrix} \hat{w}_r(0,t) \\ \hat{w}_l(0,t) \end{bmatrix} = \begin{bmatrix} C_{11} \\ C_{21} \end{bmatrix} \int_{t_o}^{t} e^{A(t-\tau)} B\varepsilon_1(\tau)\, d\tau + \begin{bmatrix} C_{12} \\ C_{22} \end{bmatrix} \int_{t_o}^{t} e^{A(t-\tau)} B\varepsilon_2(\tau)\, d\tau \qquad (3.56)$$

where ε_1 and ε_2 are the strain measurements taken at location *1*-($x=-\Delta/2$) and *2*-($x=\Delta/2$). As mentioned earlier suppose a sine wave is incident from the left arriving at sensor 1 at $t=0$. Then sensors *1* and *2* would measure the following strains

$$\varepsilon_1(t) = M \sin(\omega_o t); \quad t \geq 0$$
$$\varepsilon_2(t') = M \sin(\omega_o (t - t_o)); \quad t \geq t_o = \frac{\Delta}{c} \qquad (3.57)$$

where M and ω_o are the amplitude and frequency of the travelling wave. Substituting for ε_1 and ε_2 in equation (*3.49*) we find that

$$\begin{bmatrix} \hat{w}_r(0,t) \\ \hat{w}_l(0,t) \end{bmatrix} = \begin{bmatrix} C_{11} \\ C_{21} \end{bmatrix} \int_{0}^{t} e^{A(t-\tau)} BM \sin(\omega_o \tau)\, d\tau + \begin{bmatrix} C_{12} \\ C_{22} \end{bmatrix} \int_{0}^{t} e^{A(t-t_o-\tau)} BM \sin(\omega_o \tau)\, d\tau$$
$$t \geq 0 \qquad\qquad t \geq t_o = \frac{\Delta}{c} \qquad (3.58)$$

Substituting for matrices A and B and integrating equation (*3.58*) with all initial conditions set to zero leads to the following temporal evolution of the rightward and leftward travelling components

$$\begin{bmatrix} \hat{w}_r(0,t) \\ \hat{w}_l(0,t) \end{bmatrix} = \begin{bmatrix} C_{11} \\ C_{21} \end{bmatrix} \begin{bmatrix} \frac{-\sin(\omega_o t)}{\omega_o^2} + \frac{t}{\omega_o} \\ \frac{-\cos(\omega_o t)}{\omega_o^2} + \frac{1}{\omega_o} \end{bmatrix} M + \begin{bmatrix} C_{21} \\ C_{22} \end{bmatrix} \begin{bmatrix} \frac{-\sin(\omega_o(t-t_o))}{\omega_o^2} + \frac{t-t_o}{\omega_o} \\ \frac{-\cos(\omega_o(t-t_o))}{\omega_o^2} + \frac{1}{\omega_o} \end{bmatrix} M$$

$(t \geq 0)$ $\qquad$ $(t \geq t_o = \frac{\Delta}{c})$

(3.59)

Notice in these expressions how the restriction on the initial condition leads to steady state sinusoidal dynamics superposed upon a ramp. Fortunately, for $t > t_o$ the effect of the ramp cancels out and we are only left with the dynamics of a sinusoid. This is apparent when we substitute for the C matrices, i.e.

$$\hat{w}_r(0,t) = \left\{ \frac{-c^2 \sin(\omega_o t)}{2\Delta\omega_o^2} + \frac{c^2 t}{2\Delta\omega_o} + \frac{-c\cos(\omega_o t)}{4\omega_o} + \frac{c}{4\omega_o} \right\} M + \quad (t \geq 0)$$

$$\left\{ \frac{c^2}{2\Delta} \left(\frac{\sin(\omega_o(t-t_o))}{\omega_o^2} \right) + \frac{c}{4} \left(\frac{-\cos(\omega_o(t-t_o))}{\omega_o} \right) + \frac{c}{4\omega_o} - \frac{c^2(t-t_o)}{2\Delta\omega_o} \right\} M \quad (t \geq t_o = \frac{\Delta}{c})$$

(3.60)

and

$$\hat{w}_l(0,t) = \left\{ \frac{-c^2 \sin(\omega_o t)}{2\Delta\omega_o^2} + \frac{c^2 t}{2\Delta\omega_o} + \frac{c\cos(\omega_o t)}{4\omega_o} - \frac{c}{4\omega_o} \right\} M + \quad (t \geq 0)$$

$$\left\{ \frac{c^2}{2\Delta} \left(\frac{\sin(\omega_o(t-t_o))}{\omega_o^2} \right) + \frac{c}{4} \left(\frac{\cos(\omega_o(t-t_o))}{\omega_o} \right) - \frac{c}{4\omega_o} - \frac{c^2(t-t_o)}{2\Delta\omega_o} \right\} M \quad (t \geq t_o = \frac{\Delta}{c})$$

(3.61)

For $t < t_o$ no decoupling is achieved and the both wave component estimates undergo a transient phase which leads to a dc offset in the temporal evolution of their approximate decoupled state. This offset can be estimated for every frequency component in the spectrum of the measurement by considering only the temporal history of equations *(3.60)* and *(3.55)* up until t_o. Thus, the dc offset in the rightward and leftward wave components can be estimated at each frequency ω_o from the following expressions:

$$\hat{w}_r(0,t_o) = \left\{ \frac{c^2}{2\Delta\omega_o^2} \left(t_o - \frac{\sin(\omega_o t_o)}{\omega_o} \right) + \frac{c}{4\omega_o}(1 - \cos(\omega_o t_o)) \right\} M \approx \left(\frac{\omega_o \Delta^2}{6\beta} \right) M$$

(3.61)

$$\hat{w}_l(0,t_o) = \left\{ \frac{c^2}{2\Delta\omega_o^2}\left(t_o - \frac{\sin(\omega_o t_o)}{\omega_o} \right) + \frac{c}{4\omega_o}(\cos(\omega_o t_o) - 1) \right\} M = \left(\frac{-\omega_o \Delta^2}{24\beta} \right) M \tag{3.62}$$

For $t > t_o$ decoupling is approximately achieved; the effect of the ramp cancels and we are only left with the steady state dynamics about the dc offset for each wave component.

$$\hat{w}_r(0,t) = -\frac{cM}{\omega_o}\cos(\omega_o t) + \frac{cM}{\omega_o} + dc \quad (t \geq t_o) \tag{3.63}$$

$$\hat{w}_l(0,t) = dc \quad (t \geq t_o) \tag{3.64}$$

The above expressions are good to second order in the argument $\omega_o t_o = k\Delta$. Figure 3.7 shows the transient and steady state dynamics for a generic wave travelling to the right along a rod.

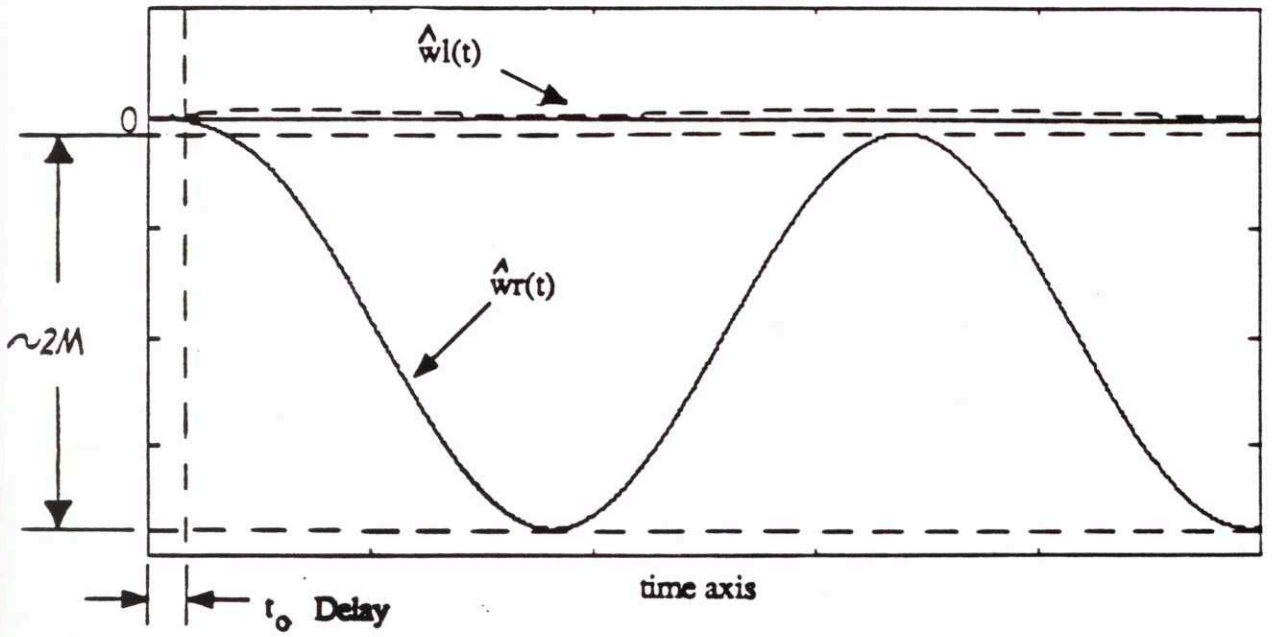

Figure 3.7: Temporal evolution of rightward and leftward propagating components along a longitudinal rod. $\varepsilon_1 = M\sin(t)$ and $\varepsilon_2 = M\sin(t - t_o)$.

3.4 Implementation Issues

The previous sections have outlined two similar approaches for observing wave components from spatially discrete local measurements along a compression rod and a Bernoulli-Euler beam. For these two examples analog circuitry will suffice to implement the elements of the observation matrix $F(\Delta,\omega)$. More specifically in the case of the beam methods have been developed which can simulate terms with $(i\omega)^{(1/2)}$ dependencies-[65]. However, the observation methods discussed in this paper are only valid in the frequency range where the mathematical models provide an accurate description of the system dynamics. Thus, the bandwidth of accuracy will not only be limited by the model accuracy but also by spatial aliasing, instrumentation and the level of the signal to noise ratio.

In addition to giving rise to the phenomenon of spatial aliasing, discretization also affects the resolution of a measured disturbance. Since a single sensor spacing stencil will only provide optimal resolution in a narrowband about $\Delta_{opt}(\omega_b)$-(b denotes bandwidth of signal), broadband signals may suffer some loss in resolution for frequencies $\omega << \omega_b$. To improve the resolution for these frequency components it may be advantageous to construct an additional wave-mode observer which has higher sensitivity in a lower frequency range(See Figure 3.8). This will require that a second sensor stencil be established to resolve the lower frequency components. The two observers can be combined by passing the higher frequency components through the first stencil and lower frequency components through the second and then summing the resulting signals. This approach leads to higher resolution broadband measurement.

3.5 Summary

In this chapter model based procedures have been developed for estimating wave components which propagate along one-dimensional members from spatially colocated and non-colocated measurements. In each procedure we have derived temporal filters which decouple wave-mode states from local physical measurements in a member. The problem with these filters, however, is that for dispersive mediums they are not guaranteed to be causal. This acausal behavior makes it difficult to observe all wave components which may propagate along a dispersive member. For certain physical geometries, however, where the response of the member is dominated by propagating dynamics, approximations can be made to render a subset of the full wave-mode vector observable by exploiting only the causal entries of the observation matrix.

Besides being limited by the dispersive nature of the medium, the non-colocated approach is also complicated by the phenomenon of spatial aliasing. This arises from the

fact that this approach uses point sensors which are some distance apart. For wavelengths small compared to sensor spacing there will be ambiguity in determining the true wavelength being resolved by this observation scheme. This restricts the non-colocated scheme to those wavelengths which are large compared to sensor spacing. Thus, a first-order approximation to the entries of the observation matrix is sufficient for practical implementation.

Sensor noise further restricts the bandwidth of the non-colocated observation scheme to those signals which are large compared to the noise level. Optimal resolution is achieved when the sensor spacing is chosen to maximize the signal-to-noise ratio of each wave component at each frequency. Of course for broadband signals multiple sensor stencils may be required to adequately resolve all frequencies which may be present in the dynamics.

The next chapter examines full-state wave-mode amplitude estimation using distributed sensors.

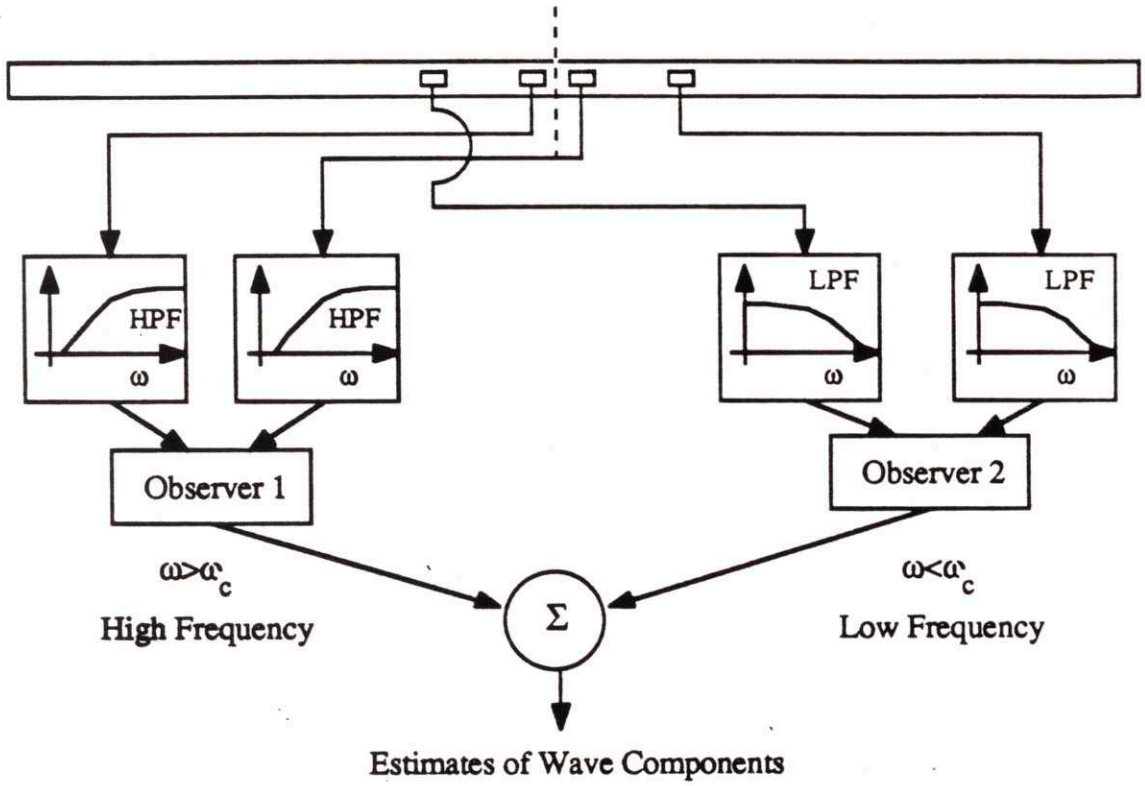

Figure 3.8: Possible scheme for resolving broadband signals. Two sensor stencils are employed to resolve the high and low frequency ends of the spectrum.

CHAPTER 4

Wave Filtering Using Distributed Sensors

4.1 Introduction

This chapter investigates the filtering of wave propagation dynamics at a cross-section along one-dimensional structures using point and distributed measurements. This work is motivated by the desire to determine the magnitude and direction of wave propagation in a member and to implement previously developed wave control designs. As in the case of discrete sensors, the solution of the partial differential equation which characterizes the dynamics of a one-dimensional structure under steady-state motion is written in terms of waves which can circumnavigate the member, interacting with structural boundaries to add constructively-(pole) or destructively-(zero). This way of viewing the response permits the application of Fourier Spectral Methods to design distributed spatial sensor weighting patterns which can be used to impart properties to the sensor output signal not normally possible using temporal filters. Some of these properties include roll-off without a phase-lag or spatial derivative without 90 degrees of phase lead. More specifically the idea is to find suitable weighting patterns for a finite distributed sensor which facilitate filtering wave propagation dynamics on a finite structure over a wide frequency range. The application of Spectral Methods achieves

this goal for a banded frequency range and a finite length sensor. This concept is illustrated for some typical one-dimensional members.

4.1.1 A Distributed Sensor: PVDF

The work of the previous chapter has motivated the need for a distributed sensor which realizes the spatial difference operators D and its derivatives. Instead of attempting to perform wave filtering with many sensors, a distributed sensor could perform this task directly and without the effects of spatial aliasing. Fortunately for the objectives of this research such a transducer does exists in the form of Polyvinylidene Fluoride, more commonly referred to as (PVDF). PVDF is a polymer which has a high piezoelectric stress coefficient that results in high electric fields under a given stress. As a transducer it has a wide range of applications; many of them being summarized in a report produced by the Pennwalt Corporation-[53,54] which manufactures several products using PVDF. Additional applications can also be found in Sessler's review-[66]. The work here, however, is concerned with the use of PVDF as a spatial filter for decoupling steady-state wave propagation dynamics. Such a filter is motivated by a desire to infer the wave-nature of 1-dimensional structures and to subsequently use this information for the purposes of structural control.

4.1.2 Previous Studies Using PVDF

The use of spatially distributed sensor and actuators is not a new concept. In fact their initial application might be traced to Hubbard and etal-[67-70] who mounted uniform PVDF actuators on both cantilever and simply-supported beams and applied Lyapunov function theory to design controllers which would damp the vibration of the first few modes of the structure. In a similar manner Connally and Hubbard attempted control of a two-dimensional structure using 4 PVDF actuators mounted on all four sides of a cantilever beam with a rectangular cross-section. Again damping of the first three modes served as the performance index. Following this attempt, Tzou demonstrated the use of PVDF as both a sensor and actuator-[71-74]. In his work he attempted both broadband isolation and damping in more than one mode of a cantilever beam. PZT-(lead zirconate-titanate) ceramic actuators were exploited by de Luis, Crawley and Hall-[75] in the design of optimal controllers for infinite-order 1-D structural models.

The use of PVDF film as a sensor, however, was first attempted by Miller and Hubbard-[76]. As before they mounted a uniform layer of PVDF on a cantilever beam to sense tip angular displacement at the free end. Feedback tests were attempted to

confirm analytical predictions. During this work they concluded that the distributed PVDF sensors were more accurate than their point counterparts since they were less sensitive to actual placement errors. This conclusion was in large part due to the fact that the distributed sensor spatially integrated the structural response. The work of Lee-[77-78] led to the next advancement in the use of PVDF as a sensor for structural control. In his work Lee derived modal sensor and actuator equations and verified his modal analysis on a stainless steel cantilever beam. He found that if the the electrode pattern of the PVDF was etched into the shape of a natural eigenfunction of a particular mode of a structure, the sensor could effectively act as a modal filter with respect to all modes which were not orthogonal to this eigenfunction. He tested this concept by fabricating modal sensors for the first and second mode of a beam. During these tests the normalized Mode One sensor had a response that was *18%* sensitive to the second mode. Similarly, the Mode Two sensor was only *3%* sensitive to the first mode. Lee also demonstrated the performance of modal actuators.

The modal sensor concept initiated by Lee,et al-[78] was verified by the work of Collins-[79] who opted to build modal sensors for a structure with more complicated dynamic behaviour than just a cantilever beam. The test article he chose was the Martin Marietta Large Space Manipulator-(LSM) link which consisted of a *1.8* meter horizontal planar arm formed by two aluminum beams with rectangular cross-section. He subsequently constructed modal sensors for the first three modes of the structure which were at *2.015, 9.829* and *35.03 Hz.* respectively. Results similar to those found by Lee were obtained for non-orthogonal modal sensitivity. Collins, Miller and von Flotow-[80] also demonstrated the use of PVDF as a spatial averaging filter for local strain measurements. They constructed sensors which yield properties such as infinite roll-off without a phase lag. However, their methods appeared to be ad-hoc; looking for a suitable averaging function for structural control.

One useful application of the spatial averaging sensors is for the purposes of filtering wave propagation dynamics-[81]. Such information lends itself quite readily to previously developed feedforward control methodologies for active isolation and damping. This chapter demonstrates the use of distributed sensors to solve the approximated full-state wave filter problem for purely propagating dynamics.

4.1.3 Realizations for Wave Filtering-(See Figure 4.1)

An array of spatially discrete measurements represents just one way in which the discrete operators D_{∞}^{0} and D_{∞}^{1} can be realized to infer local information. Although, there is flexibility in changing individual gains for the discrete spatial operators, discrete

processing of structural information may suffer from spatial aliasing and hardware constraints. Distributed sensors overcome these issues with the gains of the spatial difference operator being implemented directly in sensor interpolation pattern with the only disadvantage that once the pattern is selected it can't be changed. Nevertheless, a distributed sensor offers reduced complexity while achieving much better accuracy.

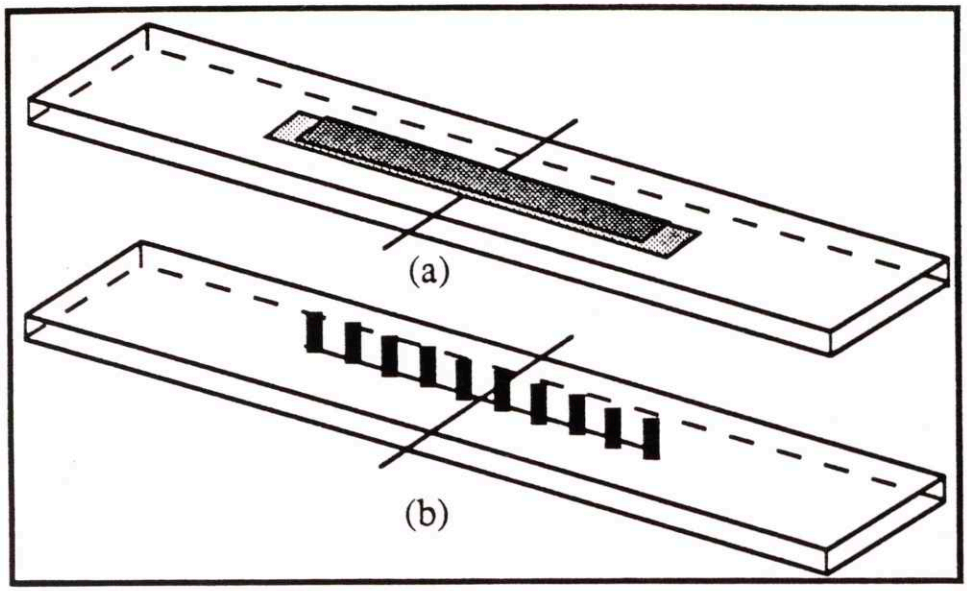

Figure 4.1: Possible Realizations:(a) Distributed PVDF Sensor. (b) Discrete Array of Point Sensors

4.2 The Distributed Sensor Equation

The modal sensors developed by Lee, Collins and others-[77-79] using PVDF film represented a unique way in which the engineer could tailor a transducer to achieve certain temporal properties such as modal filtering or arbitrary roll-off characteristics.. Since these sensors combine information which is spatially distributed along a member into a single temporal signal, all that is required is to determine the geometry of the weighting pattern which has certain desired temporal frequency properties. Fortunately, such an approach holds here in the case of wave-mode filtering of propagating dynamics where all that is required is the appropriate interpolating pattern which is sensitive to only one direction of propagation. However, before proceeding to describe the properties of such a filter, it is important to point out some of the parameters which make up the response from a PVDF film sensor. Lee found that

given a mechanical deformation of uniform beam, the charge generated by a layer of PVDF film mounted on its surface is given by

$$Q(t) = -e_{31} z \int_{-d}^{d} F(x) \frac{\partial^2 u(x,t)}{\partial x^2} dx \qquad (4.1)$$

where $Q(t)$ is the charge generated by the piezo film, z is the distance from the beam's neutral axis to the PVDF'S midplane, e_{31} is piezoelectric constant, d is the length of the sensor, $\phi(x)$ is the effective electrode width and $u(x,t)$ is the transverse displacement of the beam. The assumptions behind this equation, and the definitions of the variables can be found in Appendix A1. Since the charge generated by the PVDF film is proportional to the surface area of its electrode the sensor output can be interpreted as the weighted average of the beam's distributed strain with a weighting pattern determined by the shape of the electrode. Designing this electrode shape can be done in a number of ways as pointed out by Collins-[79]. The purpose of this chapter is to present an approach for designing such a transducer that filters wave-mode amplitudes for the purposes of structural control.

4.3 Collocated Wave-Mode Amplitude Filtering

Collocated wave-mode filtering schemes which were presented in Chapter 4 for typical 1-D members were limited by two major factors:

1. Lack of Availability of all elements of the physical cross-sectional state vector-y.
   and
2. The inability to realize elements of $Y^{-1}(\omega)$ or $F(\omega)$ which are temporally non-causal.

This section attempts to solve these problems using spatially distributed sensors whose electrodes can be shaped to a desired weighting patterns-$\phi(x)$ that makes the sensor signal sensitive to directional wave propagation.

4.3.1 Band-Limited Realization of Spatial Derivatives

The discrete approach outline in Chapter 3 exploited spatial averaging and difference operators to approximate spatial derivatives of arbitrary order. This approach, however, suffered from discretization pitfalls such as spatial aliasing, artificial dispersion and differentiation accuracy. To minimize these effects it is often necessary to increase the number of sensors and choose the sensor spacing Δ arbitrarily small. In the limit as $\Delta \Rightarrow 0$ and the number of sensors-$2m \Rightarrow \infty$, the gain of the discrete operators $D_\infty{}^0$ and $D_\infty{}^1$ approach gains of a class-$L^2 \supset X$ of continuous polynomials-[82,83] at discrete points $x_j = j\Delta$. These polynomials have the properties that they are

(i) Bounded in L^2-(The space of square integrable functions)
(ii) Band-Limited in the Spatial Frequency Domain
(iii) Trigonometric
(iv) Non-causal

The fundamental interpolant in this class corresponds to the well-known sinc function given by

$$\phi(x) = \frac{1}{2\pi}\left(\frac{2\sin(k_b x)}{x}\right) \qquad x \in [-\infty, \infty] \tag{4.2}$$

with frequency properties

$$\Phi(k) = \begin{cases} 1, & |k| < k_b \\ 0, & otherwise \end{cases} \tag{4.3}$$

where k_b defines the cut-off wave-number. The sinc function represents the banded version of the ideal delta-$\delta(x)$ function. Similarly, by computing its spatial derivative we find that

$$\phi'(x) = \frac{1}{2\pi}\left(\frac{2k_b\cos(k_b x)}{x} - \frac{2\sin(k_b x)}{x^2}\right) \tag{4.4}$$

which corresponds to the band-limited version of the 1st spatial derivative. It's frequency properties are thus given by

$$\Phi(k) = \begin{cases} ik, & |k| < k_b \\ 0. & otherwise \end{cases} \tag{4.5}$$

Equations-(4.2) and (4.4) are plotted in Figure 4.2 with the magnitude of their spatial transforms. Higher order approximations are possible by simply differentiating the fundamental interpolant as may times as desired to yield the order of interest.

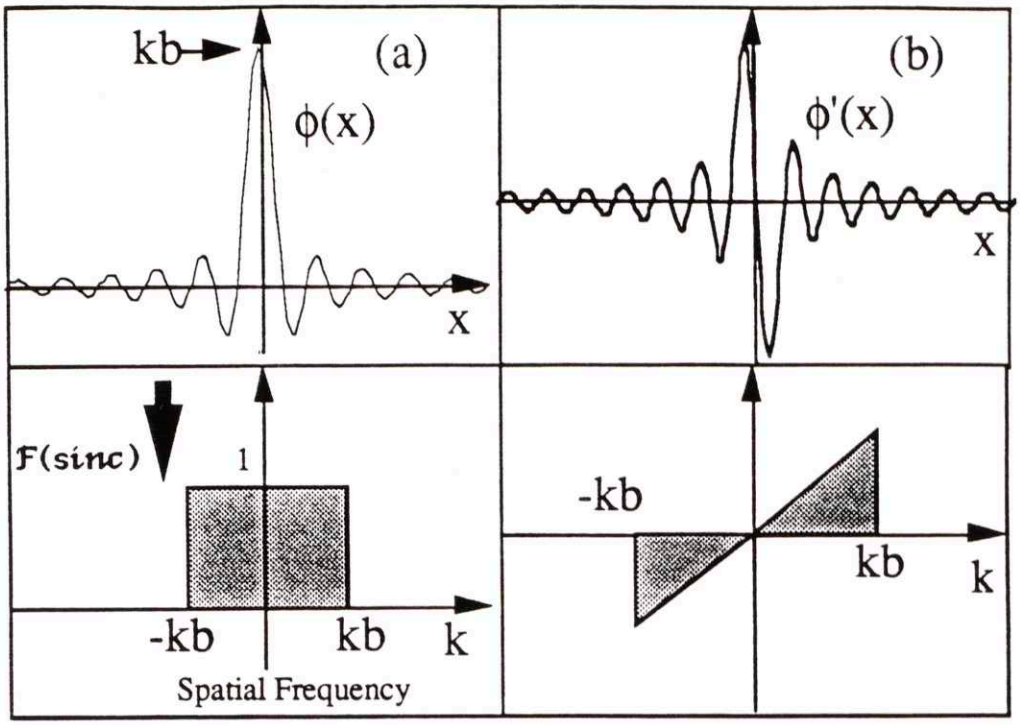

Figure 4.2: The sinc-(a) interpolant and its derivative (b)

4.3.2 Directional Sensitivity

Propagating wave solutions have the form

$$q(x,\omega) = w_{rp}(0,\omega)e^{-ikx} + w_{lp}(0,\omega)e^{ikx} \tag{4.6}$$

i.e. if no discontinuities or excitations are in the sensing domain. To observe left-going wave at $x=0$ we need a sensor sensitivity function $\phi(x)$ such that

$$\int_{-\infty}^{\infty} \phi(\xi)q(\xi,\omega)d\xi = \begin{cases} w_{lp}(0,\omega) & k > 0 \\ 0 & k < 0 \end{cases} \tag{4.7}$$

Similary for a rightward going wave at $x=0$ the relation in equation (4.7) becomes

$$\int_{-\infty}^{\infty} \phi(\xi)q(\xi,\omega)d\xi = \begin{cases} w_{rp}(0,\omega) & k > 0 \\ 0 & k < 0 \end{cases} \tag{4.8}$$

To achieve this goal $\phi(x)$ must have a complex form given by

$$\begin{aligned} &\textit{Directional Sensitivity requires } \Phi(k) = 0 \qquad k < 0 \\ &\textit{this implies } \phi(x) = \phi_r(x) - i\phi_i(x) \\ &\textit{where } \phi_i(x) = Hi(\phi_r(x)) \end{aligned} \tag{4.9}$$

Hi indicates the Hilbert Transform of $\phi_r(x)$.

Unfortunately, in this form the filter is still not realizable since the complex filter requires the implementation of a temporal 90 degree phase shift which as mentioned previously is not possible using simple analog components without suffering some loss in frequency domain properties. However, spatial realizations do exist and are discussed in the next section.

4.3.3 Implementing $i=\sqrt{-1}$ ("90° phase shifter") with a Band-Limited Spatial Hilbert Transform and Temporal Integration.

The spatial function

$$\phi_{Hi}(x) = \frac{4\sin^2(k_b x/2)}{2\pi x}, \qquad x \in (-\infty, \infty) \tag{4.10}$$

has the spatial fourier transform

$$\Phi_{Hi}(k) = \begin{cases} i\,sign(k), & |k| < k_b \\ 0 & otherwise \end{cases} \tag{4.11}$$

Thus, spatial derivatives of $\phi_{Hi}(x)$ have transforms given by

$$\Im\left(\frac{d^n}{dx^n}\phi_{Hi}(x)\right) = (ik)^n \Phi_{Hi}(k) \tag{4.12}$$

This result can be exploited for waveguides with simple polynomial dispersion relations between k and ω. For example

Non-dispersive rod

$$k = \frac{\omega}{c}$$

B-E Beam

$$k^2 = \sqrt{\frac{\rho A}{EI}}\,\omega$$

Thus, using these simple polynomial relations wave separation can be achieved as described in the following Theorem.

Theorem 4.1: ***(Filter Equivalence)***

Suppose $\phi_r(x)$ is a band-limited real-valued interpolation function such that a complex spatial filter $h(x)$ given by

$$h(x) = \phi_r(x) - iHi(\phi_r(x)); \qquad x \in (-\infty, \infty) \tag{4.13}$$

selectively filters out rightward propagating wave dynamics then an equivalent representation of $h(x)$ is given by

i. Non-dispersive-(Wavespeed-c)

$$h_R(x) = \phi_r(x) + \frac{c}{i\omega}\phi'_r(x); \qquad x \in (-\infty, \infty) \tag{4.14}$$

ii. Dispersive-(B-E Bending)

$$h_B(x) = \phi_r(x) + \frac{1}{ik^2}Hi(\phi''_r(x)); \qquad x \in (-\infty, \infty) \tag{4.15}$$

for $k \in [0, k_b]$.

Proof:

This theorem is verified by convolving $h(x)$ with e^{ikx} to show that $H(k)=0 \vee k \in [0, k_b]$

Figure 4.3 presents a pictorial illustration of the directional filtering scheme outlined in Theorem 4.1 using band-limited spatial real valued functions. Ideally, the implementation of equation (4.13)-(Step 1) on 1-D structure is desired. However, the inability to realize $i=\sqrt{-1}$ temporally or spatially results in a transformation of the ideal distributed filter into a realizable form where causal temporal filters-[63]-(Step 2) can be exploited. Such a transformation is illustrated in steps 3 and 4 using a distributed sensor on a B-E beam where directional filtering of the rightward-going wave is achieved.

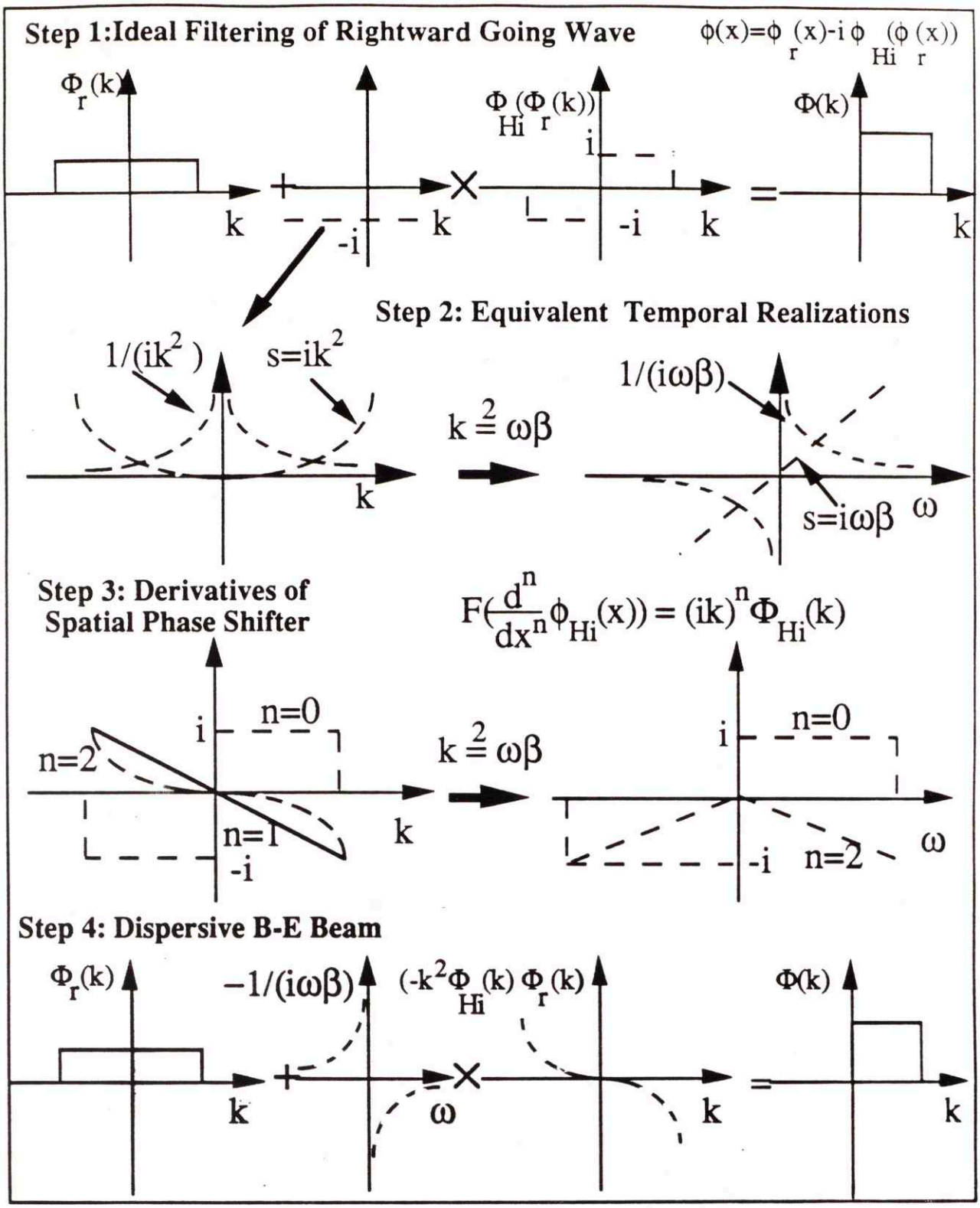

Figure 4.3 Pictorial Illustration of Desired Directional Sensitivity Properties defined in Theorem 4.1 for a rightward-going wave. Equivalent Filter representation for a Dispersive B-E beam.

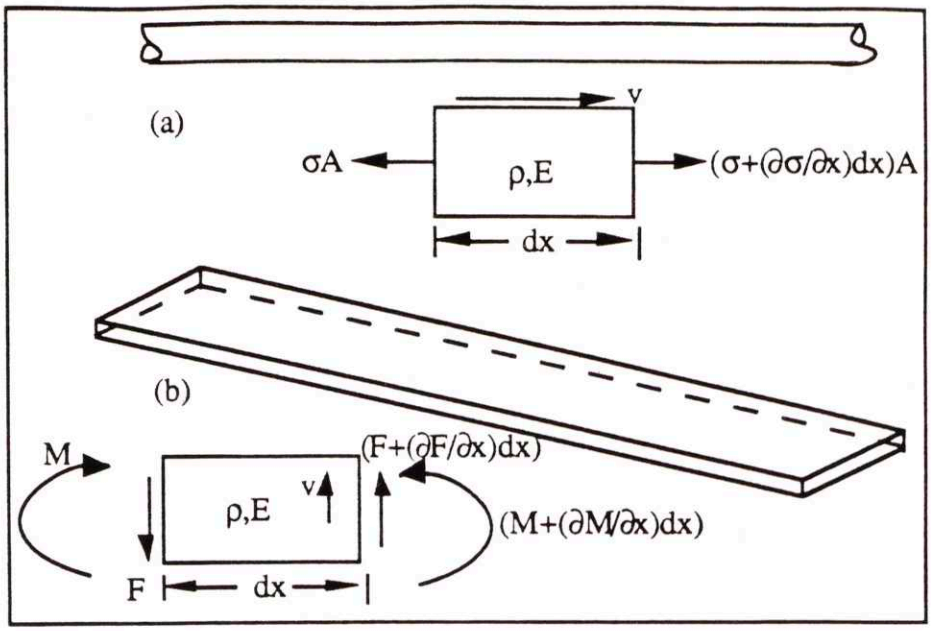

Figure 4.4: Typical 1-Dimensional Structures which support Wave Propagation-(a) Compression Rod and (b) Bernoulli-Euler Beam.

4.4 Infinite Structures

4.4.1 Longitudinal Rod:(Proof of Theorem 4.1i)

The governing partial differential equation which describes the longitudinal dynamics of a rod-(See Figure 4.4a) is given by

$$EA\frac{\partial^2 u(x,t)}{\partial x^2} = \rho A\frac{\partial^2 u(x,t)}{\partial t^2} \qquad (4.16)$$

where E is Young's modulus of elasticity, ρ is the density and A is the cross-sectional area of the member. The steady-state response of an unforced portion of the member can be written as

$$u(x,\omega) = w_{rp}(0,\omega)e^{-ikx} + w_{lp}(0,\omega)e^{ikx} \qquad (4.17)$$

where $w_{rp}(0,\omega)$ and $w_{lp}(0,\omega)$ are the rightward-(r) and leftward-(l) propagating-(p) wave amplitudes.

The output of a band-limited interpolant which would achieve directional filtering of say the rightward going strain wave amplitude-($\varepsilon_{rp}(0,\omega)=-ikw_{rp}(0,\omega)$) would have the following complex form

$$\hat{\varepsilon}_{rp}(0,\omega) = \int_{-\infty}^{\infty} \phi(\xi)\left(-ikw_{rp}(0,\omega)e^{-ik\xi} + ikw_{lp}(0,\omega)e^{ik\xi}\right)d\xi$$

$$= \int_{-\infty}^{\infty} \phi(\xi)\left(\varepsilon_{rp}(0,\omega)e^{-ik\xi} + \varepsilon_{lp}(0,\omega)e^{ik\xi}\right)d\xi$$

where the sensor sensitivity to strain, $\phi(x)$ is complex

$$\phi(x) = \phi_e(x) + i\phi_o(x)$$

$$\phi_e(x) = \frac{2\sin(k_b x)}{2\pi x} \quad \text{and} \quad \phi_o(x) = \frac{4\sin^2(k_b \frac{x}{2})}{2\pi x} \tag{4.18}$$

Of course the implementation of complex filters is not possible using temporal filters except in the case of linear *Finite Impulse Response Filters-(FIR)*-[83] where a constant phase delay is used to offset temporal non-causality. An alternative approach is to exploit the dispersion relation to form a complex filter that requires temporal integration as oppose to just a *90* degree phase shift. The form of the interpolant for this filter might have the following form

$$\phi(x) = \phi_e(x) + \frac{1}{i\omega\sqrt{\frac{\rho A}{EA}}}\phi_o(x) \tag{4.19}$$

This permits the use of a different odd interpolant for wave filtering. In this case the interpolant which achieves filtering specified in equation-(*4.9*) corresponds to the band-limited differentiator given by

$$\phi_o(x) = \frac{d}{dx}\left(\frac{2\sin(k_b x)}{2\pi x}\right) = \frac{2}{2\pi}\left(\frac{k_b\cos(k_b x)}{x} - \frac{\sin(k_b x)}{x^2}\right) \tag{4.20}$$

Therefore, the rightward going strain-wave amplitude can be filtered according to

$$\hat{\varepsilon}_{rp}(0,\omega) = \frac{1}{2\pi}\int_{-\infty}^{\infty}\left(\frac{\sin(k_b\xi)}{k_b\xi} + \frac{1}{i\omega\sqrt{\frac{\rho A}{EA}}}\left(\frac{k_b\cos(k_b x)}{\xi} - \frac{\sin(k_b\xi)}{\xi^2}\right)\right)$$
$$\left(-ikw_{rp}(0,\omega)e^{-ik\xi} + ikw_{lp}(0,\omega)e^{ik\xi}\right)d\xi \tag{4.21}$$

The same end result in equation (*4.20*) could be achieved with a point strain sensor and a distributed PVDF sensor which implements only the odd portion of the ideal filter.

Applying this approach both the rightward and leftward wave components can be found from

$$\begin{bmatrix} \hat{\varepsilon}_{rs} \\ \hat{\varepsilon}_{ls} \end{bmatrix} = F(\omega) \begin{bmatrix} \varepsilon \\ y \end{bmatrix} = \begin{bmatrix} \frac{1}{2} & \frac{1}{2s}\sqrt{\frac{EA}{\rho A}} \\ \frac{1}{2} & \frac{-1}{2s}\sqrt{\frac{EA}{\rho A}} \end{bmatrix} \begin{bmatrix} \varepsilon \\ y \end{bmatrix} \tag{4.22}$$

where $F(\omega)$ defines the observation matrix where the distributed sensor response v is given by

$$\begin{aligned} v(0,\omega) &= \int_{-\infty}^{\infty} \phi_o(\xi)\varepsilon(\xi,\omega)\,d\xi \\ &= k^2\{w_{rp}(0,\omega) + w_{lp}(0,\omega)\} \qquad k \in [-k_b, k_b] \end{aligned} \tag{4.23}$$

4.4.2 Bernoulli-Euler Beam-(Proof of Theorem 4.1ii)

The governing partial differential equation describing homogeneous transverse motion of a Bernoulli-Euler beam-(See Figure 4.4b) is given by

$$EI\frac{\partial^4 u(x,t)}{\partial x^4} = \rho A\frac{\partial^2 u(x,t)}{\partial t^2} \tag{4.24}$$

where EI is the bending stiffness, ρA is the mass per unit length.. As before, the response of the unforced segment of the beam can be written as

$$\begin{aligned} u(x,\omega) = {} & w_{rp}(0,\omega)e^{-ikx} + w_{re}(0,\omega)e^{-kx} + \\ & w_{lp}(0,\omega)e^{ikx} + w_{le}(0,\omega)e^{kx} \end{aligned} \tag{4.25}$$

where the subscripts p and e refer to propagating and evanescent wave amplitudes. A few wavelengths from structural boundaries and at high frequencies the evanescent components contribute negligibly to the response of the beam. This implies that the response can be interpreted in terms of only propagating components.

$$u(x,\omega) \approx w_{rp}(0,\omega)e^{-ikx} + w_{lp}(0,\omega)e^{ikx} \qquad \textit{high freq.} \tag{4.26}$$

The most common measurement made on a B-E beam is strain which can be computed by taking the 2nd derivative of equation-(*4.10*) and multiplying by $(-t_b/2)$. This leads to

$$\varepsilon(x,\omega) = \frac{-t_b}{2}u''(x,\omega) = \frac{t_b}{2}k^2\,(w_{rp}(0,\omega)e^{-ikx} + w_{lp}(0,\omega)e^{ikx})$$
$$= (\varepsilon_{rp}(0,\omega)e^{-ikx} + \varepsilon_{lp}(0,\omega)e^{ikx}) \qquad (4.27)$$

where ε_{rp} and ε_{lp} refer respectively to propagating rightward and leftward strain wave amplitudes at x=0.

Thus, to decouple these strain wave components it appears that only one other additional measurement is required, possibly slope or internal shear force. However, the discrete approach of Chapter 3 points out that even if all measurements were available at a point the temporal matrix transformation required to decouple waves on beam would be noncausal in time making implementation impossible. On the other hand distributed sensors attempt to overcome this problem of causality by realizing desired temporal properties in space. It is clear that both rightward and leftward wave responses could be decoupled if equation (4.27) could be combined with a sensor signal in which $\varepsilon_{rp}(0,\omega)=(t_b/2)k^2w_{rp}(0,\omega)$ and $\varepsilon_{lp}(0,\omega)=(t_b/2)k^2w_{lp}(0,\omega)$ are 180 degrees out of phase with one another for all frequencies. This condition is achieved for a rightward going strain wave using the following complex filter:

$$\hat{\varepsilon}_{rp}(0,\omega) = \frac{1}{4\pi}\int_{-\infty}^{\infty}\phi(\xi)\frac{t_b}{2}(k^2w_{rp}(0,\omega)e^{-ik\xi} + k^2w_{lp}(0,\omega)e^{ik\xi})\,d\xi$$
$$= \frac{1}{4\pi}\int_{-\infty}^{\infty}\phi(\xi)(\varepsilon_{rp}(0,\omega)e^{-ik\xi} + \varepsilon_{lp}(0,\omega)e^{ik\xi})\,d\xi$$

where

$$\phi(x) = \phi_e(x) + i\phi_o(x)$$

$$\phi_e(x) = \frac{2\sin(k_b x)}{2\pi x} \quad \text{and} \quad \phi_o(x) = \frac{4\sin^2(k_b\frac{x}{2})}{2\pi x} \qquad (4.28)$$

But again as in the case of the rod the complex filter which achieves this result requires some modification to incorporate the properties of the dispersion relation so that $\phi(x)$ becomes

$$\phi(x) = \phi_e(x) + \left(\frac{1}{ik^2}\right)\phi_o(x)$$
$$= \phi_e(x) + \left(\frac{1}{i\omega\sqrt{\frac{\rho A}{EI}}}\right)\phi_o(x) \qquad (4.29)$$

where the odd filter $\phi_o(x)$ which is suitable for this complex filter is given by

$$\phi_o(x) = \ddot{\phi}_{Hi}(x) = \frac{1}{2\pi}\left(4\left\{\frac{1-\cos(k_b x)}{x^3}\right\} - \frac{4k_b \sin(k_b x)}{x^2} + \frac{2k_b^2 \cos(k_b x)}{x^3}\right) \tag{4.30}$$

This interpolant has the following spatial frequency properties

$$\Phi_o(k) = -ik^2 \quad sign(k) \qquad k \in [-k_b, k_b] \tag{4.31}$$

where the interpolated response at $x=0$ becomes

$$\begin{aligned} v(\omega) &= \int_{-\infty}^{\infty} \phi_o(\xi)\,\varepsilon(\xi,\omega)\,d\xi \\ &= -ik^2 \varepsilon_{rp}(0,\omega) + ik^2 \varepsilon_{lp}(0,\omega); \qquad k \in [-k_b, k_b] \end{aligned} \tag{4.32}$$

With this interpolated signal, estimates of the rightward and leftward waves are obtained from

$$\begin{bmatrix} \hat{\varepsilon}_{rp} \\ \hat{\varepsilon}_{lp} \end{bmatrix} = F(\omega)\begin{bmatrix} \varepsilon \\ v \end{bmatrix} = \begin{bmatrix} \frac{-1}{2} & \frac{1}{2s\sqrt{\frac{\rho A}{EI}}} \\ \frac{1}{2} & \frac{1}{2s\sqrt{\frac{\rho A}{EI}}} \end{bmatrix}\begin{bmatrix} \varepsilon \\ v \end{bmatrix} \tag{4.33}$$

where v is a signal which does not represent any physical response of the beam, however, it can be sensed using distributed piezofilm sensors.

4.4.3 A Generalization of the Sensor Equivalence Theorem

Neglecting the presence of near field terms in the response of a Bernoulli-Euler beam makes it possible to use additional measurements such as internal shear or local slope to help realize the complex filters of equation-(*4.13-15*). For simple polynomial dispersion characteristics, these additional measurements are directly available from a distributed sensor with proper choice of interpolation function and temporal compensation.

•ROD- $\vec{y} = (u, u')^T$

$$v_1(x,\omega) = \frac{EA}{\rho A s^2}\int_{-\infty}^{\infty} \frac{1}{2\pi}\left(\frac{2k_b \cos(k_b(x-\xi))}{x-\xi} - \frac{2\sin(k_b(x-\xi))}{(x-\xi)^2}\right) u'(\xi,\omega)\,d\xi$$

(4.34)

$$v_2(x,\omega) \approx \int_{-\infty}^{\infty} \frac{1}{2\pi}\left(\frac{2\sin(k_b(x-\xi))}{x-\xi}\right)u'(\xi,\omega)\,d\xi \tag{4.35}$$

•BEAM-$\vec{y}$ = $(u,u',EIu'',-EIu''')^T$

$$v_1(x,\omega) \approx -\frac{2EI}{\rho A s^2 t_b}\int_{-\infty}^{\infty} \frac{1}{2\pi}\left(\frac{2k_b^2\sin(k_b(x-\xi))}{x-\xi} - \frac{4k_b\cos(k_b(x-\xi))}{(x-\xi)^2} + \frac{4k_b^2\sin(k_b(x-\xi))}{(x-\xi)^3}\right)\frac{-t_b}{2}u''(\xi,\omega)\,d\xi \tag{4.36}$$

$$v_2(x,\omega) \approx -\frac{2EI}{\rho A s^2 t_b}\int_{-\infty}^{\infty} \frac{1}{2\pi}\left(\frac{-2k_b^3\cos(k_b(x-\xi))}{x-\xi} + \frac{3k_b^2\sin(k_b(x-\xi))}{(x-\xi)^2} + \frac{6k_b\cos(k_b(x-\xi))}{(x-\xi)^3} - \frac{6\sin(k_b(x-\xi))}{(x-\xi)^4}\right)\frac{-t_b}{2}u''(\xi,\omega)\,d\xi \tag{4.37}$$

$$v_3(x,\omega) \approx -EI\,\frac{2}{t_b}\int_{-\infty}^{\infty} \frac{1}{2\pi}\left(\frac{2\sin(k_b(x-\xi))}{x-\xi}\right)\frac{-t_b}{2}u''(\xi,\omega)\,d\xi \tag{4.38}$$

$$v_4(x,\omega) \approx EI\,\frac{2}{t_b}\int_{-\infty}^{\infty} \frac{1}{2\pi}\left(\frac{2k_b\cos(k_b(x-\xi))}{x-\xi} - \frac{2\sin(k_b(x-\xi))}{(x-\xi)^2}\right)\frac{-t_b}{2}u''(\xi,\omega)\,d\xi \tag{4.39}$$

This implies that it might not be necessary to exploit simple polynomial dispersion relations, the Hilbert Transform filter or its derivatives to achieve directional wave filtering. For example a possible distributed interpolant which filters the rightward going strain wave amplitude might have the form

$$\phi(x) = \phi_e(x) + C_1(\omega)\phi_{o1}(x) + C_2(\omega)\phi_{o2}(x) \tag{4.40}$$

where $C_1(\omega)$ and $C_2(\omega)$ are causal temporal filters possibly having real and imaginary parts. $\phi_{o1}(x)$ and $\phi_{o2}(x)$ are odd interpolants derived from the interpolation function-

$\phi_e(x)$. More specifically, one realization which filters the rightward strain wave-mode amplitude in beam bending-($k^2 \propto \omega$) from a distributed PVDF strain sensor is given by

$$\hat{\varepsilon}_{rp}(0,\omega) = \frac{1}{3}\int_{-\infty}^{\infty} \phi(\xi)\, \varepsilon(\xi,\omega) d\xi \tag{4.41}$$

where

$$\phi(x) = \frac{2\sin(k_b x)}{2\pi x} + \left(\frac{1}{\sqrt{i\omega\sqrt{\frac{\rho A}{EI}}}}\right)\frac{d}{dx}\left(\frac{2\sin(k_b x)}{2\pi x}\right) - \frac{1}{\left(i\omega\sqrt{\frac{\rho A}{EI}}\right)^{\frac{3}{2}}}\frac{d^3}{dx^3}\left(\frac{2\sin(k_b x)}{2\pi x}\right) \tag{4.42}$$

where the fractional temporal integrations $(i\omega)^{(-1/2)}$, $(i\omega)^{(-3/2)}$ are well defined and can be easily performed in analog circuitry-[65]. This expression will be useful when we discuss truncated spatial domains since the truncation of the Hilbert transform and its derivatives lead to poor low frequency properties.

4.5 Finite Spatial Interpolants: (Truncating the spatial domain)

The wave filters presented in the previous section are idealistic; assuming that interpolation patterns can be etched on an infinite strip of PVDF film. No such strips exist. Thus, we are forced with standard signal processing problem of truncating the spatial extent of the filter while preserving as many usefull frequency properties as possible. Fortunately, several methods exist for smoothly truncating the spatial extent of a filter-[83]. One such approach involves multiplying the interpolant by another function which truncates the length of the sensor. This is commonly referred to as windowing which attempts to approximate the optimal least squares solution for truncated a filter-[84]. The other approach involves a min-max error design approach based on trying to meet certain design specifications throughout the frequency domain. Both are discussed here with more emphasis placed on windowing.

4.5.1 Ad-Hoc Truncation: Windowing

The windowing concept is based on understanding the properties of the Fourier Transform. The idea is to take a finite length window $\phi_w(x)$ defined to be zero $/x/>d$ and perform the following multiplication

$$\phi_t(x) = \phi(x)\phi_w(x) \tag{4.43}$$

where $\phi(x)$ is the infinite domain interpolant and $\phi_t(x)$ denotes its truncated form. The transform of this truncated version is now given by

$$\Phi_t(k) = \Phi(k) * \Phi_w(k), \qquad /k/ < k_b \tag{4.44}$$

which states that the frequency response of a finite-length filter is equal to the ideal frequency response $\Phi(k)$ convolved with the transform of the window function. For sharp window functions truncated transforms may suffer from the occurrence of the Gibbs phenomenon which occurs when sinusoids attempt to approximate the behaviour near a discontinuity in the frequency domain-[85]. However, this can be overcome with proper choice of window function at the expense of a smoother roll-off performance.

Some common window functions are given in Table 4.1. Figure 4.5 displays some representative examples of window functions and their corresponding transforms. The amplitude and spatial extent of these filters have been normalized for convenience of representation. All these functions are real and thus have zero phase in the region $/k/<k_b$. Beyond this point there are *180* degree phase flips for some functions whose neighboring lobes alternate in the sign.

The particular choice of window depends on how much one wants to trade side-lobe amplitude with main-lobe width. For example a rectangular window usually yields the smallest main-lobe width, however, the side-lobe amplitude is pretty large. Kaiser-[83] found the near optimal window function corresponding to a filter which maximally concentrated around $k=0$ in the frequency domain. The parameter β is his formula gives an additional factor to achieve desired window properties along with window length.

Table 4.1 Common Window Functions

1. Bartlett-(Triangular) Window

$$\phi_w(x) = \begin{cases} 1 - \dfrac{|x|}{d}, & \dfrac{|x|}{d} \le 1 \\ 0 & \dfrac{|x|}{d} > 1 \end{cases}$$

2. Generalized Cosine Window

$$\phi_w(x) = \begin{cases} a - b\cos\left(2\pi \dfrac{|x|}{d}\right) + c\cos\left(4\pi \dfrac{|x|}{d}\right), & \dfrac{|x|}{d} \le 1 \\ 0, & \dfrac{|x|}{d} > 1 \end{cases}$$

Window	a	b	c
Rectangular	1.0	0.0	0.0
Hanning	0.5	0.5	0.0
Hamming	0.54	0.46	0.0
Blackman	0.42	0.50	0.08

3. Kaiser Window

$$\phi_w(x) = \begin{cases} \dfrac{I_o\left(\beta\sqrt{1 - 2\dfrac{x}{d}}\right)}{I_o(\beta)}, & \dfrac{|x|}{d} \le 1 \\ 0, & \dfrac{|x|}{d} > 1 \end{cases}$$

4. Trigonometric Window

$$\phi_w(x) = \begin{cases} \dfrac{\pi \dfrac{x}{d}}{2\tan\left(\dfrac{\pi x}{2d}\right)}, & \dfrac{|x|}{d} \le 1 \\ 0, & \dfrac{|x|}{d} > 1 \end{cases}$$

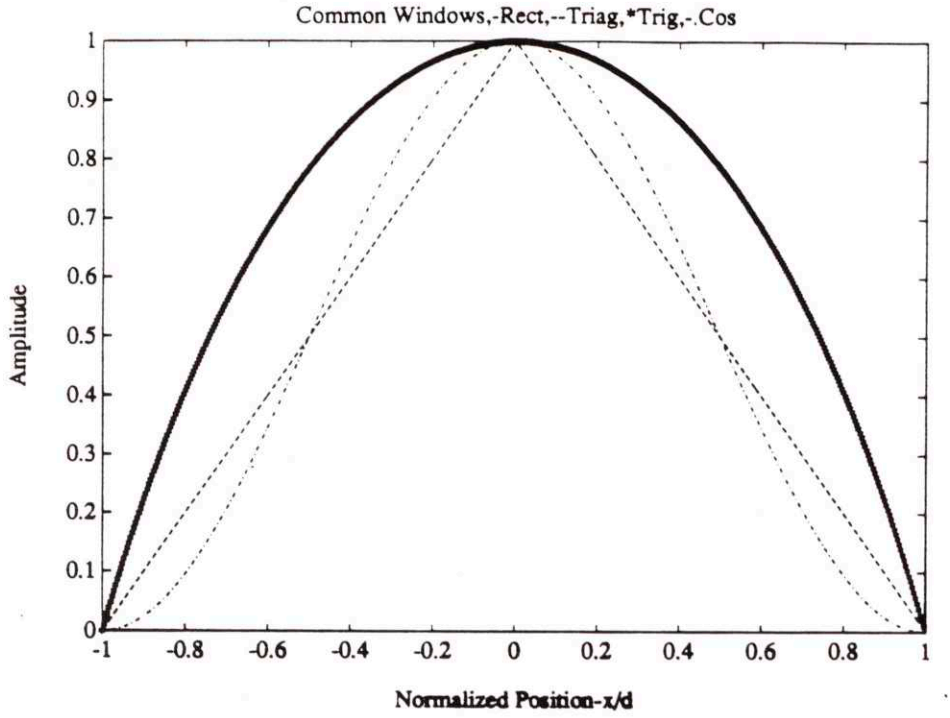

Figure 4.5: Common Windows -(Spatial Domain)

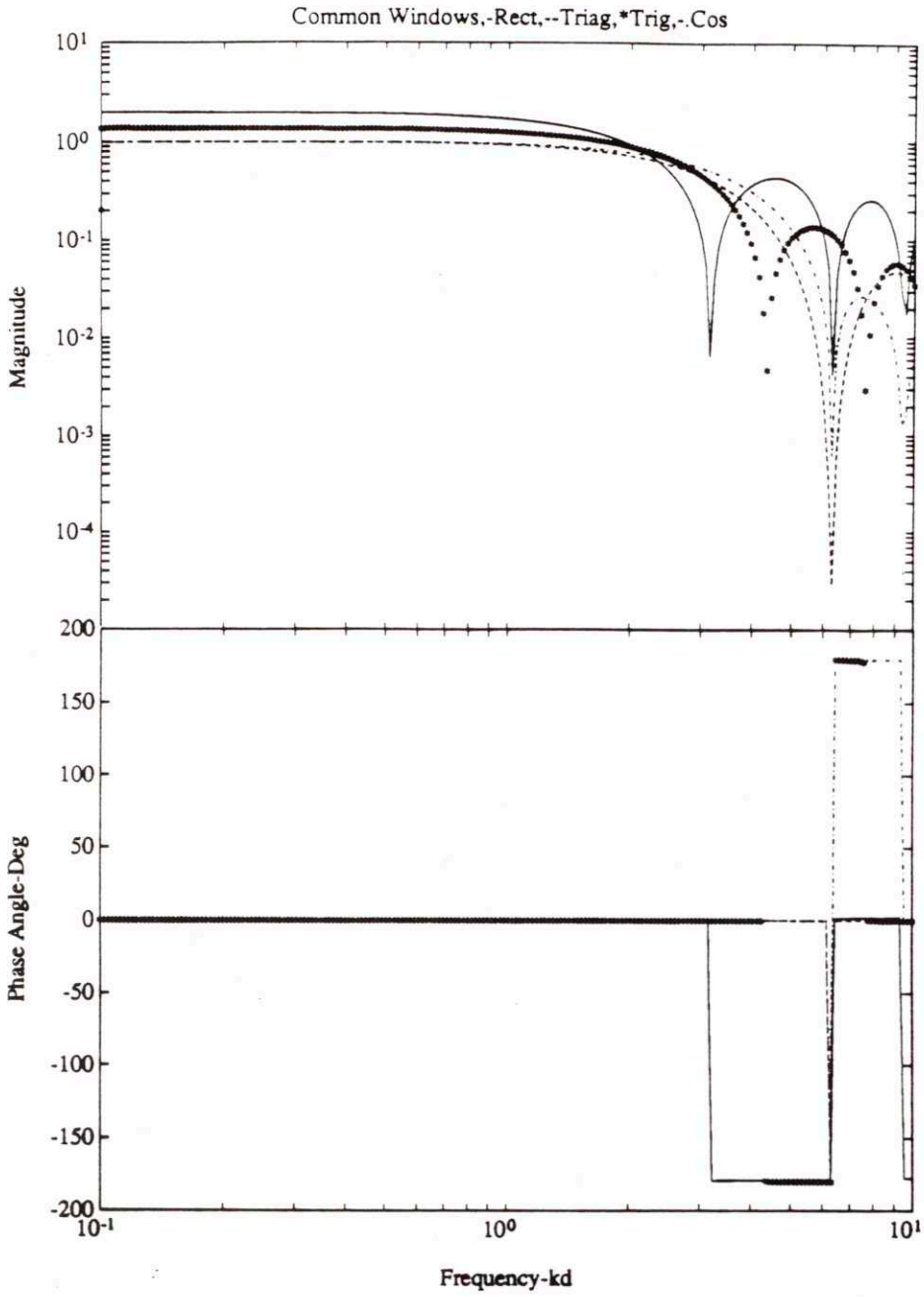

Figure 4.5-cont: Common Windows-(Frequency Domain)

4.5.2 Optimal Finite Length Filters

The design of truncated filters by the windowing method is fairly ad-hoc and requires trial and error for a particular interpolation function. An alternative to truncating the spatial extent arbitrarily might be to design optimal filters based on knowledge of frequency domain properties over a certain range of values-(See Figure 4.6). The idea is to minimize the difference between some ideal frequency response and some approximated response. This procedure follows directly from the digital signal processing literature on the optimal design of Finite Impusle Response-(FIR) filters for discrete sequence of finite length N. Here the frequency properties of the filter can be divided into various regions as defined in Figure 4.6.

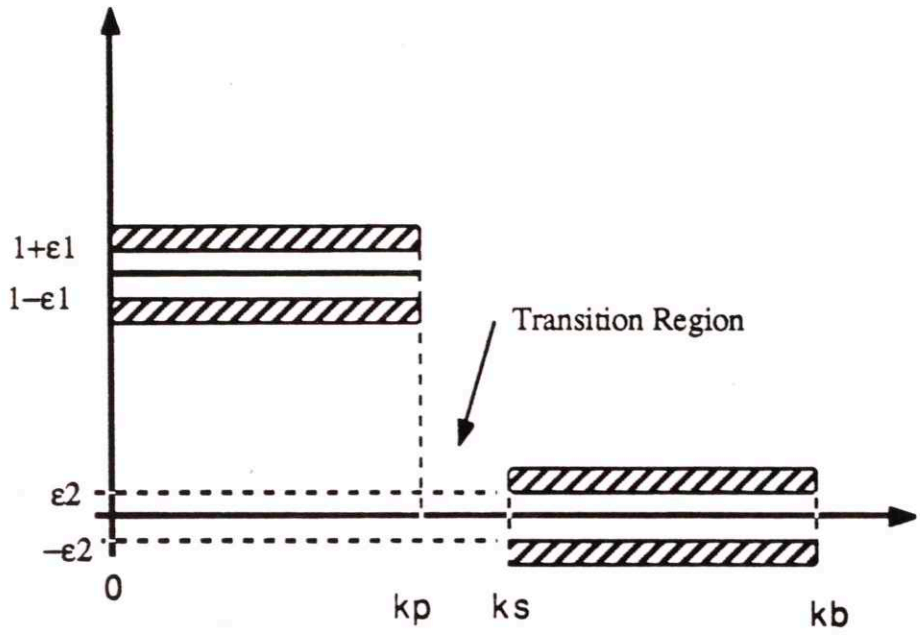

Figure 4.6: Frequency Regions used to Characterize Optimal Filter DesignParameters-(Phase Characteristics Not Included).

In the window method a least squares solution was obtained for minimizing the error between $\Phi_t(k)$ and $\Phi(k)$ over the range $|k|<k_b$. However, this approach does not always perform well near discontinuities. Better results might be possible by formulating the optimal filter problem in terms of a min/max optimization.

Lets define the error $E(k)$ between the ideal filter and its approximation as

$$E(k) = W(k)\left(\Phi(k) - \Phi_t(k)\right) \tag{4.45}$$

where $W(k)$ is the weighting function which incorporates tolerances ε_1 and ε_2 into the filter design. If the frequency response is defined on the closed sub-intervals $(0 \le k \le k_b$ and $k_s \le k \le k_f)$ then the optimal min/max optimization problem can be formulated as

$$\min_{\phi(x)} \left(\max_{k \in G} (E(k)) \right) \tag{4.46}$$

where G defines the subset of closed intervals contained in $0<k<k_f$ and N is the max length of a discrete filter. The solution to this optimization problem was given by Parks and McCllenan-[84] who also developed an algorithm for solving for the optimal filter coefficients for a Chebyshev Approximation leading to what they call the equiripple filter. Details can be found in several texts on digital signal processing-[83,84,86].

4.6 Wave Sensor Performance in Finite Structures

The infinite interpolated responses given in equation-(*4.20*) and (*4.30*) will be corrupted with resonant dynamics when the distributed sensors are placed on a finite structure subject to external loading and structural boundaries. Therefore, depending on what sensor weighting pattern is used, computed transfer functions from distributed sensor output to external excitation might have zero locations, and magnitude and phase properties that are much different than their point measurement counterparts.

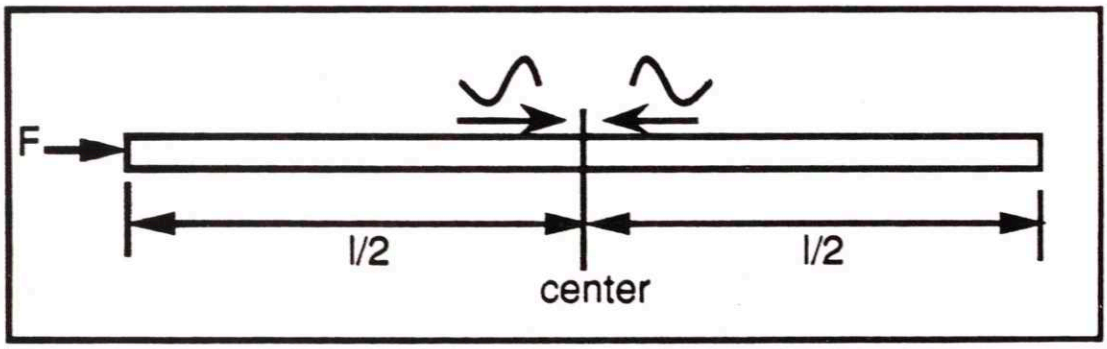

Figure 4.7: Finite Longitudinal Rod of length l with Free Boundary Conditions and External Forcing Applied at Left End.

$$\frac{v(\omega)}{f(\omega)} = -\int_{-d}^{d} \frac{ikw_{rp}(0,\omega)}{f(\omega)} \phi_t(x') e^{-ikx'} dx' + \int_{-d}^{d} \frac{ikw_{lp}(0,\omega)}{f(\omega)} \phi_t(x') e^{ikx'} dx'$$

$$= \frac{1}{EA} \left\{ \frac{-\int_{-d}^{d} \xi \phi_t(x') e^{-ikx'} dx' + \int_{-d}^{d} \xi^3 \phi_t(x') e^{ikx'} dx'}{(1-\xi^4)} \right\};$$

$$\xi = e^{-ik\frac{l}{2}} \qquad k \in [-k_b, k_b] \tag{4.47}$$

and

$$\frac{u'(\omega)}{f(\omega)} = ik\left(\frac{-w_{rp}(0,\omega)}{f(\omega)} + \frac{w'_{lp}(0,\omega)}{f(\omega)}\right) = \frac{-\xi}{EA(1-\xi^4)} + \frac{\xi^3}{EA(1-\xi^4)}$$

$$= \frac{1}{EA}\left\{\frac{-\xi}{(1+\xi^2)}\right\} \tag{4.48}$$

These transfer functions are plotted in Figure 4.9 from *0.1* to *100 kHz*. The solid and dashed-dotted curves in this figure correspond to the distributed and point transfer functions respectively. Notice that the properties of the distributed sensor displays the anticipated differentiator trend along with a smooth roll-off near *20.8 kHz*. In addition, this transfer function illustrates the effect that the odd interpolant has on the location of the zeros in the system. Because the centerline of the distributed sensor is located exactly at the midpoint of the rod, zero dynamics exactly cancel every odd mode of the structure. The point sensor transfer function exhibits pole zero cancellation of every even mode of the structure. As a result of unique sensor placement no zero dynamics appear in either transfer function. Nevertheless, these two signals can still be used for strain wave-mode estimates by applying observation scheme of equation-(*4.22*). This decoupling process leads to the following estimates for the rightward and leftward strain wave-mode amplitude transfer functions.

$$\begin{bmatrix} \frac{\hat{\varepsilon}_{rp}(\omega)}{f(\omega)} \\ \frac{\hat{\varepsilon}_{rp}(\omega)}{f(\omega)} \end{bmatrix} = F(\omega) \begin{bmatrix} \frac{u'(\omega)}{f(\omega)} \\ \frac{v(\omega)}{f(\omega)} \end{bmatrix}$$

To illustrate the accuracy of this filtering in the absence of noise and model uncertainty, Figure 4.10 compares transfer functions of the estimated rightward strain wave-mode amplitude and the ideal in frequency range from *0.1* to *100 kHz*. As expected there is close agreement up to the *15 kHz*. Between *15* and *30 kHz* a transition region exists

Table 4.2 Properties of an Aluminum Rod

Parameter	EA	ρA	l	2d
Value	1,060	0.27	5.0	1
Units	N-m^2	kg/m	m	m

4.6.1 Longitudinal Rod:

Consider the Free-Free rod depicted in Figure 4.7 of length l subject to a broadband disturbance input $f(\omega)$ applied to the left end of the member. Such an excitation generates propagating stress waves which travel away from the left end. These stress waves traverse the length of the member and subsequently reflect at the right free end. In this manner incident and reflected dynamics are superposed leading to a resonant cavity. For steady-state excitation this process continues indefinitely with equal amounts of energy flowing in both directions along the member.

If strain wave amplitudes are desired the scheme outlined in section-4.4 can be followed exactly with the only difference being that the rightward and leftward strain wave-mode amplitudes will be correlated. Therefore, in the specific case of a rod with physical properties defined in Table 4.2 the truncated interpolant-$\phi_t(x)$ required for strain wave-mode filtering is plotted in Figure 4.8(a) and corresponds to a band limited spatial differentiator with cutoff frequency $k_b=8\pi\text{--}(\omega_b=20.8\ kHz)$. The truncated form of this interpolant was obtained by multiplying the infinite interpolant in equation-(*4.20*) by a smooth Kaiser window of length-$(2d=1m)$. This operation leads to the magnitude properties shown in Figure 4.8(b) where near ω_b the magnitude rolls-off ~100 db/decade. The dashed line is this figure corresponds to the magnitude properties of an ideal spatial differentiator. Notice that below *10 kHz* there is good agreement between the ideal and band-limited differentiator.

Now transfer functions from excitations to response of both the point and distributed sensor can be found. Assuming that these two sensors are positioned halfway $(x_c=l/2)$ between each free end their transfer functions can be computed from

where the magnitude and phase properties are not well matched. Beyond *30 kHz*, however, the estimated rightward strain wave-mode transfer function approaches half the magnitude of point strain transfer function.

The ratio of $\hat{\varepsilon}_{lp}(0,\omega)$ to $\hat{\varepsilon}_{rp}(0,\omega)$ corresponds to the estimated scattering coefficient for the right free end defined by

$$\hat{S}(\omega) = \frac{\hat{\varepsilon}_{lp}(\omega)}{\hat{\varepsilon}_{rp}(\omega)} \tag{4.49}$$

This transfer function is plotted in Figure 4.11 where the difference between the ideal and estimated scattering coefficient is due to the assumed *0.1%* structural damping in the system. Again beyond *15 kHz* the scattering coefficient is not well defined since the distributed sensor response approaches zero. The phase plot shows how the leftward wave dynamics lags behind that of its rightward counterpart. The only difference occurs in the phase since the with a transition region occurring between *15* and *30 kHz*.

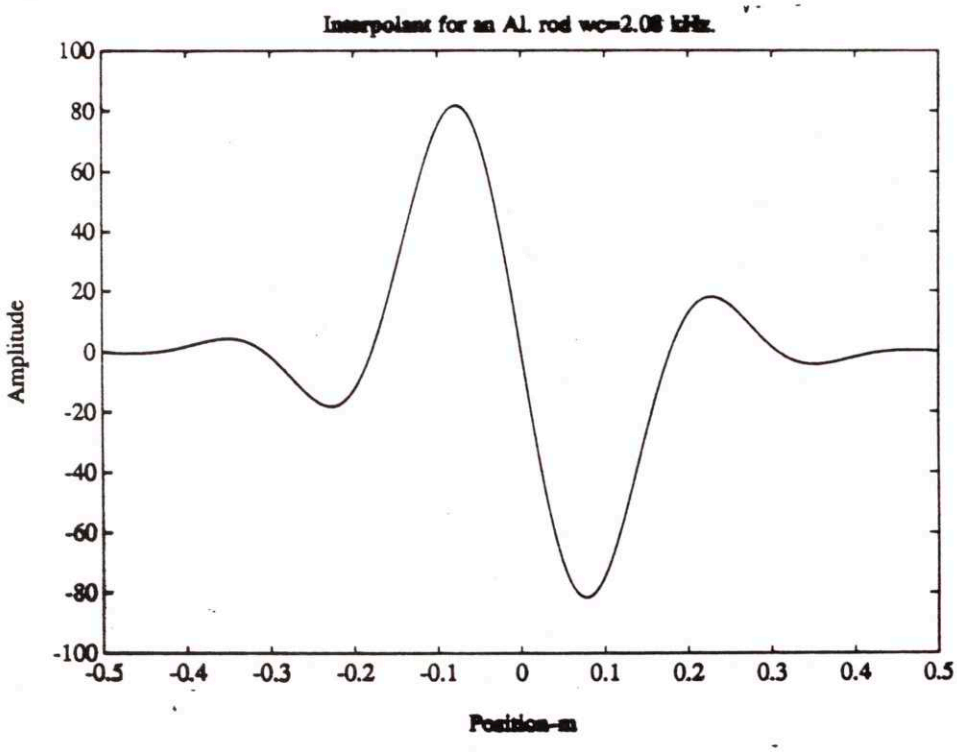

Figure 4.8: Properties of Truncated Interpolant $\phi_n(x)$: (a) Spatial Domain

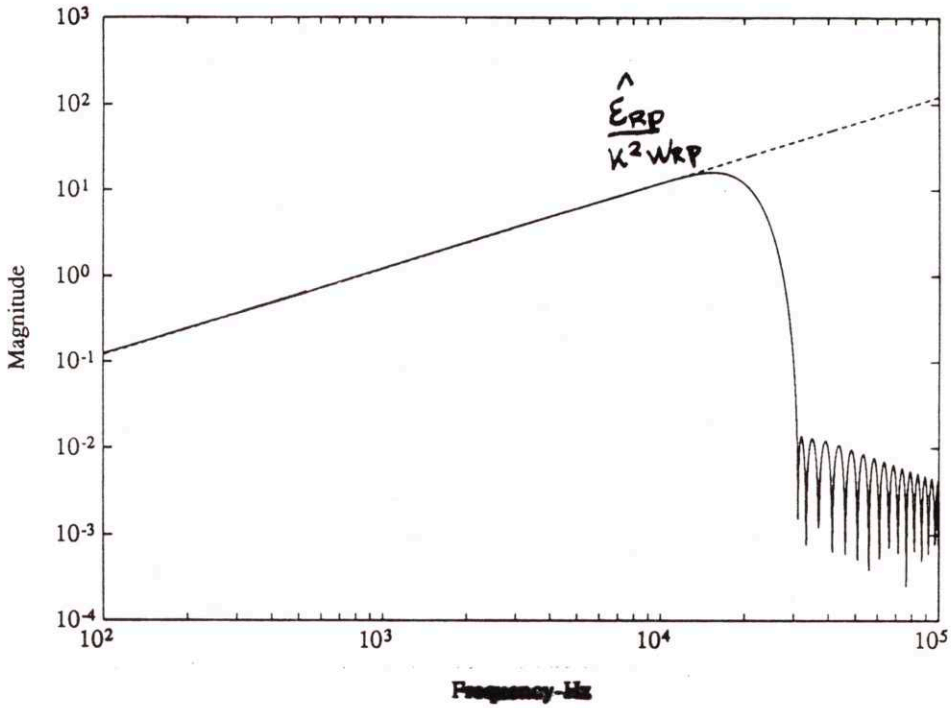

Figure 4.8: Properties of Truncated Interpolant $\phi_t(x)$: (b) Transform Domain

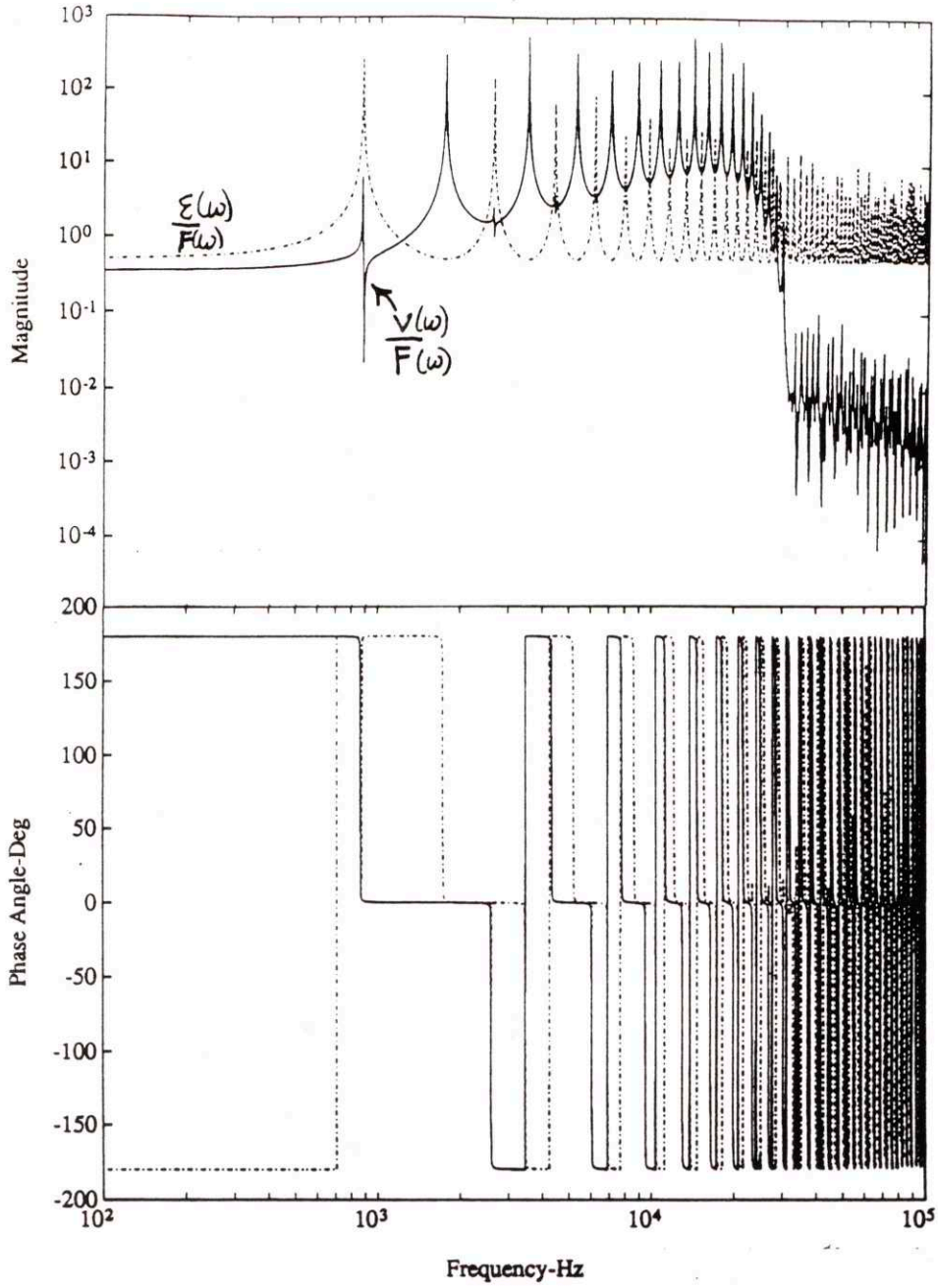

Figure 4.9: **Magnitude and Phase of Distributed and Point Strain Sensor Transfer Functions of equations-(*4.47*) and (*4.48*).**

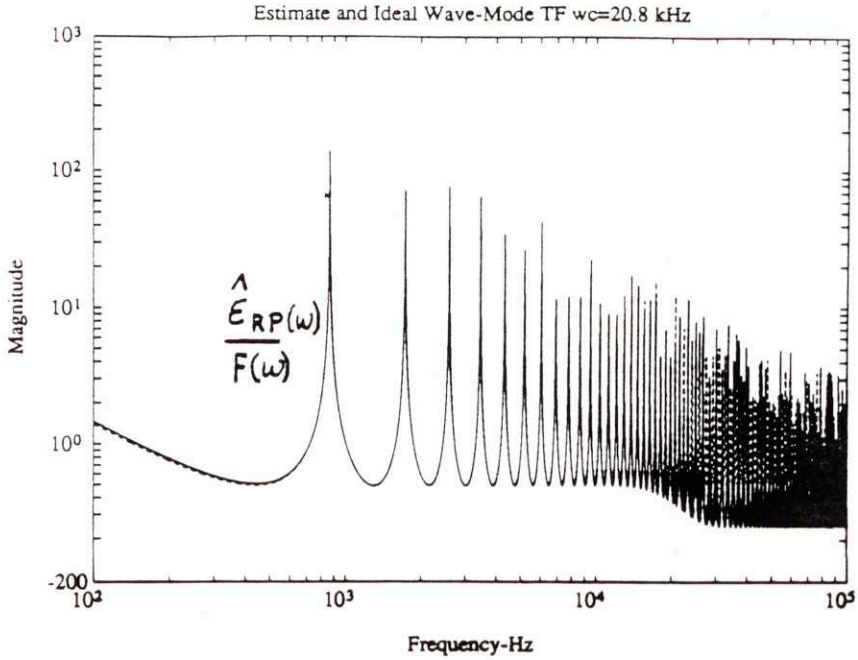

Figure 4.10: Magnitude Comparison of the Estimated-(solid) and Ideal-(dashed) Propagting Strain Wave-Mode Transfer Functions.

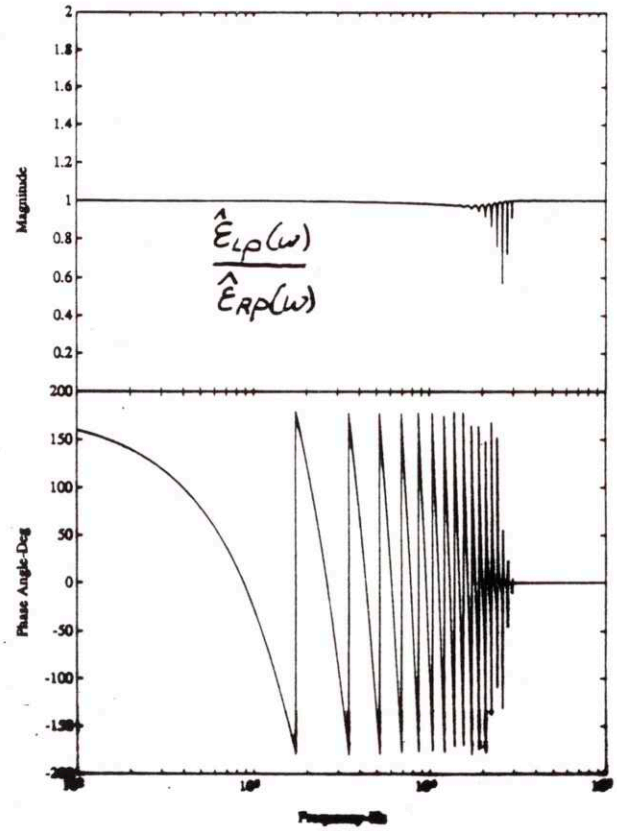

Figure 4.11: Magnitude and Phase of Reflection Coefficient for the right free end of the Rod using estimated strain-wave mode amplitudes.

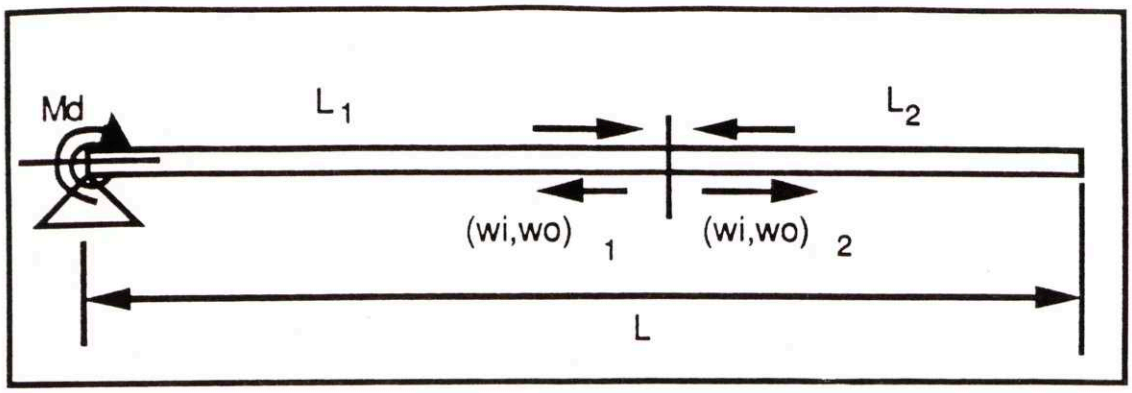

Figure 4.12: A Pinned-Free B-E Beam of length l with collocated point and distributed sensors positioned a distance l_1 from the pinned end. An external moment-M drives the response.

Table 4.3 Properties of a Brass Beam

Parameter	EI	ρA	l	l_1	l_2	2d	t_b
Value	31.1	2.85	7.32	4.77	2.55	2	0.10
Units	N-m^2	kg/m	m	m	m	m	m

4.6.2 B-E Beam

Figure 4.14 depicts a beam of length l which has both a distributed piezofilm sensor of length $2d$ and a point sensor positioned a distance l_1 from the pinned end. At the pinned end an external moment provides a broadband disturbance input which excites the resonant dynamics of the member. Therefore, if a B-E model is assumed for the dynamics, the moment applied at the pinned end will generate both propagating and near field terms emanating away from the point of excitation. As pointed out earlier the presence of these near-field terms makes wave filtering difficult since near structural discontinuities propagating components can scatter and generate near field wave dynamics. However, if measurements are taken sufficiently far way from structural discontinuities s.t. the near field terms will contribute negligibly to the response.

To illustrate this point lets consider a specific example where the parameters characterizing a pinned-free brass beam are given in Table 4.3. Now suppose that

rightward and leftward strain wave responses are desired up to a frequency of *2 kHz*. Applying the filtering concepts outlined for an infinite structure the interpolant which yields non-causal properties necessary for wave filtering must be truncated to a length $2d<<l_1,l_2$. As in the case of the rod this can be achieved smoothly by multiplying the infinite interpolant in equation-(*4.30*) by a window function which truncates the spatial extent of the sensor to a length 2d=*2 m*.. A Kaiser window achieves this end, resulting in the truncated interpolant $\phi_t(x)$ depicted in Figure 4.13a where the cutoff wavenumber-$k_b=20\pi m^{-1}$-*(~2kHz)*. Unfortunately, the truncation of the spatial domain is at the expense of poor magnitude-(See Figure 4.13b) properties at low frequency where the wavelength is comparable to the sensor length-*(ω<10 Hz)*. This can be attributed to a discontinuity in the magnitude of the interpolant at $k=0$. Good agreement with the ideal (dashed curve) magnitude curve is achieved between *30 Hz* and *2kHz*. The phase angle of the interpolant exhibits better behaviour with *90* degrees being maintained up to $k_b=20\pi m^{-1}$. However, beyond this point uncertainty in the phase results in *180* degree phase flips.

The following transfer function relating external moment-$M(\omega)$ to distributed sensor output $v(\omega)$ is

$$\frac{v(\omega)}{M(\omega)} = \frac{t_b}{2}k^2 \int_{-d}^{d} \phi_t(x')\left(\frac{w_{rp}(0,\omega)}{M(\omega)}e^{-ikx'} - \frac{w_{re}(0,\omega)}{M(\omega)}e^{-kx'} + \frac{w_{lp}(0,\omega)}{M(\omega)}e^{ikx'} - \frac{w_{le}(0,\omega)}{M(\omega)}e^{kx'}\right)dx'$$

$$= \int_{-d}^{d} \left[\frac{t_b}{2}k^2 \quad \frac{-t_b}{2}k^2\right] A^{-1}\left(\xi_1\Psi_1\begin{bmatrix}0\\1\end{bmatrix}\phi_t(x')e^{-ikx'} + \xi_1\xi_2 S_2 \xi_2 \Psi_1\begin{bmatrix}0\\1\end{bmatrix}\phi_t(x')e^{ikx'}\right)dx', \qquad k \in [-k_b, k_b]$$

(4.50)

where

$$A = (I - \xi_1 S_1 \xi_1 \xi_2 S_2 \xi_2)$$

$$\xi_1 = \begin{bmatrix} e^{-ikl_1} & 0 \\ 0 & e^{-kl_1} \end{bmatrix}; \quad \xi_2 = \begin{bmatrix} e^{-ikl_2} & 0 \\ 0 & e^{-kl_2} \end{bmatrix}; \quad \Psi_1 = \frac{1}{EIk^2}\begin{bmatrix} k^2 & -1 \\ k^2 & 1 \end{bmatrix}$$

$$S_1 = \begin{bmatrix} -1 & 0 \\ 0 & -1 \end{bmatrix}; \quad S_2 = \begin{bmatrix} -i & 1+i \\ 1+i & i \end{bmatrix}; \quad i = \sqrt{-1} \qquad (4.51)$$

Similarly, the response of a point strain sensor collocated with the center of the distributed strain sensor at $x=l_1$ can be computed from

$$\frac{\varepsilon(\omega)}{M(\omega)} = [\frac{t_b}{2}k^2 \; 0\;]A^{-1}\left\{\xi_1\Psi_1\begin{bmatrix}0\\1\end{bmatrix} + \xi_1\xi_2 S_2 \xi_2\Psi_1\begin{bmatrix}0\\1\end{bmatrix}\right\} \tag{4.52}$$

These two transfer functions are plotted in Figure 4.14 as the solid-(distributed) and dashed-dotted-(point) curves respectively. As expected the poles of both transfer functions are identical. The zeros on the other hand occur at different locations in each transfer function. For the point sensor the zeros fall between the pole locations whereas in the distributed transfer function the zeros fall exactly at every *(3m+2; m=0,1,2,3...)* mode causing pole-zero cancellation of these dynamics. This is especially true at high frequency-*(ω>10 Hz)*. The distributed sensor transfer function also displays the magnitude trend imparted by the truncated interpolant where between *20Hz* and *1kHz* the magnitude appears to increase at a rate of *20 db/decade*. Below this range the magnitude properties of the distributed transfer function are not nearly as well defined. This is partly due to the truncation of the interpolant and also to the presence of near-field terms in the low frequency regime.

4.6.2.1 Rejection of Near-Field Terms

The question arises as to how much these near-field terms contribute to the point and distributed sensor transfer function and beyond what frequency can these contributions be considered negligible. One possible way for determining the limiting effect of near-field components is to compare the ratio of the magnitude of the near-field terms to the propagating terms. If this ratio is less than some arbitrarily specified ceiling say *0.1%* than the near-field terms can be considered negligible. Mathematically this can be represented as

$$\frac{max\left(|w_{re}(\omega)|, |w_{le}(\omega)|\right)}{min\left(|w_{rp}(\omega)|, |w_{lp}(\omega)|\right)} < 0.001 \;\forall\; \omega > \omega_L \tag{4.53}$$

where ω_L corresponds to the limiting frequency beyond which the near-field terms will always remain below the ratio condition of equation-(*4.53*). ω_L will vary according to the parameters in Table 4.3 and the nature of the beam's boundary conditions. For the brass beam in this example the ratio in equation-(*4.53*) can be computed by exposing the wave-nature-(strain-wave-modes) of the point and distributed transfer functions given in equations-(*4.50*) and (*4.51*). Figure 4.15 plots the magnitude of these individual strain wave-mode amplitudes over the frequency range from *0.1* to *1.0 kHz.* for the distributed-(a) and point-(b) sensor transfer functions respectively. In Figure 4.15(a)&(b) the propagating distributed and point strain wave-mode amplitudes

correspond to solid curves with both rightward and leftward superposed on one another. The rightward and leftward near-field strain wave-mode amplitudes are shown as the dashed and dashed-dotted curves respectively in both parts of Figure 4.15. Notice that for both the distributed and point sensor transfer functions, the propagating strain wave-mode components are significantly greater than the near-field terms over most of the frequency range. This is largely due to the exponential decay of the near-field terms with location from the structural discontinuities such as boundaries and point forces. The leftward going near-field term is many orders of magnitude greater than its rightward counterpart. This disparity can be attributed to the coupling of the outgoing leftward near field wave-mode to an incoming-(rightward) propagating strain wave-mode through the scattering matrix-S at the free end. This near-field component, however, is still significantly smaller than the magnitude of the propagating strain wave amplitudes over most of the frequency range. a differentiator. Pictorially, it appears that the criterion in equation-(*4.50*) is met at approximately ω_L=*2 Hz.* which a full decade below where the distributed sensor properties are thought to be well defined. Based on this reasoning the distributed interpolant could be made longer to improve its low frequency magnitude properties that are essential for wave filtering.

4.6.2.2 Filtering of Propagating Components

With the condition in equation-(*4.53*) satisfied in the frequency range from 2 Hz to 2 kHz the point and distributed sensor transfer functions can be used to compute estimates of propagating rightward and leftward strain wave-mode amplitudes as

$$\begin{bmatrix} \dfrac{\hat{\varepsilon}_{rp}(\omega)}{M(\omega)} \\ \dfrac{\hat{\varepsilon}_{lp}(\omega)}{M(\omega)} \end{bmatrix} = F(\omega) \begin{bmatrix} \dfrac{\varepsilon(\omega)}{M(\omega)} \\ \dfrac{v(\omega)}{M(\omega)} \end{bmatrix} \qquad (4.54)$$

in the absence of noise. The magnitude of these estimated-(solid) strain wave-mode transfer functions are compared against the ideal-(dashed) strain wave-mode transfer functions in Figure 4.16. As anticipated the estimates are in close agreement in the range from *(20 Hz to 2 kHz).* However, below this band significant deviations are apparent. The reflection coefficient of the right free-end from these wave estimates is displayed in Figure 4.17.

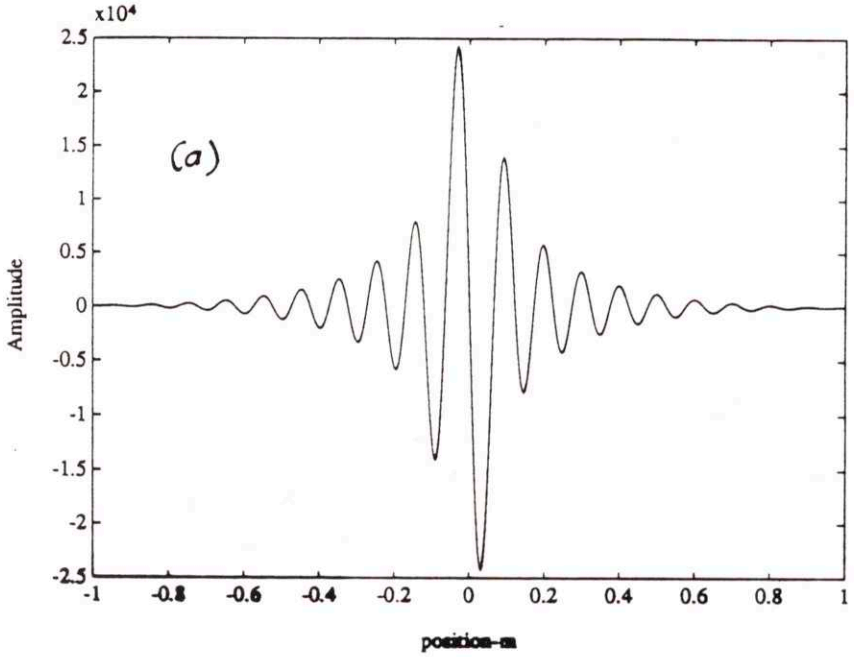

Figure 4.13: Properties of Truncated Interpolant-$\phi^B_d(x)$: (a) Spatial Domain and (b) Transform Domain. Ideal Prediction shown as dashed curve.

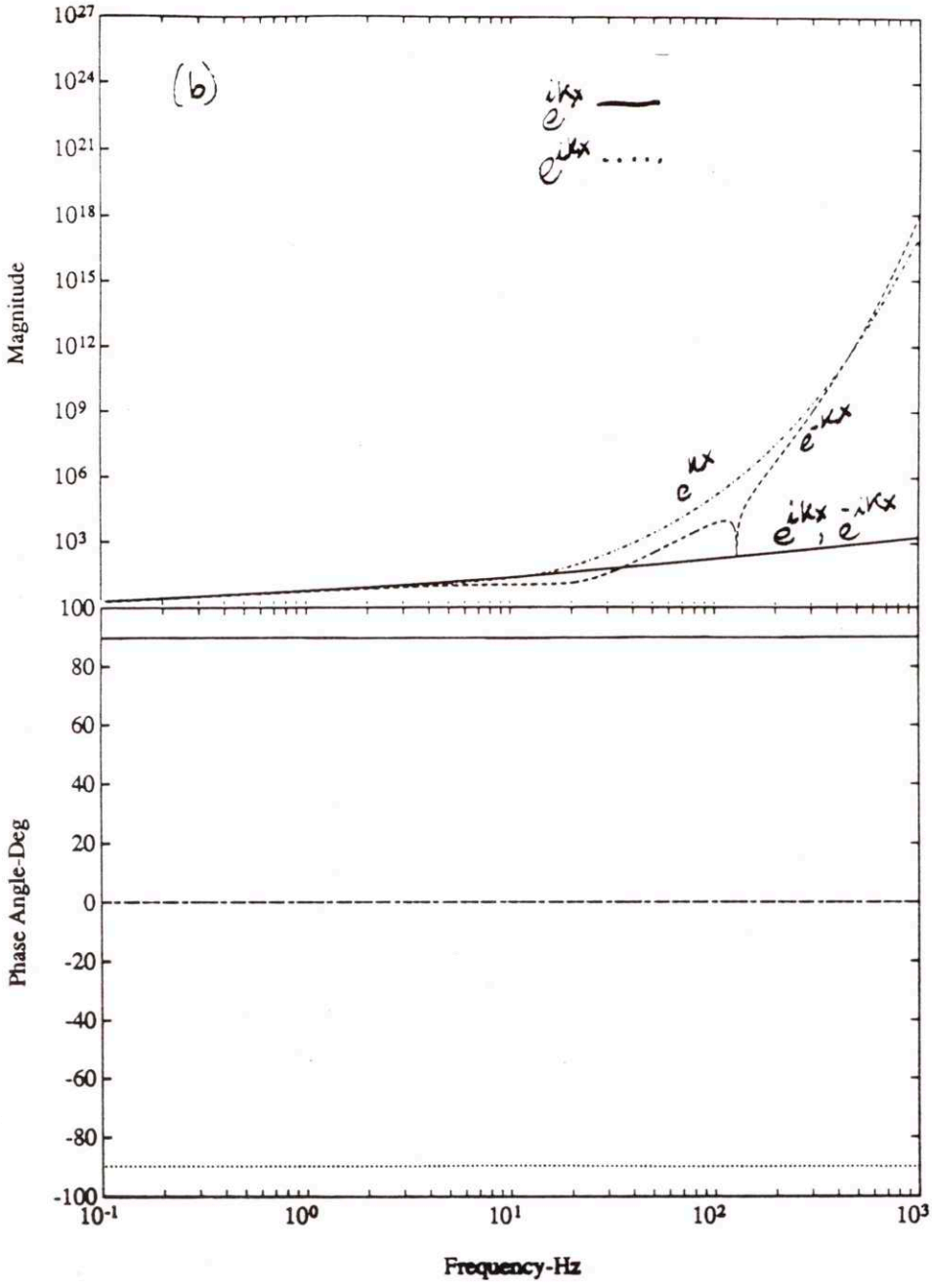
(b)
e^{ikx}
e^{ikx}
e^{kx}
e^{-kx}
e^{ikx}, e^{-ikx}
Magnitude
10^{27}
10^{24}
10^{21}
10^{18}
10^{15}
10^{12}
10^{9}
10^{6}
10^{3}
100
Phase Angle-Deg
80
60
40
20
0
-20
-40
-60
-80
-100
10^{-1}
10^{0}
10^{1}
10^{2}
10^{3}
Frequency-Hz

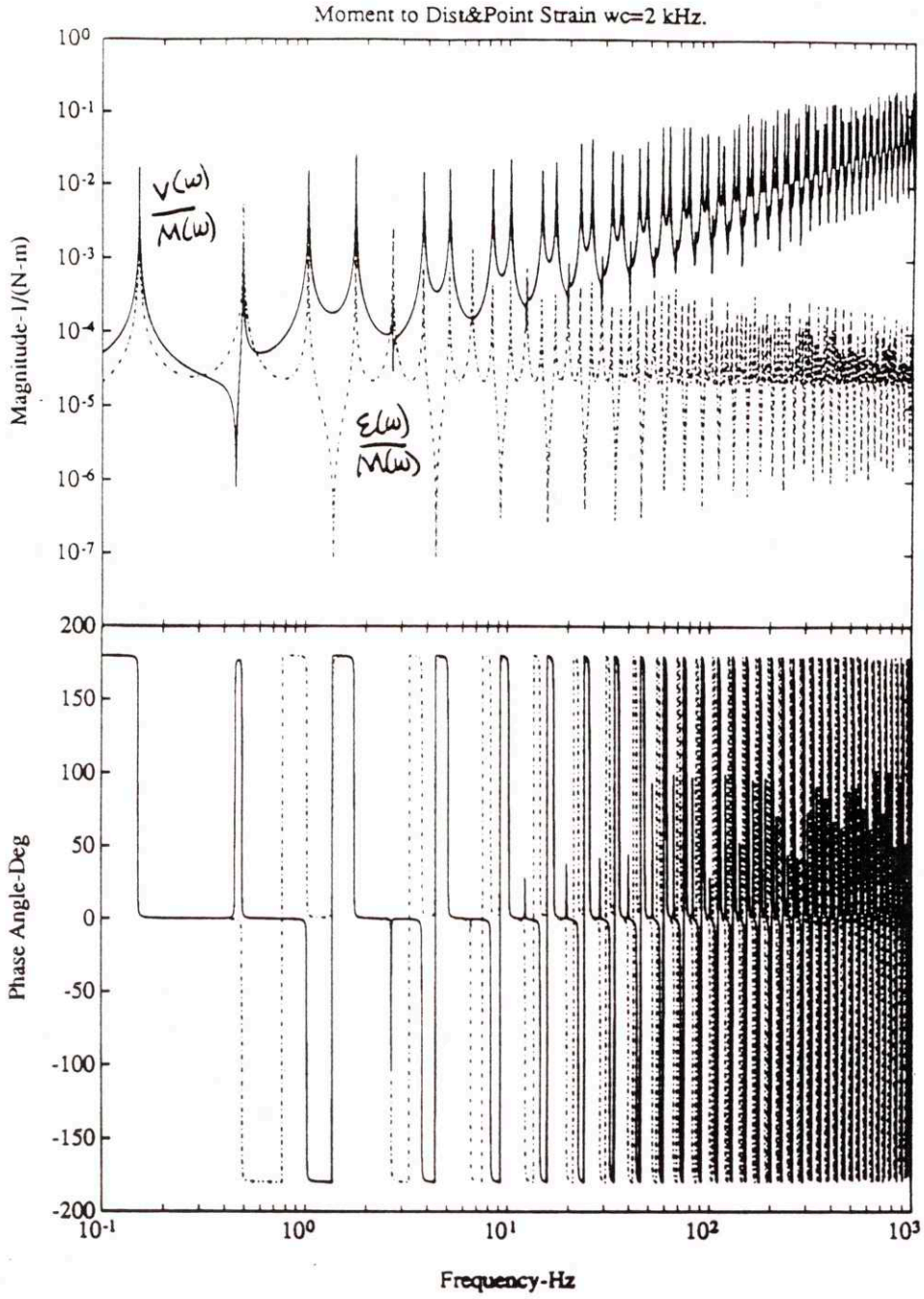

Figure 4.14: Magnitude and Phase of Point-(dashed-dotted) and Distributed-(solid) Strain Sensor Transfer Functions-$k_b=20\pi$ m^{-1}.

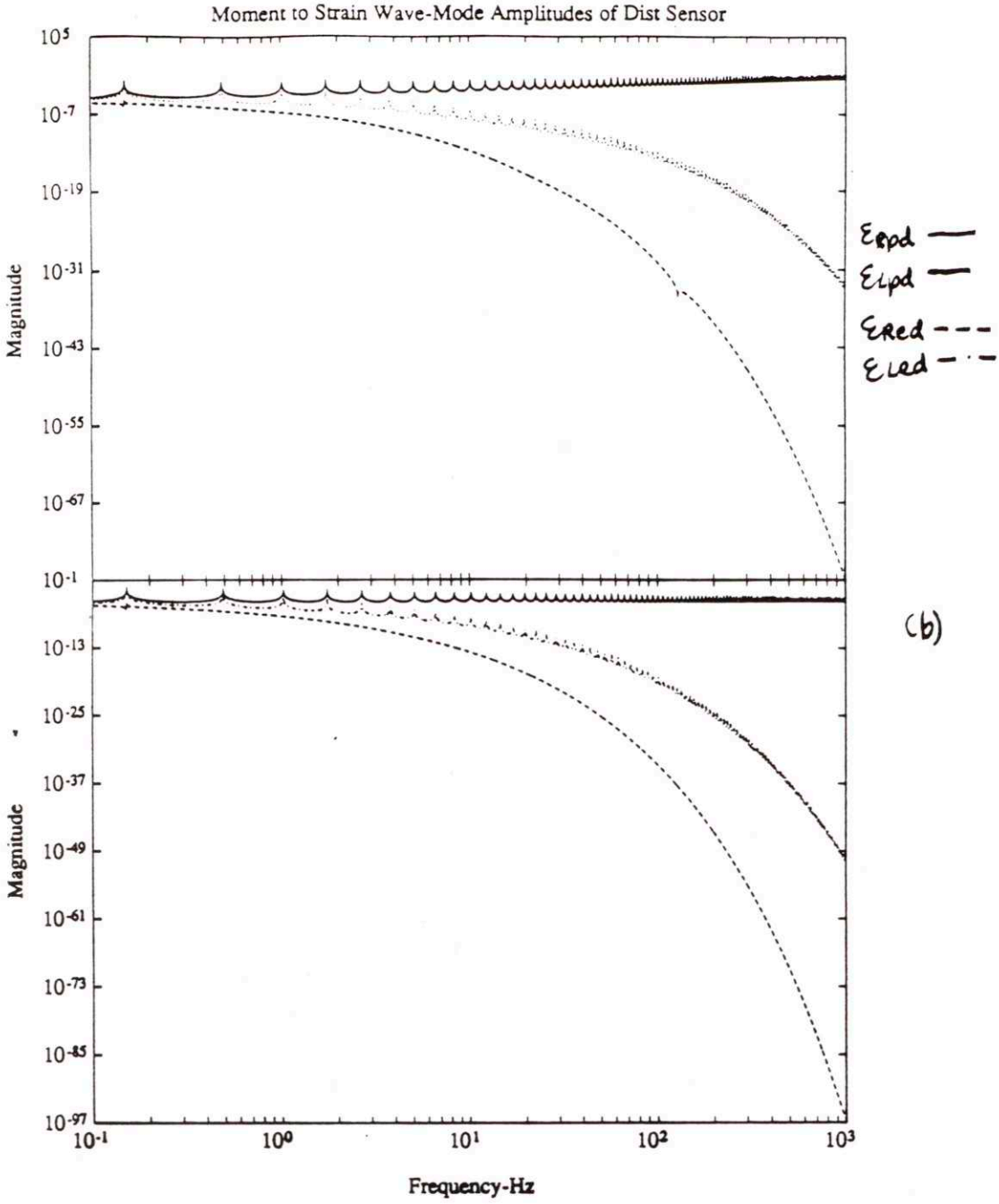

Figure 4.15: Strain Wave-Mode Amplitude Transfer Functions for both the (a)-Distributed-$(\varepsilon_{rpd}, \varepsilon_{red}, \varepsilon_{lpd}, \varepsilon_{led})$ and (b)-Point-$(\varepsilon_{rp}, \varepsilon_{re}, \varepsilon_{lp}, \varepsilon_{le})$ Sensors.

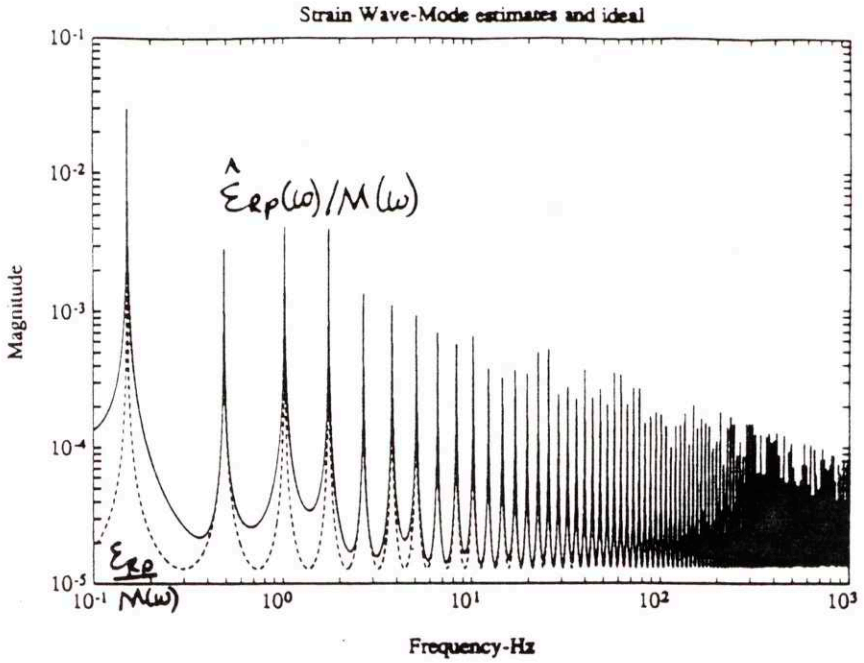

Figure 4.16: Magnitude Comparison of Estimated-(solid) and Ideal-(dashed) Propagating Strain Wave-Mode Amplitudes.

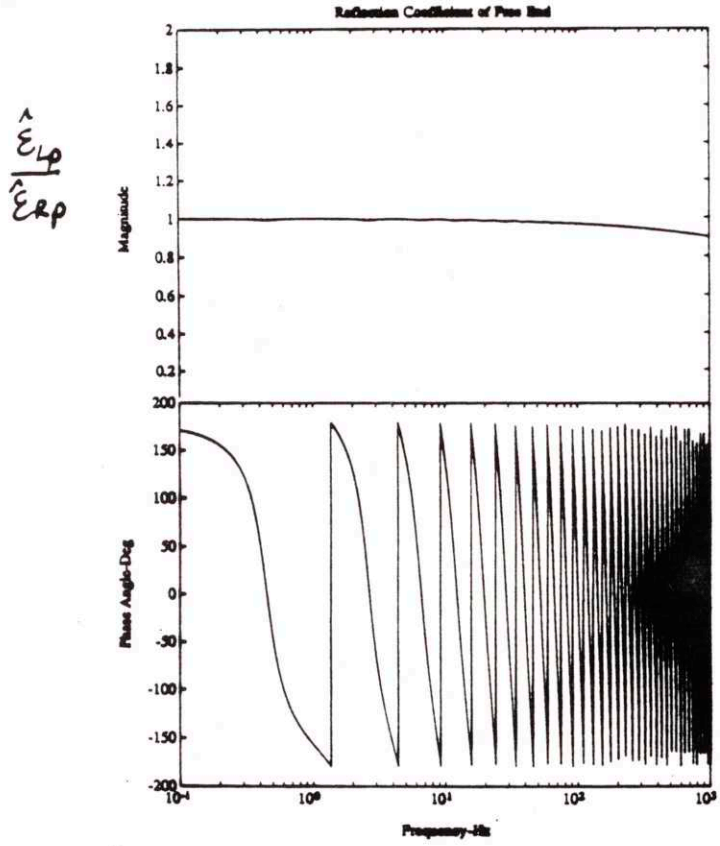

Figure 4.17: Magnitude and Phase of Reflection Coefficient for the right free end of the Rod using estimated strain-wave mode amplitudes.

4.7 Wave Sensor Transfer Function

Because of the assumed form of the solution which is used to infer wave propagation along 1-dimensional structures, an inherent difficulty associated with the decoupling of rightward and leftward wave components is the accuracy of the convolution kernels $\phi_l(x)$ in equations (4.20) and (4.30) which determine the observation matrix $F(\omega)$. It is not clear how accurate the truncated trigonometric interpolants are at realizing the spatial frequency properties required to decouple waves.

The required transfer function from actual wave-modes present to wave-mode estimates delivered by the sensor is given by

$$\hat{\vec{w}}(\omega) = \Lambda(\omega)\vec{w}(\omega) + \vec{n}(\omega) \tag{4.54}$$

where $\Lambda(\omega)$ is the wave sensor transfer function, $\vec{n}$ is the vector of uncorrelated noises, $\vec{w}$ is the vector of actual waves-modes and $\hat{\vec{w}}$ represents the vector of wave sensor estimates. In all of these approaches the wave-modes which are present in a member are inferred from a combination of physical variables and band-limited interpolated signals using a frequency dependent transformation of the form

$$\hat{\vec{w}} = F\vec{y} \tag{4.55}$$

where F is the ideal observation matrix which decouples rightward and leftward waves from their physical measurements. Thus, each approach works by attempting to mimic the band-limited F on a finite structure.

Further the physical measurements-$[u\ v]^T$ are corrupted with noise. This leads to two kinds of imperfections in the approach outlined in this chapter; $\hat{F}$ is not F because of model errors and $\hat{\vec{y}}$ is not $\vec{y}$ because of sensor noise. These imperfections are summarized in the following wave sensor transfer function:

$$\begin{aligned}\hat{\vec{w}}(\omega) &= \hat{F}(\omega)\vec{y}(\omega) \\ &= \hat{F}(\omega)(\vec{y} + \vec{n}) \\ &= \hat{F}(\omega)F^{-1}(\omega)\vec{w} + \hat{F}(\omega)(\vec{n})\end{aligned} \tag{4.56}$$

which defines $\Lambda(\omega)$ and can be thought of as the uncertainty in the wave filtering process. Ideally $\Lambda(\omega)=I$ and the noises $n=0$. But of course in practical systems this is never true. Even in the absence of noise $\Lambda(\omega)$ may still be fully populated as a result of errors in designing the spatial interpolant.

4.8 Summary

This chapter has presented a band-limited Spectral approach for decoupling wave dynamics on 1-D structures using distributed sensors. This approach exploit properties of global interpolation functions to form complex filters that enable directional wave filtering using PVDF film sensor. The distributed nature of such a sensor solves the causality problem which hinders discrete wave filtering techniques outlined earlier in Chapter 3.

Specifically, in the case of a beam whose dynamics are adequately modelled by B-E beam theory, wave filtering is possible far away from structural boundaries where near fields contribute negligibly to the response. This has been demonstrated in the specific case of a pinned-free example. The presence of near-field terms forces the filtering process to be accurate at high frequencies-(including more than 5 modes of the structure). This is in contrast to wave filtering on a rod which is valid for nearly all modes of a structure. The only major drawback is that the frequency content of the interpolant is restricted to lie in a finite frequency band-$[-k_b,k_b]$ introducing possibility of poor performance near this limit.

The next logical step, however, is to verify the approach described in this paper experimentally using similar piezofilm material used by reference-[79]. This work is addressed in Chapter 6.

Chapter 5

Wave Control using Estimated Wave States

5.1 Introduction

Wave Control represents an alternative to the linear control methodologies developed for LTI modal dynamics. Here performance metrics can formulated on a local scale based on the intuitive concept of altering the scattering properties of incoming and outgoing waves at a junction. In chapter 3 a generic junction was depicted in Figure 2.1 for a truss structural joint, however, junctions are not restricted to such configurations and can correspond to any location in a 1-D structural member such as boundaries-(clamped, pinned, free, etc.) or internally at the intersection between two members. Once a junction is established, the input/output relation of the local scattering dynamics can be transformed into incoming and outgoing waves and external disturbances.

$$\vec{w}_o(\omega) = S(\omega)\vec{w}_i(\omega) + \Psi(\omega)\vec{Q}(\omega) \tag{5.1}$$

In this form a host of active control objectives can be stated with most falling into three distinct categories-(See Figure 5.1):

(i) Active Damping

(ii) Active Isolation

(iii) Any mix of (i) and (ii)

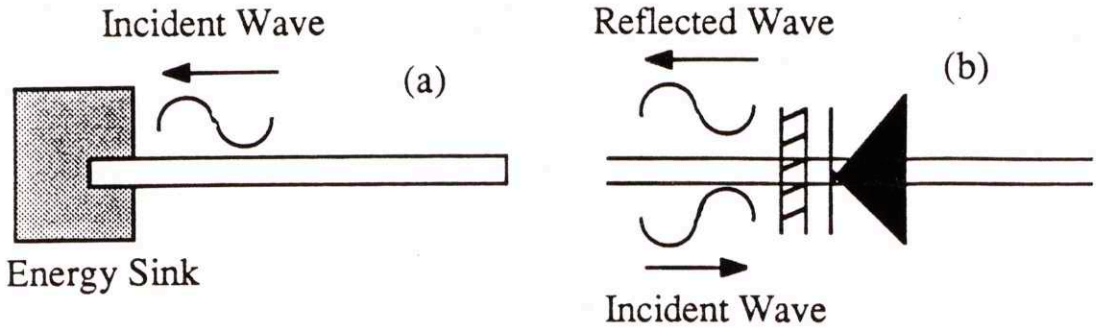

Figure 5.1: Control Objectives: (a) Active Damping-creation of an energy sink. (b) Active Isolation-creations of a structural diode.

Active Isolation refers to the shunting of energy from one particular segment of a 1-D structural member to another location. Essentially, the purpose of this kind of control is to construct a structural diode where disturbances are allowed to flow in only one direction . Thus, no dissipation of energy occurs; a portion of the structure simply becomes isolated from external sources of excitation which enter elsewhere. On the other hand *Active Damping* refers to the extraction of energy from the structure to effectively eliminate its resonant behavior. Compensators which achieve this end are derived by considering power flowing along the member or by artificially constructing matched terminating boundary conditions which attempt to match the impedance at a boundary to absorb incident disturbances. Ideally, if this is achieved the structure acts as if it were spatially infinite. Finally, combining these two control objectives leads to a condition in which a portion of the incident disturbance is prevented from being transported to other parts of the structure while simultaneously having some of its energy absorbed during the process.

In all three cases the form of the compensation is typically written in terms of wave-states in which the control is specified in terms of the feedforward of incoming waves-(See Figure 5.2a). In previous research the lack of availability of this information forced control structure to be recast into an equivalent feedback representation expressed in terms of physical measurements-(See Figure 5.2b).

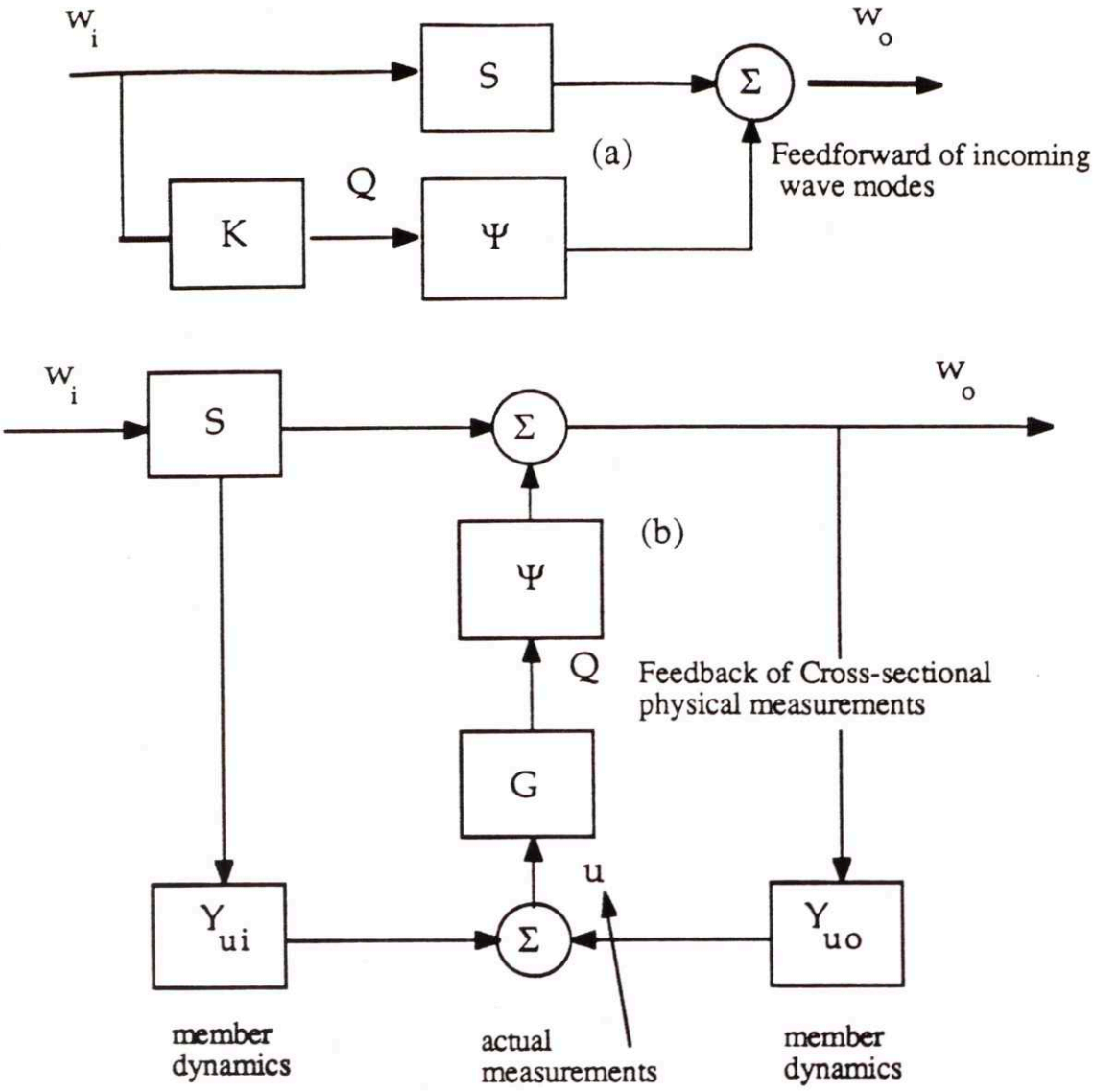

Figure 5.2: Structure of an Feedforward-(a) and Actual Feedback-(b) implementation of a typical Wave Control

Wave control designs may be further complicated by the fact that compensators which achieve active isolation or active damping for dispersive members are typically non-causal. The basic problem with non-causal solutions is that some portion of their singularities lies in the right-hand-part-(RHP) of the Laplace Plane. Singularities in the right-half-plane indicate one of two situations. Either the dynamics are affiliated with a system which is stable in negative time and thus anticipates future information or it corresponds to a dynamics which are unstable in positive time. The former situation is applicable to this work. Non-causal compensators anticipate future information which is otherwise

unavailable in time. In the spatial domain this information is available from the propagation of travelling waves along a structure. Hence,the future response at any point location in a member is given by Fourier Spatial modes which are presently propagating to that location and modes which created a response in the past are presently propagating away from the cross-section. Consequently, future and past temporal information at a point in a member can be interpreted by convolving rightward and leftward spatial wave dynamics which propagate to and from a cross-section-(See Figure 5.3). This approach was exploited in Chapter 4 to perform wave-mode filtering and also will be used to embed a portion of the control in the sensor while simultaneously performing the wave filtering process. Since the sensing is typically non-collocated with respect to the control, it will be necessary to realize phase lags using a digital computer.

This chapter explores wave filtering in conjunction with feedforward control.

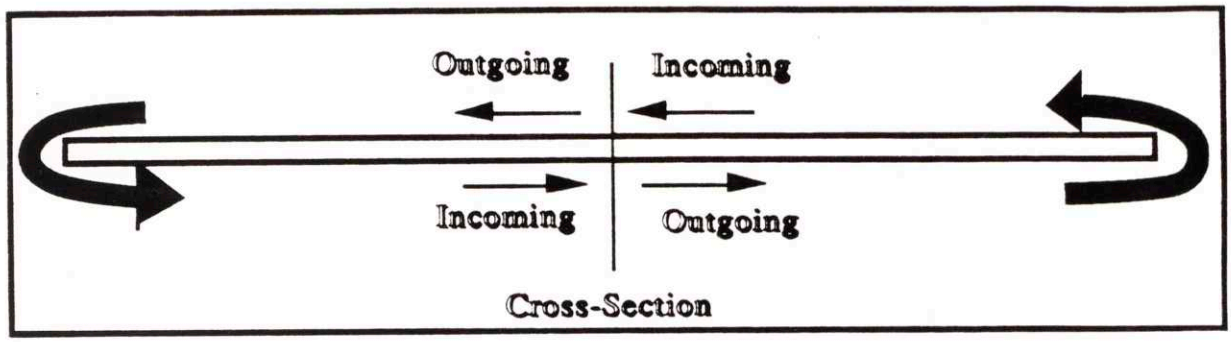

Figure 5.3: Typical 1-D Structural element illustrating how incoming and outgoing waves circumnavigate a structural member creating past, present and future responses at a cross-section in the member.

5.2 Wave Control Loop Architecture

The open loop input/output relation given in equation 5.1 describes how incoming wave-mode amplitudes at a junction are thought to scatter, creating outgoing wave amplitudes. In this relation all the homogeneous dynamics are captured in $S(\omega)$. Non-homogeneous dynamics are contained in $\Psi(\omega)$ where the presence of external forces can alter the properties of outgoing wave-modes. Thus, if the rank of the matrix $\Psi(\omega)$ is equal to the number of different incoming wave-mode mixes than a unique set of forces and moments can be used to achieve any desired control objective. Full specification of the

control is achieved if the number of unique actuator that are available equals the number of incoming wave-modes to the junction.

Assuming that the mix of incoming waves are available for measurement a feedforward form of the control can be written as

$$\vec{Q}(\omega) = K(\omega)\vec{w}_i(\omega) \tag{5.2}$$

where $K(\omega)$ is a matrix compensator. Substituting this expression into equation-(5.2) leads to

$$\begin{aligned}\vec{w}_o(\omega) &= (S(\omega) + \Psi(\omega)K(\omega))\vec{w}_i(\omega) \\ &= S_{cl}(\omega)\vec{w}_i(\omega)\end{aligned} \tag{5.3}$$

Therefore, specifying the elements of $S_{cl}(\omega)$ uniquely determines the necessary compensator required to achieve a particular performance requirement. However, the control in equation requires collocated observation of incoming wave-modes. In previous research this information was not available forcing the compensation to be realized using an equivalent feedback representation given by

$$\vec{Q}(\omega) = G(\omega)\vec{u}_d(\omega) = \tag{5.4}$$

where the vector $\vec{w}_i(\omega)$ of incoming wave-mode amplitudes has been replaced by the vector $\vec{u}_d(\omega)$ of available physical cross-section measurements. Substituting this expression into equation-(5.2) leads to

$$\begin{aligned}\vec{w}_o(\omega) &= S(\omega)\vec{w}_i(\omega) + \Psi(\omega)\vec{Q}(\omega) \\ &= S(\omega)\vec{w}_i(\omega) + \Psi(\omega)G(\omega)\vec{u}_d(\omega)\end{aligned} \tag{5.5}$$

where $\vec{u}_d(\omega)$ connects physical measurements to wave-mode amplitudes. Hence equation-(5.5) reduces to

$$\begin{aligned}\vec{w}_o(\omega) = S_{cl}(\omega) = (I - \Psi(\omega)G(\omega)Y_{uo}(\omega))^{-1} x \\ (S(\omega) + \Psi(\omega)G(\omega)Y_{ui}(\omega))\vec{w}_i(\omega)\end{aligned} \tag{5.6}$$

Solving for $G(\omega)$ leads to the following compensation matrix

$$G(\omega) = \Psi^{-1}(\omega)(S_{cl}(\omega) - S(\omega))(Y_{ui}(\omega) + Y_{uo}(\omega)S_{cl}(\omega)) \tag{5.7}$$

Thus, $G(\omega)$ and $K(\omega)$ are related through

$$G(\omega) = K(\omega)(Y_{ui}(\omega) + Y_{uo}(\omega)S_{cl}(\omega)) \tag{5.8}$$

5.3.0 Wave Control Design

5.3.1 Ad-Hoc Specification

Physical insight and intuition can be used to guide in specifying elements of the closed loop scattering matrix S_{cl} to achieve certain objectives. Such a procedure, however, may require that the number of control actuators equals the number of incoming wave-mode amplitudes to a junction. Assuming this condition is met the elements of S_{cl} can be specified freely with the necessary compensation determined by equation-(*5.9*). One special case corresponds to $S_{cl}=0$ which is referred to as the matched terminating condition-[10] and leads to zero reflection and transmission of incident components.

$$K(\omega) = \Psi^{-1}(\omega)\left(S_{cl}(\omega) - S(\omega)\right) \tag{5.9}$$

5.3.2 Partial Specification

Full specification of the closed-loop scattering matrix is dependent on full observability and controllability of all incoming wave-modes to a junction. More realistically, a reduced set of sensor and/or actuators will make it impossible to achieve full specification of the closed-loop scattering matrix-S_{cl}. This will constrain the number of elements of S_{cl} which can be freely specified leading to only partial specification. Several scenarios arise depending on how many sensor and actuator are available to affect certain elements of S_{cl}. These different scenarios are summarized in reference-[32].

5.3.3 Optimal Power Flow

As an alternative to the ad-hoc method of the previous section, Miller-[32] formulated a power flow approach to design control laws based minimizing the H_2 norm of net power flowing out of a junction. His cost function was written in the frequency domain as a quadratic function of wave-mode states.

$$J(\omega) = \frac{1}{2}E\left\{\int_{-\infty}^{\infty} \vec{w}^{H} P \vec{w} + \vec{Q}^{H} R \vec{Q}\right\} d\omega \tag{5.10}$$

where R is the control penalty matrix, P is the power flow matrix and w is the vector of incoming and outgoing wave states.

Minimization of the functional in equation-(*5.10*) leads to various forms of the optimal compensation matrix $G(\omega)$. Not all of these forms correspond to causal temporal

realizations. In fact the optimal form which achieves the lowest cost corresponds to non-causal compensation.

5.4 Non-collocated Feedforward Control

The causality constraints associated with the collocated control design approaches of the previous section can be overcome by using non-collocated wave sensors and feedforward control. Such a procedure only applies to the propagating components of the response with the near-field terms assumed to contribute negligibly to the response. Therefore, the wave filters developed in chapters 3 and 4 using point and distributed sensors can be used to tailor the response such that the non-causal portion of compensation can be realized along with wave sensing at some point away from the location of the control input into the system. The incoming portion of this signal can then be appropriately delayed to account for the non-collocation of sensor and actuator. Thus, the modified Feedforward Loop structure might take the form shown in Figure 5.4.

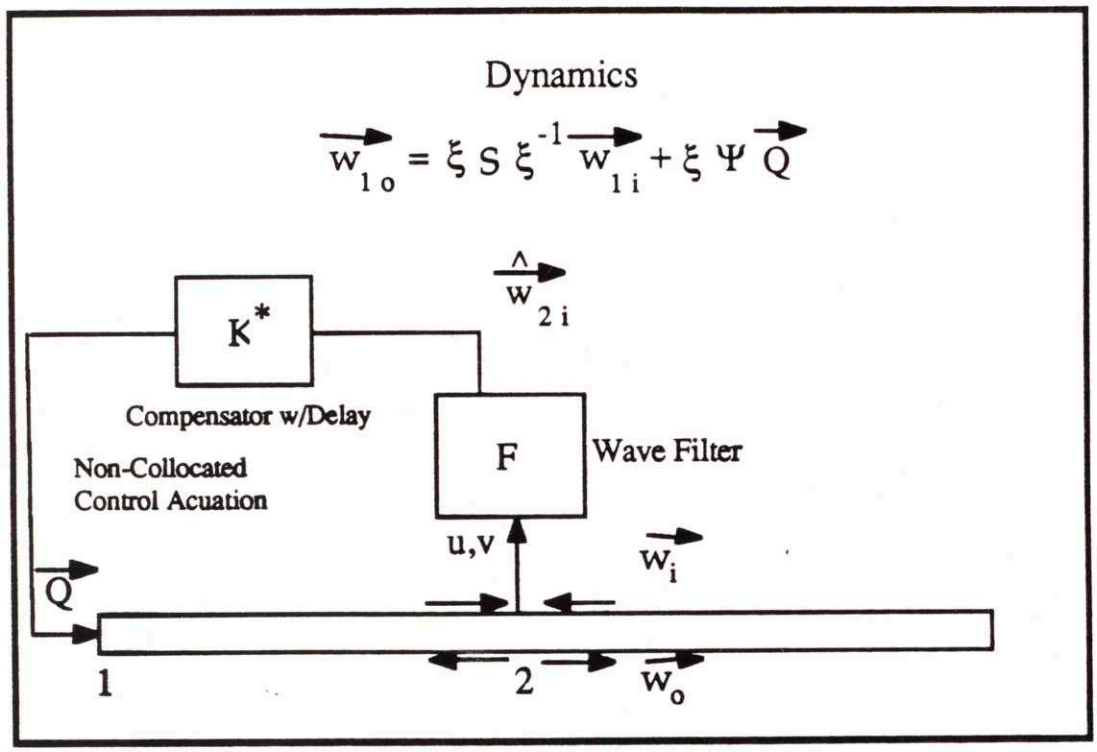

Figure 5.4: Non-collocated Feedforward Wave Control Loop using Estimated Propagating Wave-Mode Amplitudes.

If we combine the wave-filter with the junction input/output relation, we find that

$$\vec{w}_{1o} = S\,\vec{w}_{1i} + \Psi(\omega)K^{*}\,\hat{\vec{w}}_{2i} \tag{5.11}$$

where $\vec{w}_{2i}$ and $\vec{w}_{1i}$ are estimates related through the spatial transition relation which defines the degree of non-collocation between sensor and actuator.

$$\hat{\vec{w}}_{2i} = \xi^{-1}\,\hat{\vec{w}}_{1i} \tag{5.12}$$

Combining equations-(*4.56*) (*5.11*) and (*5.12*) leads to the following closed loop scattering representation

$$\vec{w}_{1o} = S_{cl}\,\vec{w}_{1i} + L_o\left(\Psi K^{*}\,\xi^{-1}F_{11}^{-1}\,\vec{n}_1 + \Psi K^{*}\,\xi^{-1}F_{11}^{-1}\,\vec{n}_2\right) \tag{5.13}$$

where

$$S_{cl} = L_o^{-1}(S + \Psi K\Lambda_{11})$$
$$L_o = (I - \Psi K\Lambda_{12})$$
$$K^{*} = \xi K$$

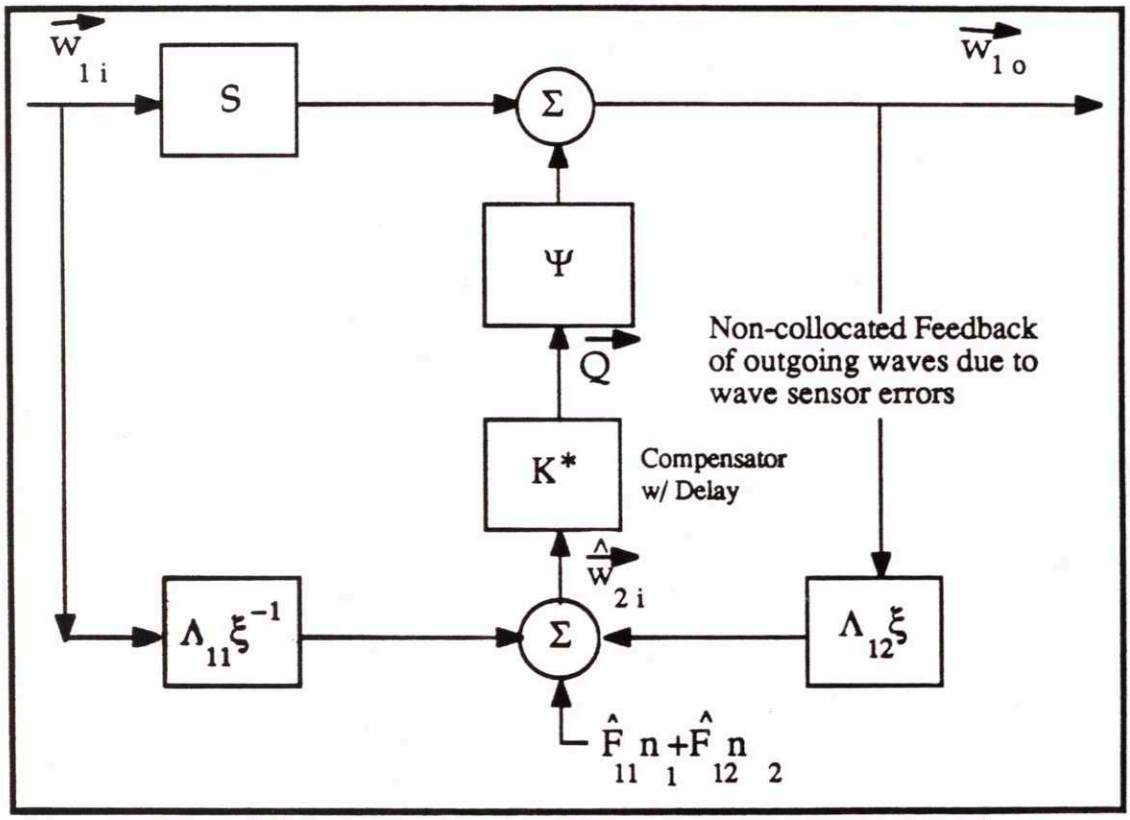

Figure 5.5: Equivalent Loop Structure accounting for Model Uncertainty, Sensor Noise and Non-collocation between Wave-Filter and Control Actuator.

Equation-(*5.13*) accounts for all the possible sources of errors due to modelling uncertainties and noisy sensors. This equation motivates an equivalent loop structure shown in Figure 5.5 which shows the effects of modelling uncertainty, non-collocation and sensor noise.

Ideally, if no modelling uncertainty were present-($\Lambda_{11}=I$, $\Lambda_{12}=0$) equation-(*5.13*) would reduce to

$$\vec{w}_{1o} = (S + \Psi K)\,\vec{w}_{1i} + \left(\Psi K^{*}\,\xi^{-1}\,F_{11}^{-1}\,\vec{n}_1 + \Psi K^{*}\,\xi^{-1}\,F_{11}^{-1}\,\vec{n}_2\right) \qquad (5.14)$$

which has almost the same appearance as equation-(*5.4*) with the exception of the presence of sensor noise. Of course if the spectrum of these noises are well defined then optimal Wiener filters could be designed to pre-filter physical measurements so as to minimize the contribution of sensor noise to wave-mode estimates. Notice that because of the commutivity of the transition matrix ξ the compensation can be embedded in the sensor by placing the matrix K^{*} in the feedforward and feedback paths of Figure 5.4. This leads to Figure 5.6 where now only a phase lag must be realized.

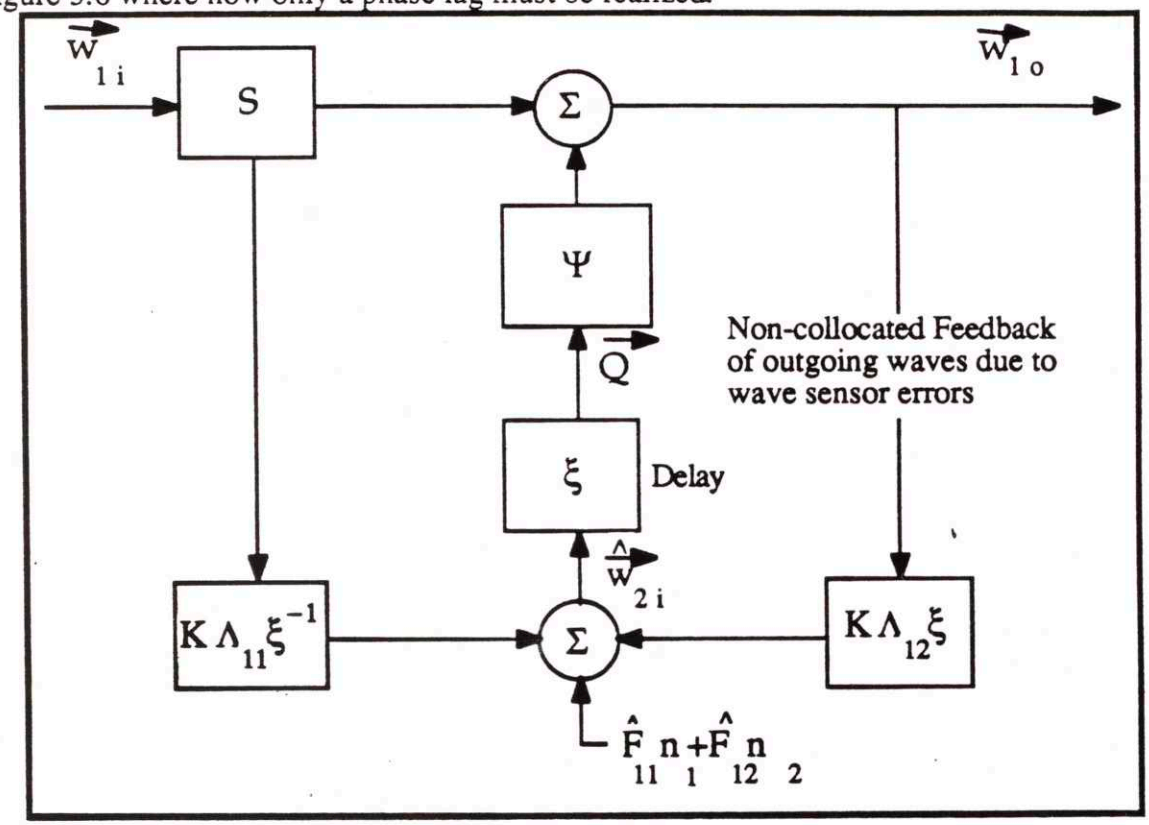

Figure 5.6: Non-collocated Feedforward Control Structure with Compensation Embedded in Wave Sensing.

5.4.1 Realization of Spatial Phase Lag

The non-collocated wave control loop of Figures 5.4-6 requires implementation of a spatial phase lag contained in the transition matrix ξ. The properties of such a frequency dependent lag vary for each 1-d structural element and are dependent on the dispersion relation for the member.

5.4.1.1 Linear Phase Lag-(Rod)

For non-dispersive 1-D structural elements the wavenumber k is proportional to temporal frequency ω. Thus, the phase lag associciated with these members is linear with frequency. Discrete-time signals can represent analog signals exactly at discrete intervals corresponding to multiples of the sampling period-T. Transforming discrete signals to their frequency domain representation requires an operation known as the Z-transform where the Discrete Laplace Transform Variable z is given by

$$z = e^{i\omega T} \tag{5.15}$$

which relates the continuous Laplace vaiable $s=i\omega$ to its discrete equivalent-z. More importantly, this equation has the properties of linear phase necessary to implement spatial phase lags associated with non-dispersive members. Therefore, if the sampling period-T is tuned to

$$T=(1/n)(\rho A/EA)^{(1/2)}L \tag{5.16}$$

then the phase lag necessary for non-collocated control can be realized by the structure shown in Figure 5.7. Ideally, the constant-n in equation (*5.20*) should be 1. But such a specification neglects the dynamics associated with the digital to analog and analog to digital conversion processes. The effects of these processes are usually modelled by the following zero-order-hold-(ZOH) transfer function:

$$H(\omega) = \frac{1 - e^{i\omega T}}{i\omega} \tag{5.17}$$

As a result of these dynamics the transfer function $\hat{w}_{2i}$ -(output of the wave sensor at station 2) and $\hat{w}_{1i}$ (output of the digitally-delayed signal) is given by

$$\frac{\hat{w}_{2i}}{\hat{w}_{1i}} = z^{-n}\left(\frac{1 - e^{-i\omega T}}{i\omega}\right) \tag{5.18}$$

which includes the linear phase term and the dynamics of discrete-time signal processing. Notice that $ZOH(\omega)$ adds both magnitude and phase distortion to the desired phase lag. To

$$\xi_{11}(\omega) = e^{-ik(x_2-x_1)} = e^{-ic\sqrt{\omega}} \tag{5.19}$$

where the difference $(x_2\text{-}x_1)$ characterizes the degree of non-collocation between observation points. Notice that the phase angle of equation (5.25) is given by

$$\angle\xi_{11}(\omega) = \sqrt{\omega}\sqrt[4]{\frac{\rho A}{EI}}(x_2 - x_1) \tag{5.20}$$

which is a non-linear function of frequency-ω. Therefore, because of this non-linear behaviour the phase lag for a dispersive structures do not lend themselves to simple analog approximation; thus causal discrete filters must be used. Again as in the case of the rod the best approach to realize the phase lag using the help of the digital computer where $\xi_{11}(\omega)$ assumes its discrete equivalent which is approximated by

$$\xi_{11}(z) = b_0 + b_1 z^{-1} + \ldots + b_n z^{-n} \tag{5.21}$$

This corresponds to a Nth order finite impulse response-(FIR) filter with all of its discrete poles concentrated at the origin. The idea then is to find the parameters-$(b_0,b_1,b_2,\ldots b_N)$ which make $\xi_{11}(z=e^{-i\omega T})$ match $e^{-i\omega(1/2)c}$ as closely as possible in the frequency domain. The coefficeints bj will correspond to the weighted impusle response at times $t=jT$ where j is an integer. The simplest approach to solving this problem is to find the Inverse Fourier Transform solution up to the nyquist frequency π/T. Thus,

$$h(mT) = \frac{1}{n}\sum_{j=0}^{n}\xi(\omega_j)e^{ijm\pi/n} \tag{5.22}$$

An alternative to this approach is to apply the methods of Mcllenan and Parks-[84] to find the optimal coefficients b_j which minimize some min/max performance criteria. This is identical to the scheme described in section 4.4 for optimal wave-mode filtering. Here, however, the objective is to find b_j such that

$$\min_{b_j}\left(\max_{\omega\in[\omega_A,\omega_B]}\left\{\xi(\omega) - \hat{\xi}(z=e^{i\omega T})\right\}\right) \tag{5.23}$$

where G is a closed subset of the normalized frequency interval $0<\omega<\pi$. Therefore, the idea is to find the FIR filter which satisfies the frequency domain criteria of equation (5.23) for some optimal unknown δ given the filter length N, the desired phase lag $\xi_{11}(\omega)$ and the closed intervals defined by G on $0<\omega<\pi$.. The solution to this problem is often called the equiripple filter and usually requires an iterative search. Algorithms for performing this search are given in many textbooks and for the sake of brevity are not presented here.

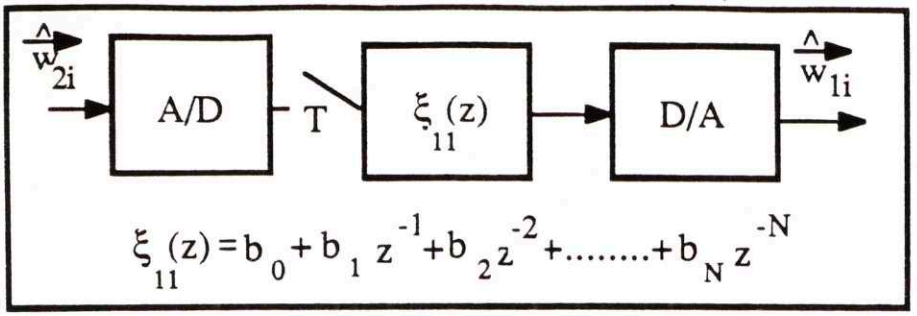

Figure 5.9: Realization of Non-Linear Spatial Phase Lag for a Dispersive Member.

To illustrate an example of a dispersive phase lag that can be adequately realized by FIR filters lets consider $\xi_{11}(\omega)$ given by

$$\xi_{11}(\omega) = e^{-i(2.8/1.8)*\sqrt{\omega}} \qquad (5.24)$$

N=32

Now lets suppose that the desired filter length is *32*. With this choice of filter length the causal FIR approximation is given by $\xi_{11}(\zeta)$ shown in Figure 5.10(a) compared with a windowed version of the same filter. The corresponding temporal filters are displayed in Figure 5.10(b). Notice that in constrast to the linear phase lags, non-linear phase lags have unit magnitude but non-linear phase. However, the linear approximation to this non-linear phase lag is in fairly good agreement for frequencies which lie in the midrange-($0<\omega<\pi$). The filter approximation suffers at low frequency for both the smooth window-(dashed) and rectangular(solid) windowed filter. This is because the low frequency dynamics are not adequately captured by the *32* sample points of the window.

N=256

A longer length filter clearly leads to better causal approximations to the non-linear phase lag of equation-(*5.24*). This is evident from the frequency domain properties shown in Figure 5.11(a). The corresponding temporal properties are shown in Figure 5.11(b). Of course this longer length filter is at the expense of additional computational burden which will indeed introduce hardware constraints on possible sampling rates.

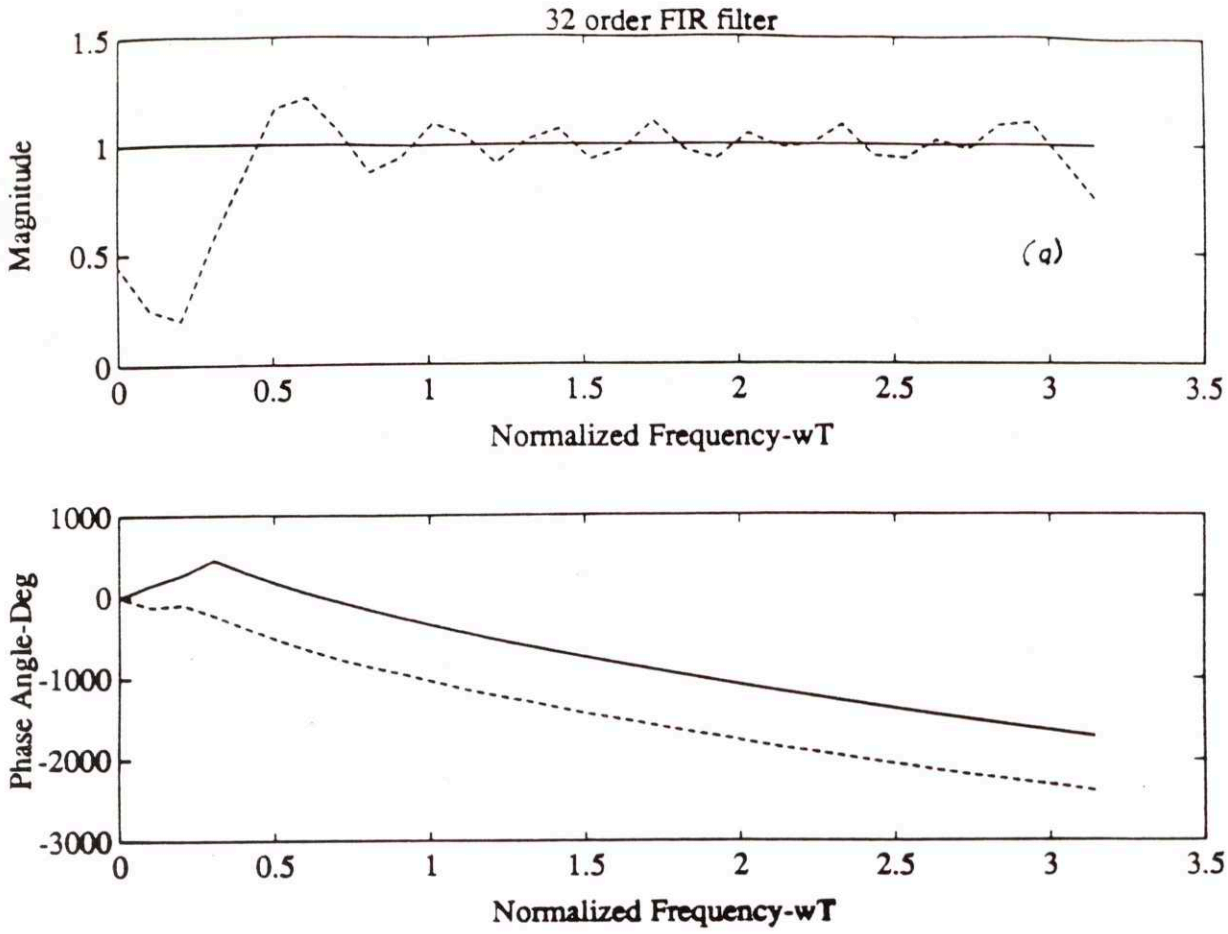

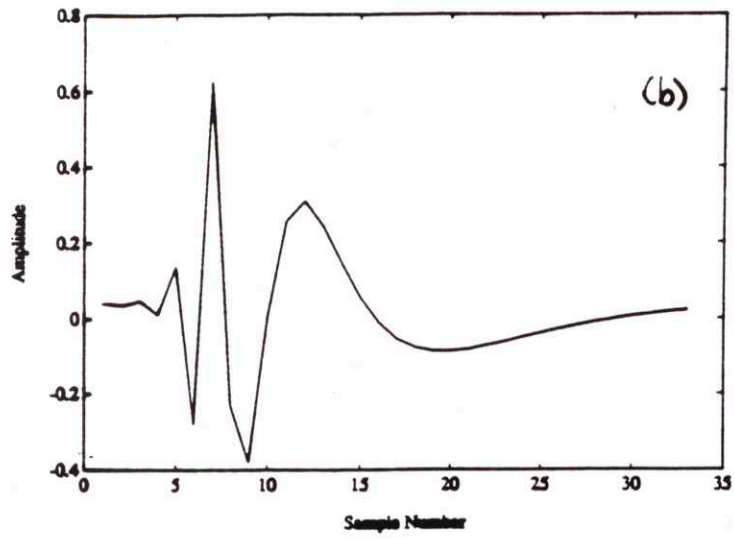

Figure 5.10: N=32 Causal FIR Filter: (a) Frequency Properties. (b) Temporal Properties.

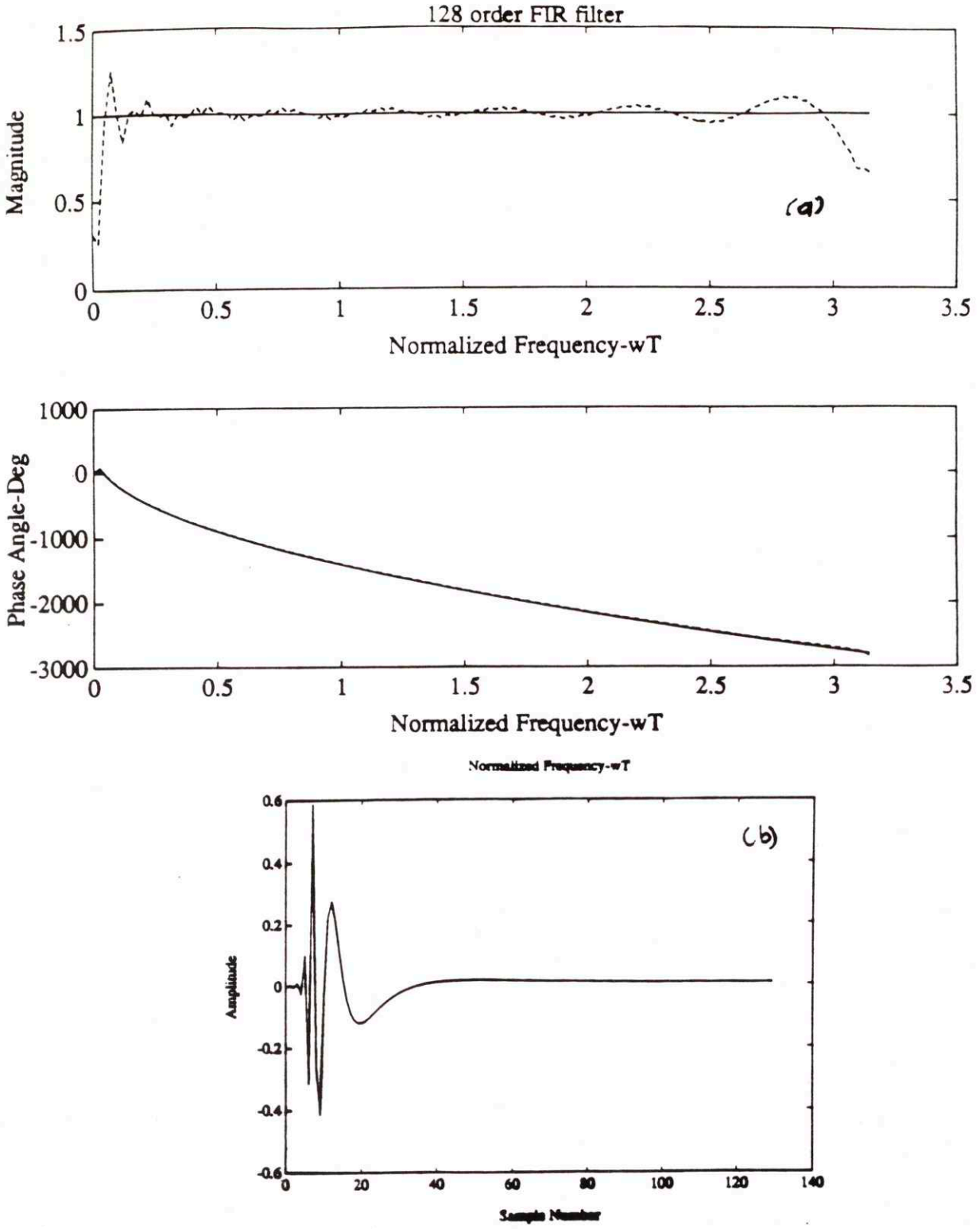

Figure 5.11: N=128 Causal FIR Filter: (a) Frequency Properties. (b) Temporal Properties.

5.5 Some 1-D Control Examples

The phase lag associated with non-collocated sensing of propagating wave-mode amplitudes makes possible active wave control of the rod and beam defined in Chapter 4. In both cases a disturbance force is applied to the right free end. Control actuators are located at the left end where the objective is to perform active damping, i.e. to absorb the incoming waves.

5.5.1 Free-Free Rod

As in Chapter 4 suppose observation is attempted at the center of the rod of Figure 4.7. To achieve ideal active damping the scattering coefficient at the left free end of the rod must be set equal to zero. This requires feedforward of the leftward propagating wave-mode amplitude estimates appropriately delayed an amount $T=L_1(\rho A/EA)^{1/2}$. Therefore, in the absence of errors, the feedforward loop structure for active damping leads to the diagnostic transfer function displayed in Figure 5.12(a) which corresponds to the disturbance force to collocated position at the right free end. Notice that as expected in the frequency range-($0<k<k_b$) in which the distributed sensors of Chapter 4 are valid the resonances of the rod disappear and the rod behaves as if it were infinte in length. However, near the k_b where roll-off occurs the closed-loop suffers as the estimated incoming leftward wave-mode amplitude becomes corrupted with rightward going dynamics and the dynamics of the distributed interpolant. This corruption is much more apparent in Figure 5.12(b) which displays the magnitude of the scattering coefficient of the left end. From this figure it is obvious that the magnitude of the scattering coefficient increases as the cutoff frequency k_b is approached. However, it never reaches its open loop magnitude of 1.0. This is because the point sensor used in lieu of the sinc sensor has no roll-off characteristics in its dynamics.

If two distributed sensors are used to observe rightward and leftward going wave dynamics on the rod of Figure 4.7. then application of the same feedfoward control strategy leads to the modified diagnostic closed-loop transfer function and scattering coefficient dynamics shown in Figures 5.13(a)&(b) respectively. Here the use of two distributed sensors constrains the frequency range of the filtering to be only valid up until k_b. Beyond this point the output of both sensors is approximately zero. Therefore, the effect of two distributed sensors results in closed-loop dynamics up to k_b with a small transition zone and then the appearance of open loop behaviour with the magnitude of the leftward scattering coefficient reaching a magnitude of 1.0.

5.5.2 Pinned-Free B-E Beam

The beam differs from the rod in two respects. First its wave dynamics are dispersive and secondly near-field terms are also present in its dynamics. Nevertheless, as was demonstrated in Chapter 4 wave sensing can be achieved on a finite beam if its is assumed that the evanescent terms contribute negligibly to the response of the member. This assumption is valid far away from structural discontinuities and at high frequencies.

Therefore, if we consider the beam of Chapter 4 with a point and distributed sensor placed at a distance of *2.73 m* from the pinned-end condition, wave sensing can be achieved in the interior of the structure with the estimated strain wave-amplitudes used in a feedforward control structure to achieve active damping. All that is required is the realization of the spatial phase lag between the wave sensing location and the moment control actuator. Figure 5.13 shows the effect of such a control scheme for a disturbance force entering at the right free-end of the beam to a position sensor placed at the same end. The idea here is to achieve active damping by zeroing the 11 component of the open loop scattering matrix which corresponds to the reflection of purely propagating dynamics. Notice that over the entire frequency range the resonances are reduced with best results being achieved in the range from *100 Hz. to 1 kHz.* However, beyond the cutoff frequency-($k_b=20\pi$) of the distributed sensor feedforward control has no affect on reducing the scattering coefficeint because the wave sensor no longer senses directional information. The same behaviour is seen when two distributed sensors are used for wave sensing-(See Figure 5.14). The magnitude of the scattering coefficient returns to 1.0.

Although the two examples considered in this section have demonstrated the effect of control in the case of actve damping, the same procedures hold for active isolation. The only difference is that the control actuator is not located at one of the structure's boundaries but at some interior point in the member.

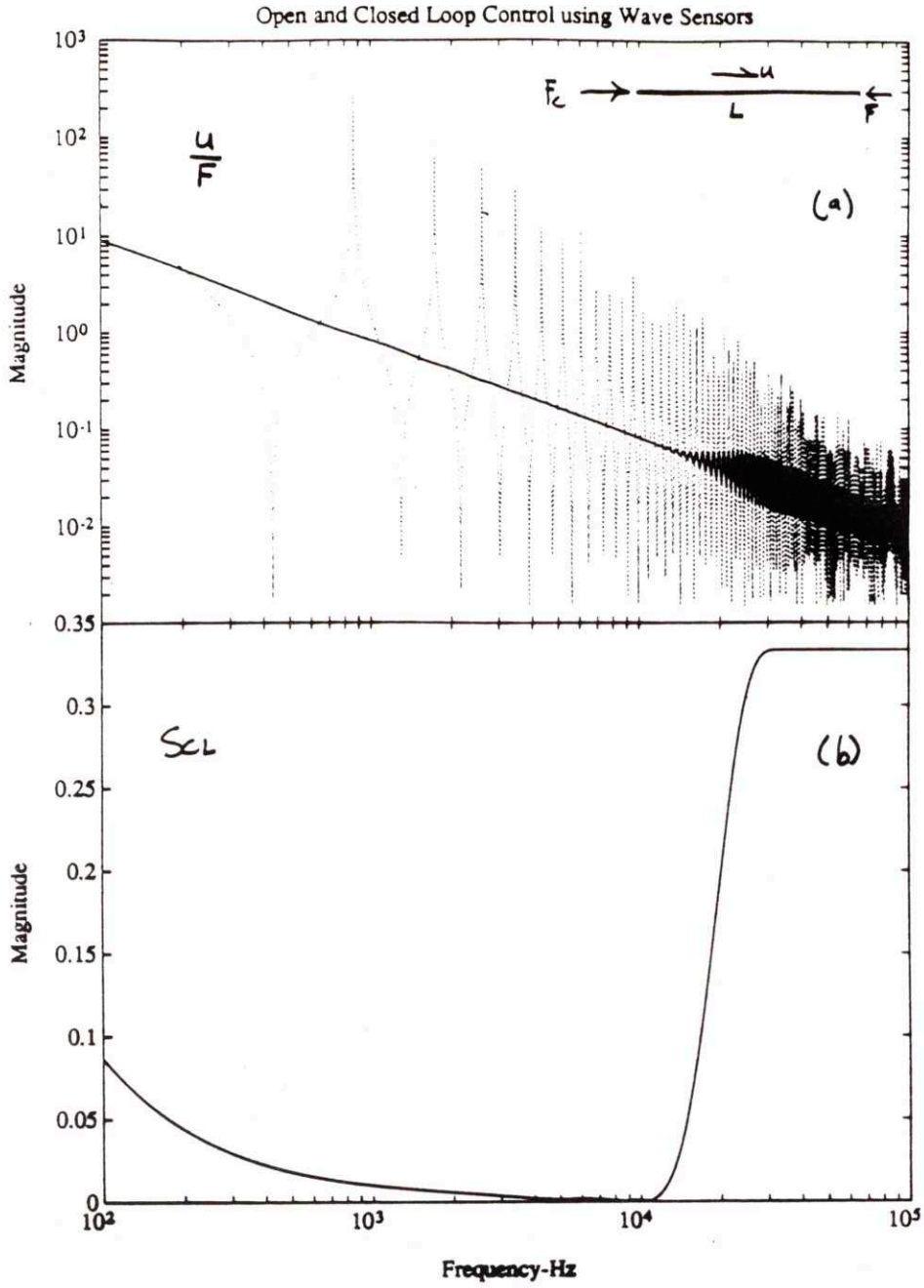

Figure 5.12: (a) Magnitude and Phase of Diagnostic Transfer Function from disturbance force-$f(\omega)$ to displacement-$u(\omega)$ at Right Free End-(Closed Loop-Solid Curve, Open-Loop-Dotted Curve). Wave Filtering performed using a Point and a Distributed Sensor (b) Magnitude of Closed-Loop Scattering Coefficient at Left Free End.

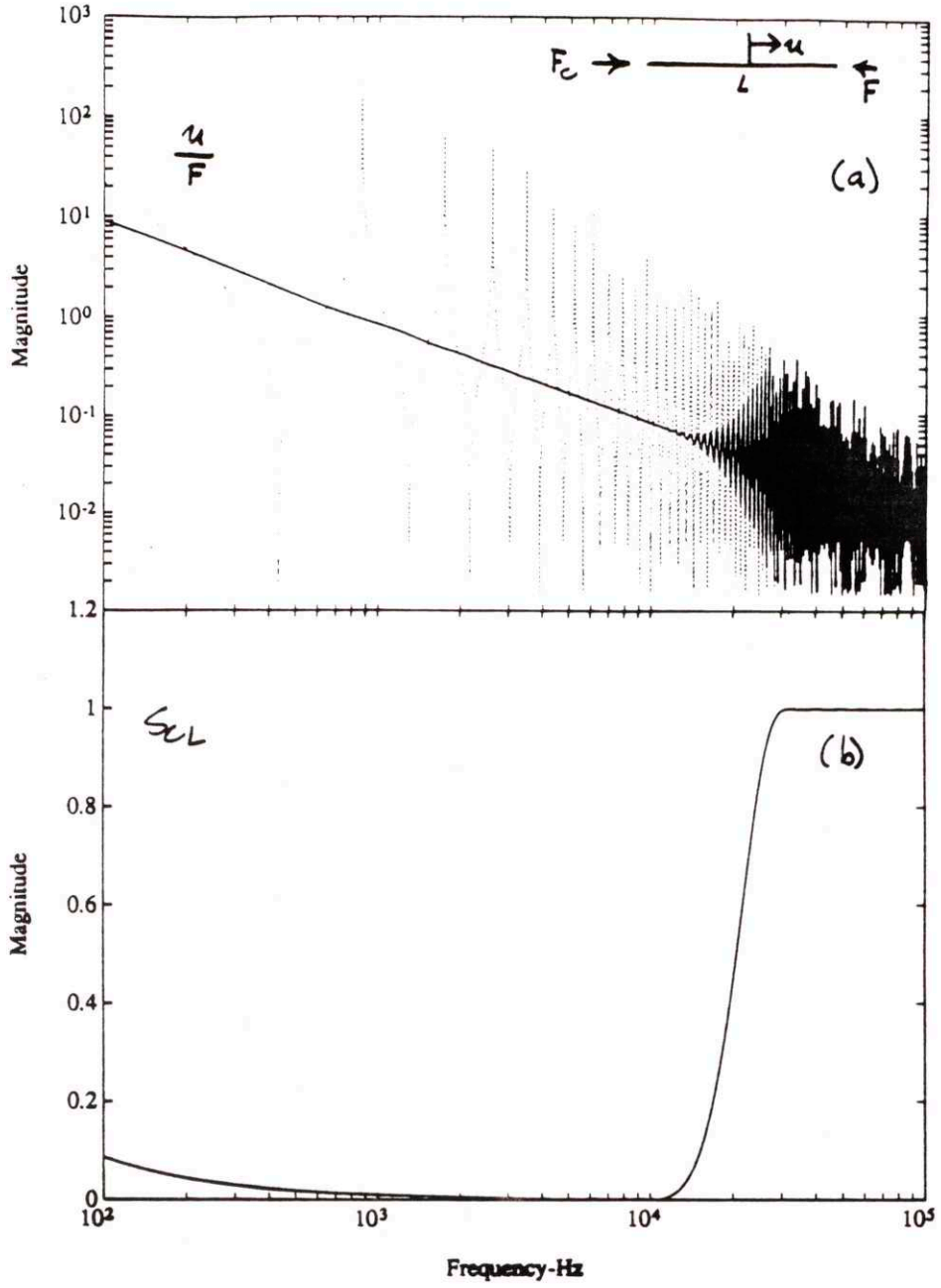

Figure 5.13: (a) Magnitude and Phase of Diagnostic Transfer Function from disturbance force-$f(\omega)$ to displacement-$u(\omega)$ at Right Free End-(Closed Loop-Solid Curve, Open-Loop-Dotted Curve). Wave Filtering performed using two Distributed Srnsors. (b) Magnitude of Closed-Loop Scattering Coefficient at Left Free End.

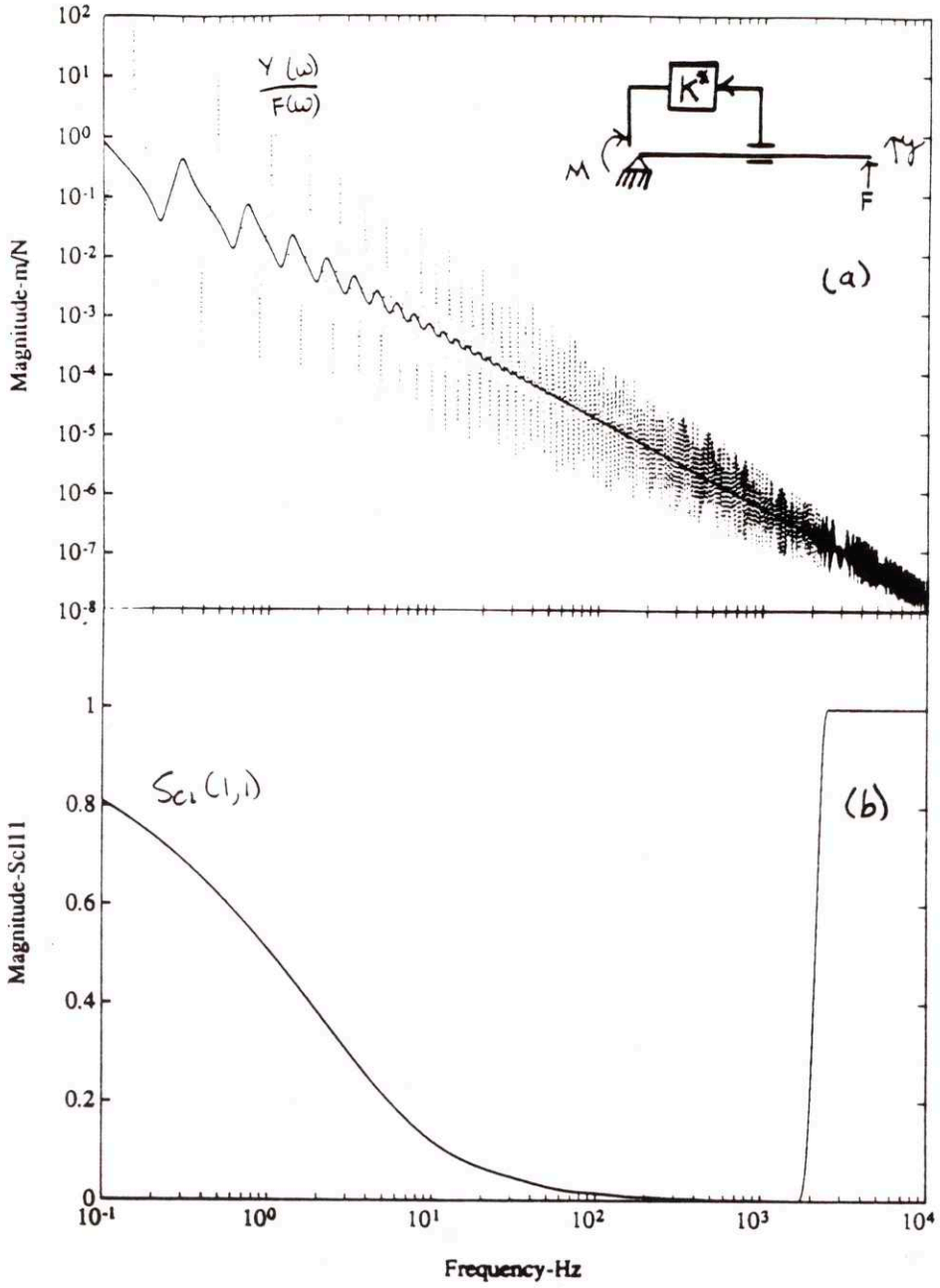

Figure 5.14: (a) Magnitude and Phase of Diagnostic Transfer Function from disturbance force-$f(\omega)$ to displacement-$u(\omega)$ at Right Free End-(Closed Loop-Solid Curve, Open-Loop-Dotted Curve). Wave Filtering performed using a Point and a Distributed Sensor (b) Magnitude of Closed-Loop Scattering Coefficient at Left Free End.

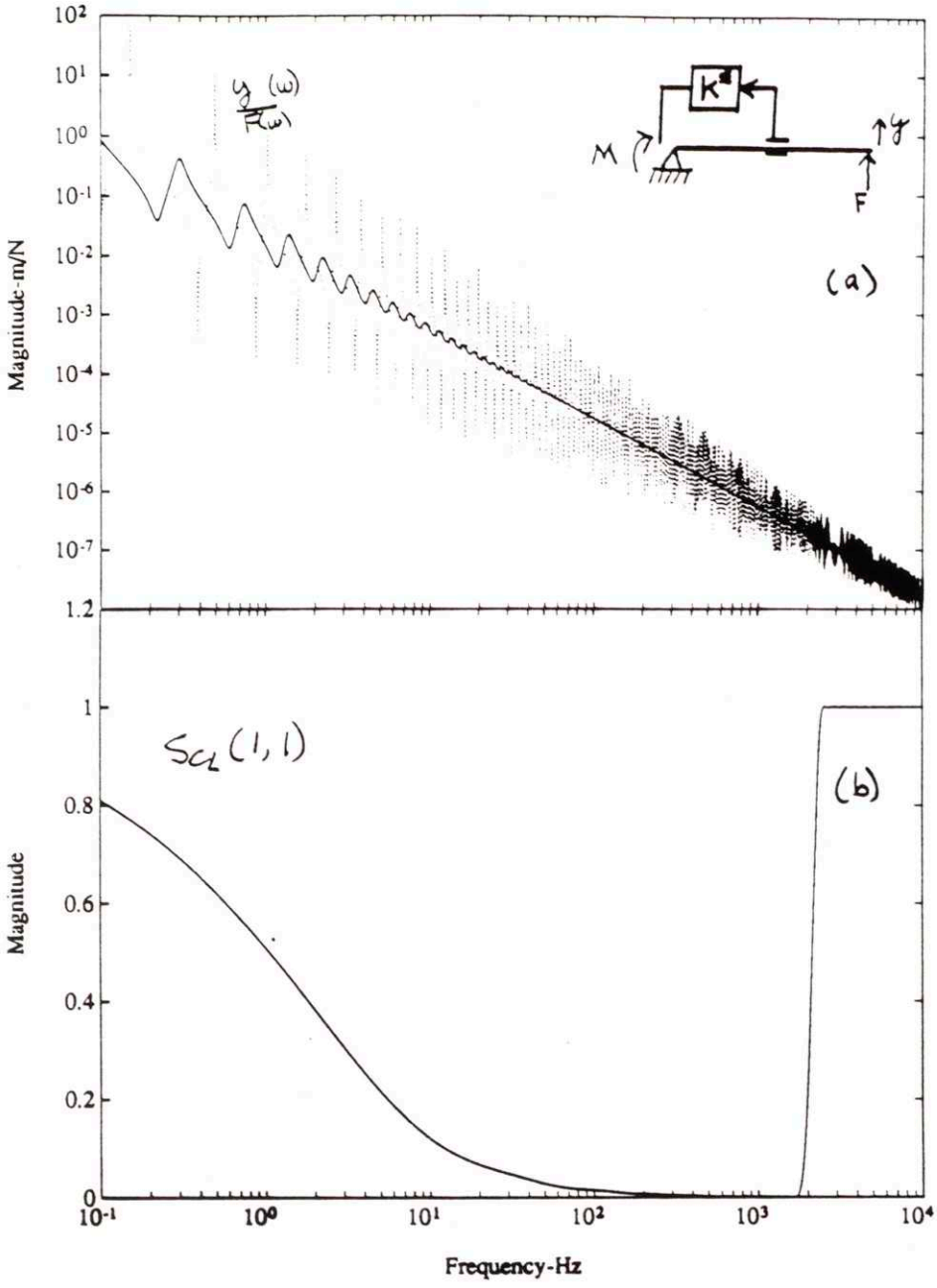

Figure 5.15: (a) Magnitude and Phase of Diagnostic Transfer Function from disturbance force-$f(\omega)$ to displacement-$u(\omega)$ at Right Free End-(Closed Loop-Solid Curve, Open-Loop-Dotted Curve). Wave Filtering performed using two Distributed Srnsors. (b) Magnitude of Closed-Loop Scattering Coefficient at Left Free End.

5.6 Summary

This chapter has presented a non-collocated approach to implementing wave control objectives formulated by references [10,32]. This scheme exploits filtering of wave-mode amplitudes at some location upstream relative to the location of the control input and uses a digital computer to account for the travel time between sensor and actuator so that control effort is imparted at the appropriate time. This method, however, only applies to propagating wave-mode amplitude estimates where measurements are taken far away from structural boundaries and point disturbances. In these regions near field terms contribute negligibly to the response except for the first few modes of the structure. Thus, for structures like B-E beams knowledge of propagating wave-mode dynamics should be sufficient to perform structural control. This is especially true at high frequencies as the pinned-free beam example has demonstrated.

The use of distributed sensors offers a unique flexibility not in just filtering wave dynamics but also in truncating the frequency properties of the response so as to insure stability of the feedforward loop structure.

CHAPTER 6

Experimental Verification

6.1 Introduction

The analysis presented in Chapters 3, 4 and 5, and the application of PVDF piezo film by many others-[74,76-79] to the controlled structures problem has motivated an experimental phase of this research. This was done for several reasons. First and foremost there is a desire to confirm the concept of directional filtering of wave propagation dynamics on an actual 1-D structural element. Analytical simulations present only an idealized prediction of the stucture's behaviour. An actual structural exposes the true limits of the concept. Secondly, several issues associated with sensor/actuator implementations are not always obvious from just analytical studies. These subtleties can only be discovered during actual hardware implementation which involve both sensor manufacture and electronic interfacing. This may help to suggest improvements in the present approach to the problem.

Experimental verification of the concept of wave filters for structural control was attempted on an experimental pinned-free Bernoulli-Euler beam and consisted of two phases. The first phase involved the implementation of the wave filtering scheme outlined

in Chapter 5 using distributed/point sensor pairs. During this phase three distributed/point sensor pairs were manufactured and tested. Each of their performance was evaluated by computing their response under both steady-state and transient structural excitation. Best results were obtained for the third distributed/point sensor pair. These results are discussed in detail in this chapter. The second phase of the experimental tests exlpoited the estimated strain wave amplitude information for non-collocated closed-loop control. The idea was to alter the local scattering properties of the pinned-end boundary of the structure. The control objective was to actively damp the resonant vibrations.

More specifically, this chapter is divided into six sections. Section 6.2 discusses the experimental apparatus which includes the structure, sensors, actuators and open loop instrumentation. This section also describes the location of the distributed/point sensor pair tested in this work. Detail regarding sensor manufacture are described in section 6.3. This includes Electrode Shaping, Sensor Assembly/Lead Attachment and Sensor/Structure Attachment. Properties of the three distributed/point sensors designs studied in this work are summarized in section 6.4.. This section also discusses some important assumptions made during this process. Section 6.5 presents Wave Sensing results for the third distributed/point sensor pair from steady-state and transient response data. Finally, section 6.6 considers non-collocated closed-loop control using wave sensing information and an FIR Filter approximation of the compensation. The compensation is realized using a digital computer.

6.2 Experimental Setup

The apparatus-(See Figure 6.1) used in all experimental tests was developed by Miller-[32] and consisted of a 7.32 m brass beam with physical and geometrical properties listed in Table 6.1. The beam was constructed from four separate segments, each 6 ft in length and connected together by lightweight aluminum sleeves using eight 5/8" threaded bolts. The entire apparatus was suspended from the laboratory ceiling by six pairs of piano wire spaced exactly at one-seventh length intervals with both ends left free for attachment of actuator hardware. The suspension was configured to suppress vertical as well as torsional motion. At the left end of the beam a PMI torque motor-(See Table 6.2) was mounted to the structure using a 6 cm long rigid aluminum moment arm which transmitted torque from the motor shaft to the left end of the beam. To create a pinned end relative to the laboratory frame the outer casing of the torque motor was clamped to a laboratory stand. During open loop wave sensing tests the right end of the beam was left free. However, during closed-

loop tests the right end was instrumented with a proof-mass shaker-(See Table 6.2) which provided a disturbance input to the structure.

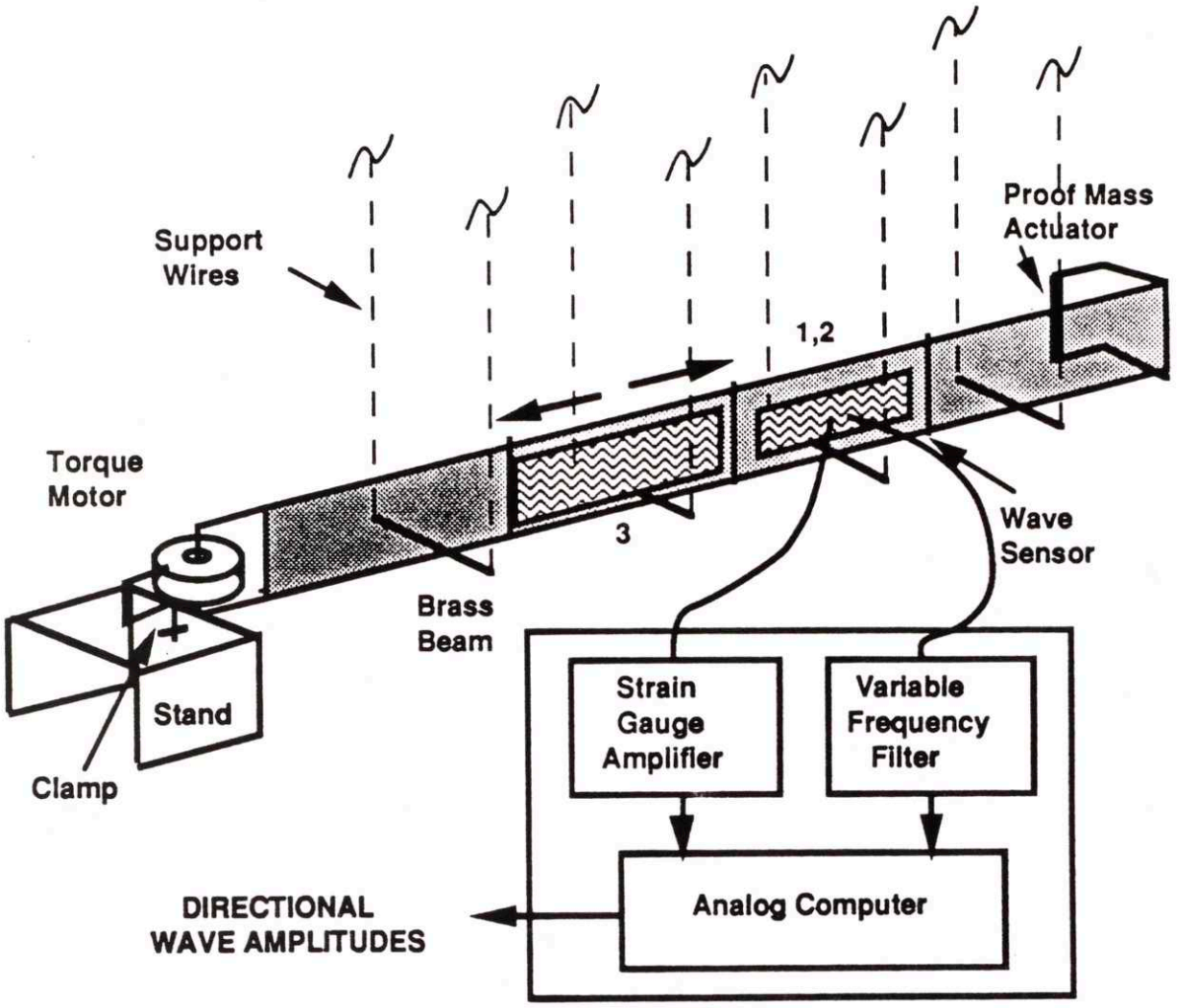

Figure 6.1: Experimental Test Apparatus for Directional Wave Filtering

Table 6.1 Beam Properties

Physical Dimensions		
Length	Width	Thickness
7.32 m	10.2 cm	0.3175 cm
Material Properties		
EI-(Stiffness)		ρA-(Mass Per Unit Length)
31.1 N-m^2		2.85 kg/m

Table 6.2 Actuator Properties

Torque Motor	
Manufacturer/Model	PMI U-9
Torque Motor Constant	0.0212 N-m/Amp
Armature plus Arm Inertia	0.000146 kg-m^2
Current Source	EG&G PA-601
Gain	-2.08 Amp/Volt
Proof Mass Actuator	
Manufacturer/Model	Pittman 7214
Torque Motor Constant	0.0357 N-m/Amp
Current Source	EG&G PA-223
Gain	-1.87 Amp/Volt

6.2.1 Sensor Placement

Three distributed/point strain sensor pairs were created to evaluate the performance of various distributed sensor designs in filtering directional dynamics. The midpoint-(See Figure 6.1) of all three pairs was positioned sufficiently away from both beam boundaries to insure that the steady-state contributions of near-field dynamics were negligible above 1 Hz.. More specifically, pairs 1 and 2 were positioned at a distance of *4.33 m* away from the pinned-end condition while the third pair which achieved the best directional wave filtering results was positioned much closer to the pinned end at a distance of *2.73 m*. The reason for this was to reduce the degree of non-collocation between the wave sensor and actuator location to help facilitate feedforward control. The greater the separation between sensor and actuator, the more phase lag present in the feedforward compensation which tends to hinder closed-loop control.

6.2.2 Signal Conditioning and Diagnostics

Several types of signal conditioning equipment was used to achieve directional wave filtering and non-collocated control-(See dashed box in Figure 6.1). Probably the most important piece of instrumentation in this group was the bridge amplifier which was used to calibrate and amplify each strain gauge signal. From this information the magnitude of the distributed strain sensor could be calibrated appropriately at a modal frequency of the structure. However, special care was required when interfacing with the distributed sensor. Because of its piezoelectric nature the impedance between the electrical boundaries of the sensor have the dynamics of a capacitor-($Z=1/\omega C_f$). Thus, when strained the piezo film has the appearance of a charge generator-(See Figure 6.2a). Its simplified Thevenin equivalent circuit is shown in Figure 6.2b. In this form it is clear that connecting the electrical boundaries of the distributed sensor to any signal conditioning device will set up a RC network with a time constant $\tau=R_i(C_f+C_i)$ or equivalent corner frequency given by $f_c=1/\tau$. Therefore, R_i must be chosen so that f_c lies below the frequency range of interest. For the distributed sensors designed in this work, a variable frequency filter instrumented with an impedance of $10\ M\Omega$, was used as the electronic interface which resulted in sensor corner frequencies that were below 1-Hz.

Finally, a PACE TR-48 analog computer was used to manipulate the output from the strain gauge conditioner and the variable frequency filter to yield estimates of directional strain wave dynamics. This information was used later for non-collocated control, however, further discussion of real-time control hardware is reserved for section 6.6.

Response data from both open and closed-loop testing was recorded using the Tektronix 2040 Personal Fourier Analyzer. This device also served as the function generator for steady-state and transient pulse inputs to the torque motor and proof-mass actuators.

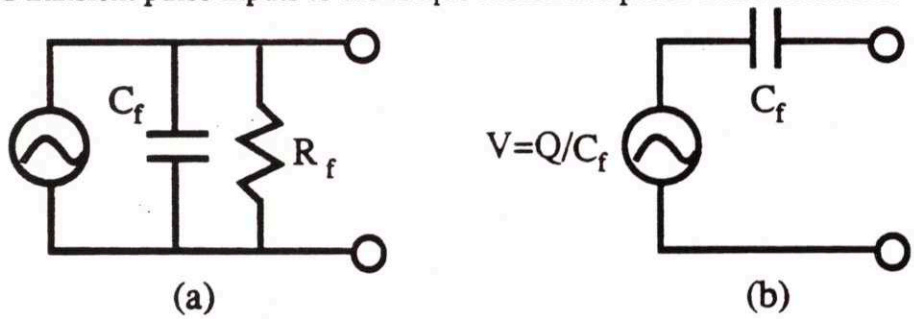

Figure 6.2: PVDF film's Thevenin Equivalent Circuits. (a) Charge Generator (b) Voltage Generator.

6.2.3 Modelling Assumptions

Formulation of wave-models for the apparatus pictured in Figure 6.1 required that several assumptions be made about its ability to simulate wave dynamics. These assumptions were noted by Miller in his PhD thesis and are summarized here as follows.

1 The segmented brass beam was modelled using B-E beam theory with spatially uniform properties. This model assumes that the dynamics of the apparatus could be sufficiently described dispersive propagating and evanescent wave components.

2. Suspension Cables and bolted aluminum sleaves were assumed not to alter the uniform physical properties of the brass beam.

3 The rotary inertia of the armature shaft was assumed to be negligible except at high frequency-(beyond *200 Hz.*).

4 The aluminum arm used to transmit torque from the motor to the beam was assumed to be rigid.

5 All other associated hardware such as the stand, clamp and actuator casings were assumed to be rigid.

6.2.4 Wave Model of Test Apparatus

A wave description of the test apparatus which incorporated the above modelling assumptions was developed in accordance with analytical framework of Chapters 2 and 4. Specifically, the approach followed the wave model developed for a pinned-free B-E beam given in section 4.4. From this section the input/output relation at the pinned-end condition which relates incoming and outgoing wave dynamics is given by

$$\begin{bmatrix} w_{rp} \\ w_{re} \end{bmatrix} = \begin{bmatrix} -1 & 0 \\ 0 & -1 \end{bmatrix} \begin{bmatrix} w_{lp} \\ w_{le} \end{bmatrix} + \frac{1}{2\,EIk^2} \begin{bmatrix} -1 \\ 1 \end{bmatrix} M \qquad (6.1)$$

where (w_{rp}, w_{lp}, w_{re}, w_{le}) are wave-mode amplitudes normalized with respect to lateral deflection. This equation shows that the propagating and evanescent components are decoupled from one another at the pinned-end. Substituting the expression for point strain given by

$$\varepsilon = \frac{-t_b}{2} k^2 \left(w_{rp} - w_{re} + w_{lp} - w_{le} \right) \tag{6.2}$$

into equation equation (6.1) gives the following transformed input/output relation

$$\begin{bmatrix} \hat{\varepsilon}_{rp} \\ \hat{\varepsilon}_{re} \end{bmatrix} = \begin{bmatrix} -1 & 0 \\ 0 & -1 \end{bmatrix} \begin{bmatrix} \hat{\varepsilon}_{lp} \\ \hat{\varepsilon}_{le} \end{bmatrix} + \frac{t_b}{4\,EI} \begin{bmatrix} 1 \\ 1 \end{bmatrix} M \tag{6.3}$$

This expression reveals that if one could sense the mix of incoming strain wave amplitudes, the scattering characteristics of the pinned-end could be altered to achieve a particular control objective such as active isolation or active damping. Unfortunately, from a point strain signal at the boundary these wave components are indistinguishable. In the interior, however, the approach outlined in Chapter 4 suggests that propagating wave components are available. More specifically, if the torque motor excites the open loop steady-state dynamics of the structure estimates of rightward and leftward going strain waves can be found by following the scheme outlined in equations *4.50* , *4.51* and *4.52*. This leads to the following expression for strain wave estimates from a point and a distributed strain sensor at a distance x=l away from the pinned-end.

$$\begin{bmatrix} \dfrac{\hat{\varepsilon}_{rp}(\omega)}{M(\omega)} \\ \dfrac{\hat{\varepsilon}_{lp}(\omega)}{M(\omega)} \end{bmatrix} = \begin{bmatrix} \dfrac{1}{2} & \dfrac{-1}{2s\sqrt{\dfrac{\rho A}{EI}}} \\ \dfrac{1}{2} & \dfrac{1}{2s\sqrt{\dfrac{\rho A}{EI}}} \end{bmatrix} \begin{bmatrix} \dfrac{\varepsilon(\omega)}{M(\omega)} \\ \dfrac{v(\omega)}{M(\omega)} \end{bmatrix} \tag{6.4}$$

where s is the Laplace variable. The distributed sensor weighting pattern which permits this filtering scheme is given by

$$\phi_t(x) = \frac{1}{2s\sqrt{\dfrac{\rho A}{EI}}} \phi''_{Hi}(x)\phi_w(x) \pm \frac{1}{2}\delta(x) \tag{6.5}$$

Using this pattern, simulation of the expression in equation 6.4 for the experimental beam yields the strain wave responses to tip moment shown in Figure 6.3. A damping of *0.1%* was assumed. These transfer functions can be directly measured in the laboratory.

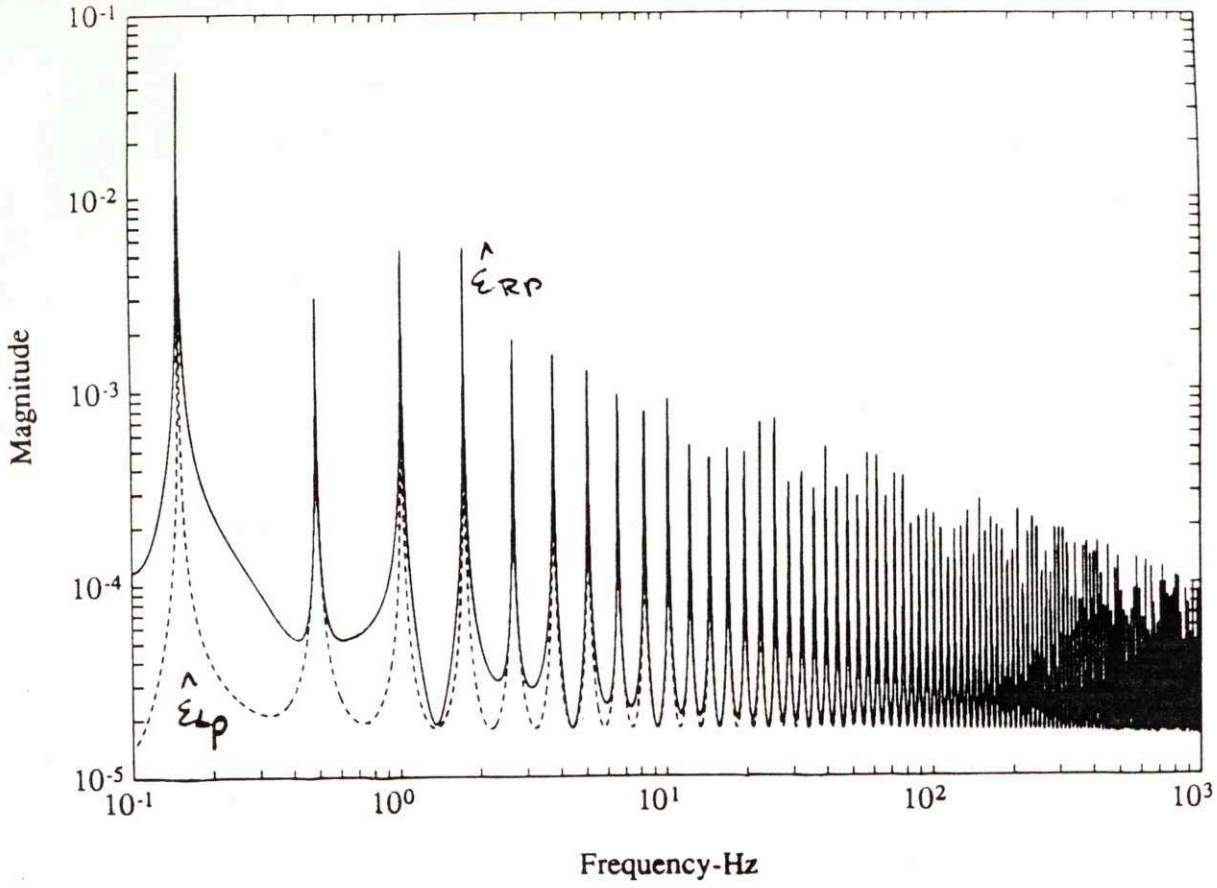

Figure 6.3: Estimated Open Loop Strain Wave Transfer Function for a value of x=2.73 m away from the pinned-end condition.

6.3 Sensor Manufacture

The performance of the collocated wave sensors developed in this work is strongly dependent on good distributed sensor design. The design and manufacture of these sensors, however, is not an easy task. Although Pennwalt's-[53,54] guide and application notes provide many useful tips regarding sensor fabrication, many useful ideas can only be discovered by experimenting with the actual piezo film itself. One type of piezo film which has found many applications in the field of controlled-structures-[74,76-79] is polyvinyldene fluoride-(PVDF). PVDF is a tough, lightweight and flexible polymer that has piezoelectric properties. One such form of this piezo film which is manufactured by the Piezo Film Division of the Atochem Corp-(formerly the Pennwalt Corp) is *Kynar* polyvinyldene flouride-(PVDF). This material has high piezoelectric stress coefficient which results in large fields being developed under a given stress. It can be purchased in one of two forms

15 cm by 30 cm sheets-(52 microns thick)

15 cm by rolls (28 microns thick)

A summary of its physical and piezoelectric properties are listed in Table 6.3. A more thorough discussion of its physical and electrical properties is described in Sesslers' review-[66] and Pennwalt's application notes-[54].

Table 6.3 Physical and Piezoelectric Properties of Kynar Piezo Film

Physical

ρ	E
1.8×10^3 kg/m^3	2 GPa

Piezoelectric

Strain Constants-(pC/N)	Strain Constants-(pC/N)	Coupling Factor
d_{31}=23	g_{31}=216	k_{31}=12%
d_{32}=3	g_{32}=19	Strain Constants
d_{33}=-33	g_{33}=-339	e_{31}=

At the purchaser's request the film can be manufactured with or without vacuum deposited metallic electrodes on either side. The electrodes are used to accumulate charges which appear on the surface of the film. The choice of electrode deposition, however, depends on the sensor designer's application. Standard electrode surfaces are typically made of a thin-(~250-1000A) CuNi or CuAg alloy. Atochem also supplies a Ag ink solution for custom electrode manufacturing, however, because of the consistency of this material it is hard to control the electrode thickness to any degree of accuracy. Thus, following the lead of Collins-[78] and others PVDF sheets with metallic electrodes were deemed adequate for achieving the desired distributed sensor properties necessary for wave sensing. This choice of electrode metallization divided sensor manufacture into three phases

Electrode Shaping
Sensor Assembly/Lead Attachment
Sensor/Structure Attachment

A discussion of each these phases follows.

6.3.1 Electrode Shaping

A critical step in achieving good distributed sensor performance dpends on how well the sensor's electrode pattern matches the actual weighting function-$\phi(x)$. Most approaches begin with the creation of a mask of the desired electrode shape. This of course can be done in many ways. The approach taken here was to exploit the use of a *Macintosh-(SE30)* computer and compatible software to program a *Matlab* macro which reproduces the desired electrode pattern to full scale on a crt screen. This image was later cut/pasted into the software *Clariscad* where final scaling of the exact electrode pattern of the distributed sensor could be made within 1/2 mm of accuracy taking particular pains to insure that the pasted version of the pattern was elongated precisely to the dimensions of the sensor that would fit on the beam. Once this was done hard copies of this pattern were obtained by sending the image to a high resolution laser printer. These printed sheets were used to define the boundaries of the electrode pattern-(See Figure 6.4).

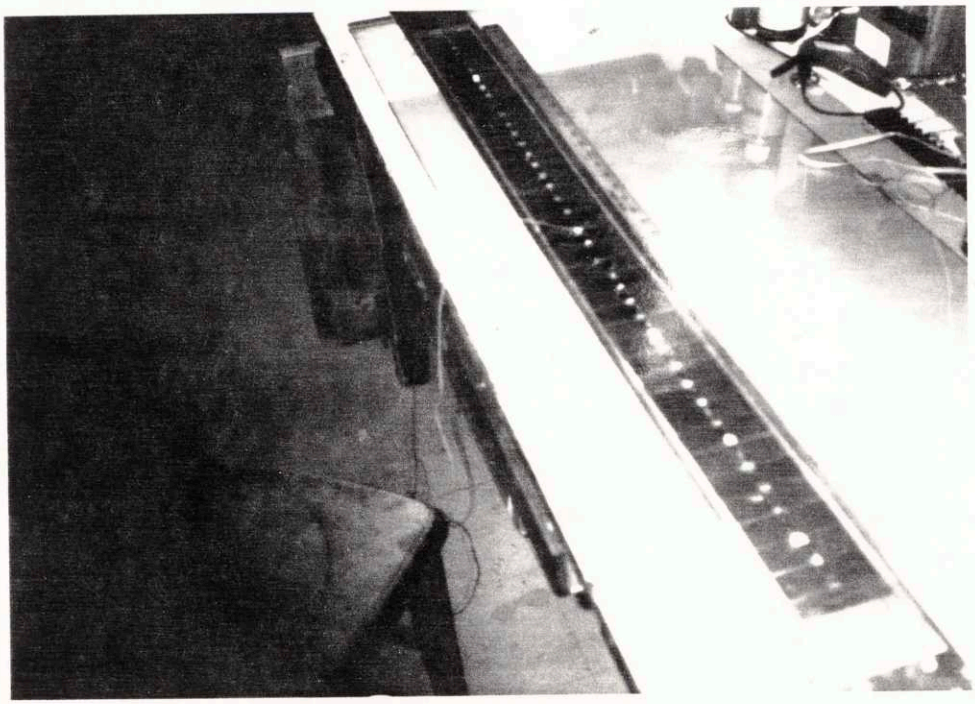

Figure 6.4: Photograph of an Experimental Distributed Sensor with Etched Electrode Pattern.

Masks were created by copying the pattern on these sheets onto a commercially available transparent material such as *Mylar*. For this work *Visiblok III* served as a suitable

alternative which was durable, flexible, transparent and could be purchased with adhesive on one side. Thus, with electrode pattern copied onto the *Visiblok III* material the mask was complete. The only other remaining step was to cut out the geometry of the electrode pattern with a pair of scissors. The mask could then placed directly on one side of the PVDF taking particular pains to insure that the mask bonds uniformly over the electrode surface. It was found that a firm bond could be achieved by wiping the surface of the mask with a solution of isopropyl alcohol. This also served to clean the surface of the exposed electrode area from any oily deposits.

With the mask in place the next phase of process centered on how best to remove the excess electrode surface area. Collins points out that if the desired electrode shape has simple geometrical properties a sharp razor of exacto knife could be used to cut the entire film to the desired electrode shape. This process appears to work well for vacuum deposited electrodes, however, there is some concern over the damage done to the film in the region near the cut. It has been found that for Ag ink electrodes such cuts produced fragmentation of the electrode resulting in shorting of the upper and lower electrode surfaces of the film. This sometimes occurs with vacuum deposited electrodes, but can be overcome by gently wiping the edges with a solution which dissolves metal fragments. An additional concern that arises when the film is cut is its ability to bond uniformly to a structure in the region near the cut.

An alternative which overcame the problems associated with cutting the film was to use a chemical etching solution such as *Ferric Chloride* to remove unwanted electrode deposits. Collins found in his work that vacuum deposited electrode metalizations could easily be removed by passing a paper towel dampened with the *Ferric Chloride* solution over the unmasked regions of the electrode. Near the edges improved accuracy of electrode removal could be achieved using cotton swabs. However, some care is required to make sure the etchant does not seep under the electrode mask. Paper towels dampened with water was then used to neutralize the residual etchant and remove it from the film's surface. Finally, *Isopropyl alcohol* was used to clean the mask/electrode/film surface. Removal of the mask resulted in a electrode pattern which was within 1 mm of accuracy with respect to the original weighting pattern.

The polarity and stretch direction of the film is usually indicated by markings on the film when purchased from the manufacturer. However, during electrode shaping these markings were often removed from the film's surface. This did not present a problem since the polarity could always be determined by connecting leads to the electrodes on each side of the film and exploiting either the piezoelectric effect or the pyroelectric effect to determine the sign of the voltage and subsequent polarity of the sensor. Polarity checks

were important for the electrode patterns manufactured in this work because the distributed sensor 's weighting function was odd. This required the senor to be manufactured in segments so properties of the weighting function would be preserved during attachment of electrical connections.

6.3.2 Sensor Assembly/Lead Attachment

The most difficult and probably the most important aspect of sensor manufacture was concerned with attaching durable leads to the distributed sensor for measurement of structural deformation. This process was further complicated by the fact that the distributed sensors manufactured in this work were segmented, forcing several additional electrical connections between the low and high side of individual segments. Although the Pennwalt Corp. application notes discuss a number of tips such as pre-shaped electrical ports made of Ag ink which have leads already soldered to them, most of these tips were of no use to this work since they either resulted in mass loading of the structure or distorted properties of the desired electrode pattern.

One approach which worked well for the segmented sensors manufactured in this work was the use of *3M(#1181)* Copper tape backed with a conductive adhesive. Even though the tape loses it tack with time as was found by Collins, it represents a quick satisfactory solution to achieving reasonable lead-electrode attachment. More consistent operation was achieved by applying a little dab of conductive epoxy-(*Tra-Con*) to the copper tape and then connected segmented parts of the sensor together. This provided for a longer lasting electrical connection. The response of the sensor was read by soldering two wires to strips of copper tape and connecting the tape to the low and high side electrodes of the segmented sensor. This was only done after the entire segmented sensor was bonded to the structure.

6.3.3 Sensor/Structure Attachment

All the work of the previous sections becomes nullified if a good bond between the sensor and the beam is not achieved. Therefore, the sensor designer before selecting a bonding procedure the sensor designer must answer three questions.

Is the sensor continuous or segmented?

What is the nature of the bonding surface-(smooth or rough)?

What are the electrical properties of the structure-(conductive or non-conductive)?

The answer to each one of these questions is critical in the selection of an appropriate sensor/structure attachment technique. For example if a sensor were continuous and the structure were metallic then a direct bond could be made from the PVDF sensor to the structure using a conductive epoxy. The structure could then serve as a ground for the network. Similarly, the structure could be made electrically neutral with respect to the sensor if a non-conductive epoxy is used as the bonding agent or if a layer of *Visiblok III* material is used to insulate the sensor from the structure with spray adhesive. Another approach might involve the use of a durable glue compound such as *Permabond 910* which is normally used for strain gauges and provides very good bonds on metallic surfaces.

Nevertheless, because the distributed sensors designed in this work were segmented, their assembly required an additional layer of *Visiblok III* material to properly align neighboring segments. Thus, it was arbitrarily decided to make the brass beam electrically isolated from the distributed sensor. *3M#6068* Spray adhesive was then used to form a strong bond between the non-sticky side of the *Visiblok III* material and the beam with particular care taken to remove any air bubbles trapped between the *Visiblok III* and the structure. The 30 to 60 second cure time of the spray adhesive provided some flexibility in properly aligning the sensor on the structure.

6.3.4 Summary of Sensor Manufacturing Design Steps

From the discussion above, good distributed sensor manufacture requires mastering 7 design steps. These steps are summarized below.

Size PVDF Sensor for Structure
Create Sensor Mask
Remove Unwanted Electrode Area
Clean Sensor with Isopropyl Alcohol and Remove Mask
Assemble Sensor and Attach Leads
Attach Sensor to Structure
Connect Final Leads for Electronic Interfaces

6.4 Distributed Sensor Designs

Following the steps outline in section 6.3.4 three distributed sensors were manufactured to mimic the transfer function properties predicted from the analysis of Chapter 4-(See Figure 6.5). Each of these distributed sensors were subsequently paired with a strain

gauge sensor at two specific locations along the experimental beam. Distributed sensors 1 and 2 were located at a distance of 4.33 m away from the pinned end whereas sensor 3 was only positioned 2.73 m from the pinned end. Thus, three distributed/point sensor pairs were formed to evaluate wave sensing. In each pair the geometrical properties of the distributed sensor were altered to study the sensitivity of directional filtering to sensor length and electrode shape. The fundamental weighting pattern remained the same throughout each distributed sensor design. A summary of the properties of the distributed sensors in these pairs is given in Table 6.4. The strain sensor in each pair consisted of a Measurements Group precision strain gauge with gauge factor of 2.

Table 6.4 Properties of Distributed Sensors

Distributed Sensor	Window	Length	Capacitance	Bonding Method
1	rectangular	0.60 m	14.0 nf	cond. epoxy
2	trigonometric	1.0 m	15.4 nf	spray adhesive
3	kaiser	1.70 m	15.9 nf	spray adhesive

It is important to note that three assumptions were made during the manufacture and implementation of the distributed sensors presented in Table 6.4. These assumptions can be described as follows.

1. The distributed sensor was assumed to add neligible mass and stiffness to the beam. If this was not true then one would expect the impedance of the sensor to cause reflections of leftward and rightward travelling waves at the endpoints of the sensor.

2. Sensor/Structure attachment was assumed to be uniform such a uniform strain field appeared over the width and length of the sensor.

3. PVDF piezo film properties were assumed to be constant over the time window-(1 month) in which open and closed-loop experiments were conducted and homogeneous over the spatial extent of the sensor.

4. Sensor was assumed not to affect the passive damping properties of the structure.

In the context of these assumptions, it is now appropriate to discuss the performance of the three distributed/point sensor pairs.

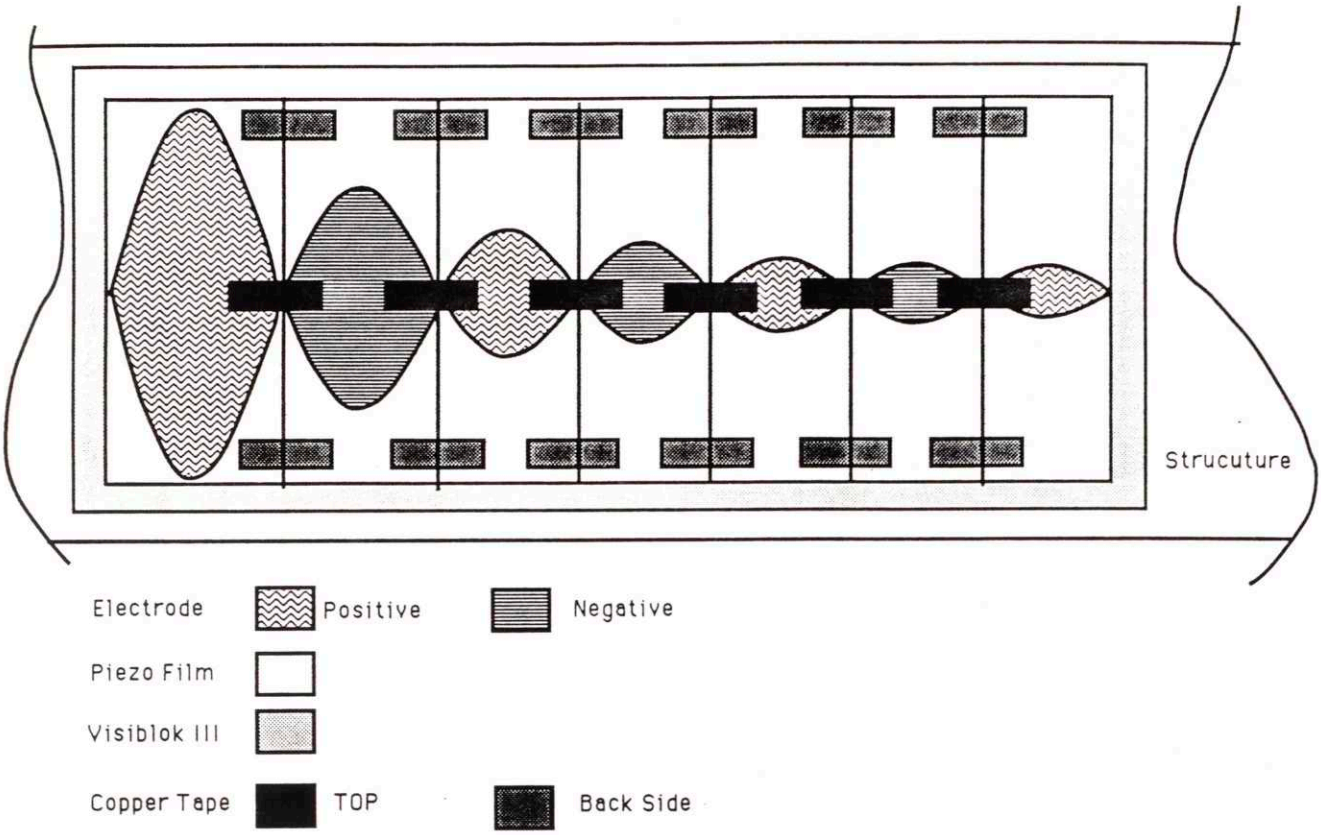

Figure 6.5: Distributed Sensor Realization of analytical weighting pattern $\phi(x)$ of equation-(4.30) over the spatial domain from $0<x<d$.

6.5 Wave Sensing Results

6.5.1 Pair 1

The distributed sensor of this pair was manufactured by shaping the CuNi electrode of the PVDF film to have the properties of the weighting pattern $\phi(x)$ in equation-(4.30) truncated with a *rectangular window*. As expected the transform properties of this sensor output are determined by the convolution of frequency transforms of the ideal weighting pattern $\Phi(k)$ with its window $\Phi_w(k)$. Upon driving the torque motor with random steady-state excitation it was found that abrupt truncation of PVDF sensor greatly distorted the magnitude properties of the sensor. As a result wave sensing could only be attempted at one narrowband frequency at a time with the gains of the analog filter varying for each frequency component

6.5.2 Pair 2

A smoother truncation-(*trigonometric window*) was manufactured for the distributed sensor of the 2nd distributed/point sensor pair. In addition, the length of the distributed sensor was increased to 1 m. Based on analytical predictions, these improvements were expected to extend the range of applicability of the sensor's low frequency range down to approximately *30 Hz*.. However, experimental results indicated that the filter had good properties down to approximately *95 Hz*. This was not considered to be a broad enough range to evaluate the concept of wave sensing since the torque motor's inertia became significant near *200 Hz*. This implied that the range of wave sensing would only extend from *95-200 Hz*. Hence a third iteration was performed to improve the compatibility of the sensing scheme with the properties of the torque motor actuator.

6.5.3 Pair 3

A more detailed discussion of the results obtained using the third distributed/point sensor is presented below for steady-state and transient excitation of the experimental beam. The distributed sensor in this pair was manufactured with a *kaiser window*.

6.5.3.1 Steady-State

Figure 6.6 shows a plot of the transfer functions from the torque motor-$M(\omega)$ to the point strain-(dotted)-ε and distributed strain-(solid)-ν sensor outputs for a broadband-(*0.1 to 1 kHz*) white noise input. As expected the strain sensor output exhibits a horizontal trend with pole and zero dynamics. Similarly, the transfer function of the distributed strain sensor exhibited the desired temporal differentiator-ω magnitude trend from approximately *20* to *200 Hz*. Closer inspection of the distributed strain sensor transfer function also

reveals that the realization of the complex number $i=\sqrt{-1}$ is characterized by the zero locations. Notice that the zero locations of the point and distributed strain sensors occur at different locations in the s-plane even though the two sensors are spatially collocated. This suggests that the distributed strain sensor weighting pattern has somehow altered the zero dynamics of the system. A more complete description of these effects can be seen by computing the ratio of the distributed sensor output to the point sensor output-(See Figure 6.6). Here both the realization of ω and $i=\sqrt{-1}$ appear in the magnitude plot of this ratio. All pole dynamics cancel and only zero dynamics from both sensors remain. If $i=\sqrt{-1}$ were not realized then the zeros of the two transfer functions would be the same and the magnitude trend would be simply a straight line proportional to ω.

The plots in Figures 6.6 and 6.7, however, are not without their share of non-idealistic behaviour. For example in both figures results beyond 200 Hz are corrupted by the strong contribution of the torque motor's inertia Thus, results beyond this range should not be considered since the motor is not responding as an ideal actuator. In addition, it is not clear what causes the abrupt phase and magnitude effects seen at 12, 16, 20 and 65 Hz respectively in these curves. Indeed this will have some affect on the performance of the directional filters.

In preparation for directional dynamics estimation, the output of the distributed strain sensor was calibrated with respect to its collocated point strain sensor output at *102.4 Hz*. This frequency corresponded to a mode of vibration of the beam and was selected based on analytical simulations which showed that the sensor magnitude properties would be better approximated from 100 Hz to 1 kHz..

After performing the necessary analog manipulations of the calibrated distributed/point sensor pair using the PACE TR48, the experimental estimated rightward-(solid) strain wave transfer function was computed and found to compare well with its analytical prediction-(0.1% structural damping is assumed) in the range from *2 to 200 Hz*.-(See Figure 6.8). Best results are achieved between *2* and *100 Hz* where the magnitude and phase are in close agreement with one another. However, beyond this frequency range the poles of the experimental transfer function appear at much higher frequencies than those of the analytical transfer function. This suggests that the structure becomes much stiffer at higher frequencies than what the model predicts. This could be because the model parameters change at high frequencies. Similar results are evident in Figure 6.9 for the leftward estimated strain wave amplitude transfer function when compared to its analytical prediction. Although the magnitude of this leftward-going strain wave transfer function appears to be the same as rightward-going strain wave it has signigicantly more phase. This is because the leftward going wave corresponds to a disturbance which travels from

the torque moment actuator and reflects off the free-end before it returns to the sensing location. On the other hand the rightward-going estimate contains information about the incident disturbance before it encounters the free-end of the beam.

The scattering coefficient of the right free end can be computed by simply taking the ratio of the leftward going wave to the rightward going wave. This leads to the scattering coefficient dynamics shown in the Figure 6.10. The dashed line in this plot indicate the magnitude of the analytical prediction of the scattering coefficient of the free end for a system with *0.1%* structural damping. The actual scattering coefficient shows the effects of a lossy system and imperfect wave sensing. The oscillatory magnitude dynamics are thought to be caused by the fact the wavenumber k is not a constant multiple of $\omega^{(1/2)}$. andto imperfections in the wave sensing scheme.

6.5.3.2 Transient Excitation

Although the steady-state results of the previous section verify that wave sensing is feasible using distributed and point sensors, it is also instructive to examine the performance of the wave sensing scheme under transient excitation. The motivation here was to compute elements of the generic wave sensor transfer function given in equation-(*4.56*) by supplying short duration pulses to the torque motor actuator. In this manner a rightward going wave could be established and the effectiveness of the wave sensing scheme evaluated.

Using the Tektronix 2040 Fourier Analyzer short duration pulses could easily be supplied to the torque motor actuator to generate incident structural disturbances. This operation simply required placing the random noise output generator in continuous burst-mode with the time intervals between successive bursts set by the user. An interval of 3 seconds between bursts was found to allow sufficient time for the energy from a random burst to travel the length of the beam interact with its boundaries and dissipate its energy. In this way a sequence of wave trains could be used to time average the response of the wave filter.

Figure 6.11 plots the computed wave sensor transfer functions from strain sensor output to estimated rightward and leftward going strain wave amplitudes. These correspond to elements Λ_{11} and Λ_{22} of equation-(4.56). They were computed by windowing the transient signal for each sensor output, and zero-padding the portion of that window which correspond to propagating wave components of the first reflection from the right free end of the beam-(See Figure 6.12). This was meant to prevent any reflected wave components from corrupting computations of the FFT of incident disturbance and strain wave amplitude estimates. This process worked well for computing the wave sensor

transfer functions, however, several averages were required to minimize the effect of noise in low level strain signals. Nevertheless, from Figure 6.11 the computed wave sensor transfer functions indicate that some wave sensor performance in filtering the incident disturbance is present from *24 Hz. to 100 Hz.* Ideally over this range, the output of the leftward going wave sensor should be close to zero. Below this frequency range filtering is not feasible. This is in part due to poor properties of the distributed sensor below 20 Hz. and the fact that a longer time window is required to include the lower frequency components. In addition, below 1 Hz. the near field terms must not be neglected.

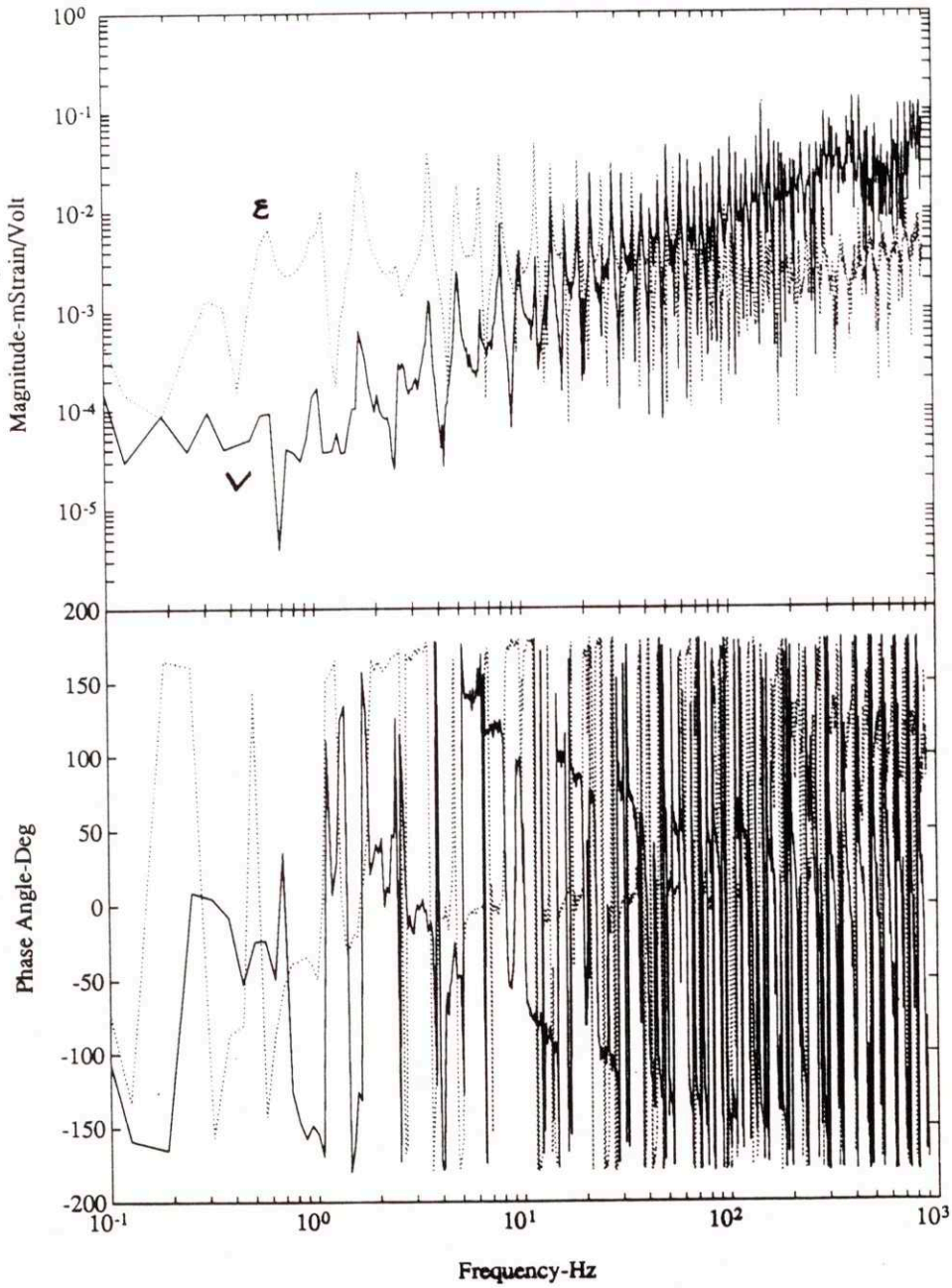

Figure 6.6: Transfer Functions of Distributed and Point Strain Sensors from Torque Motor Actuator.

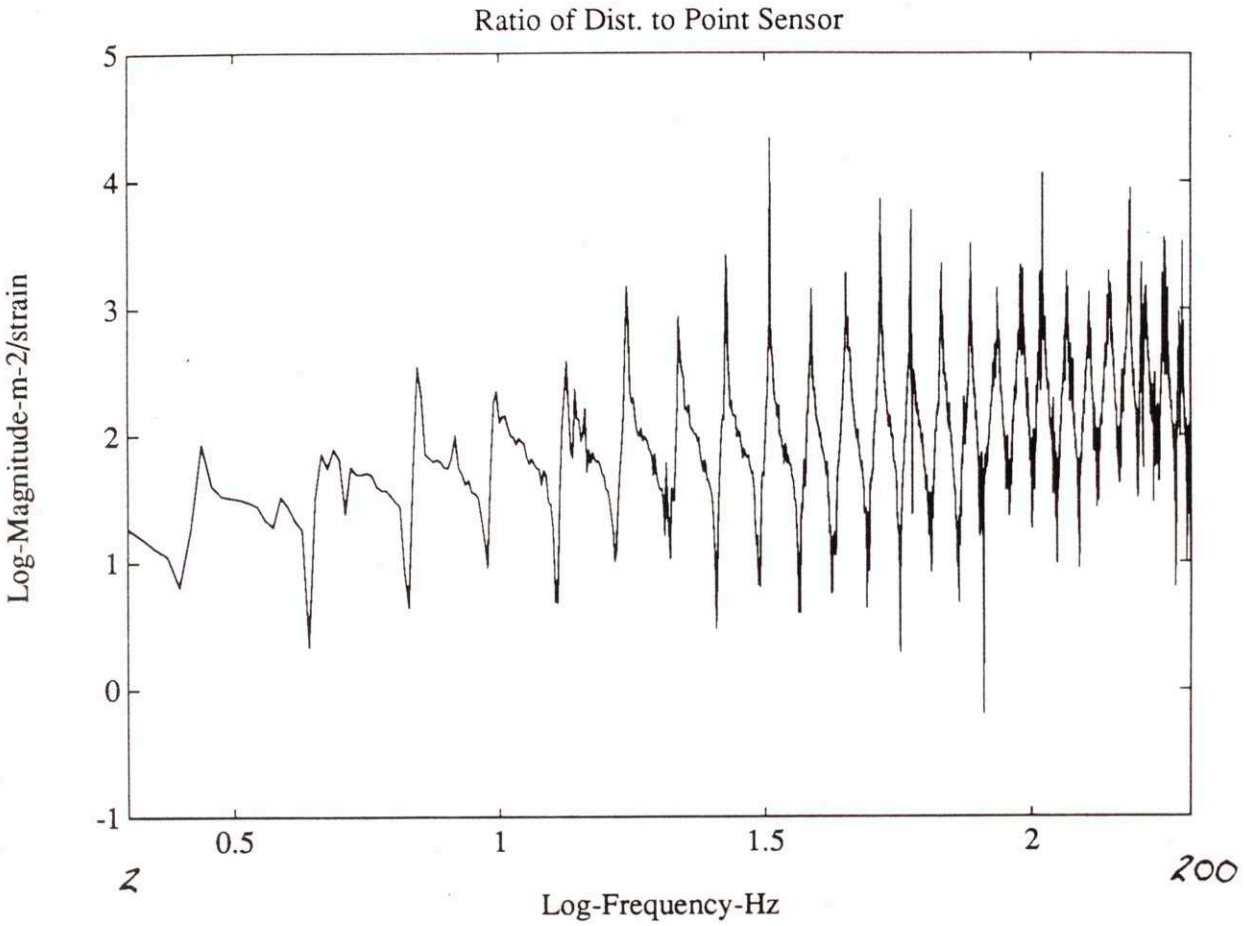

Figure 6.7: Ratio of Distributed and Point Strain sensor Transfer Functions plotted from 2 to 200 Hz. Magnitude

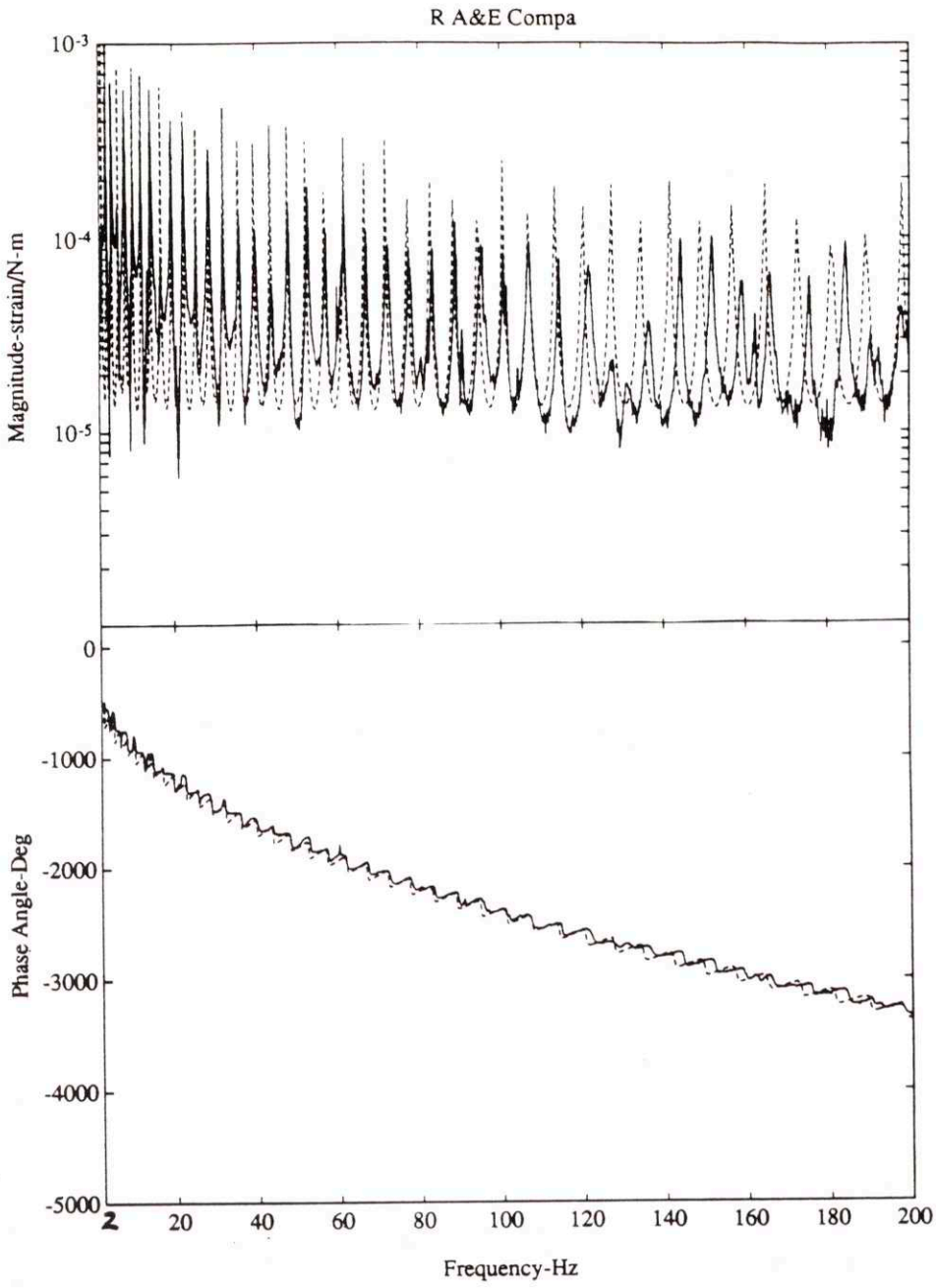

Figure 6.8: Steady-State Comparison of Analytical-(Dashed) and Experimental-(solid) Estimated Rightward-Going Strain Wave Transfer Functions plotted from 2 to 200 Hz. Magnitude and Unwrapped-Phase

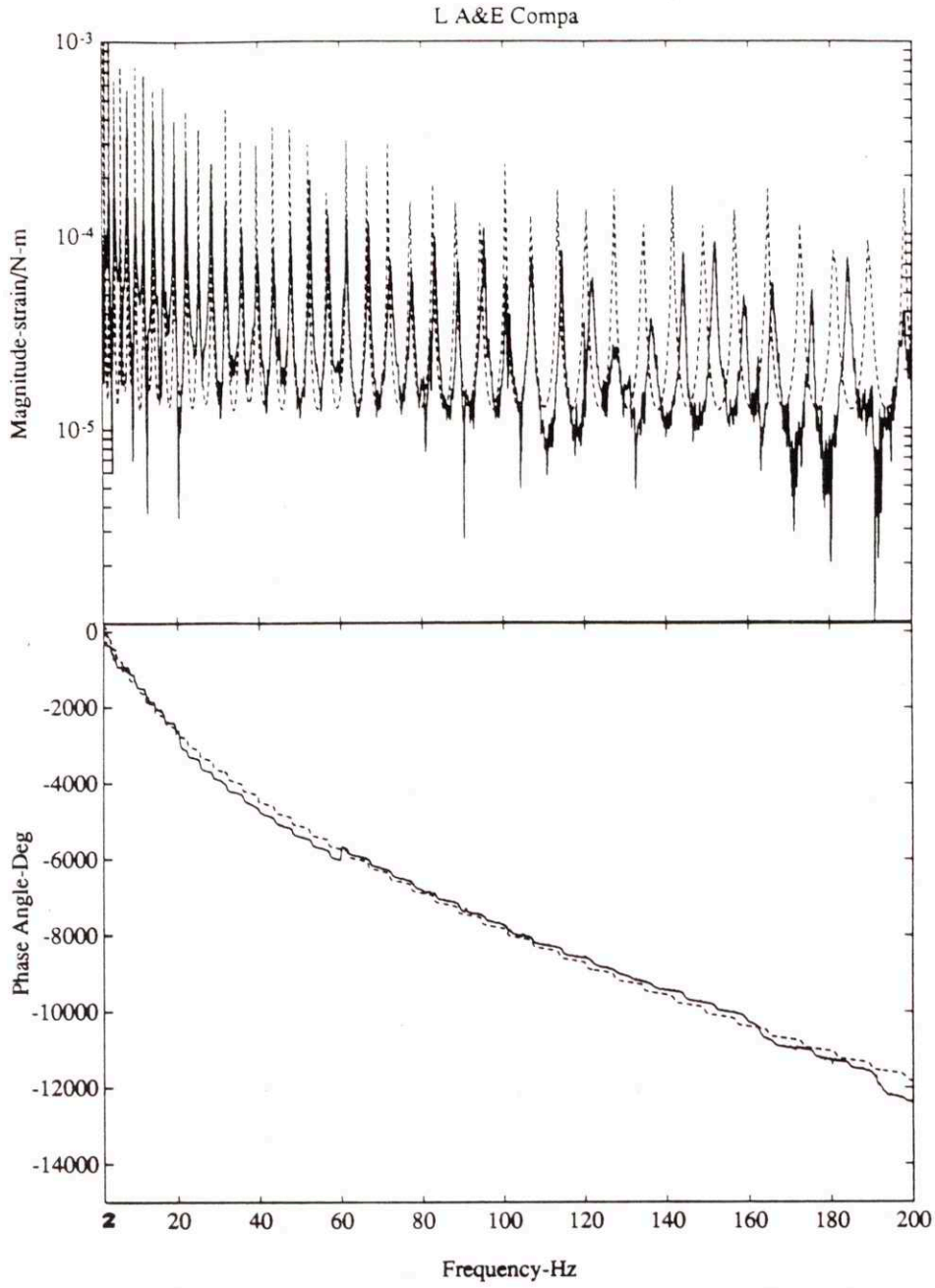

Figure 6.9: Steady-State: Comparison of Analytical-(Dashed) and Experimental-(solid) Estimated Leftward-Going Strain Wave Transfer Functions plotted from 2 to 200 Hz. Magnitude and Unwrapped-Phase.

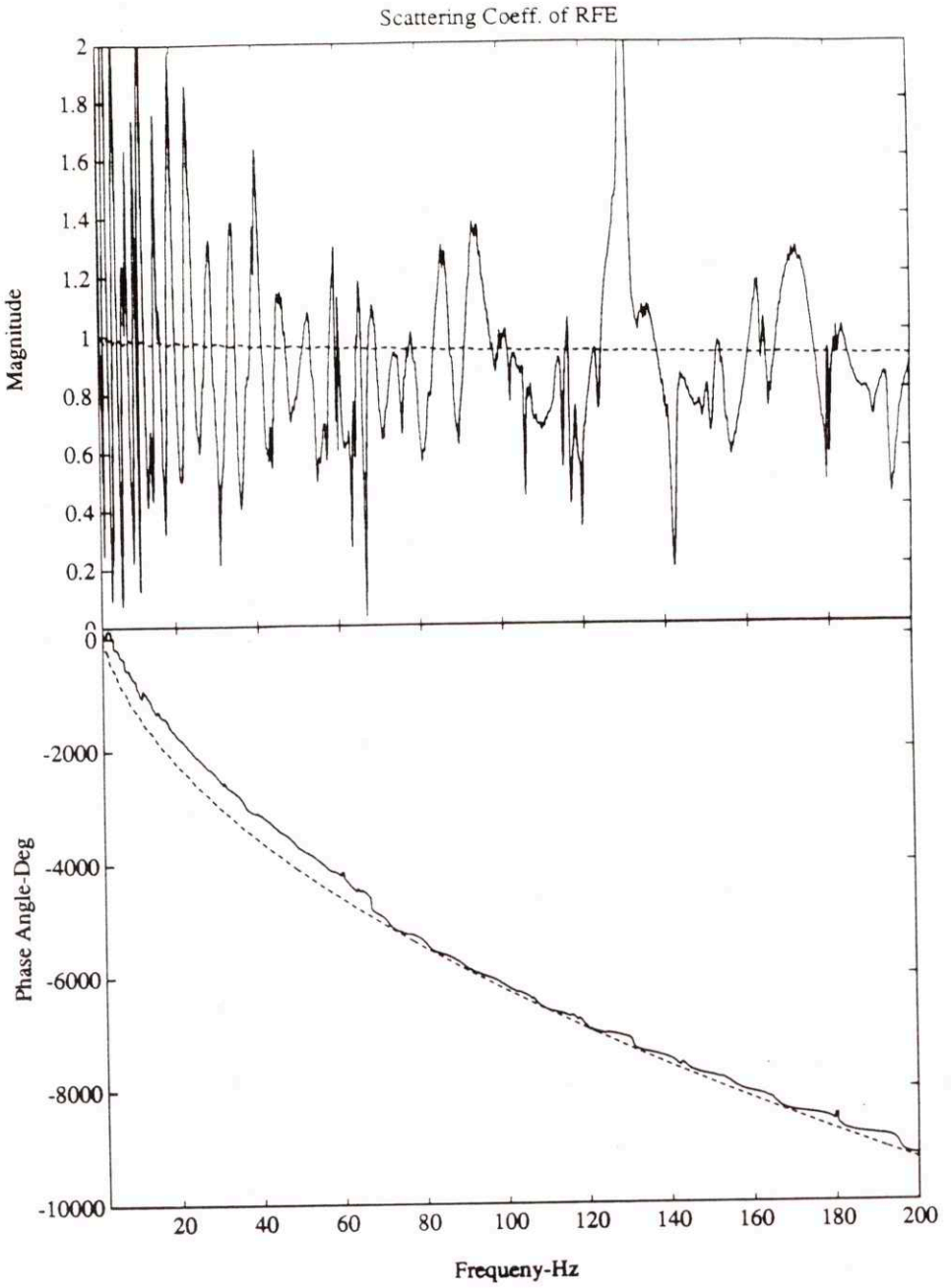

Figure 6.10: Comparison of Analytical and Experimental Reflection Coefficient from the Free End of the Beam plotted between 2 and 200 Hz. Magnitude and Unwrapped-Phase.

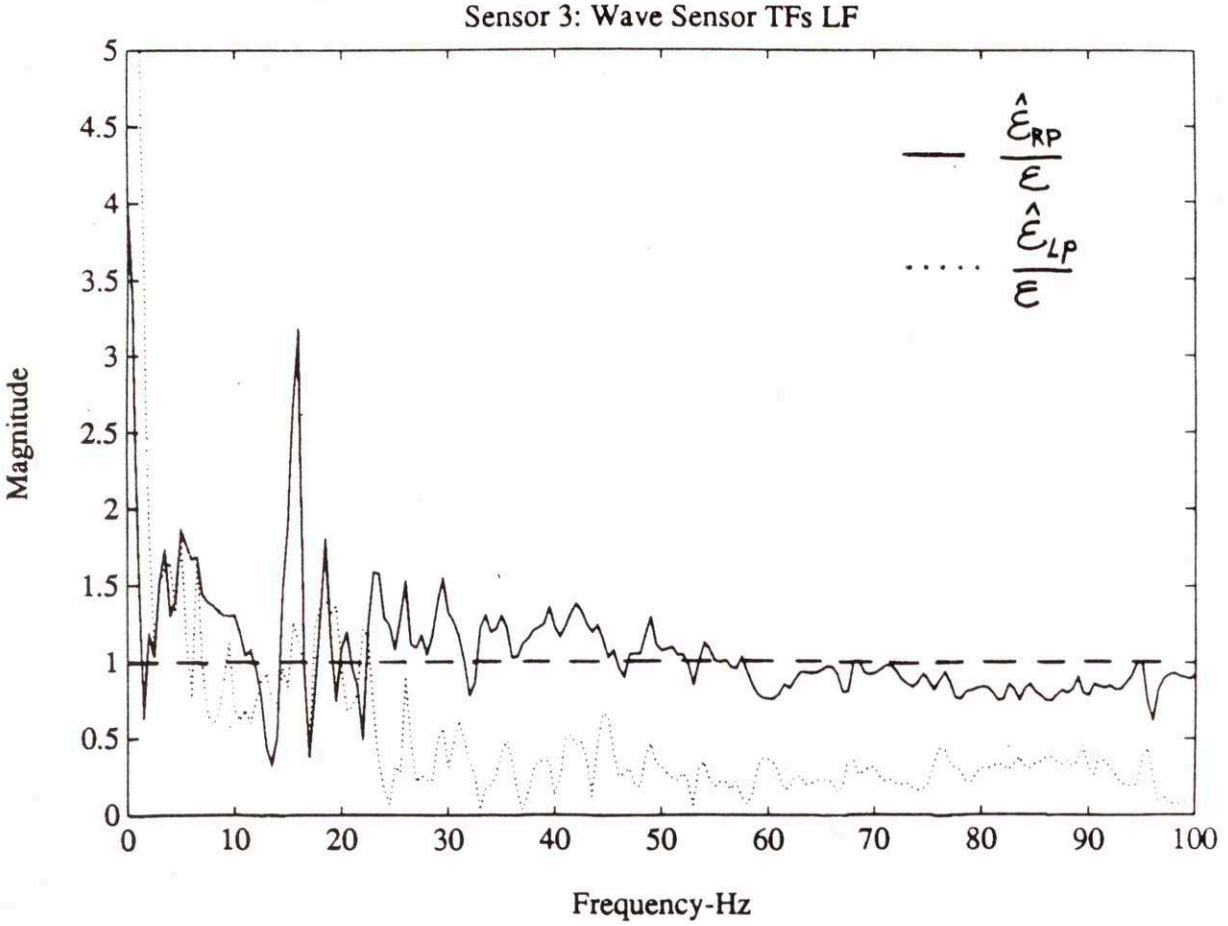

Figure 6.11: Wave Sensor Transfer Functions from Estimated Rightward and Leftward going waves obtained from Temporal Windowed data.

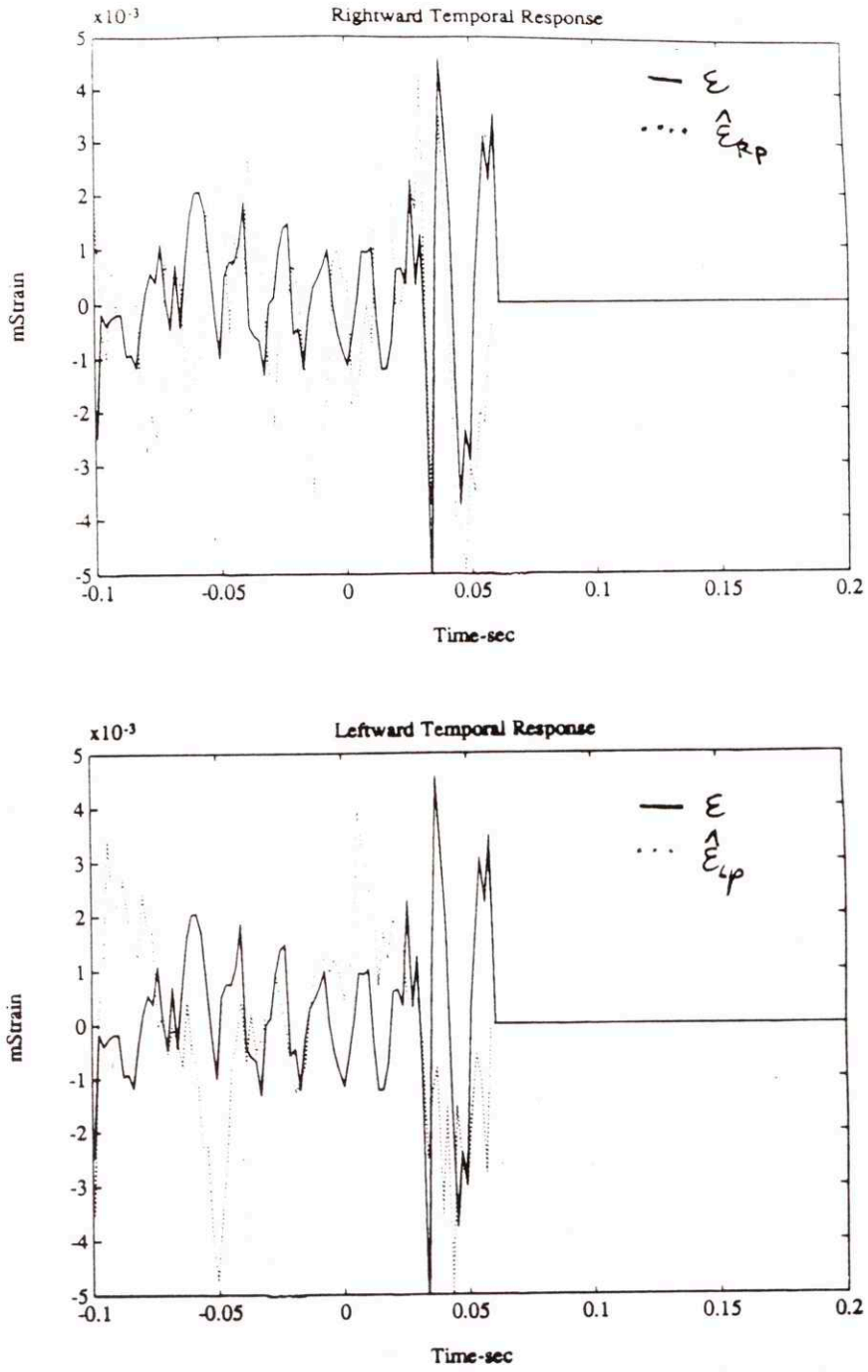

FIgure 6.12: Typical Windowed Temporal Output from Rightward and Leftward Strain Wave Filters. End of Window Padded with Zeros to remove reflected Wave Components.

6.6 Feedforward Wave Control using Wave Sensors

Throughout this work the underlying motivation behind the development of wave sensors discussed in the previous section has been the desire to suppress the resonant vibration dynamics of 1-D structures. The section describes such control of the experimental beam.

6.6.1 Junction Model/Feedforward Loop Structure

The model based Feedforward Control Loop structure is shown in Figure 6.13. This figure displays an idealized model of the disturbance force-$F(\omega)$ which was used to drive the system. Wave sensing is assumed to occur at some interior location in the member. Active control is achieved by feeding the sensed directional wave information through a frequency dependent compensator and then to the moment actuator. The form of the compensation depends on the control objective and the normalization of the sensed wave component. For the experimental apparatus considered in this work active damping is desired and the normalization is taken with respect to strain. Thus, the form of the feedforward compensation is given by

$$M(\omega) = K^{*}(\omega)\,\hat{\varepsilon}_{lp} \tag{6.6}$$

where

$$K^{*}(\omega) = e^{-ikl_1} \tag{6.7}$$

and corresponds to a spatial phase lag.

Since $k \propto \omega^{(1/2)}$ this expression does not correspond to a pure time delay. Approximate digital realizations, however, can be achieved using FIR filters which approximate the frequency properties of the spatial phase lag. Because the lag is dispersive, low frequency components will suffer since they move at much slower speeds requiring very longer FIR filters to accurately mimic their properties.

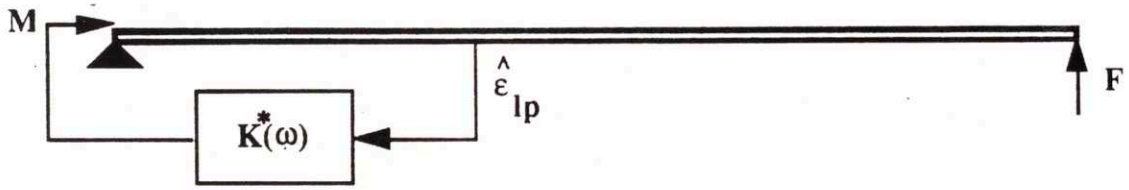

Figure 6.13: Idealized Feedforward Loop Structure.

6.6.2 Real-Time Control Hardware

The Heurikon HK68V30XE which runs at 33 MHz and has 4 Mbytes of available RAM was used to realize all feedforward compensators. It operates on a single board and uses the VME architecture to communicate to other boards over the backplane. One such board that it communicated with was the CSPI Supercard I which was used to perform fast floating point computations of vector dot products. Analog to Digital-(Input) and Digital to Analog-(Output) conversions were done using data translation cards DT1492 and DT1406 respectively. A Sun Microsystem Sparc Workstation served as the host computer which interfaced with the HK68V30XE so that macro programs in Matlab could be used to find good FIR realizations of $K^*(\omega)$. These FIR filter coefficients were then downloaded to the HK68V30XE for real-time control.

Figure 6.14 displays the real-time control hardware along the analog components required for directional wave filtering. Thus, from this figure it is obvious that active control from this perspective required a two tiered approach. This first involved analog realization of wave sensing and the second required digital realization of $K^*(\omega)$. A sampling rate of 400 Hz. was chosen for all closed-loop tests. Higher sampling rates increase the order of FIR filter approximation and are beyond the range of applicability of the actuator hardware.

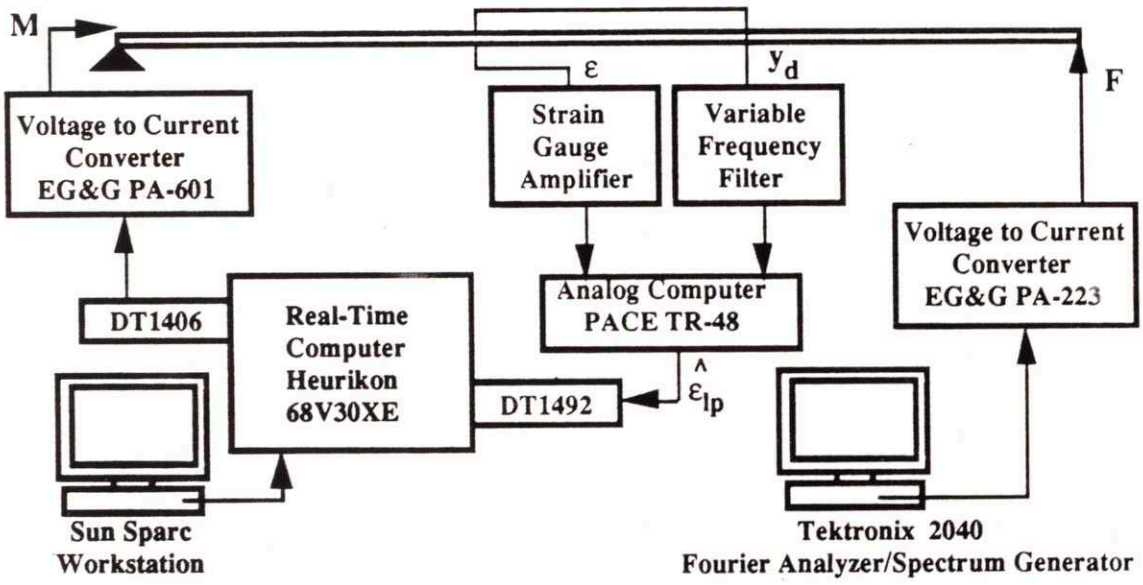

Figure 6.14: Real-Time Control Hardware.

6.6.3 Model-Based Results

Implementation of the model-based $K^*(\omega)$ by the Heurikon HK68V30XE with parameters given in Table 6.1 and an assumed structural damping of 0.1% leads to the closed-loop results shown in Figure 6.15. A strain sensor collocated with the wave sensing location serves as the diagnostic sensor. Notice that this plot shows that there is very little difference between open loop and closed loop-results for the frequency range shown.. Although 20 modes appear in this figure, only show signs of reduction.

6.6.4 Measurement Based Results

The poor performance of the model-based compensator motivated an approach that would identify the actual experimental feedforward compensation required to zero the scattering coefficient of the left pinned-end. This approach involved the determination of 4 transfer functions relating inputs $M(\omega)$ and $F(\omega)$ to outputs $\hat{\varepsilon}_{lp}(0,\omega)$ and $\hat{\varepsilon}_{rp}(0,\omega)$ -(See Loop Structure in Figure 6.14. These tranfer functions are given by

$$\hat{\varepsilon}_{rp} = H_1(\omega)M(\omega) + H_2(\omega)F(\omega) \tag{6.8}$$

$$\hat{\varepsilon}_{lp} = H_3(\omega)M(\omega) + H_4(\omega)F(\omega) \tag{6.9}$$

Now if $M(\omega)$ is defined based on feedforward of $\hat{\varepsilon}_{lp}(0,\omega)$ multiplied by a frequency dependent compensator $K^*(\omega)$ then setting $\hat{\varepsilon}_{rp}(0,\omega)=0$ and solving for $K^*(\omega)$ gives the following experimental feedforward compensation

$$K^*(\omega) = \frac{H_2}{H_1 H_4 - H_2 H_3} \tag{6.10}$$

This experimental expression-(solid) is plotted in Figure 6.16 along with an 128 order FIR filter approximation-(dotted). As pointed out by Mckinnell, control performance of the filter is determined by how well the phase of the approximate filter matches that of the actual filter. Notice that the FIR approximation includes the effect of the D/A conversion process.

With this FIR filter approximation of the experimental $K^*(\omega)$ programmed, real-time control is much improved as displayed in Figure 6.17. As in the model-based case strain information collocated with the wave sensing location is used to serve as the diagnostic sensor for evaluating the effectiveness of the control. This figure compares the open loop-(dotted) transfer function from force at free-end to diagnostic strain sensor with the closed loop-(solid) transfer function from *1* to *60 Hz*. The upper limit on the frequency range was imposed by the inertia of the proof mass actuator located at the free-end. Notice that twenty

beam modes are visible in this frequency range. Of these 20 modes 4-(8,9,11,18) remain unaffected by feedforward control, i.e. their magnitude and phase properties remain virtually the same. However, this implies that damping has been increased in 16 of the 20 modes. Some of these increases are significant as in modes 6,12,17,19 and 24, however, many exhibit only moderate increases. On the average the best reduction occurs where the wave-sensor performs well and the FIR filter approximation matches the experimental compensator in magnitude and phase. This range lies between *20* and *60 Hz*. Nevertheless, results are much improved over those found in during the model-based realization of $K^*(\omega)$.

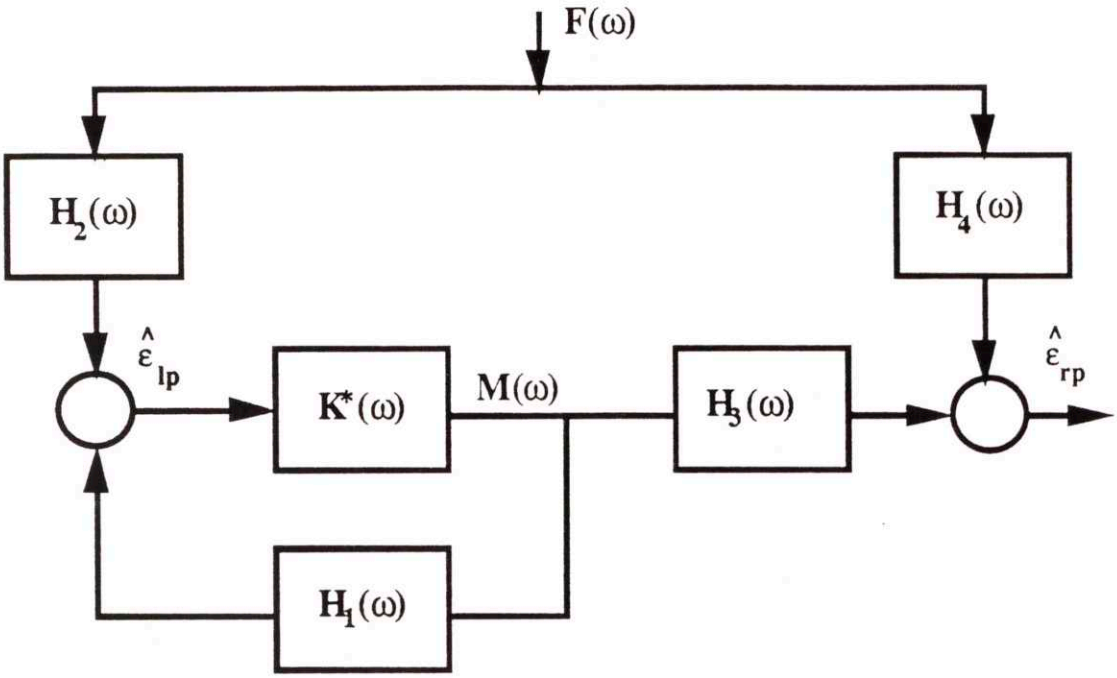

Figure 6.16: Loop Structure for Identifying $K^*(\omega)$. from Experimental Transfer Functions

6.6.5 Stability

The loop structure of Figure 6.14 contains a positive feedback loop corresponding to feedback of

leftward going waves after they reflect off the free end and return to the sensing location. Due to some sensitivity of the wave sensor to outgoing waves, the local feedback loop is

also still present. Stability of this loop is evaluated by analyzing the loop transfer function given by

$$T(\omega) = \frac{H_1 H_4}{H_2 H_3 - H_1 H_4} \qquad (6.11)$$

Figure 6.18 plots this function computed from the experimental transfer functions used to compute $K^*(\omega)$.. From this Figure it is clear that any increase in the gain should degrade performance.

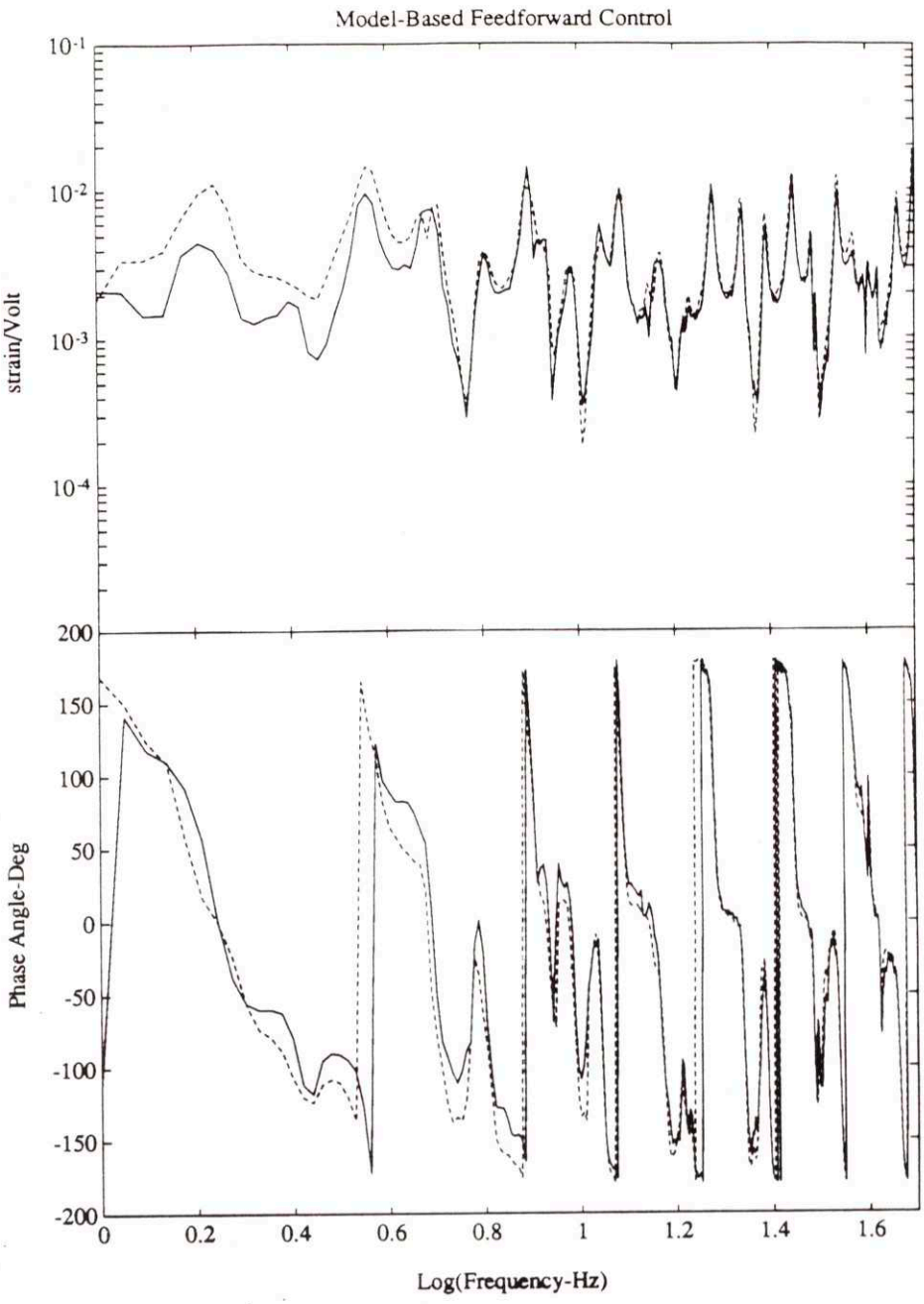

Figure 6.15: Feedforward Control. Open and Closed-Loop Results for Model-Based FIR Filter Implementation of $K^*(\omega)$. Plotted from 2 to 60 Hz.

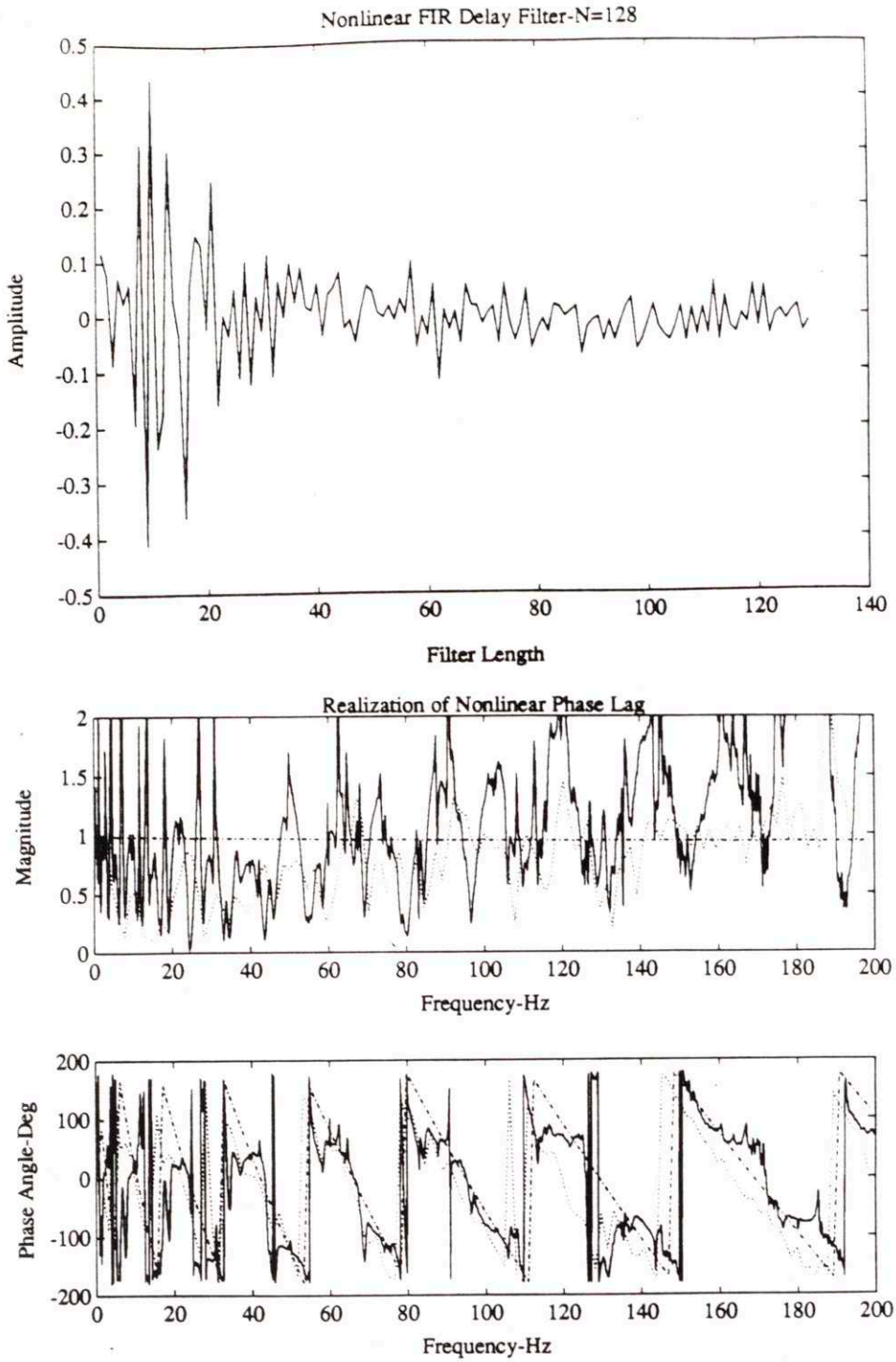

FIgure 6.17: Comparison of Measurement-Based Compensator and FIR Filter Approximation of $K^*(\omega)$.. (a) FIR Filter coefficients-N=128. (b) Frequency Properties-(dashed-dotted-model-based compensator, dashed-FIR Filter Approximation, solid-measurement based compensator.

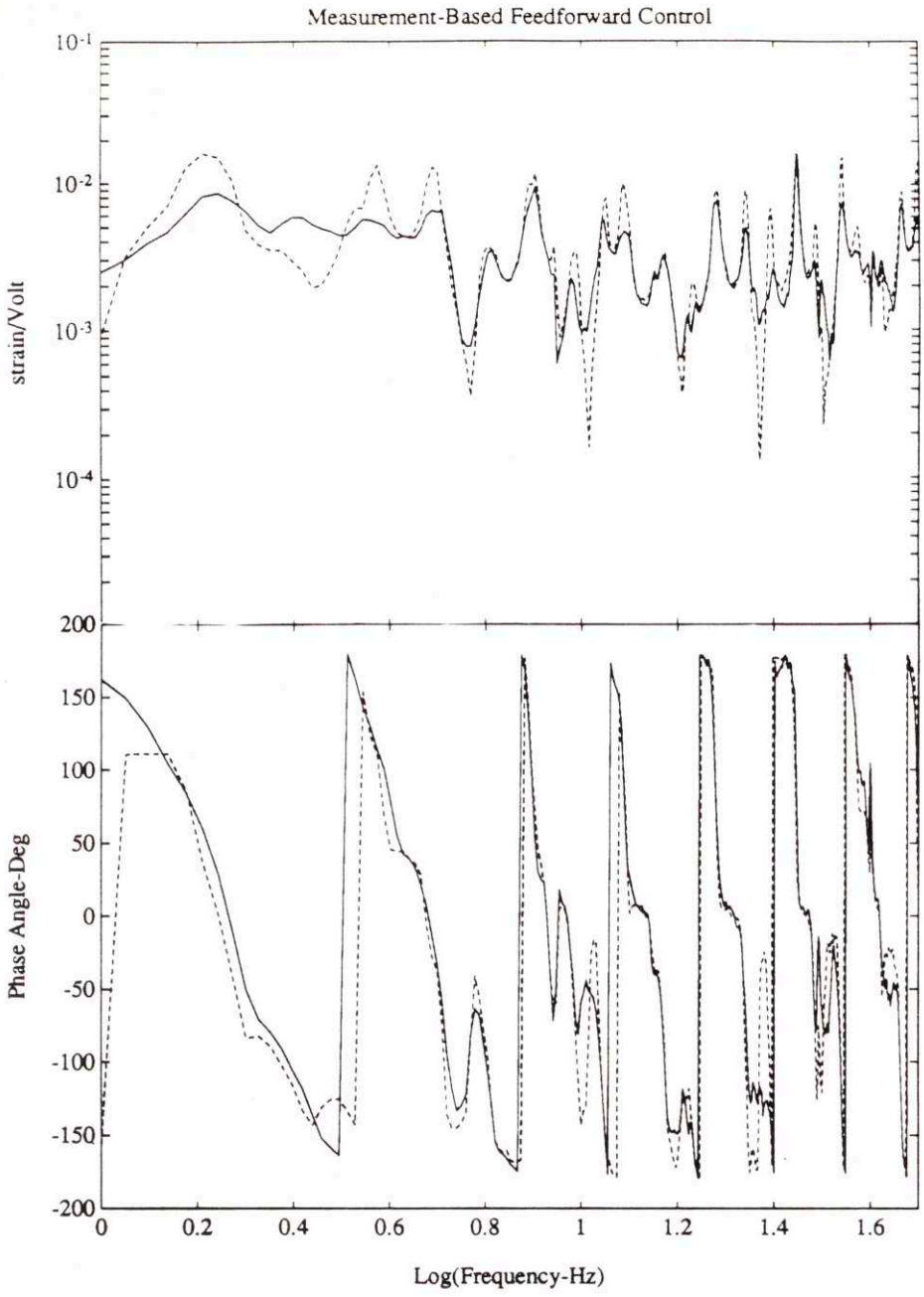

Figure 6.18: Feedforward Control. Open and Closed-Loop Results for Measurement-Based FIR Filter Implement-ation of $K^*(\omega)$. Plotted from 2 Hz to 60 Hz.

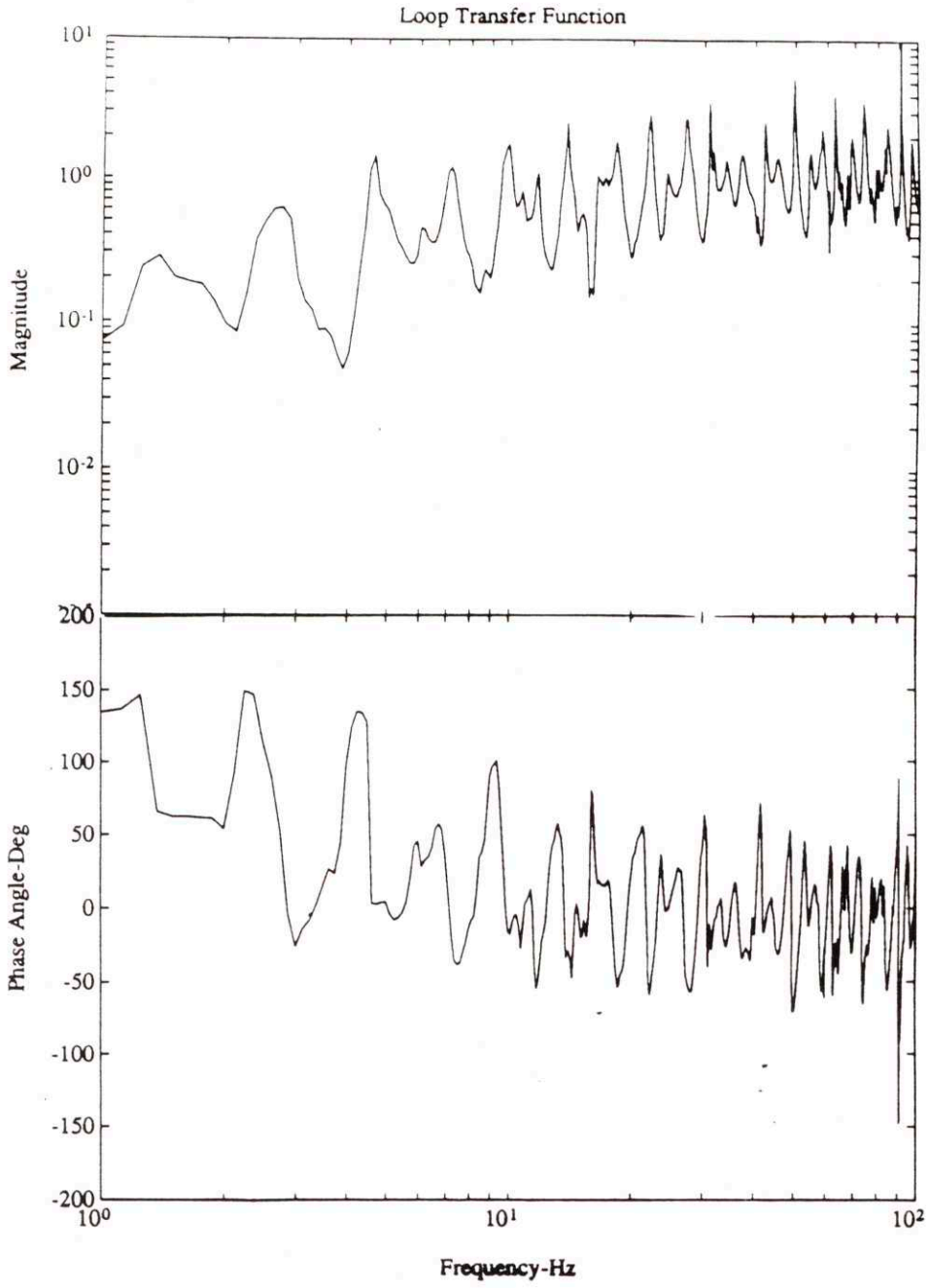

Figure 6.19: Loop Transfer Function of Resonant Beam for Feedforward of leftward going strain wave.

6.7 Summary

It is believed that the poor performance of the feedforward wave control is due to lack of compatibility between the wave filter and the control actuator. Wave sensing can be extended down to *1 Hz* by manufacturing a longer distributed sensor. However, a longer sensor makes the manufacturing process more difficult and increases the likelihood error, either during electrode shaping or sensor/structure bonding. Present electrode shaping procedures can only produce a pattern which has a resolution of *1 mm.* which may not be accurate enough to achieve good wave filtering. In addition, it is not clear whether the bonded sensor truly sees a uniform transverse strain field over its width and length. Finally, improvements in the sensing scheme will undoubtedly improve the characteristics of the compensator $K^*(\omega)$ making it more suitable for FIR filter approximations.

Chapter 7

Conclusions

7.1 Summary

This thesis has developed a novel approach to sensing wave propagation responses along simple one-dimensional structural elements for the purposes of structural control. Specifically, a method has been developed to infer directional wave propagation dynamics using only *distributed sensors*. This method exploits a class of *band-limited trigonometric functions-$\phi(x)$* which when convolved over the spatial domain with distributed position, slope, strain or internal shear force yield distributed sensor signals that are proportional to rightward or leftward going travelling wave dynamics. The use of band-limited trigonometric functions to shape distributed sensors represents a new approach which overcomes the causality limitations imposed by the use of a finite set of individual point sensors-[45,46] to infer directional wave dynamics at a location in a one-dimensional structural member. In addition, this thesis has shown that by invoking the dispersion relation-(k *vs.* ω) of a member, a portion of the temporal compensation used to suppress or alter the resonant vibrations of a finite structure, can be incorporated in the weighting function-$\phi(x)$ along with the properties necessary for directional wave filtering. Such a

directionally sensitive sensor confirms the view of one-dimensional structures based on wave-propagation models which have terminating and non-terminating boundary conditions. More importantly, such a sensor complements previously developed active control schemes based on wave propagation descriptions of one-dimensional structural dynamics. These control schemes often require knowledge of directional information to achieve certain control objectives such as Active Damping and Active Isolation. Thus, because of their directional sensitivity the sensors developed in this thesis lend themselves quite readily to many wave control schemes. This unique attribute offers many advantages over physical measurements since the properties of the temporal compensation can be greatly simplified.

The use of distributed sensors to achieve directional wave filtering was motivated by the application of *KYNAR* PVDF piezo film to the structural control problem-[73,74,76]. As a distributed sensor PVDF was found to be lightweight, compliant, durable and to exhibit a high signal-to-noise ratio for a given strain. In addition, the electrode of the film could be shaped to perform the work of an array of equally spaced point sensors whose outputs are multiplied by the value of the function at that location and then summed. This implied that tedious digital computations were not required. Thus, the distributed sensor convolved the weighting pattern-$\phi(x)$ of an electrode on one-side with the strain field seen by the piezo film to obtain the response at a point location in a structural member. A good bond between the sensor and structure was required to insure that the strain on the surface of the structure was transfered to the film. For many modal-based control objective such a sensor performed adequately, however, never before has such a sensor been used to infer directional dynamics for the purposes of structural control. This thesis has demonstrated that distributed PVDF strain sensors can be used to infer directional wave dynamics for the purposes of structural control.

Verification of the wave sensing/wave control concept was attempted on an experimental pinned-free brass beam using a single point/distributed PVDF strain sensor pair. Both steady-state and transient tests were conducted to verify analytical predictions. However, because of the inertia of the actuators used to excite and control the beam experimental results were restricted to frequencies ranging from *2 to 200 Hz* in the open loop tests, and from *2 to 60 Hz.* in the closed loop tests. In the open loop case both steady-state and transient tests showed that the wave sensor performed adequately in the frequency range from *20 to 200 Hz.* Specifically, Figures 6.8 and 6.9 showed close agreement between the analytical and experimental estimates of the rightward and leftward going strain-wave amplitudes from *20 to 100 Hz.* These figures depicted the characteristic pole-dynamics and phase lags that are consistent with predicted strain wave amplitude transfer functions. As

anticipated zero dynamics are present in such transfer functions since these transfer functions account for only the constructive interference of incident and reflected waves which circumnavigate the beam. Transient tests further verified the directional sensitivity of the wave sensor developed in this thesis, however, this method of verification suffered from low signal-to-noise ratios and temporal windowing phenomena. Nevertheless, some preliminary closed loop tests using the estimated strain wave amplitudes were attempted on the experimental beam. Results from these closed loop tests-(See Figure 6.18) lead to significant damping in at least *10*-modes of the structure, however, *4*-modes in the frequency range from *2 to 60 Hz* retained their open loop dynamics. This was in large part due to the fact that the implemented temporal compensator did not match the experimental compensator over the entire frequency range of interest.

7.2 Chapter Contributions

More specifically, contributions from the six chapters in this thesis can be summarized as follows

Chapter 1 motivated the wave sensing technique developed in this work from a controlled-structures point of view. This motivation had its origins in the work of Swinbanks, von Flotow, Scheuren, Miller, Pines, Mckinnell, Elliott and many others. The underlying component inherent in all of this work was the concept of controlling a system based on a travelling wave description of the component dynamics. From this perspective two control objectives could be addressed, Active Damping or Active Isolation. The former was attempted in this work.

Chapter 2 developed one-dimensional wave-models which provided the basis for the analysis of Chapters 3, 4, 5 and 6. Here the frequency formalism of references-[10] and [32] is adopted to obtain simple 1-D descriptions of rods and beams.

Wave sensing issues involving only point sensors were discussed in *Chapter 3*. The main issue of concern in this chapter was a discussion of causality and its influence on directional filtering. It was demonstrated that filtering of propagating wave amplitudes from point sensors all of which are positioned at a p;articular location in a member often required the implementation of non-causal temporal filters. This was especially true in the case of a Bernoulli-Euler beam. Thus, the purpose of this chapter was to demonstrate that causal realizations are possible using point sensors. Such schemes, however, typically

require digital manipulation of a finite set of equally spaced point measurements of the same kind such as deflection, slope, etc. where the separation distance between these individual measurements provides the impetus for directional wave filtering. This is because temporal phase lags between individual sensor can be manipulated to inter directional information. Similar ad-hoc schemes were devised by Scheuren-[45,46].

Besides point out the pitfalls of wave sensing using point sensors, this chapter provided an approach to optimize point sensor spacing in the presence of sensor noise. In addition, a transient analysis was presented to illustrate the effectiveness of the directional filtering process for a rod excited by a single sinusoid.

Chapter 4 presented a more systematic view of achieving directional filtering of wave dynamics using distributed sensors and served as the main contribution of this thesis. The key concept formulated in this chapter was the application of a class of band-limited trigonometric weighting functions-$\phi(x)$ to the concept of wave sensing. This chapter demonstrated that distributed sensors could be used to convolve these weighting functions with distributed position, slope, strain or internal shear force to infer directional wave dynamics. This approach eliminated the problems of causality, spatial and temporal aliasing, and digital processing errors which limit wave filtering schemes using equally-spaced point sensors. The approach developed in this chapter also permits plenty of flexibility in designing the frequency properties of the filtered rightward and leftward going wave amplitudes. This implies that generalizations of directional filtering may be possible for one-dimensional structures which have more complex dispersion relations. These advantages are not possible with point sensors.

Chapter 5 discussed the use of distributed wave sensors in non-collocated feedforward control loops for both a rod and a beam. It was shown that for non-dispersive and dispersive 1-D members that a portion of the compensation could be incorporated in the wave sensing scheme. This was done by including the properties of the temporal compensation in the weighting function-$\phi(x)$ which was convolved with physical measurements. For both the rod and beam analytical simulations demonstrated that significant damping could be added to a structure. However, in the case of the beam the presence of near-field terms in conjunction with poor properties of the distributed sensor at low frequencies limited the effectiveness of the control. The degree of non-collocation between sensor and control actuator also hindered performance by adding additional phase lag in the Feedforward Compensator. Because this lag was non-linear with frequency digital realization was required. This was done using FIR filter approximations. Because

of the finite spatial length of the sensor these approximations were not accurate for long wavelengths. However, in the range where the near-field terms were negligible and the filter estimates were good, closed-loop results demonstrated that significant damping could be added to several modes using 2 sensors and 1 actuator.

The concept of wave propagation filters for structural control was verified in *Chapter 6* on an experimental brass beam. The verification process first involved confirming the concept of wave sensing under both steady-state and transient structural excitations and subsequently using strain wave estimates to perform feedforward control Results from the sensing tests showed that the wave filtering scheme performed well in frequency range from *20 to 200 Hz*. The oscillatory behaviour seen in the estimated strain wave amplitude transfer functions was thought to be due to the cutting errors of the distributed sensor. The trend, however, of these transfer functions were comparable to those predicted by the theory.

Closed-Loop control using these estimated wave states was also attempted. This required the use of a real-time computer-(Heurikon 680V30) to approximate properties of the desired feedforward compensator. Both model based and measurement compensators were implemented. Best results were achieved using the measurement-based compensation in the frequency range from *2 to 60 Hz*. Moderate damping of the *20* structural modes in this frequency range was apparent, however, at least *4* modes retained their open loop dynamics. The distant loop transfer function from control moment to leftward-(incoming) going-wave was found to be stable for nominal control gains.

7.3 Recommendations for Future Study

Although this thesis has presented a comprehensive approach to filtering wave dynamics using distributed sensors on one-dimensional structures, there are several potential avenues for future study. I describe some of these directions below

- First of all I believe that the sensor/structure bond plays an integral role in the performance of the sensing scheme. It is clear that for distributed PVDF strain sensors any irregularity in the strain field across its width will directly affect the performance of the directional wave sensor. Thus, to improve the wave sensor's performance, a detailed experimental study of potential bonding agents is required for different sensor/structure interfaces.

- Secondly, the manufacturing process used to shape the electrode of PVDF strain sensor which duplicates the properties of a particular weighting function requires much improvement. In this thesis I have not devoted much effort to this issue other than to point out that the present manufacturing process is only capable of mimicking the analytical weighting function-$\phi(x)$ to within $1mm$ of resolution. Clearly, this will not suffice if the wave sensing scheme presented in this thesis is to achieve its full potential.

- Thirdly, optimal weighting function design methods-(See equation *4.46*) should be explored to determine how such techniques might improve the design of wave sensors using distributed sensors. These methods present the opportunity to improve the properties of the wave sensor in specific frequency ranges while sacrificing performance in another regime.

- Fourthly, I have deliberately ommitted a discussion of the possibility of point forces appearing in the distributed sensing domain from the general body of this thesis. However, I have added such a section in Appendix A5 which considers Active Isolation on a B-E beam where the control force acts in the center of the sensing domain. The analysis presented in this section accounts for only the reverberant dynamics in the member. No discussion of the dynamics of the incident wave field generated by the point control force is presented. Further study, however, is required to understand the problems created by such a force.

- Fifthly, the unique form of the output of the wave sensor lends it quite readily to Adaptive Feedforward Control schemes which exploit upstream and downstream measurements of wave dynamics. Typically this information is gathered by sensors which measure the physical response of the member at a particular location. Feeding such signals to Feedforward control loops results in local Feedback loops as described in Chapter 1. Wave sensors eliminate this problem and thus reduce the likihood of an instability.

- Sixthly, in this thesis I have only developed a method for filtering the *propagating components* on dispersive and non-dispersive one-dimensional

structures. Further study is required to develop a directional wave sensor which is also sensitive to near field-(evanescent) components of the incident and reverberant response. Such a filter would enhance active control schemes which rely on just propagating components.

- Finally, the distributed wave sensing concepts developed in this thesis should be applied to two-dimensional structures such as plates and shells.

8.0 References

[1] M.J. Balas, "Trends in Large Space Structure Control Theory: Fondest Hopes, Wildest Dreams," *IEEE Trans. on Automactic Control*, Vol. AC 27, No.3, June 1982.

[2] S.N. Atluri, A.K. Amos, Large Space Structures-Dynamics and Control, Springer Verlag, 1988.

[3] R. Vaicaitis and J.S. Mixson, "Review of Research on Structureborne Noise," *AIAA Paper 85-0786*.

[4] M. Athans, Multivariable Control Theory Lecture Notes, *Massachusetts Institute of Technology*, Cambridge, MA., 1990.

[5] R.H. Lyon, "Statistical Energy Analysis of Dynamical System: Theory and Application," *MIT Press*, 1975.

[6] R.M. Chi, "Asymptotic Modal Analysis of Structureborne Noise in Cross Beams," *United Technologies Research Center* , Report No. 84-152447-1, Oct. 1984.

[7] E.H. Dowell and Y. Kubota, "Asymptotic Modal Analysis and Statistical Energy Analysis," *J. of Applied Mechanics*, 1985.

[8] A.H. von Flotow, Travelling Wave Effects in LSS," *NASA Workshop on Applications of Distributed System Theory to the Control of Large Space Structures*, JPL, July 14-16, 1982.

[9] A.H. von Flotow, "A Travelling Wave Approach to the Dynamic Analysis of Large Space Structures," *24th SDM Conference*, South Lake Tahoe, CA., May 2-4, 1983.

[10] A.H. von Flotow, "Disturbance Propagation in Structural Networks," *PhD Dissertation*, Dept. of Aeronautics and Astronautics, Stanford University, Stanford, CA.,1984.

[11] M.A. Swinbanks, "The Active Control of Sound Propagating in Long Ducts," *J. of Sound and Vibration*, 27, pp.411-436, 1973.

[12] J.H.B. Poole and H.G. Leventhall, "An experimental study of Swinbank's method of active attenuation of sound in ducts," *J. of Sound and Vibration*, 49, pp. 257-266, 1976.

[13] M. Berengier and A. Roure, "Broadband active sound absorption in a duct carrying uniformly flowing fluid," *J. of Sound and Vibration*, 68, pp. 437-449, 1980.

[14] C.F. Ross, "An adaptive digital filter for braoadband active sound control," *J. of Sound and Vibration*, 80,pp. 381-388, 1982.

[15] J.E. Ffowcs Williams, I. Roebuck and C.F. Ross, "Anti-Phase Noise Reduction," *Physics Technology*, 16, 1985, pp. 19-24.

[16] J. Scheuren, "Active Control of Bending Waves in Beams," *Proceedings of Inter-Noise 85*, Munich, FDR, pp 591-594, Sept 1985.

[17] A.H. von Flotow and B. Schaefer, "Experimental Comparison of Wave Absorbing and Modal Based Low-Authority Controllers for Flexible Beam," *AIAA Guidance and Control Conference*, Snowmass, Co., August, 1985.

[18] A.H. von Flotow, "Travelling Wave Control for Large Spacecraft Structures," *J. of Guidance, Control and Dynamics*, Vol. 9, No. 4, July-Aug, pp 462-468, 1986 .

[19] A.H. von Flotow, "Disturbance Propagation in Structural Networks," *J. of Sound and Vibration*, 106(3), pp 433-450, 1986.

[20] A.H. von Flotow and B. Schaefer, "Wave-Absorbing Controllers for a Flexible Beam", *J. of Guidance, Control and Dynamics*, Vol. 9 No. 6, pp 673-680, Nov-Dec 1986.

[21] P. Hagedorn and J. Schmidt, "Active Vibration Damping of Flexible Structures using the Travelling Wave Approach," *Proceedings of the 2nd International Symposium on Spacecraft Flight Dynamics*, ESA SP-255, Darmstadt, FDR,1986.

[22] P. Hagedorn and J. Schmidt, "On the Active Vibration Control of Distributed Parameter Systems," *Proceedings of the 6th VPI &SU/AIAA Symposium on Dynamics & Control of Large Space Structures*, Blacksburgh, VA., pp 359-373, 1987.

[23] J. Schmidt, "Entwurf von Reglern zur Aktiven Schwingungsdampfung an flexiblen mechanischem Strukturen," *PhD Dissertation*, TH Darmstadt, FDR.,1987

[24] R.J. Nagem, "Control of One-Dimensional Distributed Structure based on Wave Propagation Analysis," *PhD Dissertation*, Department of Mechanical Engineering, Massachusetts Institute of Technology, Cambridge, Mass.,1987.

[25] B.R. Mace, "Active Control of Flexural Vibrations," *J. of Sound and Vibration*, 114(2), pp. 253-270, 1987.

[26] W. Redman-White, P.A. Nelson, A.R.D. Curtis, "Experiments on the Active Control of Flexural Wave Power Flow," *J. of Sound and Vibration*, 112(1), pp 187-191, 1987.

[27] J. Signorelli and A.H. von Flotow, "Wave Propagation in a Periodic Truss Beam," *Proceedings of AIAA Dynamics Specialist Conference, Monterey*, CA., April 9-10, 1987.

[28] D.W. Miller, A.H. von Flotow, and S.R. Hall, "Active Modification of Wave Reflection and Transmission in Flexible Structures," *Proceedings of the American Control Conference-ACC, Mineapolis*, Minnesota, June10-12, 1987.

[29] A.H. von Flotow, "The Acoustic Limit of Structural Dynamics," *Large Space Structures; Dynamics and Control*, chapter edited by S. Atluri and T. Amos, Springer Verlag, 1987.

[30] A.U. Kuehnle, "Control and Simulation of Longitudinal Wave Propagation with Voigt Damping," *PhD Dissertation*, Department of Mechanical Engineering, Massachusetts Institute of Technology, Cambridge, Mass.,1988.

[31] R.J. Mckinnell, "Active Vibration Isolation by Cancelling Bending Waves," *PhD Dissertation, Cambridge University*, Cambridge, CB21PZ, U.K.,1988.

[32] D.W. Miller, "Modelling and Active Modification of Wave Scattering in Structural Networks," *PhD Dissertation*, Department of Aeronautics and Astronautics, *Massachusetts Institute of Technology*, Cambridge, Mass.,1988.

[33] J. Scheuren, "Non-Reflecting Termination for Bending Waves in Beams by Active Means," *Internoise-88.*

[34] ARD. Curtis, "The theory and Application of Quadratic Minimisation in the Active Reduction of Sound and Vibration," *PhD Dissertation*, University of Southampton, U.K.,1988

[35] A.U. Kuehnle, "Control of Longitudinal Waves in a Rod with Voigt Damping," *Proceedings of the American Control Conference*, Pittsburgh, PA., pp 206-211, 1989.

[36] D.W. Miller, S.R. Hall and A.H. von Flotow, "Optimal Control of Power Flow at Structural Junctions," *Proceedings of the American Control Conference*, Pittsburgh, PA., pp 212-220, June 21-23, 1989.

[37] D.J. Pines and A.H. von Flotow, "Active Control of Bending Waves at Acoustic Frequencies," *Proceedings of the Automatic Control Conference*, Pittsburgh, Pa., pp 221-29, June 21-23, 1989.

[38] J.K. Bennighof and L. Meirovitch, "Active Suppression of Traveling Waves in Structures," *J. of Guidance, Control and Dynamics*, Vol. 12, No. 4, July-Aug, 1989.

[39] D.W. Miller and S.R. Hall, "Experimental Results Using Travelling Wave Power Techniques,"*1989 ASME Winter Conference*, San Francisco, CA., Dec. 11-15, 1989.

[40] C.H. Hansen, S.D. Snyder and C.R. Fuller, "Active Control of Structurally-Radiated Noise using Piezoceramic Actuators," *Internoise-89*, Newport Beach, CA., Dec., 1989.

[41] D. MacMartin, "An H_∞ Power Flow Approach to the Control of Uncertain Structures," *SM Thesis*, MIT Department of Aeronautics and Astronautics, October 1989.

[42] R.J. Mckinnell, "Active Vibration Isolation by Cancelling Bending Waves," *Proceedings of the Royal Society of London*, A 421, pp 357-393, 1989.

[43] H. Fuji, T. Ohtsuka and T. Murayama, "Wave Absorbing Control for Flexible Space Structures with Non-colocated Sensors and Actuators," *AIAA Guidance, Navigation and Control Conference*, Boston, MA., August, 1989.

[44] P. Hagedorn, J. Wallaschek and P. Chen, "Active Vibration Damping in Beams," *Proceedings of the American Control Conference*, Pittsburgh, PA., June 21-23, 1989.

[45] J. Scheuren, "Iterative Design of Band-limited FIR-Filters with Gain Constraints For Active Control of Wave Propagation," *ICA SSP 89*, Glasgow, Scotland, May 23-26, 1989.

[46] J.Scheuren, "Active Attenuation of Bending Waves in Beams," *Proceeding of the Institute of Acoustics*, Southamption, United Kingdom, Vol.12:Part 1, pp 623-629, 1990.

[47] D. MacMartin and S.R. Hall, "Control of Uncertain Structures Using an Hoo Power Flow Approach, *Journal of Guidance, Control, and Dynamics*, Vol14, No. 3, May-June, pp 521-530, 1991.

[48] D. MacMartin and S.R. Hall, "Structural Control Using Active Broadband Impedance Matching," *First Conference on Recent Advances in Active Control of Sound and Vibration*, Blacksburg, VA., 1991.

[49] S.J. Elliott, I.M. Stothers and L. Billet , "Adaptive Feedforward Control of Flexural Waves Propagating in a Beam," *1990 Proc. Institute of Acoustics*, 12(1),pp 613-622.

[50] R.J. Nagem and James H. Williams Jr., "Control of a One-Dimensional Distributed Structure Based on Wave Propagation Analysis," *Mech. Struct.&Mach.*, 18(1),pp. 33-57, 1990.

[51] C.R. Fuller, G.P. Gibbs and R.J. Silcox, "Simulaneous Active Control of Fexural and Extensional Power Flow in Beams," *International Congress on Recent Developments in Air and Structure-Borne Sound and Vibration*, Auburn, Al., March 6-8, 1990, pp 657-662.

[52] H.Fuji, K. Miyachi, T. Ohtsuka and S. Anazawa, "Experiment on Wave Absorbers Control for Flexible Space Structures," *presented on the 17th International Symposium on Space Technology and Science-(ISTS)*, Tokyo, Japan, May, 1990.

[53] *KYNAR* Piezo Film Technical Manual, *Pennwalt Corp.*, Valley Forge, PA., 1987, 65pp.

[54] Pennwalt Corp. Application Notes, PA., 198

[55] P.H. White, "Cross Correlation in Structural Systems: Dispersion and Nondispersion Waves," *J. Acoustical Society of America*, 45, pp 1118-1128, 1969.

[56] W. Redman-White, "The measurement of Structural Wave Intensity," 1983 PhD Dissertation, Univeristy of Southampton, Southampton, U.K.

[57] D.U. Noiseux, "Measurement of Power Flow in Uniform Beams and Plates," *J. Acoustical Society of America*, 47, pp.238-247, 1970.

[58] G. Pavic, "Separation of Dynamically Induced low-frequency Stresses in Rods and Pipes," *Experimental Mechanics*, pp. 1-9, 1983.

[59] G. Pavic, "Measurement of Structure-Borne Wave Intensity Part I: Formulation of the methods," *J. of Sound and Vibration*, 49(2), pp 221-230, 1976.

[60] G. Pavic, Measurement of Vibrations By Strain Gauges, Part I: Theoretical Basis," *J. of Sound and Vibration*, 102(2), pp 153-163, 1985.

[61] G. Pavic, Measurement of Vibrations By Strain Gauges, Part II: Selection of Measurement Parameters," *J. of Sound and Vibration*, 102(2), pp 163-188, 1985.

[62] P.D. Taylor, "Nearfield Structureborne Power Flow Measurements," *International Congress on Recent Developments in Air and Structure-Borne Sound and Vibration*, Auburn, Al., pp. 339-345, 1990.

[63] B. Fornberg, "Generation of Finite Difference Formulas on Arbitrarily Spaced Grids," *Math. Comp.*, 55, 1988, pp. 699-706.

[64] J.J. D'Azzo and C.H. Houpis, Feedback Control System Analysis and Synthesis, 2nd ed., McGraw-Hill Book Company, New York, 1966, 824pp.

[65] C.A. Halijak and G.E. Carlson, "Approximation of Fractional Operators $(1/s)^{1/n}$ by a Regular Newton Process," *IEEE Transactions on Circuit Theory*, June 1964, pp. 210-213.

[66] G.M. Sessler, "Piezoelectricity in Polyvinylidenefluoride," *J. of Acoustical Socieity of America*, Dec. 1981, pp. 1567-1576.

[67] T. Bailey and J.E. Hubbard Jr., "Distributed Piezoelectric-Polymer Active Vibration Control of a Cantilever Beam," *J. of Guidance, Control and Dynamics*, 8 (5), Sept.-Oct., 1985, pp. 605-611.

[68] J.M. Plump, J.E. Hubbard Jr. and T. Bailey, "Nonlinear Control of a Distributed System: Simulation and Experimental Results," *J. of Dynamic Systems, Measurements and Controls*, 109 (2), June 1987, pp. 133-138.

[69] S.E. Burke and J.E. Hubbard Jr., "Active Vibration Control of a Simply Supported Beam Using a Spatially Distributed Actuator," *IEEE Control Systems Magazine*, 7 (4), Aug. 1987, pp. 25-30.

[70] J.A. Connally and J.E. Hubbard Jr., "Low Authority Control of a Composite Cantilever Beam in Two Dimensions," *Proc. of the 1988 American Control Conference*, Atlanta, GA, June 15-17, 1988, pp. 1903-1908.

[71] H.S. Tzou and M. Gadre, "Active Vibration Isolation by Polymeric Piezoelectric with Variable Feedback Gains," *AIAA Journal*, 26 (8), Aug. 1988, pp. 1014-1017.

[72] H.S. Tzou and M. Gadre, "Theorectical Analysis of a Multi-Layered Thin Shell Coupled with Piezoelectric Shell Actuators for Distributed Vibration Controls," *J. of Sound and Vibration*, 132(3), Aug 1989, pp.433-450.

[73] H.S. Tzou, "Integrated Distributed Sensing and Active Vibration Suppression of Flexible Manipulators Using Distributed Piezoelectrics," *J. of Robotic Systems*, 6 (6), Dec. 1989, pp. 745-757.

[74] H.S. Tzou and C.I. Tseng, "Distributed Piezoelectric Sensor/Actuator Design for Dynamic Measurement/Control of Distributed Parameter Systems: A Piezoelectric Finite Element Approach," *J. of Sound and Vibration*, 138 (1), April 1990, pp.17-34.

[75] J. de Luis, E.F. Crawley and S.R. Hall, "Design and Implementation of Optimal Controllers for Intelligent Structures Using Infinite Order Structural Models," *Space Systems Laboratory Report No. 3-89*, Massachusetts Institute of Technology, Cambridge, MA., Jan. 1989, 198 pp.

[76] S.E. Miller and J. Hubbard, "Theoretical and Experimental Analysis of Spatially Distributed Sensors on a Bernoulli-Euler Beam," *C.S. Draper Laboratory Report CSDL-C-5953*, Cambridge, MA., July 1987, 35 pp.

[77] C-K. Lee, "Piezoelectric Laminates for Torsional and Bending Modal Control: Theory and Experiment," *PhD Thesis, Dept. of Theoretical and Applied Mechanics*, Cornell University, Ithaca, NY, May 1987, 199 pp.

[78] C-K. Lee, W-W. Chiang and T.C. O'Sullivan, "Piezoelectric Modal Sensors and Actuators Achieving Critical Active Damping on a Cantilever Plate," *Proceedings of the 30th SDM Conference*, Mobile, AL., April 3-5, 1989, pp. 2018-2026.

[79] D.W. Miller, S.A. Collins and S.P. Peltzman, "Development of Spatially Convolving Sensors for Structural Control Applications," *Proceedings of the 31st SDM Conference*, Long Beach Ca. , April 4-6, 1990.

[80] S.A. Collins, D.W. Miller, and A.H. von Flotow, "Piezopolymer Spatial Filters for Active Structural Control," *First Conference on Recent Advances in Active Control of Sound and Vibration*, Blacksburg, VA., 1991.

[81] D.J. Pines, "The Application of Spectral Methods to Filtering of Wave Propagation Dynamics along 1-D Structures using Point and Distributed Sensors," *First Joint US/JAPAN Conference on Adaptive Structures*, Maui, Hawaii, November, 1990.

[82] D. Gottlieb and S.A. Orszag, Numerical Analysis of Spectral Methods: Theory and Applications, *Society of Industrial and Applied Mathematics*, Philadelphia, Penn, 1977.

[82] C. Canuto, M.Y. Hussanini, A. Quarteroni and T.A. Zang, Spectral Methods in Fluid Dynamics, *Springer Verlag*, New York, 1988.

[83] A.V. Oppenheim and R.W. Schafer, "Discrete-Time Signal Processing," *Prentice-Hall, Inc.*, Englewood Cliffs, New Jersey, 1989

[84] T.W. Parks and C.S. Burrus, "Digital Filter Design," *John Wiley & Sons*, Inc., New York, 1987.

[85] R.N. Bracewell, The Fourier Transform and Its Applications, 2nd Edition, McGraw-Hill Book Co., New York, 1978, 444 pp.

[86] J.V. Candy, Signal Processing, McGraw-Hill Book Co., New York, 1988.

[87] H. Kolsky, Stress Waves in Solids, *Clarendon Press*, Oxford, U.K., 1953.

[88] J. Miklowitz, The Theory of Elastic Waves and Waveguides, *North Holland*, Amsterdam, 1978.

[89] R.A. Scott, "Linear Elastic Wave Propagation: An annotated Biliography; Parts I and II, " *Shock and Vibration Digest*, 10 (2/3), 1978, pp.25-41.

[90] K.F. Graff, Wave Motion in Elastic Solids, *Clarendon Press*, Oxford, U.K., 1975.

[91] M.M. Al-Mousawi, "Theoretical Studies on Flexural Wave Propagation in Beams: A Comprehensive Review-Part I: Historical Background," *Shock and Vibration Digest*, 1986, pp. 11-18.

[92] M.M. Al-Mousawi, "On Experimental Studies of Longitudinal and Flexural Wave Propagations: An Annotated Bibliography," *Applied Mechanics*, 39 (6), 1986, pp. 853-865.

[93] Fresnel, 1816

[94] L. Euler, "Elastic Curves-(An English Translation)," *Isis*, 20, Nov. 1933, pp. 1.

[95] D. Bernoulli,Comment, Academic Petro, Vol. 13.

[96] B.D. Saint-Venant, "Sur le chou longitudinal de deux barres elastiques," *J. of Mathemat-(Liouville)*, 72, 1867, pp.257 and 376.

[97] B.D. Saint-Venant, *Journal of Mathematic-(Liouville)*, ser. 2, Vol.1, 1856.

[98] M. Bresse, Cours de Macanique appliquee, *Successeur de Mallet-Bachelier*, Paris, FR., 1866.

[99] J. Boussinesq, *Phil. Magazine.*, 1895

[100] L. Pochhammer, "Uber die Fortpflanzugsgeschwindigkeiten kleiner Schwingungen in einem umbegrenzten isotropen Kreiscylinder," *Z. Math.*, 81, 1876, pp. 33-61.

[101] C. Chree, "The Equations of an Isotropic Elastic Solid in Polar and Cylinder Coordinates, Their Solution and Application," *Trans. Camb. Phil. Soc.*, 14, 1889, pp 250-369.

[102] J.W.S. Rayleigh, The Theory of Sound Vol.1, *Dover Publications*, New York, 1943-(Reprint),1894.

[103] H. Lamb, "On Waves in an Elastic Plate," *Proceedings of the Royal Society of London*, 93 (A), 1917, pp. 114-128.

[104] S.P. Timoshenko, "Zur Frage nach der Wirkung eines Stosses auf einen Balken, *Z. Math. Physics*, 62, 1913, pp. 198-209.

[105] S.P. Timoshenko, "On the Correction for Shear of the Differential Equation for Transverse Vibration of Prismatic Bars," *Phil. Magazine*, 43 (6), 1921, pp. 744-746.

[106] S.P. Timoshenko, "On the Transverse Vibration of Bars of Uniform Cross Section," *Phil Magazine*, 43 (6), 1922, pp. 125-131.

[107] J.E. Sears, On Longitudinal Impact of Metal Rods with Rounded Ends," *Proceedings of Cambridge Phil. Society*, 14, 1908, pp. 257.

[108] C. Ramsauer, "Experimentelle und theoretische Grundlagen des elastichen und mechanischen Stosses," *Ann. Physik*, 4 (30), 1909, pp. 417-495.

[109] E.W. Tschudi, "Duration of Impact of Bars," *Physics Review*, 2 (18), 1921, pp. 423-430.

[110] J.E.P. Wagstiff, "Experiments on the Duration of Impacts, mainly of Bars with Rounded Ends, in Elucidation of the Elastic Theory," *Proceedings of the Royal Society of London*, A (105), 1924, pp. 544-570.

[111] R. Fanning and W.V. Bassett, "Measurement of Impact Strains by a Carbon Strip Extensometer," *ASME Transactions*, 62, 1940, pp. A24-A28.

[112] S.K. Shear and A.B. Focke, "Dispersion of Supersonic Waves in Cylindrical Rods of Polycrsystalline Silver, Nickel and Magnesium," *Physics Review*, 15, 1940, pp. 532-537.

[113] C.O. Dohrenwend and W.R. Mehaffrey, "Measurement of Dynamic Strain," *J. of Applied Mechanic*, 10, 1943, pp. A-85-92.

[114] B. Hopkinson, "A Method for Measuring the Pressuring Produced in the Detonation of High Explosive or by the Impact of Bullets," *Phil. Transactions of the Royal Society of London*, A (213), 1913, pp. 437-456.

[115] H. Kosky and D.Y. Hsieh, "An Experimental Study of Pulse Propagation in Elastic Cylinders," *Proceedings of the Physics Society*, 71, 1958, pp. 608-612.

[116] NP Suh, "Stress Wave Propagation in Truncated Cones Against "Rigid" Wall," *Experimental Mechanics*, 7, 1967, pp. 541-544.

[116] E.D.H. Davies and S.C. Hunter, "The Dynamic Compression Testing of Solids by the Method of Split Hopkinson Pressure Bar, " *J. of Mechanics, Physics and Solids*, 11, 1963, pp. 155-181.

[117] S. Ellwood, L.J. Griffiths and D.J. Parry, "A Tensile Technique for Material Testing at High Strain Rates," *J. of Physics, Engineering Science and Instrumentation*, 15, 1982, pp. 1169-1172.

[118] T. Nicholas, "Tensile Testing of Materials at High Rates of Strain," *Experimental Mechanics*, 21, 1981, pp. 177-185.

[119] H. Cox, "On Impact on Elastic Beams," Cambridge Philosophical Transactions, 9 (1), 1849, pp. 73-78.

[120] J. Lennertz,"Beitrag zur Frage nacyh der wirkung eines Querstosses auf einen Stab," Ing. Arch., 8, 1937,pp. 37-46.

[121] J.P. Lee and H. Kolsky, "The Generation of Stress Pulses at the Junction of Two Noncollinear Rods," *J. of Applied Mechanics*, 39, 1972, pp. 809-813.

[122] W.H.H. Hoppmann, "Experimental Study of the Transverse Impact of a Mass on a Column," *Proceedings of SESA*, 10 (1), 1952, pp 21-30.

[123] I. Vigness, "Transverse Waves in Beams," Proceedings of SESA, 8, 1951, pp. 69-82.

[124] D.M. Cunningham and W. Goldsmith, "An Experimental Investigation of Beam Stresses Produced by Oblique Impact of a Steel Sphere, " *J. of Applied Mechanics*, 23, 1956.

[125] K.E. Barnhart and W. Goldsmith, "Stresses in Bending During Transverse Impact," *J. of Applied Mechanics*, 24, 1957, pp. 440-446.

[126] D.M. Cunningham, G.W. Brown and J.C. Griffith, "Photoelastometric Recording of Stress Waves," *Proceedings of Experimental Stress Analysis*, 16 (2), 1970, pp. 114-119.

[127] H. Schwieger, "A Simple Calculation of the Transverse Impact on Beams and its Experimental Verification," *Experimental Mechanics*, 5, 1965, pp. 244-250.

[128] A. Kuske, "Photoelastic Research on Dynamic Stresses," *Experimental Mechanics*, 1, 1966, pp. 105-112.

[129] R. Aprhamian, D.A. Evensen, et al, "Application of Pulsed Holographic Interferometry to the Measurement of Propagating Transverse Waves in Beams, *Experimental Mechanics*, 11, 1971, pp. 309-314.

[130] J.F. Doyle and S Kamle, "An Experimental Study of the Reflection and Transmission of Flexural Waves at Discontinuities," *J. of Applied Mechanics*, 52, 1985, pp. 669-673.

[131] Y.A. Liu and L. Lapidus, "Observer Theory for Distributed-Parmeter Systems," *International J. of Systems Science*, 7, pp. 731-742, 1976.

A 1

Wave Propagation in 1-Dimensional Structures: A Historical Perspective

A1.1 Two Centuries of Wave Propagation Research

The study of wave propagation in 1-dimensional structures has a rich history with publications extending well into the early 18th century. During these early years, several theoretical tools were extensively developed to characterize the dynamics of simple 1-D structures. Most of these efforts were focused around trying to predict transient wave propagation in rods and beams subject to impact. This work was motivated by a desire to determine the material properties and understand how structures behave under certain compressive and tensile loading conditions. Other researchers were interested in verifying the validity of continuum 1-D models proposed by Bernoulli-Euler, Rayleigh, Pochammer and Timoshenko. More recently, a renewed interest in wave propagation dynamics has been undertaken to predict and control the steady-state dynamic motion of large flexible structures made up of 1-D structural elements. This section attempts to bridge the gap between past research in wave propagation and problems facing researchers today-(See Histogram in Figure A1.1). However, this historical perspective is by no means

comprehensive. More exhaustive reviews can be found in books by references-[87-90] and a series of papers presented by Al-Mousawi-[91,92]. The purpose of this summary is to simply bring the field to present state of the art while pointing out some areas for future research.

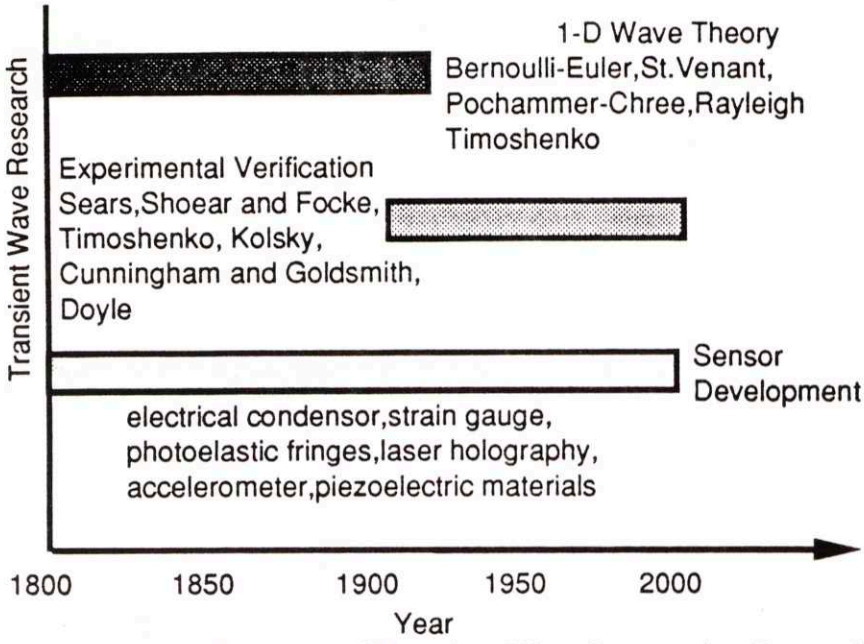

Figure A1.1: Histogram of Transient Wave Propagation Research

A1.2 1-Dimensional Wave Theory

The original concept concerning the notion of transverse vibration being transmitted through a medium was originally based on a theory formulated by Fresnel in 1816-[93]. He used the concept of transverse waves to explain the propagation of light which was at the time thought to be a disturbance propagating in an elastic ether. However, the theory of transverse waves in elastic solids had its beginnings in the 18th century work of Leonard Euler-[94] and Daniel Bernoulli-[95] who independently derived the partial differential equation governing flexural vibrations of a bar by invoking stationarity of its strain energy function. Later a researcher by the name of Boree de Saint-Venant-[96] examined the two primary assumptions of Bernoulli-Euler beam theory, namely that plane sections remain plane and that the longitudinal fibers at any cross-section are either under a state of tension or compression. He showed that these two assumptions are satisfied only in the case of uniform bending, i.e. when the beam is subjected to two equal an opposite couples applied at an end. The assumptions are not applicable when shearing stress cause warping of the cross-section. Saint-Venant also pointed out that the B-E theory holds only if the length is

many times its cross-section dimensions. Saint-Venant-[97] continued his research well into the 1880's on formalizing approximate solutions for both longitudinal and transverse motion of bars. Bresse-[98] followed this work and suggested correction terms for both rotatory inertia and transverse shear. In 1895 Boussineq-[99] presented a general wave solution for the equation of motion describing longitudinal impact dynamics on a bar in terms of rightward and leftward travelling waves.

Following these approximate methods, a more rigorous approach to describing the dynamics of 1-D structures was first undertaken by Pochammer-[100] and later verified by Chree-[101]. They applied the theory of elasticity to derive accurate equations of motion governing longitudinal, torsional and flexural vibrations of infinitely long beams of uniform cross-section. This approach led to first and second order approximations for longitudinal and flexural vibrations. Their first order approximations was later exploited by Lord Rayleigh-[102] who 1894 included a correction term to account for the rotatory inertia of the lateral vibrations of a rod. Although Bresse[103] suggested this addition years earlier Rayleigh received credit for appending it to the equation of motion. Lamb-[104] also showed that the B-E beam model was flawed. The final approximation to the work of Pochammer and Chree was proposed by Timoshenko-[33] in 1913-(English translation-[105,106]-1921). He included correction terms to account for both shear deformation and rotatory inertia.

In this form Timoshenko Beam theory did not predict infinite wave speed for a localized disturbance as was the main pitfall of Bernoulli-Euler beam theory, especially in the case of transient wave propagation. Nevertheless, both theories have found wide applications in steady-state wave propagation for long slender members.

A1.3 Verification of 1-Dimensional Wave Theory

The verification of theories characterizing longitudinal and transverse vibration of long slender members has relied heavily on transient experimental tests. Typically these have involved impact tests of short duration where reflected components are ignored in the analysis.

A1.3.1 The Existence of Longitudinal Waves

The first results verifying the wave-nature of longitudinal motion was presented by Sears-[107] in 1908. He examined the collision of two rods to obtain the velocity of wave propagation by observing the impact duration-t_d. He found that the impact duration was greater than the time required to travel twice the length of either bar. In 1909, Ramsauer-

[108] verified Sears conclusions and showed that the length and the shape of the striking bar played a important role in determining the duration of the impact. Tschudi-[109] found that duration of impact depended on both striker length and impact speed. Wagstiff-[110] followed up on this work and performed several impact tests with bars that had various length to diameter ratios-(L/d) and found certain results agreed well when modelled according to Hertz contact theory while others were akin to use St. Venant contact theory. These results, however, were difficult to judge since there was no knowledge of the deformations the bars were actually undergoing.

The invention of the strain gauge in 1940-[111], however, paved the way for obtaining a wealth of information concerning longitudinal wave dynamics. Using strain gauges Shear and Focke-[112] measured wave velocities at supersonic frequencies-(750kHz), however, their results were also corrupted by the appearance of effects due to torsional and longitudinal vibration. In a lower frequency range Dohrenwad and Mehudffrey-[113] found that strain gauges worked well at measuring dynamic stress levels in bars. Many others have used the impact of two bars for various other applications such as yield stress measurements and acoustic radiation with data gathering being obtained in the form of strain measurements.

Along with development of better sensors the verification of wave theories followed closely the development of transient test apparati which could impart repeatable pulses of finite duration to one end of a bar. A novel approach to this problem was achieved by Hopkinson-[114] who constructed apparatus known as the "Hopkinson Pressure Bar" which consisted of a short bar and a long bar in contact and subjected to impact by a bullet. Hopkinson found that this device could achieve good repeatable impacts. Later this apparatus was modified by Kolsky-[115] who used it to verify the theory of Pochammer and Chree by measuring the arrival times of longitudinal, dilational and transverse waves. He found results agreed well with theory for bars with large L/d ratios. With the use of strain sensors other researchers-[116-119] found that both tensile and compressive stress-strain curves could be obtained.

A1.3.2 The Existence of Transverse Waves

Experimental verification of transverse vibration has lagged somewhat behind successes achieved in verifying longitudinal theory. This primarily due to two factors. The first and probably most significant contributor to this delay period is the fact that an adequate approximate theory describing transverse motion was not available until the work of Timoshenko in 1913. Secondly, hardware for achieving repeatable impact dynamics was being developed during the same time period along with contact theory for two colliding

bodies. Nevertheless, even before adequate contact laws and beam models were available Cox-[120] in 1849 attempted to study transverse waves in a simply supported beam by impacting it with a steel sphere. During these tests he measured transverse deflection for several impact velocities. Although not a true verification of the wave-nature of a beam, his most significant contribution was an experimental method for generating transverse wave motion. Since then several advances in testing methods have been made, however, all are restricted to transient wave propagation due to impact. The difference between these methods is determined by the degree of flexibility afforded in generating impulses of various durations and magnitudes. For example.many researchers have used a cylindrical striking bar to represent the impacting body while others have used projectiles..

Such methods motivated Timoshenko in 1922-[106] to use a steel sphere to excite transverse motion of simply supported beam with a cross-sectional area of $10\ mm^2$. He compared experimental and analytical results for deflection and internal deformation using B-E beam theory and found considerable disagreement. This motivated his corrections to the B-E beam theory, accounting for shear and rotatory inertia of a cross-section. Following this work closely Lennertz-[121] was able to determine the fundamental frequency of a simply supported beam by using impacts which were short compared to length of the structure. Lee and Kosky-[122] improved upon the work of Lennertz by incorporating a modified Hertzian contact law to account for local indentations.

The true wave-nature of a beam became apparent in the work of Hoppman-[123] who instrumented multispan beams with newly developed resistive strain gauges to measure transverse waves due to impact of a steel sphere. He also measured maximum deflection using a micrometer. Theoretical comparisons were made by approximating the impulse as a half sign wave. Similar observations were made by Vigness-[124] using strain sensors and an impacting pendulum on a cantilever beam. Thus, as in the case of longitudinal waves the invention of the resistive strain gauge resulted in a number of experiments which attempted to verify Timoshenko beam theory. One of the more interesting studies was conducted by Cunningham and Goldsmith-[125], who in 1956 impacted a steel ball at various angles with a uniform beam. They used strain gauges to determine bending stress as a function *angle of incidence* of the impacting ball. They found that peak amplitude undergoes an inversion as it propagates along the beam. They also noted that high frequency components are more apparent further away from the impact where the slower frequency near field components dominate the response closer to the site of impact. These conclusions verified the dispersive wave-nature of both B-E and Timoshenko beam theory. From this work Barnhart and Goldsmith-[126] were able to develop a theory of transverse

impact of spheres on elastic beams which agreed well with responses measured very close to the impact site.

Studies beyond the work of Barnhart and Goldsmith-[127-129] were centered around developing better measurement schemes for inferring wave dynamics. During this period photoelastic materials and laser holography were used to determine the strain and deflection patterns for various beams. However, none of these approaches were capable of separating incident waves from their reflections in real-time and thus were restricted to just providing global deformation patterns.

With the development of the FFT algorithm many investigators attempted to verify wave theories by working in the frequency domain and then finding the inverse transform to obtain predictions of the distributed response-[130]. This approach required post processing of impact data and the use of temporal windowing to capture only the incident wave dynamics from a single strain sensor. Of course during this process low frequency information suffered since this information is propagated at very slow wave speeds. However, many experimental tests have demonstrated the merits of post processing transient impact data from beams.

A1.3.3 Steady-State Wave Dynamics

The study of wave motion has not only been restricted to transient investigations. In fact in the last decade the use of steady-state wave analysis has found applications in a number of fields including, Active Control of Large Space Structures and Structural Acoustics-[8-10,16-52]-(See Figure A1.2. One of the earliest publications using this approach was formulated by von Flotow-[10] in his 1984 PhD thesis. In this work he formulated a uniform frequency based approach to describe the dynamics and control of 1-dimensional structural elements. Following von Flotow's approach, a host of other researchers have applied similar methods to solve a number of structural control problems. One of the more notable contributions was achieved by Miller-[28,32,36] who formulated an optimal power flow approach to the control of Structural Networks. In this work Miller derived optimal causal, non-causal and fixed-form control strategies for a beam based on Bernoulli-Euler Theory. Experimentally, he verified his causal solutions on an experimental beam and found good agreement between theory and experiment.

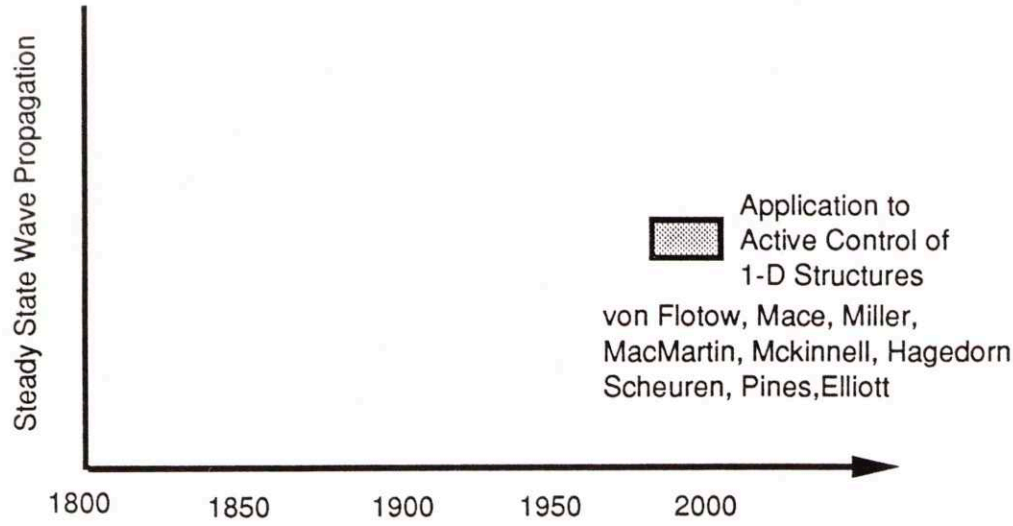

Figure A1.2: Historgram for Steady-State Analysis of Wave Propagationwith Application to Active Control of 1-D Structures.

A1.4 Wave Response of a 1-D Structure: (Understanding the physics)

The historical anecdote of the previous section supports the original claim made by Fresnel-[93] regarding the existence of transverse waves in continuous media. Since that time the study of wave propagation has advanced significantly, both in theory and experiment. But even today the picture of 1-dimensional wave propagation is not entirely complete. For example, intuition suggests that if a slender rod is excited along its length, then a longitudinal pulse will start to propagate away from the point of excitation at a finite speed. Similarly, if excited perpendicular to its spatial axis.transverse motion results causing the rod to move perpendicular to its spatial axis. These intuitive idealizations, however, are only approximate. Much more is actually going than is actually apparent. For instance at the site of excitation, the forcing acts over a finite domain and not at a point. Attempts to achieve excitation of one or other mode usually results in the excitation of many wave phenomena such as dilational waves or Rayleigh surface waves. In addition, upon initial excitation the structure behaves as if it is semi-infinite, requiring a finite amount of time before the incident disturbance encounters the finite dimensionality of the member. Thus, on a time scale which incorporates many scale lengths of the structure the response at any point along the member becomes a complex superposition of the incident wave front plus several reflections from the boundaries.

Clearly, the true wave response incorporates all of these factors. The question then arises as to what factors truly dominate the response for a given excitation. The answer to this usually implies assumption ultimately leads to mathematical representations of the wave dynamics. However, before this attempted in the next chapter, there are a number of tools available which are fundamental to the existence of wave motion along 1-dimensional structures. These include the wavenumber relation, phase speed and the group speed.

A1.4.1 Wavenumber Relation

The general form of a wavenumber relation for 1-dimensional structure can be written as

$$k(\omega) = k_r(\omega) + ik_i(\omega) \qquad (A1.1)$$

where k_r and k_i refer to the real and imaginary parts of the wavenumber. The functional dependency of k on ω can be either linear or non-linear. If it is linear the nature of the wave-motion is termed non-dispersive, however, if it is non-linear then the wave motion is termed dispersive. Knowledge of the dispersion relation permits the response of a 1-dimensional member for a wave travelling in one direction to be written as

$$u(x,t) = \sum_n A_n e^{k_i x} e^{-i(k_r x - \omega t)} \qquad (A1.2)$$

where A_n is the normalized amplitude spectrum of the wave packet being propagated. Therefore, the response consists of a spatially decaying term multiplying a sinusoidal term evolving in both space and time.

A1.4.2 Phase Speed

The argument of the complex term in equation-(*A1.2*) defines the relation between individual sinusoids and their location in space and time. For sinusoids with the same phase it is possible to determine the phase speed by differentiating the argument w.r.t. time to obtain

$$c_p = \frac{\omega}{k} = \frac{dx}{dt} \qquad (A1.3)$$

which corresponds to the velocity of a single sinusoid. In non-dispersive members the velocity is the same for all frequency components.

A1.4.3 Group Speed

The response in equation-(*A1.2*) corresponds to the superposition of a group of harmonics travelling in one direction. Viewing the dynamics of a single harmonic in this

group is virtually impossible unless it has an amplitude far greater then other components. However, what will be apparent is the motion of the response as a group. The motion of the wave packet is characterized by a quantity called the group speed

$$c_g = \frac{d\omega}{dk} \qquad (A1.4)$$

which represents an average of how the arrival of the packet behaves as a group.

Equations (*A1.1-A1.3*) effectively capture the essential dynamics associated with the propagation of an incident wave along a 1-dimensional structure.

A1.5 Wave Response in Typical 1-D Elements

With the tools of the previous section the wave response for typical 1-D structures can be can be understood in terms of how individual frequency components evolve in time and space.

A1.5.1 Longitudinal Wave Response

Consider a compression rod subject to a square pulse generated by a force at one end at time t_1.-(See Figure A1.3). At some time-(t_2) later the pulse measured by a strain gage has retained its shape but has traversed a distance l corresponding to half the length of the rod. The shape of this pulse has not changed because all frequency components travel at the same phase speed for a non-dispersive member. Further down the rod the square pulse encounters a structural discontinuity corresponding to a free end. This free end causes the pulse to change its direction with a 180 degree phase change. Thus, superposition of the incident and reflected strain wave-pulse at time t_3 leads to cancellation of the stress near the free end. As the reflected emerges from the discontinuity only an tensile strain wave pulse travelling to the left survives. This process continues indefinitely until the energy associated with the pulse is dissipated through either structural damping or lossy boundaries.

The transient wave response shown in Figure A1.3 corresponds to the evolution of strain wave amplitude on a free-free rod resulting from a finite duration excitation applied to the left free end. Although Figure A1.3 summarizes the evolution of the member's strain distribution pattern, the same excitation gives rise to a very different displacement distribution pattern. To obtain this information requires only a spatial integration of the strain field in the member at times t_1,t_2,t_3,and t_4. Performing this integration leads to the displacement wave response of the transient excitation shown in Figure A1.4. Notice that

now the square-pulse has been transformed into a propagating ramp-step pulse which moves to the right as time evolves. As this pulse passes the midpoint-(t_2,x_2) of the rod all particles in its wake assume the same displacement level. Particles far beyond this point are still at rest and await the arrival of the incident disturbance. The 90 degree phase difference between the displacement and strain wave response insures that the displacement response appears before the strain response. As the displacement pulse reaches the right free-end-(t_3) the amplitude of the response doubles. Some time-t_4 later a displacement wave emerges that is double in amplitude but moving towards the left.

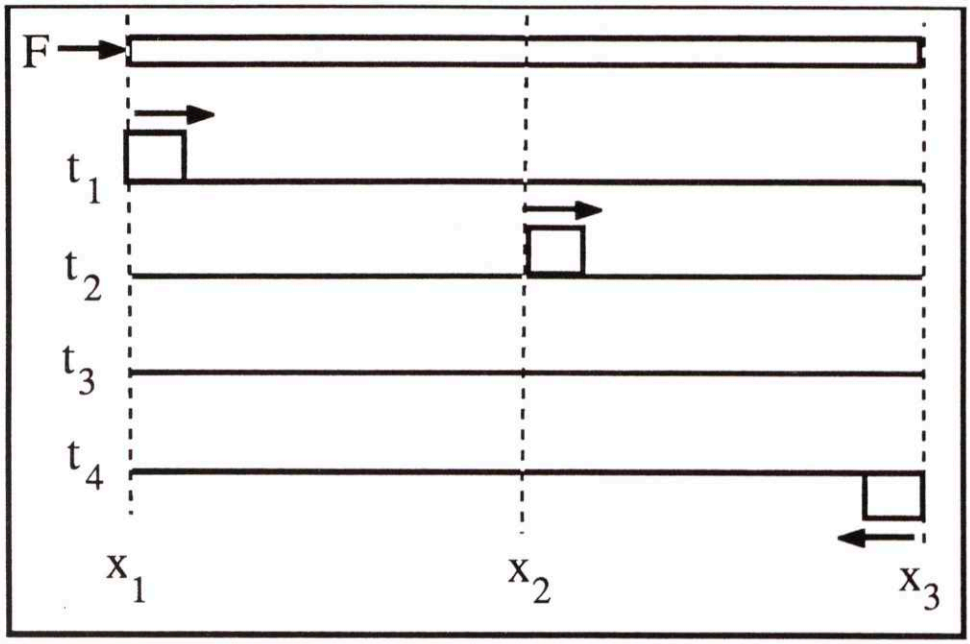

Figure A1.3: Strain Wave Response to transient Force excitation applied to left end of a compression rod. Square pulse remains undistorted as it propagates.

a 1-D beam. Timoshenko-[91] points out that as frequency increases beam dynamics become non-dispersive; characterized by both transverse and shear wave motion. Therefore, the arrival times of the incident disturbance will be determined by the wave speeds of these two competing phenomena. One might expect the response at station 2 to exhibit some of this non-dispersive behaviour in the form of an impulse followed by slower dispersive dynamics consisting of near-field and far-field contributions. This can be seen in the time history of the strain response at station 2. A small DC offset can be seen in this plot as a result of near-field terms. However, as the non-collocation between actuator and sensor becomes even more profound near field dynamics become negligible and the dynamics become dominated by purely propagating terms which are both dispersive and non-dispersive. Here the nature of dipsersion is more evident as the dipsersive tail becomes more oscillatory as faster moving dynamics start to pull away from their slower moving counterparts. The non-dispersive wave dynamics remain unchanged, their arrival times simply increase.

Boundaries associated with finite structures complicate matters as incident dispersive and non-dispersive beam wave dynamics scatter, often changing direction, magnitude and phase to subsequently add to the incident waveform. This superposition can be tracked temporally but is better summarized by examining steady-state motion.

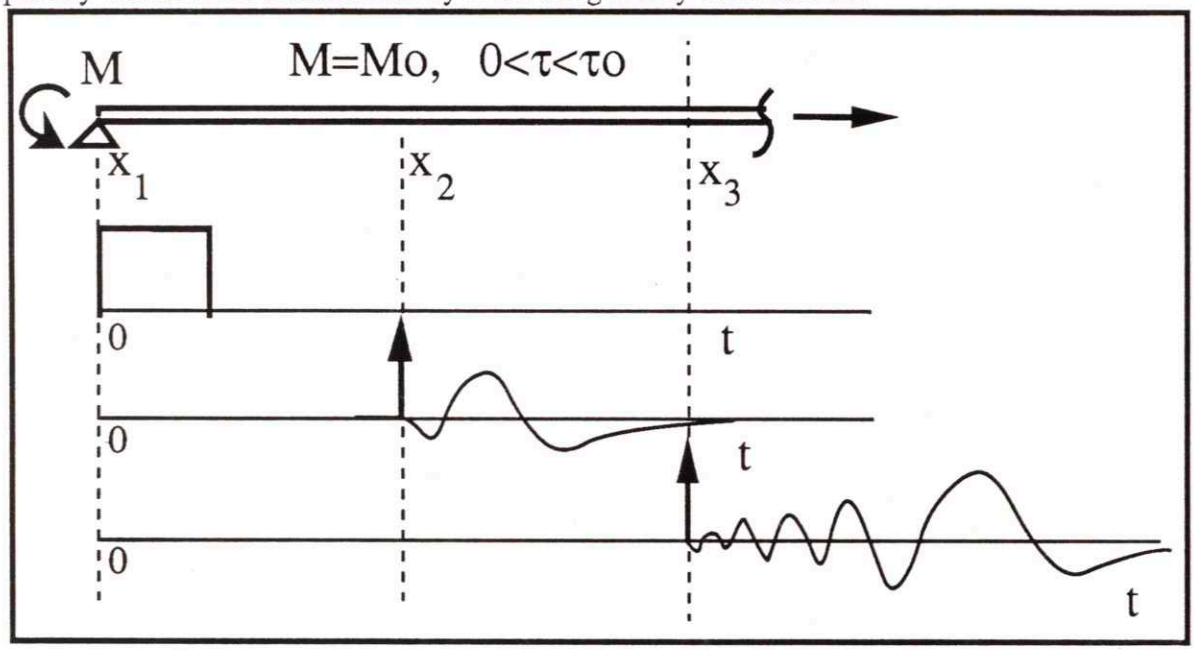

Figure A1.5: Strain wave-mode response of a semi-infinite beam to a moment pulse applied at the pinned-end. High frequency components pull away from slower low frequency waves. Wave distorts as it propagates.

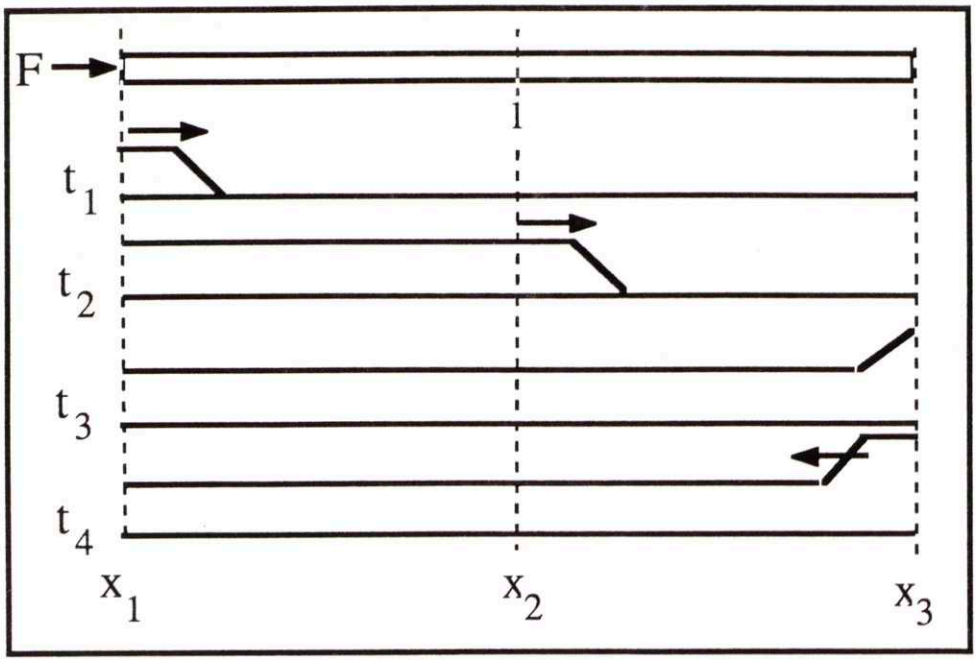

Figure A1.4: Position Wave Response to Transient Force Excitation applied at the left end of a compression rod. Ramp-Step Pulse propagates but does not change its shape.

A1.5.2 Transverse Wave Response

The wave response of a rod is fairly easy to characterize since longitudinal dynamics are non-dispersive. The wave dynamics of a beam, however, are complicated by the fact that the dynamics are dispersive and that near field terms can dominate the response at low frequency near structural discontinuities. Nevertheless, to examine the response of such a structure to transient excitation lets consider a pinned-free semi-infinite beam subject to a square pulse generated by a external moment applied to the pinned end-(See Figure A1.5). Now lets further assume that strain sensors are placed and strategic locations-(stations 1, 2, and 3) along the member to capture the incident transient waveform as it evolves over the spatial domain. Previous studies-[118-121] have shown that at low frequencies the dynamics are dominated by near field effects, especially if measurements are made near the discontinuity. Therefore, at station 1 it is anticipated that the response will consist of near field and far field terms which superpose upon one another. A strain sensor placed near this disturbance yields a response that has the same shape as the input disturbance pulse. Further down the beam, however, the near field terms begin to decay exponentially with distance and the far field behavior starts to domainate the response. Here several competing factors which affect the structural dynamics start to become noticeable. One of these factors is associated with the high frequency limit of the dispersion characteristics for

A1.5.3 Steady-State Response

The preceding section have focused on the wave response as being a transient phenomena occuring on idealized structural domains. However, contrary to this belief-[16-52] wave-models are still valid when steady-state excitation occurs, with the only difference being that the wave response consists of an infinite superposition of incident and reflected dynamics for all time. A useful way of interpreting these dynamics is to view this behavior in the frequency domain where the relation between the excitation and the response is contained in the form of a complex transfer function. This transfer function corresponds to the superposition of disturbance information travelling in both directions along a finite 1-dimensional structural element. The interaction of these spatially evolving wave-modes at a point in a member can either lead to constructive-(pole) or destructive-(zero) interference. The constructive interference is also called a mode of vibration of the structure and occurs at several temporal frequencies. Similarly, depending on placement of a point sensor relative to the location of the point excitation, destructive interference may or may not occur. A typical transfer function is given Figure A1.6.

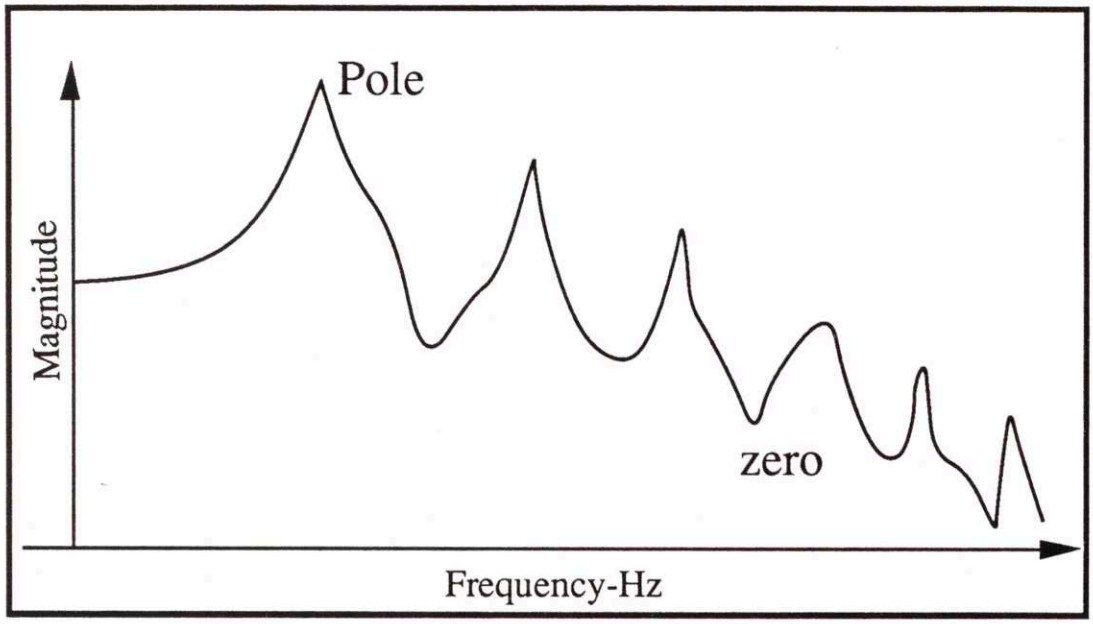

Figure A1.6: Magnitude of Steady-State Wave Superposition in the frequency domain of a typical sensed variable.

A1.6 Summary

Indeed perceiving the dynamics of 1-dimensional structural elements in terms of their underlying wave behaviour is not a new idea, however, it is only recently that this approach has been applied to the controlled-structures problem. This approach is unique since previous research has shown that by cancelling wave motion in one direction along a B-E beam it might be possible to eliminate all of a structure's resonances with a single point sensor and actuator. So far such a lofty goal has not been achieved with point sensors and actuators because the compensators required to meet this goal are non-causal even for a dual-sensor actuator pair. An equivalent form simply requires feedforward of incoming wave-dynamics which can be obtained anywhere on the structure and passed through a causal delay for subsequent control. The filltering of this wave behaviour is subject of this research and may also be applicable to the field of transient wave dynamics due to impact. But first we must define some 1-D wave-models of typical structural elements. This is done in the next chapter.

A 2

The Sensor Equation

A2.1 The Sensor Equation

Lee-[77] derived an equation relating the charge generated by a piezoelectric lamina to the mechanical deformation of a two-dimensional structure; this relation correponds to distributed sensor equation given in equation-(*4.1*). This equation was derived based on the following assumptions about the piezoelectric lamina:

made of PVDF
isotropic
constant properties along its length
deformations across its width are negligible

The sensor output is a function of the effective electrode width *F(x)*, which includes the physical width of the electrode and the polarization of the film, making negative widths possible. To define *F(x)* for an arbitrary sensor shape, let *F(x,y)* denote the spatial pattern of the electrode (*1* or *0*, depending on whether the point *(x,y)* is covered by an electrode or not). Let *P(x,y)* be the polarization profile of the piezopolymer. Allowing any orientation of the poling axis, *P* is the dot product of the film's poling axis(the *3* axis) and the axis of mechanical deformation (the *z* axis)

$$P(x,y) = \vec{p_z} \cdot p_3(x,y) \qquad (A2.1)$$

where p_i is the unit normal aligned with axis i. But we have assumed the piezo film's axes are aligned with the principal structural axes, and its is known that commerical PVDF is typically poled through the thickness, so P indicates whether the poling axis has the same sign as the deformation axis, i.e. P will be 1 for poled PVDF. In equation *(A2.1)* notice that p_3 can vary from point to point on the film. Integrating the product of F and P across the width of the beam b, the effective electrode width is

$$F(x) = \int_{-b/2}^{b/2} F(x,y) P(x,y)\, dy \qquad (A2.2)$$

If the PVDF lamina has a single continuous electrode on each side and is of uniform polarity, then equation-*(A2.2)* reduces to

$$F(x) = \pm b_{pz}(x) \qquad (A2.3)$$

where where b_{pz} is the width of the piezoelectric film's electrode. With the effective electrode width defined, the sensor equation for a PVDF sensor on a uniform beam can be expressed using the piezoelectric coefficient-e_{31}, which is the ratio of the charge per unit electrode area to the mechanical strain. The strain in the x direction is determined by multiplying the moment-curvature realtion for a symmetric beam subjected to pure bending by the moment arm z

$$\varepsilon(x,t) = -z\frac{\partial^2 u(x,t)}{\partial x^2} \qquad (A2.4)$$

where z is the distance from the beam's neutral axis to the lamina's midplane. Then, the effective electrode width is integrated along the length of the sensor to obtain the electrode area, resulting in the sensor equation given by

$$Q(t) = -e_{31} z \int_{-d}^{d} F(x) \frac{\partial^2 u(x,t)}{\partial x^2} dx \qquad (A2.5)$$

where $Q(t)$ is the charge generated by the PVDF lamina, d is sensor's length and $u(x,t)$ is the transverse displacement of the beam. The piezoelectric field intensity constant e_{31}, can be expressed in terms of the piezoelectric strain coefficients as

$$e_{31} = (d_{31} + \nu_{pz} d_{32}) \frac{E_{pz}}{1 - \nu_{pz}^2} \qquad (A2.6)$$

where the subscript pz indicates a property of the piezoelectric lamina.

A 3

Distributed Wave Observers

A3.1 Introduction

Chapters 3 and 4 have presented an approach for full-state estimation of propagating dynamics along 1-D structures using both discrete and distributed sensors respectively. Neither of these chapters, however, address the problem of wave filtering based on limited physical measurments. This section attempts to address this issue by exploiting well-defined Luenberger/Kalman-[131] Filtering Theory to define spatial weighting patterns which facilitate wave-filtering. This approach digresses from the band-limited scheme of Chapter 4 and assumes the structure is infinite. For finite windowing can be used to truncate the spatial extent of the sensor.

A3.2 Motivation

The application of distributed parameter methods to the problem of wave-amplitude estimation in 1-dimensional structures is motivated by the desire to implement both non-causal temporal filters and compensators in real-time for the purposes of structural wave control. The term non-causal refers to the fact that the elements of these filters and compensators have portions of their singularities which are not analytic in the right-half Laplace-(s) plane. This implies that part of their dynamics produces either signals which are stable in negative time, anticipating future information, or signals which are unstable in

positive time violating conservation of energy conditions. If the former interpretation is chosen and member dynamics are described in terms of travelling waves, information thought to propagating in negative time may be actually circulating the structure via spatial Fourier modes affecting past, future and present dynamics at discrete cross-sections in the member-(See Figure A3.1).

Waves which are thought to be propagating towards a cross-section will affect the future response at that location, whereas waves propagating away from the cross-section will have created a response in the past. This is synonymous with acausal temporal anticipation of a wave which is propagating in negative time being mapped into positive and negative space. Consequently, future and past temporal information at a point in a member can be interpreted by convolving rightward and leftward spatial wave dynamics which propagate to and from a cross-section.

Fortunately, distributed sensors which can be shaped to any desired pattern perform this convolution directly-(See Figure A3.2a). The same convolution, however, could be achieved using an array of discrete sensors each separated by a distance Δ(See Figure A3.2b). The problem with the discrete approach, however, is threefold. First the use of many sensors makes it difficult to keep track of phase lags and leads between individual sensors. Secondly each sensor output signal will require a specific weighting value or gain. For a large array this could be computationally intensive reducing real-time capability. Finally, many sensors would be much more costly than one distributed sensor. In addition, the use of discrete sensors introduces the unwanted problem of spatial aliasing.

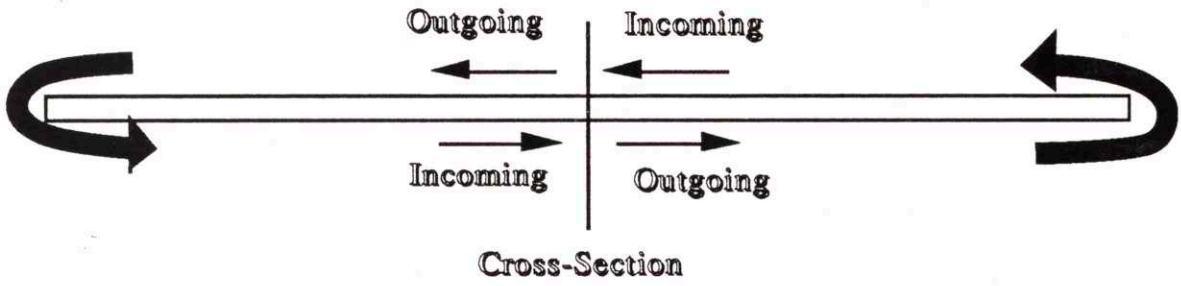

Figure A3.1: Typical 1-D Structural element illustrating how incoming and outgoing waves circumnavigate a structural member creating past, present and future responses at a cross-section in the member

Thus, distributed sensors represent a logical choice for wave-observers.

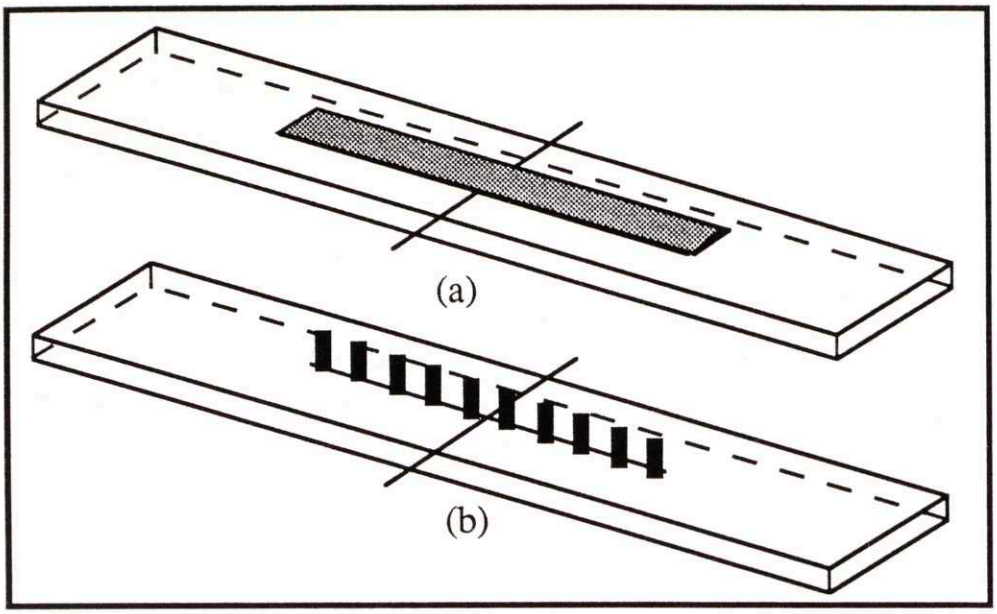

Figure A3.2: (a) Distributed Sensor Arrangement for Detecting Wave Dynamics. (b) Discrete Sensor Array Equivalent.

A3.3 Observer Theory for PDE's

A3.3.1 Problem Statement

Consider a well-posed linear distributed parameter system described by a linear partial differential equation on a infinite spatial domain, Ω, that is an open connected subset of a real n-dimensional Euclidean vector space, R^n. The boundary of Ω is denoted by $\partial\Omega$ and the closure by $\Omega=\Omega U\partial\Omega$, with the notation $d\Omega$ and $d(\partial\Omega)$ representing differential volume elements of the domain and boundary respectively.

In general a linear distributed-parameter system is described by an equation of the form

$$\frac{\partial \vec{v}(x,t)}{\partial t} = A_x \vec{v}(x,t) + B_x \vec{f}(x,t) \; ; \qquad x \in \Omega$$
$$y(x,t) = C_x \vec{v}(x,t) \qquad (A3.1)$$

where the matrices $A_x(x)\in C^{nxn}$, $B_x(x)\in C^{nxm}$ and $C_x(x)\in C^{pxn}$ are assumed to be bounded linear operators in a spatial Hilbert Space $\mathcal{H}$, defined to be $L^2(-\infty,\infty)$, the space of bounded square integrable functions. The boundary and initial conditions are specified as

$$(i)\; A_b v(x,t) = 0 \; ; \qquad x \in \partial\Omega$$
$$(ii)\; v(x,o) = 0$$

where the subscript b refers to the operator acting on the boundary-$\partial\Omega$. In a similar manner an equivalent spatial representation of the system dynamics takes the following form

$$\frac{\partial \vec{v}(x,t)}{\partial x} = A_t \vec{v}(x,t) + B_t \vec{f}(x,t) \; ; \qquad t \in [0,\infty)$$
$$y(x,t) = C_t \vec{v}(x,t) \tag{A3.2}$$

where $A_t(t) \in C^{nxn}$, $B_t(t) \in C^{nxm}$ and $C_t(t) \in C^{pxn}$ are bounded linear operators in a temporal Hilbert Space defined by $\mathcal{H}=L_2[0,\infty)$.

Thus, the goal of this research is to exploit these distributed representations to derive temporal and spatial full-order observers for determining wave-mode coordinates.

A3.3.2 Temporal Observer

Following the lead of Liu-[132] a specific full-order observer with unspecified gain operator $K_x(x)$ can be represented as

$$\begin{aligned}\frac{\partial \hat{\vec{v}}(x,t)}{\partial t} &= A_x \hat{\vec{v}}(x,t) + B_x \vec{f}(x,t) + K_x\left(y(x,t) - C_x \hat{\vec{v}}(x,t)\right) \; ; x \in \Omega \\ &= \left\{A_x - K_x C_x\right\} \hat{\vec{v}}(x,t) + B_x \vec{f}(x,t) + K_x y(x,t) \\ &\equiv D_x \hat{\vec{v}}(x,t) + B_x \vec{f}(x,t) + K_x y(x,t) \\ A_b \hat{\vec{v}}(x,t) &= 0 \; ; \qquad x \in \partial\Omega\end{aligned} \tag{A3.3}$$

where $v(x,t)$ represents the observed state vector of physical coordinates. The state reconstruction error can be defined as

$$\vec{e}(x,t) = \hat{\vec{v}}(x,t) - \vec{v}(x,t) \tag{A3.4}$$

Combining equations (*A3.1*), (*A3.3*) and (*A3.4*) the error dynamics evolve according to

$$\begin{aligned}\frac{\partial \vec{e}(x,t)}{\partial t} &= (A_x - K_x C_x)\vec{e}(x,t) \; ; \qquad x \in \Omega \\ &= D_x \vec{e}(x,t)\end{aligned} \tag{A3.5}$$

where $D_x(x)$ is a linear operator acting on the reconstruction error dynamics. Therefore, it follows from functional analysis that if $A_x(x)$ is an infinitesimal generator of a strongly continuous semi-group-$(\Phi(t);t>0)$ and both $K_x(x)$ and $C_x(x)$ are bounded linear operators

then $D_x(x)$ can be an infinitesimal generator of a strongly continuous semi-group-$(\Lambda(t);t>0)$. Assuming that this is true Liu shows that a sufficient condition for exponential stability of the state reconstruction error dynamics is that there exist a Lyapunov Functional $Q(e)$ such that the time derivative satisfies for positive constant $C>0$ and $e \in \mathcal{D}(D_x(x))\mathcal{H}$

$$\dot{Q}\left(\vec{e}(x,t)\right) \leq h\left\|\vec{e}(x,t)\right\| \tag{A3.6}$$

where $h>0$ and

$$Q\left(\vec{e}(x,t)\right) = [\vec{e},\vec{e}] = \int_{-\infty}^{\infty} \vec{e}^{T} P \vec{e}\, dx\,; \qquad x \in \Omega \tag{A3.7}$$

with P being a constant bounded positive definite matrix operator. Taking the temporal derivative of this expression we find that

$$\dot{Q}\left(\vec{e}(x,t)\right) = 2\int_{-\infty}^{\infty} trace\left\{\vec{e}\,\vec{e}^{T}\left(A_x - K_x C_x\right)^{T} P^{T}\right\} dx\,; \qquad x \in \Omega \tag{A3.8}$$

This implies that for exponential stability of the error dynamics

$$A_x(x)\text{-}K_x(x)C_x(x) < 0$$
$$\Rightarrow K_x(x)C_x(x) > A_x(x)$$
$$or\ \lambda_i(A_x(x)\text{-}K_x(x)C_x(x)) < 0\ for\ i=1,\ldots,n$$

A3.4 Spatial Observer

Analogously, a full order spatial observer can be represented as

$$\begin{aligned}\frac{\partial \hat{v}(x,t)}{\partial x} &= \left\{A_t - K_t C_t\right\}\hat{v}(x,t) + B_t \vec{f}(x,t) + K_t y(x,t)\,; \quad t \in [0,\infty) \\ &= G_t \hat{v}(x,t) + B_t \vec{f}(x,t) + K_t y(x,t) \\ A_b \hat{v}(x,t) &= 0\,; \qquad x \in \partial\Omega\end{aligned} \tag{A3.9}$$

where as before $v(x,t)$ is the estimated state vector with initial condition $v(-\infty,t)=0$ for $-\infty<x<0$ or ($v(\infty,t)=0$ for $0<x<\infty$). The spatial reconstruction error dynamics for $x \in \Omega$ are given by

$$\begin{aligned}\frac{\partial e(x,t)}{\partial x} &= \left\{A_t - K_t C_t\right\} e(x,t) \quad t \in [0,\infty) \\ &= G_t e(x,t)\end{aligned} \tag{A3.10}$$

where $e \in \mathcal{D}(G_t)\mathcal{H}=L^2[0,\infty)$. Similar to the temporal case G_t will be an infinitesimal generator of a strongly continuous semi-group ($x>0$) iff $A_t(t)$ is and both $K_t(t)$ and $C_t(t)$ are bounded linear operators. Again the direct method of Lyapunov yields the following condition for exponential stability of the state reconstruction error:

$$\lambda_i(A_t(t)-K_t(t)C_t(t)) < 0 \quad for\ x>0\ for\ i=1,...,n$$
$$\lambda_i(A_t(t)-K_t(t)C_t(t)) > 0 \quad for\ x<0\ for\ i=1,...,n$$

A3.5 Observability

The previous sections have developed stable temporal and spatial observers for obtaining estimates of physical and wave-states of 1-D members, However, neither approach has attempted to consider the issue of reconstruction-(or observability) of the entire state-space from limited output information. Consider the general temporal and spatial output relations given by

$$temporal: \ y = C_x \vec{v}(x,t); \qquad spatial: \ y = C_t \vec{v}(x,t)$$

where C_x and C_t are bounded linear operators in a Hilbert Space. Since both output relations map internal states $v(x,t)$ to a reduced state-space y, we can define this mapping by sets

$$M_t = \left\{ \vec{v}(x,t) \,\middle|\, C_x \Phi(t) \vec{v}(x,t) = 0 \ \forall\ t \in R \right\}$$
$$M_x = \left\{ \vec{v}(x,t) \,\middle|\, C_t \Phi(t) \vec{v}(x,t) = 0 \ \forall\ x \in R \right\} \qquad (A3.11)$$

which represent subspaces of the set of all $v(x,t)\ \mathcal{H}$. In this form the system is said to be observable if the only element contained in these sets correspond to the null solution-$v(x,t)=0$. Transforming equations (*A3.3*) and (*A3.9*) to the temporal-(s) or spatial-(p) Laplace domains a simple approach exist for verifying the observability of LTI-(Linear Time Invariant) and LSI-(Linear Space Invariant) systems. This approach involves finding the rank of the system observability matrix denoted by

$$O = \left[C^t \quad A^t C^t \quad \ldots\ldots\ldots\ldots \quad (A^t)^{n-1} C^t \right] \qquad (A3.12)$$

where the matrices-(A,C) now refer to their Laplace-(s *or* p) domain equivalents with the space and time subscripts suppressed. Thus, if the rank(O)=n then the system is said to observable and the entire state space is reconstructible from only output information.

A3.6 Pole-Placement

It follows from Linear Systems Theory that if a LTI-{LSI} system is completely observable then then characteristic values of the observer dynamics can be arbitrarily located in the complex plane(with the restriction that complex poles occur in complex conjugate pairs). This ensures that the reconstruction error dynamics-$e(x,t)$ can be made asymptotically stable irrespective of initial errors in time or space. Therefore, given an observable with only one output measurement available and with desired characteristic equation given by

$$\begin{aligned} \beta(s) &= s^n + \beta_1 s^{n-1} + \ldots\ldots + \beta_n \quad or \quad \beta(p) = p^n + \beta_1 p^{n-1} + \ldots\ldots + \beta_n \\ &= \prod_{i=1}^{n} (s + a_i) \qquad\qquad = \prod_{i=1}^{n} (p + a_i) \end{aligned} \tag{A3.13}$$

the observer gain vector $K(s)$-$\{K(p)\}$ can be computed from

$$K = \left[(OW)^t \right]^{-1} (\vec{\beta} - \vec{\alpha}) \tag{A3.14}$$

where O is the observability matrix, W is an upper triangular toeplitz matrix given by

$$W = \begin{bmatrix} 1 & \alpha_1 & & \alpha_{n-1} \\ 0 & 1 & & \alpha_{n-2} \\ & \ldots\ldots\ldots\ldots\ldots\ldots & & \\ 0 & 0 \ldots\ldots\ldots\ldots & & 1 \end{bmatrix} \tag{A3.15}$$

and b and a are vectors corresponding to the coefficients of the characteristic equations of the matrices sI-$A(p)$+$K(p)C(p)$-$\{pI$-$A(s)$+$K(s)C(s)\}$ and sI-$A(p)$-$\{pI$-$A(s)\}$ respectively. Notice that the observer gains are not constant, instead they vary as a function of frequency.

A3.7 Determination of Wave-Mode Coordinates

Because wave states are not directly measured by typical sensors they must be inferred from physical measurements through temporal or spatial decoupling matrices. These matrices represent the space of similarity transformations which diagonalize the system matrices $A(p)$ and $A(s)$. A generic transformation might be of the form

$$\Gamma(p) = T^{-1}(p) A(p) T(p) \qquad or \qquad \Gamma(s) = T^{-1}(s) A(s) T(s)$$

where T represents the transformation matrix which maps physical coordinates to wave coordinates. Here the diagonal elements of $\Gamma(p)$ relate temporal wave-modes which propagate in both positive and negative, whereas the diagonal elements of $\Gamma(s)$ correspond to spatial wave-modes which propagate both rightward and leftward along a 1-D member. The units of these normalized wave-coordinates is determined by the choice of similarity transformation which operates on the vector of physical states. For instance if the elements of the transformation matrix are normalized relative to physical deflection then the units of the wave coordinates will be in terms of meters-(feet). Clearly, the choice of normalization is arbitrary with the only requirement being that the columns of T maintain a given direction in C^n.

A3.7.1 Temporal Wave Transformation

Consider the general form of the temporal observer of equation (*A3.3*) with estimated physical states $v(p,t)$. By diagonalizing the operator matrix $A(p)$ the temporal wave states can be related to their physical counterparts using the following transformation relation:

$$\vec{w}(p,t) = Y^{-1}(p)\vec{v}(p,t) \qquad (A3.16)$$

with

$$Y^{-1}(p) = A(p)(\Gamma(p)Y(p))^{-1}$$

where the elements of $w(p,t)$ are estimated wave amplitudes which can propagate in both positive and negative time. Equation (*A3.16*) is interpreted as yielding the estimated temporal wave response at any point along the member from the spatial convolution of past and future estimated physical state information at particular instant in time.

A3.7.2 Spatial Wave Transformation

Similarly, for a spatial observer there exists a temporal decoupling matrix $Y(s)$ which attempts to filter wave states from physical states at a particular location in a member This temporal transformation has the form

$$\vec{w}(x,s) = Y^{-1}(s)\vec{v}(x,s) \qquad (A3.17)$$

with

$$Y^{-1}(s) = A(s)(\Gamma(s)Y(s))^{-1}$$

where $w(x,s)$ corresponds to estimates of rightward and leftward wave amplitudes respectively. Here $Y(s)$ represents a temporal filter operating on point estimates of

decouple spatial wave states from physical states are non-causal. This is especially true for non-hyperbolic systems. Nevertheless, at steady-state far from structural discontinuities the equivalence between space and time makes it possible to replace temporal filters by causal spatial filters. This is because spatial Fourier modes and are analytic over the entire spatial domain relative to observation at a cross-section.

Table A3.1 Typical Hilbert Transforms

f(x)	$F_{Hi}(x)$
cos(x)	-sin(x)
sin(x)	cos(x)
sin(x)/x	(cos(x)-1)/x
$\delta(x)$	$-1/(\pi x)$

A3.9 1-D Examples

Compression rods and flexible beams represent typical 1-D structures which support wave propagation dynamics-(See Figure A3.3). Unfortunately, however, these characteristic dynamics are often suppressed in favor of classical modal response representations. In this section spatial observers are developed for rods and beams to selectively filter out the characteristic wave dynamics. This approach makes use of the observer theory presented previously to produce causal filters.

elements of the physical state vector. Realization of equation (*A3.17*), however, is complicated by the fact that some of the elements of $Y(s)$ are acausal. This is typically the case for simple B-E beams. Therefore, an alternative approach must be found to observe wave components on members which are characterized by parabolic pde's.

A3.8 Causality and the use of Hilbert Transforms

The relation between acausal temporal filtering and causal spatial filtering is made more obvious by application of Hilbert Transform Theory where given a function $\phi(t)$ we define the Hilbert Transform to be

$$\phi_{Hi}(\phi(t)) = \frac{1}{\pi}\int_{-\infty}^{\infty}\frac{\phi(t')}{t'-t}dt' = \frac{-1}{\pi} * \phi(t) \qquad (A3.18)$$

where * denotes the convolution operation. The divergence of the integral at $t=t'$ is allowed for by computing the principal value of the integral. Now taking the Fourier Transform of the expression in equation (*A3.18*) leads to

$$\Phi_{Hi}(\omega) = isign(\omega)\Phi(\omega) \qquad (A3.19)$$

where

$$sign(\omega) = \begin{cases} 1 & \omega \geq 0 \\ -1 & \omega < 0 \end{cases}$$

Therefore, the effect of convolving a function with the Hilbert Kernel-($-1/\pi t$) is to shift its response by 90 degrees. This property of the Hilbert Transform is directly related to causality for analytic functions of the form

$$h(t) = \phi(t) - i\phi_{Hi}(t) \qquad (A3.20)$$

where $h(t)$ denotes a complex function composed of real functions $\phi(t)$ and $\phi_{Hi}(t)$. If $\phi(t)$ and $\phi_{Hi}(t)$ form a Hilbert Transform pair then the function f is said to be analytic in positive time. For instance if $\phi(t)=cos(\omega t)$ then $\phi_{Hi}(t)=-sin(\omega t)$ $h(t)=e^{j\omega t}$ which correponds to a temporal Fourier mode propagating in positive time-(See Table A3.1). This condition is equivalent to the Hilbert Transforms of the real and imaginary parts of the transfer function $\Phi(\omega)$ being related according to

$$Re(\Phi(\omega)) = \frac{1}{\pi}\int_{-\infty}^{\infty}\frac{Im(\Phi(\omega'))}{\omega'-\omega}d\omega' \quad and \quad Im(\Phi(\omega)) = \frac{1}{\pi}\int_{-\infty}^{\infty}\frac{Re(\Phi(\omega'))}{\omega'-\omega}d\omega' \qquad (A3.21)$$

Transfer functions which satisfy this equation are said to be causal in the temporal domain with effects never preceeding their causes. Unfortunately, many temporal filters which

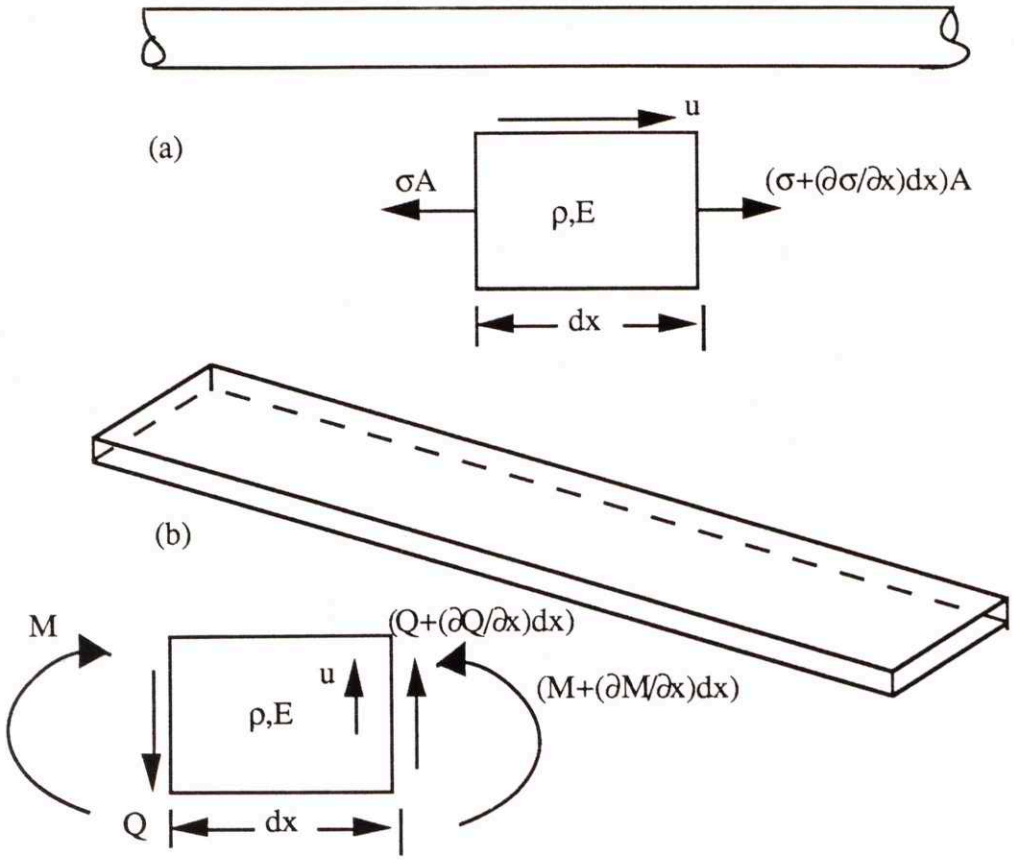

Figure A3.3: Typical 1-Dimensional Structures which support Wave Propagation-(a) Compression Rod and (b) Bernoulli-Euler Beam.

A3.9.1 Compression Rod

Example L1-(Longitudinal Waves in a Rod)

The homogeneous longitudinal dynamics of a compression rod can be modelled by the following pde:

$$\frac{\partial^2 u(x,t)}{\partial t^2} = \frac{EA}{\rho A}\frac{\partial^2 u(x,t)}{\partial x^2} \quad ; \quad -\infty < x < \infty \qquad (A3.22)$$

where $u(x,t)$ is the longitudinal deflection. Taking the Laplace transform of this equation these dynamics can be put in state-space form as

$$s^2 u(x,s) = \frac{EA}{\rho A}\frac{\partial^2 u(x,s)}{\partial x^2} \quad ; \quad -\infty < x < \infty \qquad (A3.23)$$

where

$$A(s)=\begin{bmatrix} 0 & 1 \\ \frac{\rho A}{EA}s^2 & 0 \end{bmatrix} \quad \text{and} \quad \vec{v}(x,s)=\begin{bmatrix} u(x,s) \\ u'(x,s) \end{bmatrix} \tag{A3.24}$$

If strain is only available for measurement the output vector is given by

$$y(x,s)=C(s)\,\vec{v}(x,s) \tag{A3.25}$$

where the bounded operator $C(s)=[0\ 1]$.

In this form a full-order spatial observer for this system based on past and future strain information is given by

$$\frac{d}{dx}\begin{bmatrix} \hat{u}(x,s) \\ \hat{u}'(x,s) \end{bmatrix}=\left\{\begin{bmatrix} 0 & 1 \\ \frac{\rho A}{EA}s^2 & 0 \end{bmatrix}-\begin{bmatrix} 0 & K_1(s) \\ 0 & K_2(s) \end{bmatrix}\right\}\begin{bmatrix} \hat{u}(x,s) \\ \hat{u}'(x,s) \end{bmatrix}+\begin{bmatrix} K_1(s) \\ K_2(s) \end{bmatrix}y(x,s) \tag{A3.26}$$

where $v(x,s)=[u(x,s)\ \ u'(x,s)]^T$ represents the estimated state vector and $K(s)$ is the observer gain matrix. Now taking the spatial transform of this equation leads to the following transfer functions relating estimated states to measured strain information

$$\begin{bmatrix} \frac{\hat{u}(p,s)}{y(p,s)} \\ p\frac{\hat{u}(x,s)}{y(p,s)} \end{bmatrix}=\frac{1}{\phi(p)}\begin{bmatrix} K_1(s)p+K_2(s) \\ K_2(s)p+\frac{\rho A}{EA}s^2K_1(s) \end{bmatrix} \tag{A3.27}$$

with characteristic equation given by

$$\phi(p)=p^2+K_2p+\frac{\rho A}{EA}s^2(-1+K_1) \tag{A3.28}$$

Placing the spatial poles at $-a_1$ and $-a_2$-(or at a_1 and a_2 for $x<0$), the coefficients of equation (*A3.28*) are found to be

$$K_1(s)=a_1a_2(EA/\rho As^2)+1$$

$$K_2(s)=a_1+a_2$$

Substituting for these gains and $\phi(p)$ in equation (*A2.28*) leads to the following observer transfer functions:

$$\begin{bmatrix} \frac{\hat{u}(p,s)}{y(p,s)} \\ p\frac{\hat{u}(p,s)}{y(p,s)} \end{bmatrix}=\begin{bmatrix} \frac{\left\{a_1a_2\frac{EA}{\rho As^2}+1\right\}p+(a_1+a_2)}{(p+a_1)(p+a_2)} \\ \frac{(a_1+a_2)p+\left\{a_1a_2+\frac{\rho A}{EA}s^2\right\}}{(p+a_1)(p+a_2)} \end{bmatrix} \tag{A3.29}$$

In non-dimensional form these transfer functions can be represented as

$$\begin{bmatrix} \hat{u}_{ndp} \\ \hat{u}_{nds} \end{bmatrix} = \begin{bmatrix} \dfrac{(s_{nd} + \dfrac{1}{s_{nd}})p_{nd} + \gamma s_{nd}}{p_{nd}^2 + \gamma p_{nd} + 1} \\ \dfrac{\gamma_{nd} p_{nd} + (s_{nd}^2 + 1)}{p_{nd}^2 + \gamma p_{nd} + 1} \end{bmatrix};$$

$$p_{nd} = \frac{p}{\sqrt{a_1 a_2}}, \; s_{nd} = s\sqrt{\frac{\rho A}{a_1 a_2 EA}}, \; \gamma = \frac{a_1 + a_2}{\sqrt{a_1 a_2}} \qquad (A3.30)$$

where the non-dimensional estimates of position and strain are given by

$$\hat{u}_{ndp} = s\sqrt{\frac{\rho A}{EA}}\frac{\hat{u}(p,s)}{y(p,s)} \quad \text{and} \quad \hat{u}_{nds} = p\frac{\hat{u}(p,s)}{y(p,s)} \qquad (A3.31)$$

The pole-zero diagram for these transfer functions are shown in Figure A3.4 where the zero of the first transfer function is shown to asymptotically approach the location -γas snd increases.whereas the zero of the strain estimate transfer function migrates to negative infinity along the real axis in the p-plane. The purpose of the migration of the transfer function zeros is to ensure proper phasing between measured distributed responses and their estimates which are comprised of rightward and leftward waves propagating towards a cross-section of interest. This behavior is a bit more obvious from the transfer functions of equation (*A2.38*) which are plotted in Figure A3.5. Here for three sets of values of the constants (γ and s_{nd}) we see that at the desired temporal frequency-s_{nd} of interest the observer tries to maintain zero phase difference and unity gain betweeen estimated dynamics and actual dynamics. From this figure this appears to work well for low frequency wave dynamics, however at high frequency the magnitude condition tends to suffer some.

Now by expanding into partial fractions the transfer functions in equation-(*A3.30*) become

$$\begin{bmatrix} \dfrac{\hat{u}(p,s)}{y(p,s)} \\ p\dfrac{\hat{u}(x,s)}{y(p,s)} \end{bmatrix} = \begin{bmatrix} \dfrac{-a_1(\dfrac{a_1 a_2}{\dfrac{\rho A}{EA}s^2} + 1) + (a_1 + a_2)}{\dfrac{-a_1 + a_2}{p \pm a_1}} + \dfrac{-a_2(\dfrac{a_1 a_2}{\dfrac{\rho A}{EA}s^2} + 1) - (a_1 + a_2)}{\dfrac{-a_1 + a_2}{p \pm a_2}} \\ \dfrac{-a_1(a_1 + a_2) + (\dfrac{\rho A}{EA}s^2 + a_1 a_2)}{\dfrac{-a_1 + a_2}{p \pm a_1}} + \dfrac{-a_2(a_1 + a_2) - (\dfrac{\rho A}{EA}s^2 + a_1 a_2)}{\dfrac{-a_1 + a_2}{p \pm a_2}} \end{bmatrix}$$

(A3.32)

This form can be transformed back into the spatial domain to yield the following spatial weighting pattern for point estimates of position and strain based on distributed strain measurement

$$\begin{bmatrix} \hat{u}(x,s) \\ \hat{u}'(x,s) \end{bmatrix} = \begin{bmatrix} \int_{-\infty}^{\infty} \{ \frac{-a_1(\frac{a_1a_2}{\frac{\rho A}{EA}s^2}+1)+(a_1+a_2)}{-a_1+a_2} e^{-a_1|\xi|} + \frac{-a_2(\frac{a_1a_2}{\frac{\rho A}{EA}s^2}+1)-(a_1+a_2)}{-a_1+a_2} e^{-a_2|\xi|} \} y(x-\xi)\,d\xi \\ \int_{-\infty}^{\infty} \{ \frac{-a_1(a_1+a_2)+(\frac{\rho A}{EA}s^2+a_1a_2)}{-a_1+a_2} e^{-a_1|\xi|} - \frac{a_2(a_1+a_2)+(\frac{\rho A}{EA}s^2+a_1a_2)}{-a_1+a_2} e^{-a_2|\xi|} \} y(x-\xi)\,d\xi \end{bmatrix} \quad (A3.33)$$

Combining this with the temporal transformation $Y_r^{-1}(s)$, the point position normalized rightward and leftward wave-mode amplitudes can be found from

$$\begin{bmatrix} \hat{w}_r(x,s) \\ \hat{w}_l(x,s) \end{bmatrix} = \begin{bmatrix} \frac{1}{2} & \frac{-1}{2s}\sqrt{\frac{EA}{\rho A}} \\ \frac{1}{2} & \frac{1}{2s}\sqrt{\frac{EA}{\rho A}} \end{bmatrix} \begin{bmatrix} \frac{\hat{u}(x,s)}{y(x,s)} \\ \frac{\hat{u}'(x,s)}{y(x,s)} \end{bmatrix} \quad (A3.34)$$

Example L2-(Longitudinal Waves in a Rod):

If the elements of the state vector describing longitudinal dynamics along a rod are chosen to be velocity and strain as opposed to position and strain the homogeneous state space dynamics for a rod become

$$\frac{d}{dx}\begin{bmatrix} su(x,s) \\ u'(x,s) \end{bmatrix} = \begin{bmatrix} 0 & s \\ \frac{\rho A}{EA}s & 0 \end{bmatrix} \begin{bmatrix} su(x,s) \\ u'(x,s) \end{bmatrix}; \qquad -\infty < x < \infty \quad (A3.35)$$

A spatial observer for this system yields the following transfer functions relating estimated states to distributed strain measurement

$$\begin{bmatrix} s\dfrac{\hat{u}(p,s)}{y(p,s)} \\ p\dfrac{\hat{u}(p,s)}{y(p,s)} \end{bmatrix} = \frac{1}{\phi(p)} \begin{bmatrix} K_1(s)p + K_2(s)s \\ K_2(s)p + \dfrac{\rho A}{EA} s K_1(s) \end{bmatrix} \tag{A3.36}$$

where K_1 and K_2 are the observer gains and the characteristic equation is given by

$$\phi(p) = p^2 + K_2 p + \frac{\rho A}{EA} s(K_1 - s) \tag{A3.37}$$

Choosing the same pole locations as in example L1 leads to observer gains

$$K_1(s) = s + (EA/rA)(a_1 a_2/s)$$

$$K_2(s) = (a_1 + a_2)$$

Again substituting these gains into equation (*A2.45*) leads to

$$\begin{bmatrix} s\dfrac{\hat{u}(p,s)}{y(p,s)} \\ p\dfrac{\hat{u}(p,s)}{y(p,s)} \end{bmatrix} = \begin{bmatrix} \dfrac{(s + a_1 a_2 \dfrac{EA}{\rho A s})p + (a_1 + a_2)s}{(p + a_1)(p + a_2)} \\ \dfrac{(a_1 + a_2)p + (\dfrac{\rho A}{EA} s^2 + a_1 a_2)}{(p + a_1)(p + a_2)} \end{bmatrix} \tag{A3.38}$$

The non-dimensional form of this equation and its corresponding pole-zero pattern is identical to that found in example L1. The only advantage of this choice of the state vector lies in the wave decoupling transformation which if normalized relative to velocity leads to velocity wave amplitude estimates given by the impulsive temporal convolution

$$\begin{bmatrix} \hat{w}_{rv}(x,s) \\ \hat{w}_{lv}(x,s) \end{bmatrix} = \begin{bmatrix} \frac{1}{2} & \frac{1}{2}\sqrt{\frac{EA}{\rho A}} \\ \frac{1}{2} & \frac{-1}{2}\sqrt{\frac{EA}{\rho A}} \end{bmatrix} \begin{bmatrix} s\dfrac{\hat{u}(x,s)}{y(x,s)} \\ \dfrac{\hat{u}'(x,s)}{y(x,s)} \end{bmatrix} \tag{A3.39}$$

where v refers to velocity amplitudes. These are related to position estimates by a temporal integration

$$\begin{bmatrix} \hat{w}_r(x,s) \\ \hat{w}_l(x,s) \end{bmatrix} = \frac{1}{s} \begin{bmatrix} \hat{w}_{rv}(x,s) \\ \hat{w}_{lv}(x,s) \end{bmatrix} \tag{A3.40}$$

Example L3-(Longitudinal Waves in a Rod)

The two previous examples developed spatial observers for a rod. Temporal observers, however, can be formulated to filter narrowband dynamics exploiting point measurements and static filter gains or broadband dynamics using distributed sensors with spatially

dependent filter gains. Following the analysis presented in section A2.3.0 a temporal observer for a longitudinal rod based on axial strain measurement is given by the time invariant equation

$$\frac{d}{dt}\begin{bmatrix} \dot{\hat{u}}(p,t) \\ p\,\hat{u}(p,t) \end{bmatrix} = \begin{bmatrix} 0 & \frac{EA}{\rho A}p \\ p & 0 \end{bmatrix}\begin{bmatrix} \dot{\hat{u}}(p,t) \\ p\,\hat{u}(p,t) \end{bmatrix} + \begin{bmatrix} K_1 \\ K_2 \end{bmatrix}\left(z(p,t) - C\,\hat{v}(p,t) \right) \tag{A3.41}$$

where the state vector $v = [u(p,t)\ pu(p,t)]$ is composed of velocity and axial strain and $A(p)$ is diagonalized according to

$$\Gamma(p) = \begin{bmatrix} \frac{1}{2} & \frac{-1}{2}\sqrt{\frac{EA}{\rho A}} \\ \frac{1}{2} & \frac{1}{2}\sqrt{\frac{EA}{\rho A}} \end{bmatrix}\begin{bmatrix} 0 & \frac{EA}{\rho A}p \\ p & 0 \end{bmatrix}\begin{bmatrix} 1 & \frac{1}{\sqrt{\frac{\rho A}{EA}}} \\ -\sqrt{\frac{\rho A}{EA}} & \frac{1}{\sqrt{\frac{\rho A}{EA}}} \end{bmatrix}$$

If we transform equation-(*A3.41*) into the temporal frequency domain the transfer functions relating estimated physical states to strain measurement becomes

$$\begin{bmatrix} s\frac{\hat{u}(p,s)}{z(p,s)} \\ \frac{p\,\hat{u}(p,s)}{z(p,s)} \end{bmatrix} = \begin{bmatrix} \frac{K_1 s + K_2 \frac{EA}{\rho A}p}{\phi(s)} \\ \frac{K_2 s + K_1 p}{\phi(s)} \end{bmatrix} \tag{A3.42}$$

with temporal characteristic equation as of function of observer gains K_1 and K_2 given by

$$\phi(s) = s^2 + K_2 s + K_1 p - \frac{EA}{\rho A}p^2 = 0 \tag{A3.43}$$

As in the case of the spatial observer we can place the temporal poles along the real axis at $-a_1$ and $-a_2$. This leads to $\phi(s)=s+(a_1+a_2)s+a_1a_2$. Substituting for $\phi(p)$ and the temporal observer gains-(K_1,K_2) the observer transfer functions become

$$\begin{bmatrix} s\frac{\hat{u}(p,s)}{z(p,s)} \\ \frac{p\,\hat{u}(p,s)}{z(p,s)} \end{bmatrix} = \begin{bmatrix} \frac{(\frac{EA}{\rho A}p + \frac{a_1 a_2}{p})s + (a_1 + a_2)\frac{EA}{\rho A}p}{s^2 + (a_1 + a_2)s + a_1 a_2} \\ \frac{(a_1 + a_2)s + (\frac{EA}{\rho A}p^2 + a_1 a_2)}{s^2 + (a_1 + a_2)s + a_1 a_2} \end{bmatrix} \tag{A3.44}$$

These expressions show that broadband temporal observation of physical states at a point requires spatial convolution of axial strain with the observer gain operator. However, to detect a single wavenumber the observer gain is a complex static function of the state

permitting wave states to be filtered using only point measurements. On the other hand broadband observation at a point in a structures requires both temporal and spatial convolution of the measured physical dynamics. To simplify this problem the spatial part of the two convolutions can be evaluated to yield the following expression for the rightward and leftward velocity wave components

$$\hat{w}_{rv}(0,s) = \frac{\left\{\frac{EA}{\rho A}u''(0,s) + a_1 a_2 u(0,s)\right\}s + (a_1 + a_2)\frac{EA}{\rho A}u''(0,s)}{2(s+a_1)(s+a_2)}$$

$$-\frac{1}{2}\sqrt{\frac{EA}{\rho A}}u'(0,s)$$

$$= s\frac{1}{2}u(0,s) - \frac{1}{2}\sqrt{\frac{EA}{\rho A}}u'(0,s) \qquad (A3.46a)$$

$$\hat{w}_{rv}(0,s) = \frac{\left\{\frac{EA}{\rho A}u''(0,s) + a_1 a_2 u(0,s)\right\}s + (a_1 + a_2)\frac{EA}{\rho A}u''(0,s)}{2(s+a_1)(s+a_2)}$$

$$+\frac{1}{2}\sqrt{\frac{EA}{\rho A}}u'(0,s)$$

$$= s\frac{1}{2}u(0,s) + \frac{1}{2}\sqrt{\frac{EA}{\rho A}}u'(0,s) \qquad (A3.46b)$$

where point observation occurs at $x=0$. This is equivalent to having the full collocated physical state available for measurement.

A3.9.2 B-E Beam

Example B1-(Transverse Waves in B-E Beam):

The equation of motion which governs homogeneous transverse dynamics of a Bernoulli-Euler beam is given by

$$\frac{\partial^2 u(x,t)}{\partial t^2} + \frac{EI}{\rho A}\frac{\partial^4 u(x,t)}{\partial x^4} = 0 \; ; \qquad -\infty < x < \infty \qquad (A3.47)$$

Again taking the Laplace transform of this equation and choosing the state vector to be

$$\vec{v}(x,s) = [u(x,s), u'(x,s), EIu''(x,s), EIu'''(x,s)]^T$$

we can form a spatial observer for a beam in state-space form as

$$\frac{d}{dx}\begin{bmatrix} \hat{u} \\ \hat{u}' \\ EI\ \hat{u}''' \\ EI\ \hat{u}'' \end{bmatrix} = \begin{bmatrix} 0 & 1 & 0 & -K_1 \\ 0 & 0 & 0 & 1-K_2 \\ \frac{-\rho A}{EI}s^2 & 0 & 0 & -K_3 \\ 0 & 0 & 1 & -K_4 \end{bmatrix} \begin{bmatrix} \hat{u} \\ \hat{u}' \\ EI\ \hat{u}''' \\ EI\ \hat{u}'' \end{bmatrix} + \begin{bmatrix} K_1 \\ K_2 \\ K_3 \\ K4 \end{bmatrix} y(x,s) \qquad (A3.48)$$

where v(x,s) represents the estimated state vector with distributed curvature

$$y(x,s) = C(s)\vec{v}(x,s)$$
$$= [0\ 0\ 0\ 1]\vec{v}(x,s)$$

as the only state available for measurement. $K(s)=[K_1\ K_2\ K_3\ K_4]^T$ represents the vector of observer gains. Transforming this expression into the spatial frequency domain the observer transfer functions become

$$\begin{bmatrix} \frac{\hat{u}(p,s)}{y(p,s)} \\ p\frac{\hat{u}(p,s)}{y(p,s)} \\ EIp^3\frac{\hat{u}(p,s)}{y(p,s)} \\ EIp^2\frac{\hat{u}(p,s)}{y(p,s)} \end{bmatrix} = \frac{1}{D(p)}\begin{bmatrix} K_1p^3 + K_2p^2 + K_4p + K_3 \\ K_2p^3 + K_4p^2 + K_3p - \lambda s^2K_1 \\ K_3p^3 - K_1\lambda s^2p^2 - K_2\lambda s^2p - \lambda s^2K_4 \\ K_4p^3 + K_3p^2 - K_1\lambda s^2p - \lambda s^2K_2 \end{bmatrix}; \lambda = \frac{\rho A}{EI} \qquad (A3.49)$$

with characteristic equation

$$\phi(p) = p^4 + K_4p^3 + K_3p^2 - K_1\lambda s^2p + (1-K_2)\lambda = 0 \qquad (A3.50)$$

As in the case of the compression rod the spatial observer poles can be placed along the negative real axis-(for $x>0$) at locations defined by $-a_1$,$-a_2$, $-a_3$ and-a_4. For these particular pole locations the required observer gains are

$$K_1(s) = \frac{-1}{\lambda s^2}\{a_1a_2(a_3+a_4) + a_3a_4(a_1+a_2)\}$$
$$K_2(s) = \frac{-(a_1a_2a_3a_4)}{\lambda s^2} + 1$$
$$K_3(s) = a_1a_3 + a_1a_4 + a_2a_3 + a_2a_4 + a_1a_2$$
$$K_4(s) = a_1 + a_2 + a_3 + a_4$$

which leads to the factored form of the characteristic equation

$$D(p) = (p+a_1)(p+a_2)(p+a_3)(p+a_4) = 0 \qquad (A3.51)$$

With this form of the characteristic equation partial fraction expansion of the transfer functions given in equation (*A3.49*) define appropriate weighting functions for estimating the unknown elements of the physical state vector. However, obtaining from wave states from these physical measurements is not as easy since the wave transformation matrix-$Y_b^{-1}(s)$ for a B-E beam is acausal.

Example-B2-(Transverse Waves on a B-E Beam):

In an attempt to overcome the problems associated with acausal temporal filtering we can formulate a temporal observer using velocity and curvature as state variables and exploit properties between time and space to help realize causal spatial filters. Consider the homogeneous dynamics of a B-E beam in the temporal domain described by

$$\frac{d\vec{v}(p,t)}{dt} = A(p)\vec{v}(p,t) = \begin{bmatrix} 0 & -p^2\mu \\ p^2 & 0 \end{bmatrix} \vec{v}(p,t) \quad for \; t > 0 \; ; \; -\infty < x < \infty \tag{A3.52}$$

where $\mu=\beta^{-1}$, $v(p,t)=[u(p,t)\; p^2u(p,t)]^T$ and one useful diagaonalization is given by

$$\Gamma(p) = Y^{-1}(p)A(p)Y(p) = \begin{bmatrix} \frac{1}{2} & \frac{-j}{2}\sqrt{\mu} \\ \frac{1}{2} & \frac{j}{2}\sqrt{\mu} \end{bmatrix} \begin{bmatrix} 0 & -p^2\mu \\ p^2 & 0 \end{bmatrix} \begin{bmatrix} 1 & 1 \\ \frac{j}{\sqrt{\mu}} & \frac{-j}{\sqrt{\mu}} \end{bmatrix} \tag{A3.53}$$

with output relation given by $y(p,t)=C(p)v(p,t)$ For this system a temporal observer can be represented as

$$\frac{d\hat{\vec{v}}(p,t)}{dt} = \{A(p) - K(p)C(p)\}\hat{\vec{v}}(p,t) + K(p)y(p,t) \; ; \; t > 0 \tag{A3.54}$$

As before curvature-($C(p)=[0\; 1]$) is chosen as the available state measurement. Notice that because of the parabolic form of the equation of motion for a simple beam the temporal observer is only of second order. This makes pole placement slightly less difficult since only two gains are required to locate two temporal observer poles. Thus, placing these poles at $-a_1$ and $-a_2$ results in observer gains given by

$$K_1(p) = \frac{a_1 a_2}{p^2} - \mu p^2$$

$$K_2(p) = a_1 + a_2$$

Substituting these gains into equation (*A3.54*) and transforming into the Laplace-(s) domain leads to the following non-dimensional transfer functions relating state estimates and measured curvature:

$$\begin{bmatrix} \hat{u}_{ndv} \\ \hat{u}_{ndc} \end{bmatrix} = \begin{bmatrix} \dfrac{\left(\frac{1}{2} - p_{nd}^2\right) s_{nd} - \gamma p_{nd}^2}{s_{nd}^2 + \gamma s_{nd} + 1} \\ \dfrac{\gamma s_{nd} + (1 - p_{nd}^4)}{s_{nd}^2 + \gamma s_{nd} + 1} \end{bmatrix}$$

$$s_{nd} = \frac{s}{\sqrt{a_1 a_2}}\ ;\ p_{nd} = \sqrt[4]{\mu}\,\frac{p}{\sqrt[4]{a_1 a_2}}\ ;\ \gamma = \frac{a_1 + a_2}{\sqrt{a_1 a_2}} \qquad (A3.55)$$

where u_{ndv} and u_{ndc} are defined as

$$\hat{u}_{ndv} = \frac{s\,\hat{u}(p,s)}{\sqrt{\mu}\,y(p,s)}\ ;\ \hat{u}_{ndc} = \frac{p^2\,\hat{u}(p,s)}{y(p,s)}$$

The temporal pole-zero diagrams for the transfer functions of equation (*A3.55*) are given in Figure A3.6. From this figure we see that the pole-zero behavior of the estimated velocity transfer function is similar to that found in Example L1. However, for the estimated curvature transfer function the zero introduces non-minimum phase dynamics as the spatial frequency-p_{nd} increases. The migration of the temporal zero into the righthand plane is required if broadband observation of physical and wave-states is desired. Narrowband estimation of wave states is achieved for static values of the observer gains K_1 and K_2 where the dispersion relation is satisfied at one particular frequency. This can be seen in Figure A3.7 where only at the frequency of interest is the gain and phase of measured response equal to that of its estimate at steady-state.

Exploiting the diagonalization of $A(p)$ given in equation (*A3.53*) we find that the appropriate transformation relating estimates of velocity and curvature to normalized temporal wave coordinates is given by

$$\begin{bmatrix} \hat{w}_{+v}(p,t) \\ \hat{w}_{-v}(p,t) \end{bmatrix} = \begin{bmatrix} \frac{1}{2} & \frac{-j}{2} \\ \frac{1}{2} & \frac{j}{2} \end{bmatrix} \begin{bmatrix} \dot{\hat{u}}(p,t) \\ p^2\,\hat{u}(p,t) \end{bmatrix}\ ;\ j = \sqrt{-1} \qquad (A3.56)$$

where (+) and (-) correspond to amplitude propagating in positive and negative time respectively, and v refers to temporal velocity wave amplitudes. If it can be assumed that the spatial evanescent wave components of the steady-state response are negligible then the propagating temporal velocity wave amplitudes are directly equivalent to their propagating spatial counterparts. Thus, the causal spatial convolution-(sensor realization shown in Figure A3.8) is given by

$$\begin{bmatrix} \hat{w}_{rpv}(x,s) \\ \hat{w}_{lpv}(x,s) \end{bmatrix} = \begin{bmatrix} \int_{-\infty}^{\infty} \left\{ \frac{1}{2}\delta(x')\,\hat{\dot{u}}(x-x',s) + \frac{-\sqrt{\mu}}{2\xi}\,\hat{u}''(x-x',s) \right\} d\xi \\ \int_{-\infty}^{\infty} \left\{ \frac{1}{2}\delta(x')\,\hat{\dot{u}}(x-x',s) + \frac{\sqrt{\mu}}{2\xi}\,\hat{u}''(x-x',s) \right\} d\xi \end{bmatrix} \quad (A3.57)$$

Of course position wave component estimates require only a temporal integration.

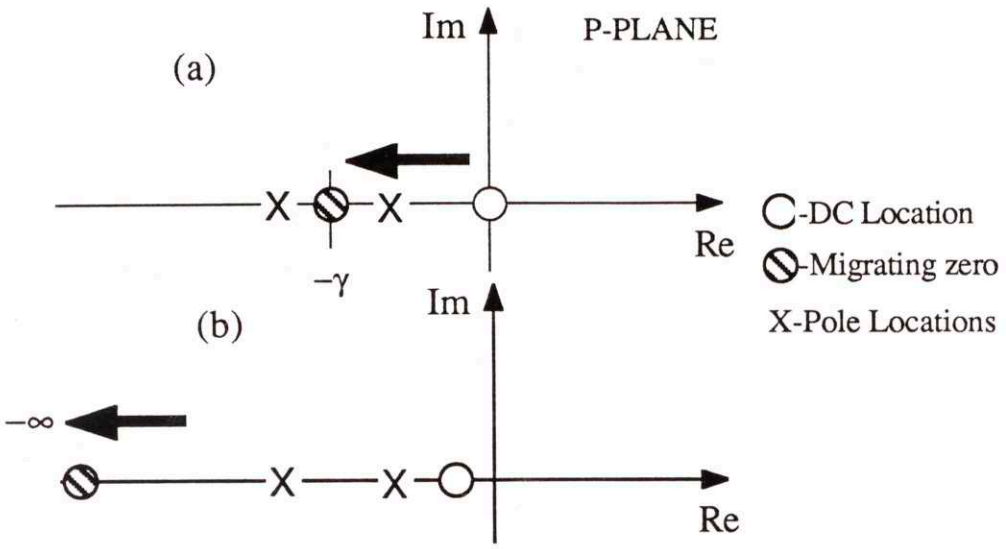

Figure A3.4: Relative pole-zero locations for Spatial Observer: (a) estimated position transfer function (b) esitmated strain transfer function.

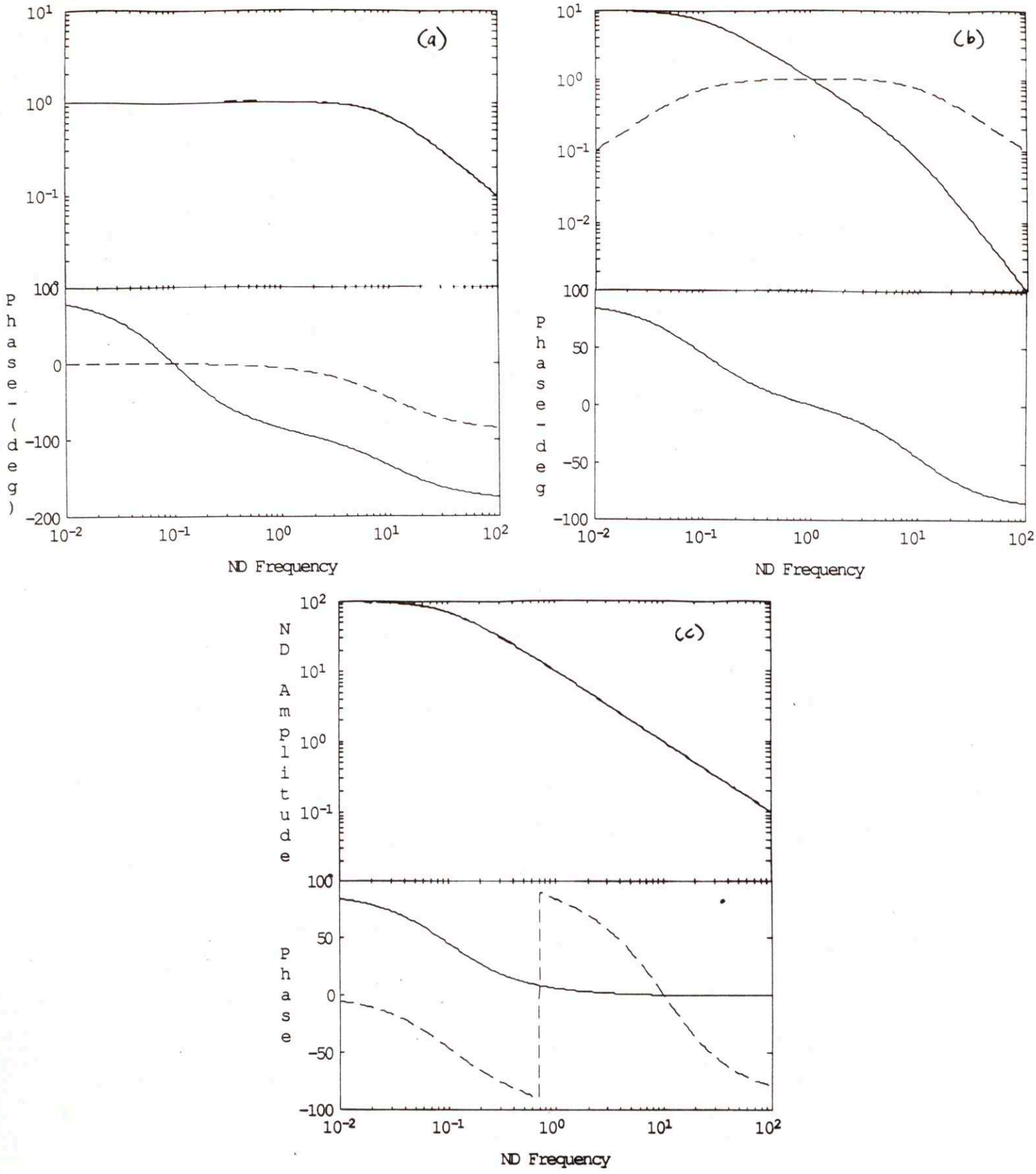

Figure A3.5: Plots of Estimated Position-(solid) and Strain-(dashed) of Spatial Transfer Functions for Longitudinal Dynamics along a Rod-(a)-snd=0.1,(b)-snd=1 and (c)-snd=10.

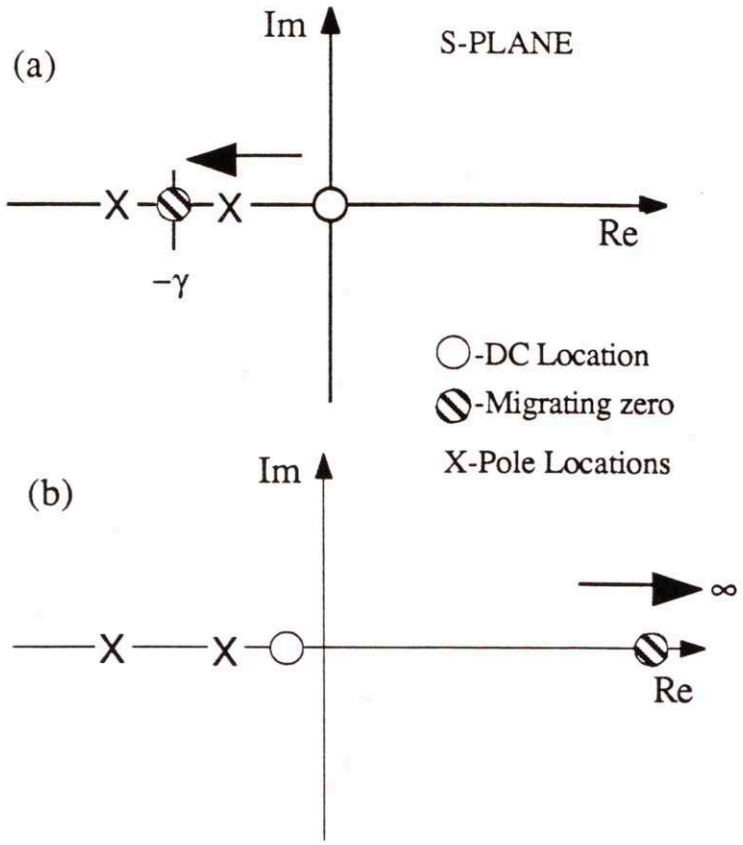

Figure A3.6: Relative pole-zero locations for Temporal Observer: (a) estimated velocity transfer function (b) esitmated strain transfer function.

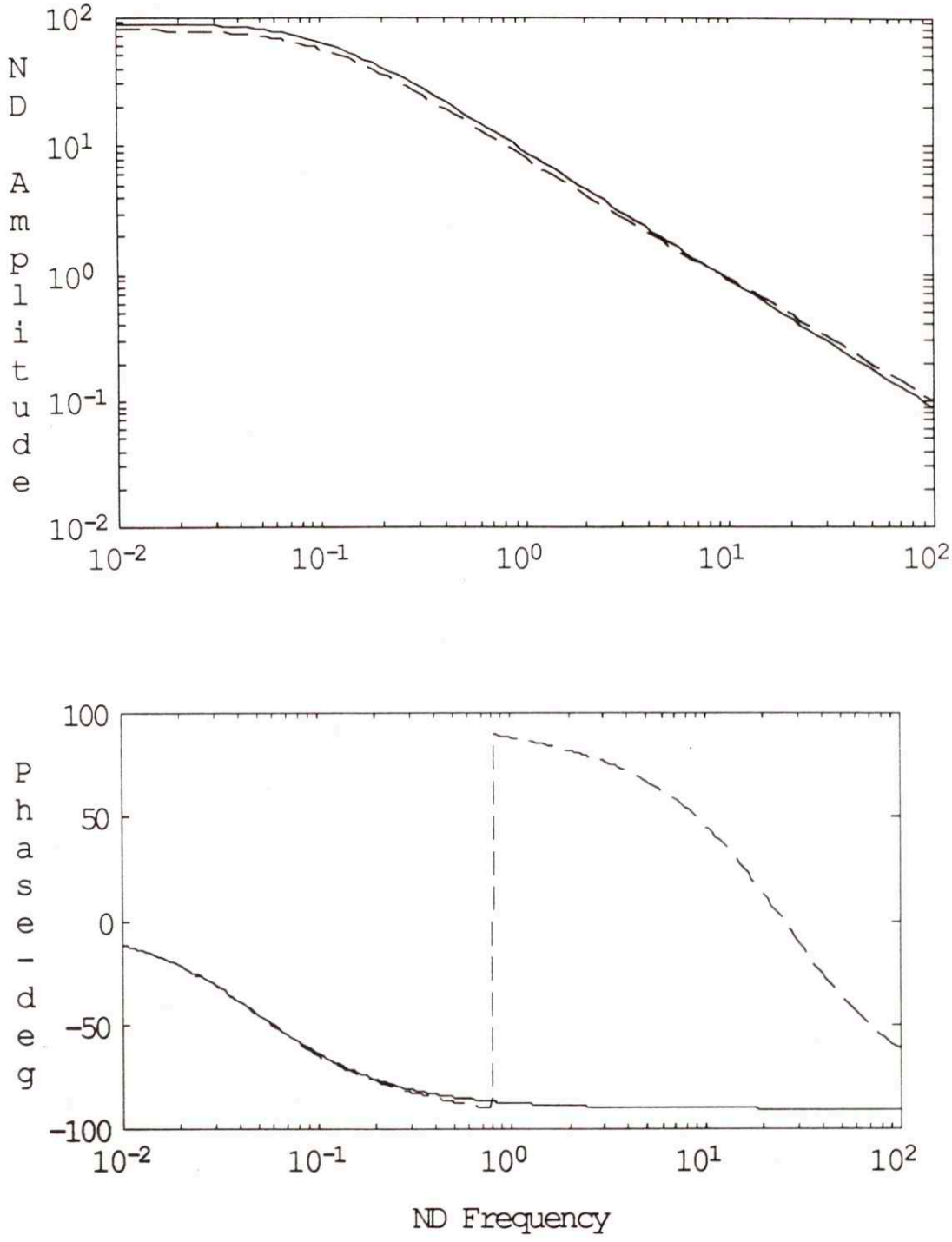

Figure A3.7: Magnitude and Phase of Estimated Position-(solid) and Strain-(solid) of Spatial Transfer Functions for Transverse Dynamics of B-E beam-($|p_{nd}|=5,\gamma=20$)

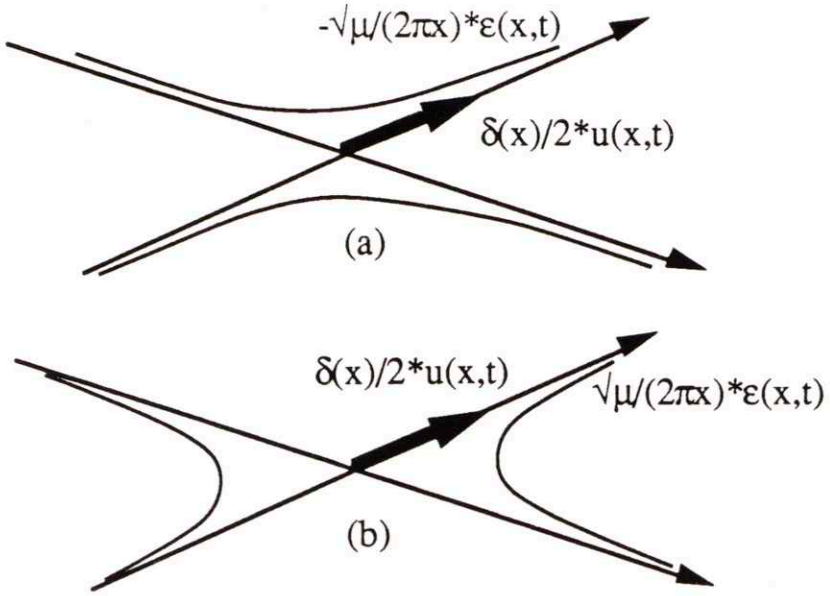

Figure A3.8: Spatial Convolution for decoupling (a)-rightward and (b)-leftward propagating wave components on a B-E beam.

A 4

Identifying the Wave-Model

Distributed Sensors have unique advantages over their point counterparts, especially when it comes to determining the characteristic wave-model-(k *vs.* ω) for a particular 1-D member. Previous research by Scheuren-[45,46] has shown that the dispersion relation can be determined using three point sensors as

$$k = \frac{2}{\Delta} cos^{-1}\left\{\frac{1}{2}\left(\frac{u\left(\frac{-\Delta}{2}, \omega\right)}{u(0, \omega)} + \frac{u\left(\frac{\Delta}{2}, \omega\right)}{u(0, \omega)}\right)\right\} \qquad (A4.1)$$

where Δ is separation distance between individual discrete sensors. Notice that this relation exploits the phase lag that exists between each sensor. The only requirement is that all point sensors be of the same type, i.e. strain, displacement, etc.

The same relation can be computed from the use of only distributed sensors which are collocated. This requires that an interpolant be found whose frequency properties correspond to $cos(k\Delta)$ over the frequency range of interest. Such a interpolant falls directly into the class of band-limited spectral filters presented in Chapter 4. Therefore, the interpolant which achieves this behaviour is given by

$$\phi(x) = \frac{1}{2\pi}\left(\frac{sin\left(k_b\left(x - \frac{\Delta}{2}\right)\right)}{\left(x - \frac{\Delta}{2}\right)} + \frac{sin\left(k_b\left(x + \frac{\Delta}{2}\right)\right)}{\left(x + \frac{\Delta}{2}\right)}\right); \qquad x \in (-\infty, \infty) \qquad (A4.2)$$

with frequency properties given by

$$\Phi(k) = \cos\left(\frac{k\Delta}{2}\right); \qquad k \in [-k_b, k_b] \tag{A4.3}$$

Now combining equation (*A4.2*) with the output of a collocated band-limited sinc interpolant leads to the following equation for the dispersion relation:

$$k = \frac{2}{\Delta}\cos^{-1}\left(\frac{v_2(0,\omega)}{v_1(0,\omega)}\right)$$

$$= \frac{2}{\Delta}\cos^{-1}\left(\frac{\frac{1}{2\pi}\int_{-\infty}^{\infty}\left(\frac{\sin(k_b(\xi-\frac{\Delta}{2}))}{(\xi-\frac{\Delta}{2})}+\frac{\sin(k_b(\xi+\frac{\Delta}{2}))}{(\xi+\frac{\Delta}{2})}\right)u(\xi,\omega)\,d\xi}{\frac{1}{2\pi}\int_{-\infty}^{\infty}\frac{2\sin(k_b(\xi))}{\xi}u(\xi,\omega)\,d\xi}\right) \tag{A4.4}$$

Of course for finite structures the spatial extent of the two interpolants will have to be truncated.

A 5

Active Isolation

A5.1.0 A Free-Free B-E Beam Example

The ideas of Chapter 5 are not restricted to implementing active damping and active isolation control objectives using non-collocated wave sensors and control actuators. Collocated control schemes are also possible. This section investigates the case of active isolation on a free-free beam using a collocated wave sensor and a force actuator located at the center of the member.

Consider the free-free beam displayed in Figure A5.1. A force acts at the right free-end of the beam and provides a broadband disturbance which excites the resonant dynamics of the structure. This resonant behaviour can be viewed in terms of waves which originate from the right free-end, traverse the length of the beam and reflect from the left free-end in such a manner that they close upon themselves. One potential control objective is to isolate a portion of the structure from the incident disturbance. The idea is to concentrate the energy in a particular region by effectively creating a structural diode. This causes the remaining portion of the structure to be unaffected by the disturbance. By suppressing the evanescent dynamics of the member only a single actuator is required for feedforward control. Figure A5. displays the control actuator at the center of the beam.

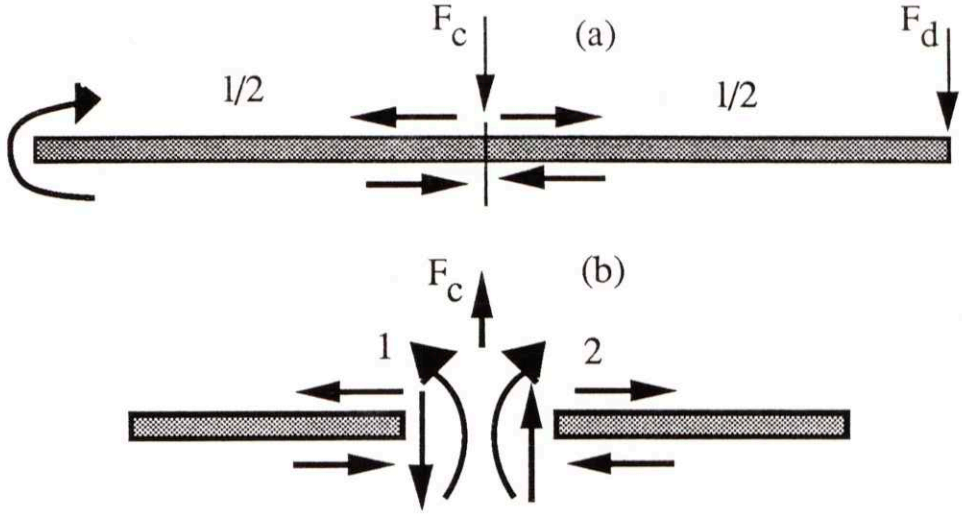

Figure A5.1 (a) A free-free B-E Beam. (b) Junction at center of beam showing internal and external forces and moments along with scattering dynamics.

A5.1.1 Junction Dynamics

In the beam of Figure A5.1a an artificial junction relation can be established by dividing the beam into two sections-(See Figure A5.1b). This exposes the internal moments and forces which act to transmit energy from one section of the beam to the other. Thus, the transmission of energy can be represented by waves which propagate to and from this section in the beam. Such a formulation leads to the following junction input/output relation which assumes that both an external force and moment are available for achieving the control objective.

$$\begin{bmatrix} w_{lp_1} \\ w_{le_1} \\ w_{rp_2} \\ w_{re_2} \end{bmatrix} = \begin{bmatrix} 0 & 0 & 1 & 0 \\ 0 & 0 & 0 & 1 \\ 1 & 0 & 0 & 0 \\ 0 & 1 & 0 & 0 \end{bmatrix} \begin{bmatrix} w_{rp_1} \\ w_{re_1} \\ w_{lp_2} \\ w_{le_2} \end{bmatrix} + \frac{1}{4\,iEIk^3} \begin{bmatrix} 1 & -ik \\ -i & ik \\ 1 & ik \\ -i & -ik \end{bmatrix} \begin{bmatrix} F_c \\ M_c \end{bmatrix} \tag{A5.1}$$

This wave input/output formulation permits the feedforward control to be written as

$$\begin{bmatrix} F_c \\ M_c \end{bmatrix} = 4\,iEIk^3 \begin{bmatrix} K_{11} & K_{12} & K_{13} & K_{14} \\ \frac{K_{21}}{k} & \frac{K_{22}}{k} & \frac{K_{23}}{k} & \frac{K_{24}}{k} \end{bmatrix} \vec{w}_i \tag{A5.2}$$

where K represents the feedforward compensation matrix. This form of the control suggests that if all the wave-modes were available for control then a collocated feedforward

implementation might be feasible. However, this assumption overlooks the fact that the term Eik^3 is non-causal. Thus, not only must one consider the availability of the wave-modes w but also how to realize the compensation. Fortunately, this methods outlined in Chapter 4 permit such a realization for propagating components using distributed and point sensors.

A5.1.2 Form of Feedforward Control

Again suppressing knowledge of the evanescent terms the compensation can be embedded in the wave sensing scheme. This implies that input/output relation in equation-(*A5.1*) can be rewritten to remove the frequency dependence on the feedforward compensators K as

$$\begin{bmatrix} s_{lp_1} \\ s_{le_1} \\ s_{rp_2} \\ s_{re_2} \end{bmatrix} = \begin{bmatrix} 0 & 0 & 1 & 0 \\ 0 & 0 & 0 & 1 \\ 1 & 0 & 0 & 0 \\ 0 & 1 & 0 & 0 \end{bmatrix} \begin{bmatrix} s_{rp_1} \\ s_{re_1} \\ s_{lp_2} \\ s_{le_2} \end{bmatrix} + \frac{1}{4} \begin{bmatrix} 1 & -ik \\ -i & ik \\ 1 & ik \\ -i & -ik \end{bmatrix} \begin{bmatrix} F_c \\ M_c \end{bmatrix} \qquad (A5.3)$$

where now shear force wave-mode amplitudes-s are desired. Similarly, the feedforward form of the control becomes

$$\begin{bmatrix} F_c \\ M_c \end{bmatrix} = 4 \begin{bmatrix} K_{11} & K_{12} & K_{13} & K_{14} \\ \frac{K_{21}}{k} & \frac{K_{22}}{k} & \frac{K_{23}}{k} & \frac{K_{24}}{k} \end{bmatrix} \vec{s}_i \qquad (A5.4)$$

This form of the control shows that there is still a frequency dependence on the compensation which involves the control moment. However, this control force can't be used with collocated distributed strain sensors since a concentrated moment results in a discontinuity in the strain field over the length of the sensor. Thus, the final form of the feedforward control becomes

$$[F_c] = 4 \begin{bmatrix} K_{11} & K_{12} & K_{13} & K_{14} \end{bmatrix} \vec{s}_i \qquad (A5.5)$$

A5.1.3 Sensing shear force wave components for control.

With the frequency dependence of the compensation transfered to the sensed wave components, the only thing left to do is to determine the form of filter which can be used

infer rightward and leftward shear-force wave components. The filter which achieves this goal is given by

$$\phi(x) = \pm\left(\phi'_{Hi}(x) \pm \phi'_{sin\,c} + \sqrt[4]{\frac{\rho A}{EI}}\, s^{\frac{1}{2}}\, \delta(x) \right) \qquad (A5.6)$$

where +/- refer to separation of rightward and leftward wave components respectively. Of course equation (*A5.6*) assumes convolution with a distributed strain field as is the case with PVDF sensors.

A5.1.4 Active Isolation of the left-half portion of the beam.

Ideally, active isolation of the left-half portion of the free-free beam can be achieved by feeding the leftward going shear force wave components to the force actuator 180 degrees out of phase. This choice would lead to control gains K in equation (*A5.6*) given by

$$K=[0\ 0\ -1\ -i]$$

which would lead to the following closed-loop scattering matrix

$$\begin{bmatrix} s_{lp_1} \\ s_{le_1} \\ s_{rp_2} \\ s_{re_2} \end{bmatrix} = \begin{bmatrix} 0 & 0 & 0 & -i \\ 0 & 0 & i & 0 \\ 1 & 0 & -1 & -i \\ 0 & 1 & i & -1 \end{bmatrix} \begin{bmatrix} s_{rp_1} \\ s_{re_1} \\ s_{lp_2} \\ s_{le_2} \end{bmatrix} \qquad (A5.7)$$

However, the near-field components are not available in this sensing scheme. Thus, feedforward control is based solely on the approximate sensing of the propagting components. At high frequency-(i.e. beyond the fifth mode of the member) this becomes a good assumption.